E-ISSN: 2147-1959

MIRT

Molecular Imaging and Radionuclide Therapy

June 2023 Volume 32 Issue 2 www.tsnm.org

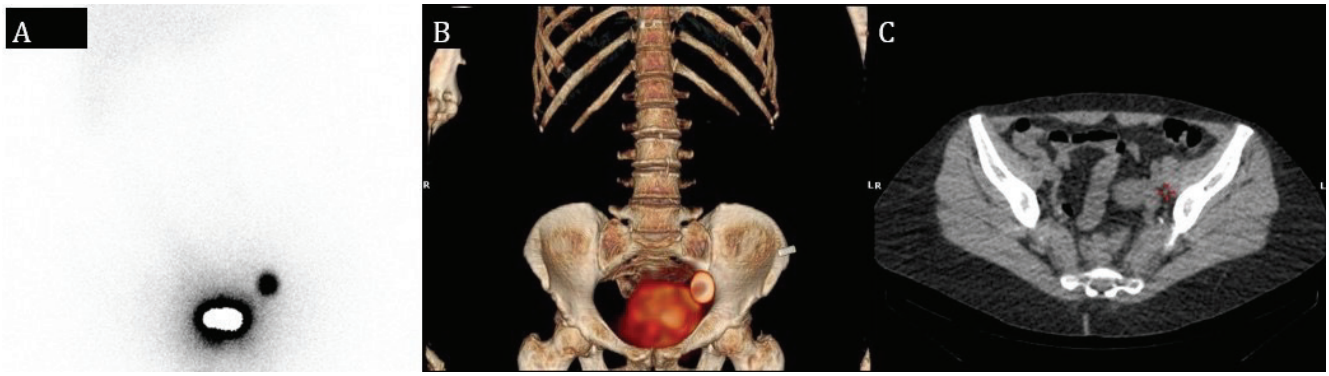

"Official Journal of the Turkish Society of Nuclear Medicine"

galenos yayınevi

TURKISH SOCIETY OF NUCLEAR MEDICINE 1975

MIRT

Molecular Imaging and Radionuclide Therapy

MIRT

Molecular Imaging and Radionuclide Therapy

Turkish Society of Nuclear Medicine
Cinnah Caddesi Pilot Sokak No: 10/12 Çankaya 06650 Ankara, Turkey **Phone:** +90 312 441 00 45 **Fax:** +90 312 441 12 95 **Web:** www.tsnm.org **E-mail:** dernekmerkezi@tsnm.org
"Formerly Turkish Journal of Nuclear Medicine"

Reviewing the articles' conformity to the publishing standards of the Journal, typesetting, reviewing and editing the manuscripts and abstracts in English, creating links to source data, and publishing process are realized by Galenos.

Publisher Contact
Address: Molla Gürani Mah. Kaçamak Sk. No: 21/1 34093 İstanbul, Turkey
Phone: +90 (212) 621 99 25 **Fax:** +90 (212) 621 99 27
E-mail: info@galenos.com.tr/yayin@galenos.com.tr
Web: www.galenos.com.tr
Publisher Certificate Number: 14521

Online Publication Date: June 2023
ISSN: 2146-1414 **E-ISSN:** 2147-1959
International scientific journal published quarterly.

MIRT

Molecular Imaging and Radionuclide Therapy

ABOUT US

Molecular Imaging and Radionuclide Therapy (formerly Turkish Journal of Nuclear Medicine) is the official publication of Turkish Society of Nuclear Medicine.

Focus and Scope

Molecular Imaging and Radionuclide Therapy (Mol Imaging Radionucl Ther, MIRT) is a double-blind peer-review journal published in English language. It publishes original research articles, invited reviews, editorials, short communications, letters, consensus statements, guidelines and case reports with a literature review on the topic, in the field of molecular imaging, multimodality imaging, nuclear medicine, radionuclide therapy, radiopharmacy, medical physics, dosimetry and radiobiology. MIRT is published three times a year (February, June, October). Audience: Nuclear medicine physicians, medical physicists, radiopharmaceutical scientists, radiobiologists.

The editorial policies are based on the "Recommendations for the Conduct, Reporting, Editing, and Publication of Scholarly Work in Medical Journals (ICMJE Recommendations)" by the International Committee of Medical Journal Editors (2016, archived at http://www.icmje.org/) rules.

Molecular Imaging and Radionuclide Therapy is indexed in **Pubmed, Pubmed Central (PMC), Emerging Sources Citation Index (ESCI), TUBITAK-ULAKBIM, DOAJ, Scopus, Gale/Cengage Learning, EBSCO databases, Embase, ProQuest Health & Medical Complete, CINAHL, Index Copernicus, J-Gate, IdealOnline, ROOT INDEXING, Türkiye Atıf Dizini-Turkiye Citation Index, Turk Medline, EuroPub, Hinari, GOALI, ARDI, OARE** and **AGORA.**

Open Access Policy

This journal provides immediate open access to its content on the principle that making research freely available to the public supports a greater global exchange of knowledge.

Open Access Policy is based on rules of Budapest Open Access Initiative (BOAI) (http://www.budapestopenaccessinitiative.org/). By "open access" to [peer-reviewed research literature], we mean its free availability on the public internet, permitting any users to read, download, copy, distribute, print, search, or link to the full texts of these articles, crawl them for indexing, pass them as data to software, or use them for any other lawful purpose, without financial, legal, or technical barriers other than those inseparable from gaining access to the internet itself. The only constraint on reproduction and distribution, and the only role for copyright in this domain, should be to give authors control over the integrity of their work and the right to be properly acknowledged and cited.

Subscription Information

Manuscripts can only be submitted electronically through the Journal Agent website (http://www.journalagent.com/mirt/?plng=eng) after creating an account. This system allows online submission and review.

All published volumes in full text can be reached free of charge through the website http://mirt.tsnmjournals.org

Copyright Statement

Instructions for Authors

Instructions for authors are published in the journal and on the website http://mirt.tsnmjournals.org

Material Disclaimer

Scientific and legal responsibilities pertaining to the papers belong to the authors. Contents of the manuscripts and accuracy of references are also the author's responsibility. The Turkish Society of Nuclear Medicine, the Editor, the Editorial Board or the publisher do not accept any responsibility for opinions expressed in articles.

Financial expenses of the journal are covered by Turkish Society of Nuclear Medicine.

Correspondence Address

Editor in Chief Prof. Murat Fani Bozkurt, MD, FEBNM Hacettepe University, Medical School, Department of Nuclear Medicine, Ankara, Turkey

E-mail: fanibozkurt@gmail.com

Web page: http://mirt.tsnmjournals.org/

Publisher Corresponding Address

Galenos Yayınevi Tic. Ltd. Şti.
Address: Molla Gürani Mah. Kaçamak Sk. No: 21/1 34093 Fındıkzade, İstanbul, Turkey
Phone: +90 212 621 99 25
Fax: +90 212 621 99 27
E-mail: info@galenos.com.tr

MIRT

Molecular Imaging and Radionuclide Therapy

INSTRUCTIONS TO AUTHORS

Molecular Imaging and Radionuclide Therapy (Mol Imaging Radionucl Ther, MIRT) publishes original research articles, short communications, invited reviews, editorials, case reports with a literature review on the topic, interesting images, consensus statements, guidelines, letters in the field of molecular imaging, multimodality imaging, nuclear medicine, radionuclide therapy, radiopharmacy, medical physics, dosimetry and radiobiology. MIRT is published by the Turkish Society of Nuclear Medicine three times a year (February, June, October).

Molecular Imaging and Radionuclide Therapy does not charge any article submission or processing fees.

GENERAL INFORMATION

MIRT commits to rigorous peer review, and stipulates freedom from commercial influence, and promotion of the highest ethical and scientific standards in published articles. Neither the Editor(s) nor the publisher guarantees, warrants or endorses any product or service advertised in this publication. All articles are subject to review by the editors and peer reviewers. If the article is accepted for publication, it may be subjected to editorial revisions to aid clarity and understanding without changing the data presented.

Manuscripts must be written in English and must meet the requirements of the journal. The journal is in compliance with the uniform requirements for manuscripts submitted to biomedical journals published by the International Committee of Medical Journal Editors (NEJM 1997; 336:309-315, updated 2016). Manuscripts that do not meet these requirements will be returned to the author for necessary revision before the review. Authors of manuscripts requiring modifications have a maximum of two months to resubmit the revised text. Manuscripts returned after this deadline will be treated as new submissions.

It is the authors' responsibility to prepare a manuscript that meets ethical criteria. The Journal adheres to the principles set forth in the Helsinki Declaration October 2013 (https://www.wma.net/policies-post/wma-declaration-of-helsinki-ethical-principles-for-medical-research-involving-human-subjects/) and holds that all reported research involving "Human beings" conducted in accordance with such principles.

Reports describing data obtained from research conducted in human participants must contain a statement in the MATERIALS AND METHODS section indicating approval by the ethical review board (including the approval number) and affirmation that INFORMED CONSENT was obtained from each participant.

All manuscripts reporting experiments using animals must include a statement in the MATERIALS AND METHODS section giving assurance that all animals have received humane care in compliance with the Guide for the Care and Use of Laboratory Animals (www.nap.edu) and indicating approval by the ethical review board.

If the study should have ethical approval, authors asked to provide ethical approval in order to proceed the review process. If they provide approval, review of the manuscript will continue.

In case report(s) and interesting image(s) a statement regarding the informed consent of the patients should be included in the manuscript and the identity of the patient(s) should be hidden.

Subjects must be identified only by number or letter, not by initials or names. Photographs of patients' faces should be included only if scientifically relevant. Authors must obtain written consent from the patient for use of such photographs. In cases of image media usage that potentially expose patients' identity requires obtaining permission for publication from the patients or their parents/guardians.

If the proposed publication concerns any commercial product, the author must include in the cover letter a statement indicating that the author(s) has (have) no financial or other interest with the product or explaining the nature of any relations (including consultancies) between the author(s) and editor the manufacturer or distributor of the product.

All submissions will be screened by Crossref Smilarity Check powered by "iThenticate". Manuscripts with an overall similarity index of greater than 25%, or duplication rate at or higher than 5% with a single source will be returned back to authors.

MANUSCRIPT CATEGORIES

1. Original Articles

2. Short Communications are short descriptions of focused studies with important, but very straightforward results.

3. Reviews address important topics in the field. Authors considering the submission of uninvited reviews should contact the editor in advance to determine if the topic that they propose is of current potential interest to the Journal. Reviews will be considered for publication only if they are written by authors who have at least three published manuscripts in the international peer reviewed journals and these studies should be cited in the review. Otherwise only invited reviews will be considered for peer review from qualified experts in the area.

4. Editorials are usually written by invitation of the editor by the editors on current topics or by the reviewers involved in the evaluation of a submitted manuscript and published concurrently with that manuscript.

5. Case Report and Literature Reviews are descriptions of a case or small number of cases revealing a previously undocumented disease process, a unique unreported manifestation or treatment of a known disease process, unique unreported complications of treatment regimens or novel and important insights into a condition's pathogenesis, presentation, and/or management. The journal's policy is to accept case reports only if it is accompanied by a review of the literature on the related topic. They should include an adequate number of images and figures.

6. Interesting Image

One of the regular parts of Molecular Imaging and Radionuclide Therapy is a section devoted to interesting images. Interesting image(s) should describe case(s) which are unique and include interesting findings adding insights into the interpretation of patient images, a condition's pathogenesis, presentation, and/or management.

7. Consensus Statements or Guidelines may be submitted by professional societies. All such submissions will be subjected to peer review, must be modifiable in response to criticisms, and will be published only if they meet the Journal's usual editorial standards.

8. Letters to the Editor may be submitted in response to work that has been published in the Journal. Letters should be short commentaries related to specific points of agreement or disagreement with the published work.

Note on Prior Publication

Articles are accepted for publication on the condition that they are original, are not under consideration by another journal, or have not been previously published. Direct quotations, tables, or illustrations that have appeared in

MIRT

Molecular Imaging and Radionuclide Therapy

INSTRUCTIONS TO AUTHORS

copyrighted material must be accompanied by written permission for their use from the copyright owner and authors. Materials previously published in whole or in part shall not be considered for publication. At the time of submission, authors must report that the manuscript has not been published elsewhere. Abstracts or posters displayed at scientific meetings need not be reported.

MANUSCRIPT SUBMISSION PROCEDURES

MIRT only accepts electronic manuscript submission at the web site http://www.journalagent.com/mirt/. After logging on to the website Click the 'online manuscript submission' icon. All corresponding authors should be provided with a password and a username after entering the information required. If you already have an account from a previous submission, enter your username and password to submit a new or revised manuscript. If you have forgotten your username and/or password, please send an e-mail to the editorial office for assistance. After logging on to the article submission system please read carefully the directions of the system to give all needed information and attach the manuscript, tables and figures and additional documents.

All Submissions Must Include:

1. Completed Copyright Assignment & Disclosure of Potential Conflict of Interest Form; This form should be downloaded from the website (provided in the author section), filled in thoroughly and uploaded to the website during the submission.
2. All manuscripts describing data obtained from research conducted in human participants must be accompanied with an approval document by the ethical review board.
3. All manuscripts reporting experiments using animals must include approval document by the animal ethical review board.
4. All submissions must include the authorship contribution form which is signed by all authors.

Authors must complete all online submission forms. If you are unable to successfully upload the files please contact the editorial office by e-mail.

MANUSCRIPT PREPARATION

General Format

The Journal requires that all submissions be submitted according to these guidelines:

- Text should be double spaced with 2.5 cm margins on both sides using 12-point type in Times Roman font.
- All tables and figures must be placed after the text and must be labeled.
- Each section (abstract, text, references, tables, figures) should start on a separate page.
- Manuscripts should be prepared as a word document (*.doc) or rich text format (*.rtf).
- Please make the tables using the table function in Word.
- Abbreviations should be defined in parenthesis where the word is first mentioned and used consistently thereafter.
- Results should be expressed in metric units. Statistical analysis should be done accurately and with precision. Please consult a statistician if necessary.
- Authors' names and institutions should not be included in the manuscript text and should be written only in the title page.

Title Page

The title page should be a separate form from the main text and should include the following:

- Full title (in English and in Turkish). Turkish title will be provided by the editorial office for the authors who are not Turkish speakers.
- Authors' names and institutions.
- Short title of not more than 40 characters for page headings.
- At least three and maximum eight keywords. (in English and in Turkish). Do not use abbreviations in the keywords. Turkish keywords will be provided by the editorial office for the authors who are not Turkish speakers. If you are not a native Turkish speaker, please reenter your English keywords to the area provided for the Turkish keywords. English keywords should be provided from http://www.nlm.nih.gov/mesh (Medical Subject Headings) while Turkish keywords should be provided from http://www.bilimterimleri.com.
- Word count (excluding abstract, figure legends and references).
- Corresponding author's e-mail and address, telephone and fax numbers.
- Name and address of person to whom reprint requests should be addressed.

Original Articles

Authors are required to state in their manuscripts that ethical approval from an appropriate committee and informed consents of the patients were obtained.

Original Articles should be submitted with a structured abstract of no more than 250 words. All information reported in the abstract must appear in the manuscript. The abstract should not include references. Please use complete sentences for all sections of the abstract. Structured abstract should include background, objective, methods, results and conclusions. Turkish abstract will be provided by the editorial office for the authors who are not Turkish speakers. If you are not a native Turkish speaker, please reenter your English abstract to the area provided for the Turkish abstract.

- Introduction
- Materials and Methods
- Results
- Discussion
- Study Limitations
- Conclusion

May be given for contributors who are not listed as authors, or for grant support of the research.

References should be cited in numerical order (in parentheses) in the text and listed in the same numerical order at the end of the manuscript on a separate page or pages. The author is responsible for the accuracy of references. Examples of the reference style are given below. Further examples will be found in the articles describing the Uniform Requirements for Manuscripts Submitted to Biomedical Journals (Ann Intern Med.1988; 208:258-265, Br Med J. 1988; 296:401-405). The titles of journals should be abbreviated according to the style used in the Index Medicus. Journal Articles and Abstracts: Surnames and initials of author's name, title of the article, journal name, date, volume number, and pages. All authors should be listed regardless of number. The citation of unpublished papers, observations or personal communications is not permitted. Citing an abstract is not recommended. Books: Surnames and initials of author's names, chapter title, editor's name, book title, edition, city, publisher, date and pages.

MIRT
Molecular Imaging and Radionuclide Therapy

INSTRUCTIONS TO AUTHORS

Sample References

Journal Article: Sayit E, Söylev M, Capa G, Durak I, Ada E, Yilmaz M. The role of technetium-99m-HMPAO-labeled WBC scintigraphy in the diagnosis of orbital cellulitis. Ann Nucl Med 2001;15:41-44.

Erselcan T, Hasbek Z, Tandogan I, Gumus C, Akkurt I. Modification of Diet in Renal Disease equation in the risk stratification of contrast induced acute kidney injury in hospital inpatients. Nefrologia 2009 doi: 10.3265/Nefrologia.2009.29.5.5449.en.full.

Article in a journal published ahead of print: Ludbrook J. Musculovenous pumps in the human lower limb. Am Heart J 2009;00:1-6. (accessed 20 February 2009).

Lang TF, Duryea J. Peripheral Bone Mineral Assessment of the Axial Skeleton: Technical Aspects. In: Orwoll ES, Bliziotes M (eds). Osteoporosis: Pathophsiology and Clinical Management. New Jersey, Humana Pres Inc, 2003;83-104.

Books: Greenspan A. Orthopaedic Radiology a Pratical Approach. 3th ed. Philadelphia, Lippincott Williams Wilkins 2000, 295-330.

Website: Smith JR. 'Choosing Your Reference Style', Online Referencing 2(3), http://orj.sagepub.com (200, accessed October 2008).

- Tables

Tables must be constructed as simply as possible. Each table must have a concise heading and should be submitted on a separate page. Tables must not simply duplicate the text or figures. Number all tables in the order of their citation in the text. Include a title for each table (a brief phrase, preferably no longer than 10 to 15 words). Include all tables in a single file following the manuscript.

– Figure Legends

Figure legends should be submitted on a separate page and should be clear and informative.

– Figures

Number all figures (graphs, charts, photographs, and illustrations) in the order of their citation in the text. At submission, the following file formats are acceptable: AI, EMF, EPS, JPG, PDF, PPT, PSD, TIF. Figures may be embedded at the end of the manuscript text file or loaded as separate files for submission. All images MUST be at or above intended display size, with the following image resolutions: Line Art 800 dpi, Combination (Line Art + Halftone) 600 dpi, Halftone 300 dpi. Image files also must be cropped as close to the actual image as possible.

Short Communications:

Short communications should be submitted with a structured abstract of no more than 200 words. These manuscripts should be no longer than 2000 words, and include no more than two figures and tables and 20 references. Other rules which the authors are required to prepare and submit their manuscripts are the same as described above for the original articles.

Invited Review Articles:

- Title page (see above)
- Abstract: Maximum 250 words; without structural divisions; in English and in Turkish . Turkish abstract will be provided by the editorial office for the authors who are not Turkish speakers. If you are not a native Turkish speaker, please reenter your English abstract to the area provided for the Turkish abstract.
- Text
- Conclusion
- Acknowledgements (if any)
- References

Editorial:

- Title page (see above)
- Abstract: Maximum 250 words; without structural divisions; in English and in Turkish. Turkish abstract will be provided by the editorial office for the authors who are not Turkish speakers. If you are not a native Turkish speaker, please re enter your English abstract to the area provided for the Turkish abstract.
- Text
- References

Case Report and Literature Review

- Title page (see above)
- Abstract: Approximately 100-150 words; without structural divisions; in English and in Turkish. Turkish abstract will be provided by the editorial office for the authors who are not Turkish speakers. If you are not a native Turkish speaker, please re-enter your English abstract to the area provided for the Turkish abstract.
- Introduction
- Case report
- Literature Review and Discussion
- References

Interesting Image:

No manuscript text is required. Interesting Image submissions must include the following:

Title Page: (see Original article section)

Abstract: Approximately 100-150 words; without structural divisions; in English and in Turkish. Turkish abstract will be provided by the editorial office for the authors who are not Turkish speakers. If you are not a native Turkish speaker, please re-enter your English abstract to the area provided for the Turkish abstract.

Image(s): The number of images is left to the discretion of the author. (See Original article section)

Figure Legend: Reference citations should appear in the legends, not in the abstract. Since there is no manuscript text, the legends for illustrations should be prepared in considerable detail but should be no more than 500 words total. The case should be presented and discussed in the Figure legend section.

References: Maximum eight references (see original article section).

Letters to the Editor:

- Title page (see above)
- Short comment to a published work, no longer than 500 words, no figures or tables.
- References no more than five.

Consensus Statements or Guidelines: These manuscripts should typically be no longer than 4000 words and include no more than six figures and tables and 120 references.

Proofs and Reprints

Proofs and a reprint orders are sent to the corresponding author. The author should designate by footnote on the title page of the manuscript the name and

MIRT
Molecular Imaging and Radionuclide Therapy

INSTRUCTIONS TO AUTHORS

address of the person to whom reprint requests should be directed. The manuscript when published will become the property of the journal.

Archiving

The editorial office will retain all manuscripts and related documentation (correspondence, reviews, etc.) for 12 months following the date of publication or rejection.

Submission Preparation Checklist

As part of the submission process, authors are required to check off their submission's compliance with all of the following items, and submissions may be returned to authors that do not adhere to these guidelines.

1. The submission has not been previously published, nor is it before another journal for consideration (or an explanation has been provided in Comments to the Editor).
2. The submission file is in Microsoft Word, RTF, or WordPerfect document file format. The text is double-spaced; uses a 12-point font; employs italics, rather than underlining (except with URL addresses); and the location for all illustrations, figures, and tables should be marked within the text at the appropriate points.
3. Where available, URLs for the references will be provided.
4. All authors should be listed in the references, regardless of the number.
5. The text adheres to the stylistic and bibliographic requirements outlined in the Author Guidelines, which is found in About the Journal.
6. English keywords should be provided from http://www.nlm.nih.gov/mesh(Medical Subject Headings), while Turkish keywords should be provided fromhttp://www.bilimterimleri.com
7. The title page should be a separate document from the main text and should be uploaded separately.
8. The "Affirmation of Originality and Assignment of Copyright/The Disclosure Form for Potential Conflicts of Interest Form" and Authorship Contribution Form should be downloaded from the website, filled thoroughly and uploaded during the submission of the manuscript.

TO AUTHORS

Copyright Notice

The author(s) hereby affirms that the manuscript submitted is original, that all statement asserted as facts are based on author(s) careful investigation and research for accuracy, that the manuscript does not, in whole or part, infringe any copyright, that it has not been published in total or in part and is not being submitted or considered for publication in total or in part elsewhere. Completed Copyright Assignment & Affirmation of Originality Form will be uploaded during submission. By signing this form;

1. Each author acknowledges that he/she participated in the work in a substantive way and is prepared to take public responsibility for the work.
2. Each author further affirms that he or she has read and understands the "Ethical Guidelines for Publication of Research".
3. The author(s), in consideration of the acceptance of the manuscript for publication, does hereby assign and transfer to the Molecular Imaging and Radionuclide Therapy all of the rights and interest in and the copyright of the work in its current form and in any form subsequently revised for publication and/or electronic dissemination.

Privacy Statement

The names and email addresses entered in this journal site will be used exclusively for the stated purposes of this journal and will not be made available for any other purpose or to any other party.

Peer Review Process

1. The manuscript is assigned to an editor, who reviews the manuscript and makes an initial decision based on manuscript quality and editorial priorities.
2. For those manuscripts sent for external peer review, the editor assigns at least two reviewers to the manuscript.
3. The reviewers review the manuscript.
4. The editor makes a final decision based on editorial priorities, manuscript quality, and reviewer recommendations.
5. The decision letter is sent to the author.

Contact Address

All correspondence should be directed to the Editorial Office:
Cinnah Caddesi Pilot Sokak No:10/12 06650 Çankaya / Ankara, Turkey
Phone: +90 312 441 00 45
Fax: +90 312 441 12 97
E-mail: info@tsnmjournals.org

MIRT
Molecular Imaging and Radionuclide Therapy

CONTENTS

Original Articles

Interesting Images

MIRT
Molecular Imaging and Radionuclide Therapy

CONTENTS

Original Article
Mol Imaging Radionucl Ther 2023;32:94-102 DOI:10.4274/mirt.galenos.2022.97658

Value of Dynamic ^{18}F-FDG PET/CT in Predicting the Success of Neoadjuvant Chemotherapy in Patients with Locally Advanced Breast Cancer: A Prospective Study

Lokal İleri Evre Meme Kanserli Hastalarda Neoadjuvan Kemoterapi Yanıtı Öngörüsünde Dinamik ^{18}F-FDG PET/BT'nin Değeri: Prospektif Çalışma

Osman Kupik[1], Murat Tuncel[2], Pınar Özgen Kıratlı[2], Meltem Gülsün Akpınar[3], Kadri Altundağ[4], Figen Başaran Demirkazık[3], Belkıs Erbaş[2]

[1]*Muğla Training and Research Hospital, Clinic of Nuclear Medicine, Muğla, Turkey*
[2]*Hacettepe University Faculty of Medicine, Department of Nuclear Medicine, Ankara Turkey*
[3]*Hacettepe University Faculty of Medicine, Department of Radiology, Ankara, Turkey*
[4]*MKA Breast Cancer Clinic, Ankara, Turkey*

Abstract

Objectives: This prospective study was planned to compare the predictive value of dynamic ^{18}F-fluorodeoxyglucose (FDG) positron emission tomography/computed tomography (PET/CT) in locally advanced breast cancer patients (LABC) receiving neoadjuvant chemotherapy (NAC).

Methods: Twenty seven patients with LABC [median age: 47, (26-66)] underwent a dynamic ^{18}F-FDG PET study at baseline, and after 2-3 cycles of (NAC) were included (interim). Maximum standardized uptake value (SUV_{max}) values and SUV ratios for the 2nd, 5th, 10th, and 30th minutes and dynamic curve slope (SL) values and SL ratios were measured using ^{18}F-FDG dynamic data. In addition, the values of SUV_{mean} (2minSUVmean), SULpeak (2minSULpeak), metabolic volume (2minVol), and total lesion glycolysis (2minTLG) were measured for the first 2 min. Percent changes between baseline and interim studies were calculated and compared with the pathological results as the pathological complete response (PCR) or the pathological non-complete response (non-PCR). Receiver operating characteristic curves were obtained to calculate the area under the curve to predict PCR. Optimal threshold values were calculated to discriminate between PCR and non-PCR groups.

Results: Baseline study SUV 30 (p=0.044), SUV 30/2 (p=0.041), SUV 30/5 (p=0.049), SUV 30/10 (p=0.021), SL 30/2 (p=0.029) and SL 30/5 (p=0.027) values were statistically significant different between PCR and non-PCR groups. The percentage changes of 2minVol between PCR and non-PCR groups were statistically significant. For the threshold value of -67.6% change in 2minVol, the sensitivity, specificity, positive predictive value, negative predictive value, and accuracy were 87.2%, 77.8%, 63.6%, 93.3%, and 80.7%, respectively (area under the curve: 0.826, p=0.009).

Conclusion: Semiquantitative parameters for dynamic ^{18}F-FDG PET can predict PCR. % changes in 2minVol can identify non-responding patients better than other parameters.

Keywords: Breast cancer, dynamic positron emission tomography, fluorodeoxyglucose, neoadjuvant therapy

Öz

Amaç: Bu prospektif çalışmada neoadjuvan kemoterapi (NAC) alan lokal ileri meme kanseri hastalarda (LABC) dinamik ^{18}F-florodeoksiglukoz (FDG) pozitron emisyon tomografisi/bilgisayarlı tomografinin (PET/BT), NAC yanıt öngörüsünü araştırdık.

Yöntem: LABC'li 27 hastaya [medyan yaş: 47, (26-66)] NAC öncesi ve 2-3 kür kemoterapi sonrası dinamik ^{18}F-FDG PET çalışması uyguladık. Dinamik çalışmanın 2., 5., 10 ve 30. dakikalarında maksimum standartlaştırılmış alım değeri (SUV_{maks}) değerleri, SUV oranları ile dinamik eğri eğim (SL)

Address for Correspondence: Osman Kupik MD, Muğla Training and Research Hospital, Clinic of Nuclear Medicine, Muğla, Turkey
Phone: +90 252 214 13 23 **E-mail:** osmankupik@gmail.com ORCID ID: orcid.org/0000-0001-9473-7940
Received: 29.08.2022 **Accepted:** 18.12.2022

değerleri ve SL oranları, ^{18}F-FDG dinamik verileri kullanılarak ölçüldü. Ayrıca ilk 2 dakika için SUVmean (2minSUVmean), SULpeak (2minSULpeak), metabolik volume (2minVol), and total lezyon glikoliz (2minTLG) değerlerini hesapladık. Parametrelerin tedavi öncesi ve interim çalışma arasındaki yüzde değişimlerini hesapladık ve patolojik sonuçlar [patolojik tam yanıt (PCR) olan ve olmayan (non-PCR)] ile karşılaştırdık. Parametrelerin patolojik yanıtı (PCR ve non-PCR) ayırt edebilmesi için ROC eğrisi kullanarak en uygun eşik değerleri hesapladık.

Bulgular: Tedavi öncesi SUV 30 (p=0,044), SUV 30/2 (p=0,041), SUV 30/5 (p=0,049), SUV 30/10 (p=0,021), SL 30/2 (p=0,029) ve SL 30/5 (p=0,027) değerleri PCR ve non-PCR hasta grupları arasında istatistiksel anlamlı farklı idi. Yüzde (%) değişim 2minVol, PCR ve non-PCR hasta grupları arasında istatistiksel olarak anlamlı farklılık vardı. 2minVol'deki -%67,6 değişim eşik değeri için duyarlılık %87,2, özgüllük %77,8, pozitif öngörü değeri %63,6, negatif öngörü değeri %93,3 ve doğruluk %80,7 idi (eğrinin altındaki alan: 0,826, p=0,009).

Sonuç: Dinamik ^{18}F-FDG PET parametreleri patolojik yanıtı öngörebilir. 2minVol'deki % değişiklikler, non-PCR hastaları diğer parametrelerden daha iyi belirleyebilir.

Anahtar kelimeler: Meme kanseri, dinamik pozitron emisyon tomografi, fluorodeoksiglukoz, neoadjuvan tedavi

Introduction

Neoadjuvant chemotherapy (NAC) is administered as a standard treatment for locally advanced breast cancer. Some of the main goals of NAC are to increase the rate of breast-conserving surgery and to predict the prognosis by monitoring the response of the tumor to treatment (1,2). The pathological complete response (PCR) in breast cancer patients receiving NAC is an important indicator of disease-free and overall survival (3,4).

Response to NAC is essential to be predicted at an early stage. Because in patients who do not respond to NAC it may be possible to change ineffective chemotherapy to minimize its toxic effects and prevent unnecessary costs. Successful results have been obtained in predicting the response to NAC with ^{18}F-fluorodeoxyglucose (FDG) positron emission tomography/computed tomography (PET/CT), which evaluates the metabolic activity of the tumor (5).

Obtaining dynamic data with ^{18}F-FDG enables a more detailed quantitative analysis of ^{18}F-FDG kinetics. Classically, a dynamic study requires recording 60 minute serial images and quantitatively evaluating the obtained data using a 2-compartment analysis. Various studies have shown that dynamic analysis is superior to semiquantitative analysis, with only standardized uptake values (SUV) in the diagnostic evaluation of the tumor and the follow-up of the response to treatment (6). Dynamic studies with ^{18}F-FDG have become uptodate again in recent years. Publications are increasingly applying clinical studies in a shorter time and with different analysis methods (7,8,9,10).

This prospective study investigated the success of baseline and interim dynamic PET parameters and percentage changes between them in predicting NAC response in patients with locally advanced breast cancer (LABC).

Materials and Methods

Study Cohort

We included 41 patients [median age: 47 years old, (26-66)] diagnosed with LABC and planned to receive NAC. Ethics Committee approval was obtained from Hacettepe University Faculty of Medicine (approval no: GO 13/45-29). We included patients with stage IIB, IIIA, IIIB, or IIIC according to the staging criteria of the American Joint Committee on Cancer 7th edition (11) without distant metastases and with ^{18}F-FDG uptake by a primary tumor in baseline imaging. Written informed consent forms were obtained from the patients who agreed to participate in the study. We did not include uncooperative patients or patients with uncontrolled diabetes mellitus. In addition, we excluded patients with dose infiltration and suboptimal image quality. Breast cancer diagnosis in all patients was confirmed histopathologically from biopsy materials. Estrogen, progesterone, and HER2 receptor determination were evaluated immunohistochemically. We grouped the patients as those with PCR or pathological non-complete response (non-PCR) according to the results of the histopathological evaluation. Patients were scanned with ^{18}F-FDG PET/CT before treatment (baseline), after 2-3 cycles of NAC (interim), and after the end of treatment, before surgery.

Imaging Protocol: Patients laid comfortably in the prone position with arms raised and breasts droop. A unique breast coil produced for this study was used. Attention was paid to fast for a minimum of 6 h before imaging and a maximum blood glucose 170 mg/dL during the injection. Dynamic images were obtained in a single bed position, including the primary tumor and the axilla, starting immediately after ^{18}F-FDG injection from the arm on the opposite side of the breast tumor or lower extremity. Dynamic phase images were recorded for 32 min, including ten frames of 30 min, five frames of 1 min, five frames of 2 min each, and four frames of 3 min (12). Iterative image processing was applied to the images (2 iterations, 21 subsets). CT images were obtained using a 4-slice device (140 kV, 80 mA), and attenuation correction was made with CT slices.

Data Analysis: Two nuclear medicine physicians with more than 20 years of expertize and a research assistant

performed the images at the AW-46 workstation. We evaluated the obtained dynamic images using the "DynamicVue" program on the Advantage workstation (GE Healthcare, USA). We obtained time-activity curves by plotting areas of interest on the lesion, symmetrical breast tissue, and aorta in the plane where the primary lesion is most prominent (Figure 1).

We first evaluated the curves visually. For semiquantitative evaluation, we measured SUV_{max} values (SUVmax2, SUVmax5, SUVmax10, SUVmax30) for the 2nd, 5th, 10th, and 30th minutes (Figure 2).

The slope (SL) values of the time-activity curves were calculated separately for the 0-2, 0-5, 0-10, and 0-30 minutes time periods of the obtained curves (SL2, SL5, SL10, SL30).

In addition, SUV_{mean} (2minSUV), SULpeak (2minSULpeak), volume (2minVol), and total glycolytic index (2minTLG) values were calculated by combining images taken between 0 and 2 min.

The percentage change of all measured numerical parameters after 2-3 cycles was c alculated according to the following formula [% change = (value after chemotherapy - baseline value) / baseline value x 100].

Statistical Analysis

The conformity of the variables to the normal distribution was examined with the Kolmogorov-Smirnov test. Continuous variables were expressed as median (minimum-maximum) and mean with standard deviation. Chi-square, Fisher's Exact, t-test, or Mann-Whitney U tests were used, depending on the analysis of NAC response with univariate analyses. The diagnostic decision-making properties of the calculated parameters in predicting the surgical response were analyzed by Receiver operating characteristic curve (ROC) analysis. The sensitivity, specificity, positive and negative predictive values, and accuracy were calculated in the presence of significant threshold values. P values <0.05 was considered statistically significant. Statistical analysis were performed using SPSS 18.

Results

Study Cohort: We performed baseline imaging in 29 patients and interim imaging in 41 patients and analyzed 27 patients [median age: 47, (26-66)] with baseline and interim imaging. The histopathological diagnosis of 22 patients was invasive ductal carcinoma, and five was mixed type (ductal + lobular) invasive carcinomas. While the primary tumor was unifocal in 23 patients, it was multicentric/multifocal in 4. Tumor size ranged from 16 to 96 mm (median: 44 mm). One patient had T1, 12 patients had T2, 12 patients had T3 and two had T4 tumors. The tumors of 13 patients were grade 2, while 14 was grade 3. Eighteen patients were in the hormone receptor-positive group, 4 in the TN group, and 5 in the HER2+ group. Ten patients were postmenopausal and 17 were premenopausal. There was no difference in the distribution between the groups according to receptor and menopausal status. The clinical information of the patients is given in Table 1.

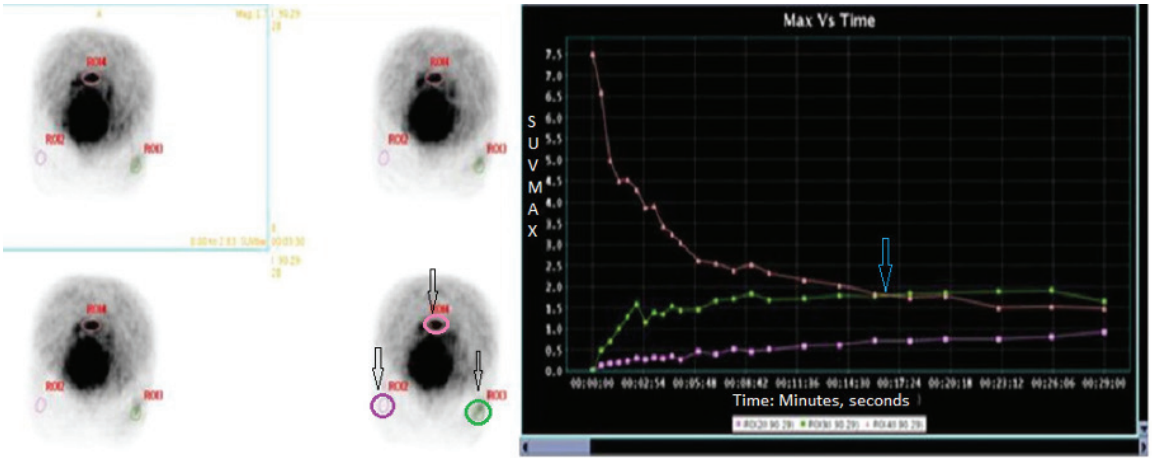

Figure 1. Time-activity curves. Right breast IDC, grade 2 tumor, 63 years-old patient. Patient was on the prone position. A green ROI was drawn to the right breast tumor, a purple ROI to the contralateral breast tissue, and a pink ROI to the aorta. Arrows indicate all three ROIs. The SUV_{max}-time graph is shown on the right. The SUV_{max}-time curve of each ROI is shown in the same color. While the contralateral breast tissue draws a low-slope SUV-time curve at the end of 29 minutes (purple curve), the tumor shows a significant SUV-time increase compared to normal tissue (green curve). While the SUV value in the aorta is initially high, it decreases rapidly over time (pink curve). At approximately 16 minutes, the aorta and tumor curves intersect (blue arrow)

IDC: Invasive ductal carcinoma, mixt, invasive ductal and lobular carcinoma, ROI: Region of interest, SUV_{max}: Maximum standardized uptake value

Surgical Response Assessment: One patient did not want to be operated on after NAC, and the remaining 26 patients underwent modified radical mastectomy. PCR was detected in 8 patients. In the remaining 18 patients, residual tumors ranging from 10 to 70 mm (median: 30 mm) were observed.

Neoadjuvant Chemotherapy Regimen: The chemotherapy regimen included four cycles of adriamycin and cyclophosphamide every 21 days, followed by weekly paclitaxel for 12 weeks. Patients with HER2+ breast cancer also received concomitant weekly trastuzumab with paclitaxel.

Baseline Study: SUV2, SUV5, SUV10, and SUV30 tumor and contralateral breast tissue values increased significantly (p=0.0001) (Figure 3). Tumor/contralateral breast SUV ratios did not change significantly over time. Figure 4 shows tumor and contralateral breast tissue dynamic SUV values and tumor/contralateral breast tissue SUV ratios

Response to Neoadjuvant Chemotherapy

SUV Values (2, 5, 10, and 30 minutes): We calculated the percentage changes in SUV values in 26 patients with complete baseline and interim data. Eight of 26 patients had a PCR, and 18 had a residual tumor. We did not find a statistically significant difference in baseline and interim study SUV values between the PCR and non-PCR groups. In addition, there was no statistically significant difference in the percentage change of SUV values. Only the baseline study SUV30 differed significantly between the groups (p=0.44). The baseline SUV30 value was higher in the PCR group (Table 2).

SUV Ratios: Baseline and interim ratio values were statistically different (p<0.001). There was a statistically significant difference in baseline SUV 30/2, 30/5, and 30/10 values between groups with and without PCR (p=0.041, 0.049, 0.021, respectively). SUV rates were higher in the PCR group (Table 3).

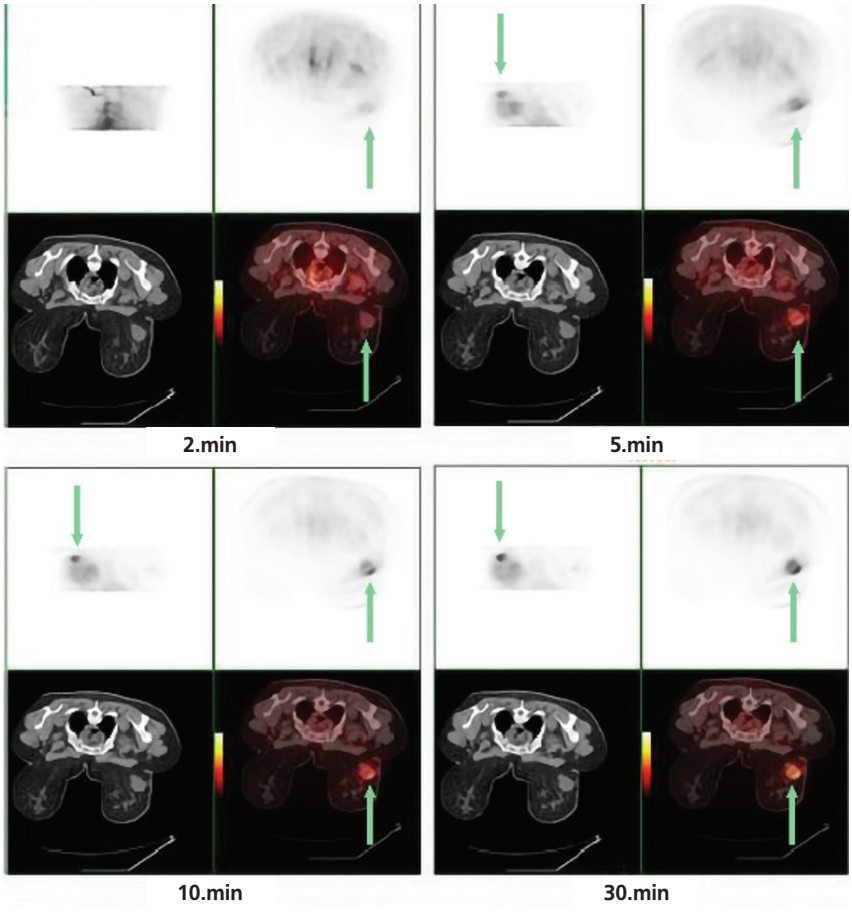

Figure 2. Right breast IDC grade 3 tumor, 56 years-old patient. Images at the 2^{nd,} 5th, 1^{0th} and 30th minutes were obtained using data acquired in the dynamic phase. Arrows indicate the same tumor
IDC: Invasive ductal carcinoma, mixt, invasive ductal and lobular carcinoma

Table 1. Patients characteristics

Patient no	Age	Histology	Tumor grade	ER	PR	HER-2	Menopause status	T	N	Tumor focality
1	43	IDC	2	+	+	-	Pre	2	1	Multifocal
2	49	IDC	2	+	+	-	Post	2	1	Unifocal
3	66	IDC	2	+	+	-	Post	2	1	Unifocal
4	32	IDC	2	+	-	-	Pre	3	1	Unifocal
5	48	Mixt	3	+	+	-	Pre	2	0	Unifocal
6	65	IDC	3	+	+	-	Post	2	1	Unifocal
7	66	IDC	2	+	+	-	Post	2	0	Unifocal
8	47	Mixt	2	+	+	-	Pre	3	3	Unifocal
9	56	IDC	3	-	-	-	Post	3	2	Unifocal
10	56	Mixt	2	+	+	-	Post	3	3	Multifocal
11	36	IDC	2	+	-	-	Pre	2	1	Unifocal
12	32	Mixt	3	-	-	-	Pre	3	3	Unifocal
13	48	IDC	3	-	-	-	Post	1b	2	Multifocal
14	32	IDC	2	+	-	+	Pre	3	1	Unifocal
15	63	IDC	3	+	+	-	Post	2	1	Unifocal
16	44	Mixt	2	-	-	+	Pre	3	3	Unifocal
17	33	IDC	3	+	+	-	Pre	3	1	Unifocal
18	40	IDC	2	+	+	-	Pre	2	1	Unifocal
19	46	IDC	3	+	+	-	Pre	3	1	Unifocal
20	28	IDC	2	-	-	+	Pre	3	1	Multifocal
21	41	IDC	2	+	+	-	Pre	3	3	Unifocal
22	56	IDC	3	-	-	+	Post	2	0	Unifocal
23	52	IDC	3	-	-	+	Pre	4	1	Unifocal
24	39	IDC	3	+	+	-	Pre	3	3	Unifocal
25	26	IDC	3	-	-	-	Pre	2	3	Unifocal
26	37	IDC	3	-	-	+	Pre	4	2	Unifocal
27	54	IDC	3	-	-	+	Post	2	2	Unifocal

ER: Estrogen receptor, PR: Progesterone receptor, HER-2: Human epidermal growth factor receptor 2, IDC: Invasive ductal carcinoma, mixt, invasive ductal and lobular carcinoma

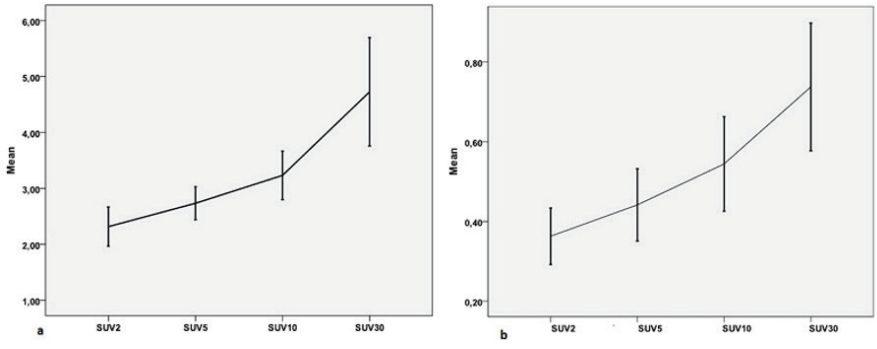

Figure 3. Increase in tumor (a) and contralateral breast tissue (b) SUV values over time in the baseline study
SUV: Maximum standardized uptake value

Dynamic Curve Slope Values: From the second minute to the 30th minute, tumor SL values showed a statistically significant decrease (p<0.001). There was no statistically significant difference in tumor SL values between groups with and without PCR (Table 4).

Slope Ratios: Baseline and interim SL ratios were statistically different (p<0.001). Baseline study SL 30/2 and SL 30/5 values significantly differed between the PCR and non-PCR groups (p=0.029 and 0.027, respectively). The values were higher in the PCR group (Table 5).

0-2 Minutes Values: 2minSUVmean, 2minSUVpeak, 2minTLG, and 2minVol values obtained from the 2nd minute of dynamic data were statistically different in baseline and interim study (p<0.001). Only percentage change 2minVol was statistically different between the PCR and non-PCR groups (p=0.009). The percentage change 2minVol values were higher in the non-PCR group (-84.8% vs. -52.55%) (Table 6).

We performed ROC analysis prediction of 2 minVol for PCR (area under the curve: 0.826, p=0.009). For the threshold value of -67.6% change, the sensitivity, specificity, positive predictive value, negative predictive value, and accuracy were 87.2%, 77.8%, 63.6%, 93.3%, and 80.7%, respectively.

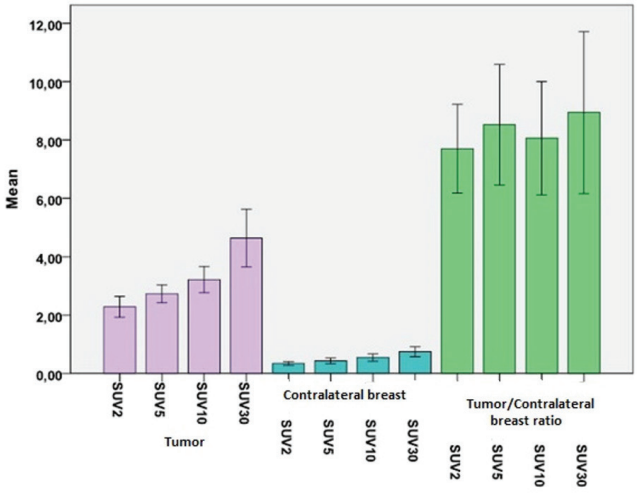

Figure 4. Tumor and contralateral breast tissue SUV values and tumor/contralateral SUV ratios
SUV: Maximum standardized uptake value

Discussion

This study investigated dynamic ^{18}F-FDG parameters predicting NAC response in patients with LABC. In dynamic imaging, ^{18}F-FDG uptake of tumor and normal breast tissue increased with time. While the SUV value in the tumor tissue was 2 on average in the 2nd minute, it increased to 5 in a short time. It was observed that the SUV value in normal breast tissue increased from 0.4 to around 0.8 within 30 min. Thus, in 30 min, tumor tissue shows ^{18}-FDG uptake at a rate of 6-10 times compared to normal tissue. Only a few groups are working on the dynamic study of breast cancer and prediction of NAC response, and generally with small patient groups (8,13,14,15).

A study comparing dynamic ^{18}F-FDG PET/CT with standard whole-body ^{18}F-FDG PET/CT in predicting response to NAC showed that K1 and Ki values were more accurate than SUV values and were associated with overall survival and disease-free survival (8). In multivariate analysis, K1 was the only independent predictor of survival. Thus, the dynamic study was more advantageous than the standard

Table 2. Baseline and interim study SUV values, % changes, and their relation with pathological complete response

Parameter	Imaging	All patients	PCR	non-PCR	p
SUV2min	Baseline	2.37 (0.50, 4.53)	2.195 (0.96, 4.53)	2.47 (1.04, 3.90)	NS
	Interim	0.80 (0.1, 4.27)	0.77 (0.1, 3.32)	0.98 (0.14, 3.88)	NS
	Change %	-46.19 (-93.01, 53.22)	-58.22 (-86.37, -26.74)	-45.67 (-93.01, 53.22)	NS
SUV5min	Baseline	2.85 (1.03, 3.92)	3.085 (1.48, 3.89)	2.57 (1.48, 3.92)	NS
	Interim	1.31 (0.22, 4.04)	1.11 (0.23, 3.23)	1.41 (0.22, 4.04)	NS
	Change %	-51.95 (-84.09, 38.74)	-62.14 (-84.09, -11.03)	-41.25 (-82.88, 38.74)	NS
SUV10min	Baseline	3.28 (1.27, 6.54)	3.54 (1.82, 6.54)	-41.25 (-82.88, 38.74)	NS
	Interim	1.61 (0.39, 5.15)	1.41 (0.47, 3.19)	2.82 (1.67, 5.0)	NS
	Change %	-47.02 (-88.48, 38.59)	-50.88 (-88.48, 3.84)	1.64 (0.39, 5.15)	NS
SUV30min	Baseline	4.19 (1.39, 12.20)	6.03 (2.92, 12.2)	3.78 (2.05, 8.45)	0.044
	Interim	1.97 (0.86, 6.37)	1.63 (0.86, 5.35)	2.01 (0.86, 6.37)	NS
	Change %	-43.28 (-88.57, 10.69)	-59.81 (-88.57, -22.65)	-40.28 (-69.04, 10.69)	NS

NS: Statistically non-significant, PCR: Pathological complete response, SUV: Standardized uptake value

Table 3. Baseline and interim study SUV ratio values and relationship with pathological complete response					
Parameter	**Imaging**	**All patients**	**PCR**	**non-PCR**	**p**
SUV30/2min	Baseline	1.98 (0.79, 6.57)	2.93 (1.15, 6.57)	1.94 (0.79, 5.09)	**0.041**
	Interim	2.21 (0.90, 8.45)	3 (0.90, 8.45)	2.120 (0.93, 6.12)	NS
SUV30/5min	Baseline	1.41 (0.81, 3.19)	2.05 (1.14, 3.19)	1.35 (0.99, 2.74)	**0.049**
	Interim	1.570 (0.92, 4.0)	1.790 (0.92, 3.68)	1.515 (0.97, 4)	NS
SUV30/10min	Baseline	1.34 (0.84, 2.0)	1.65 (1.11, 20)	1.27 (0.84, 1.90)	**0.021**
	Interim	1.19 (0.88, 2.36)	1.19 (0.88, 2.36)	1.205 (0.98, 2.22)	NS
NS: Statistically non-significant, PCR: Pathological complete response, SUV: Standardized uptake value					

Table 4. Baseline and interim study slope values. Relationship with the pathological complete response					
Parameter	**Imaging**	**All patients**	**PCR**	**non-PCR**	**p**
Slope 2min	Baseline	0.0173 (0.0042, 0.214)	0.0158 (0.0074, 0.034)	0.0186 (0.0075, 0.214)	NS
	Interim	0.0068 (0.0008, 0.0329)	0.0058 (0.0008, 0.0158)	0.0078 (0.0010, 0.0270)	NS
Slope 5min	Baseline	0.0069 (0.0018, 0.0125)	0.0068 (0.0039, 0.0119)	0.0072 (0.0018, 0.0125)	NS
	Interim	0.0040 (0.0006, 0.008)	0.0034 (0.0008, 0.0059)	0.0042 (0.0006, 0.008)	NS
Slope 10min	Baseline	0.0034 (0, 0.0096)	0.0033 (0.002, 0.0096)	0.0034 (0, 0.0065)	NS
	Interim	0.0019 (0.0004, 0.005)	0.0014 (0.0007, 0.0037)	0.002 (0.0004, 0.005)	NS
Slope 30min	Baseline	0.0013 (-0.0001, 0.0065)	0.0025 (0.0006, 0.0065)	0.0012 (-0.0001, 0.0039)	NS
	Interim	0.0007 (-0.0003, 0.006)	0.0007 (0, 0.0024)	0.0012 (-0.0001, 0.0039)	NS
NS: Statistically non-significant, PCR: Pathological complete response					

Table 5. Baseline and interim study slope ratio values. Relationship with the pathological complete response					
Parameter	**Imaging**	**All patients**	**PCR**	**non-PCR**	**p**
Slope 30/2min	Baseline	0.1 (-0.01, 0.42)	0.19 (0.03, 0.42)	0.09 (0, 0.30)	0.029
	Interim	0.12 (-0.01, 0.98)	0.19 (0.3, 0.75)	0.115 (-0.1, 0.98)	NS
Slope 30/5min	Baseline	0.21 (0.04, 0.55)	0.47 (0.11, 0.55)	0.19 (0.04, 0.44)	0.027
	Interim	0.25 (-0.05, 2.14)	0.29 (0, 0.75)	0.235 (-0.5, 2.1)	NS
Slope 30/10min	Baseline	0.48 (0.15, 0.83)	0.675 (0.27, 0.78)	0.42 (0.15, 0.83)	NS
	Interim	0.42 (-0.25, 3.0)	0.43 (0.02, 0.86)	0.42 (-0.25, -3)	NS
NS: Statistically non-significant, PCR: Pathological complete response					

whole-body ^{18}F-FDG PET/CT study in predicting the surgical response and prognosis. In their comparative study with 15 H_2O and ^{18}F-FDG PET/CT, the same study group showed that blood flow measured directly with 15 H_2O was correlated with K1 values measured with ^{18}F-FDG, and that K1 values were a parameter that indirectly showed blood flow (14). FDGK1 reflects glucose transport from blood to tissue and FDGKi is a flow constantly. It is assumed that ^{18}F-FDG is transported from blood to tissue at a linear transfer rate of K1 relative to blood flow. K1, a measure of capillary permeability and perfusion, has been shown to have a prognostic value in cancer therapy. A dynamic PET study in patients with soft tissue sarcoma also found a strong relationship between SUV obtained between 1.5 and 2.5 min and K1 values (r=0.79, p<0.05) (16). In a study on lung cancer, it was shown that there is a strong correlation (r=0.83, p=0001) between K1 values obtained with dynamic ^{18}F-FDG PET and early phase imaging (0-2 minutes) (17).

In our study, the perfusion parameters (2minSUV, 2minSULpeak, 2minTLG, and 2minVol) were obtained from the first 2 min images, which were created assuming that the perfusion of the tumor showed a significant decrease in response to NAC. In a study comparing contrast-enhanced dynamic MRI with dynamic ^{18}F-FDG PET/CT, the change in K1 and Ki values, the enhancement peak showing vascularity in MRI, and the change in tumor volume were compared. They found a higher rate of change in

Table 6. Pathological complete response relationship of parameters obtained from images between 0-2 minutes, and their percentage changes

Parameter	Imaging	All patients	PCR	non-PCR	p
2minSUV	Baseline	0.86 (0.16, 1.80)	1.08 (0.44, 1.8)	0.94 (0.29, 1.68)	NS
	Interim	0.32 (0, 2.08)	0.33 (0, 2.08)	0.31 (0, 1.66)	NS
2minVol	Baseline	21.27 (3.52, 151)	24.88 (4.5, 100)	17.45 (4.4, 151.0)	NS
	Interim	3.33 (0, 73.05)	1.96 (0, 21.91)	3.42 (0, 34.72)	NS
	Change %	-66.3 (-100, -22.3)	-84.8 (-100,-63.8)	-52.55 (-100, -22.3)	**0.009**
2minTLG	Baseline	17.75 0.56,226.5)	22.55 (2.88, 180)	16.35 (1.54, 226.5)	NS
	Interim	1.32 (0, 8.3)	0.55 (0, 45.6)	1.63 (0, 42.8)	NS
	Change %	-82.1 (-100, 6.5)	-95.2 (-100,-74.7)	-78.45 (-100, 6.5)	NS
2minSULpeak	Baseline	0.74 (0.1, 1.89)	0.93 (0.50, 1.89)	0.66 (0.32, 1.83)	NS
	Interim	0.24 (0, 1.86)	0.24 (0, 0.98)	0.25 (0, 1.86)	NS
	Change %	-67.9 (-100, 45.3)	-74.75 (-100, -18.3)	-64.45 (-100, 45.3)	NS

NS: Statistically non-significant, PCR: Pathological complete response, SUV: Standardized uptake value, TLG: Total lesion glycolysis

patients who fully responded to treatment (15). A two-compartment analysis of ^{18}F-FDG yields five constants: Four transport rates (k1, k2, k3, k4) describe the exchange of tracer between blood and tissue. In the case of ^{18}F-FDG, k1 reflects the influx, k2 the efflux, k3 the phosphorylation rate, and k4 the dephosphorylation rate of the glucose analog. Ki= (k1xk3/k2+k3). Through these, the metabolic rate can be quantitatively measured. However, since this process requires time and a unique computer program, we calculated the SL values of time-activity curves, which are practical for routine studies. A group working on dynamic ^{18}F-FDG studies used the SL and intercepted values obtained by linear regression analysis applied to time-activity curves as parametric images (18).

It is stated that the SL values reflect the trapping function of ^{18}F-FDG. Based on this information, we calculated the SL values in different periods of the 30-min dynamic study. While the SL values were high in the early periods, they decreased in tumor and normal breast tissue over time. At the same time, the SL values did not differ between the groups in predicting the NAC response. The values of baseline SL ratios SL30/2 and SL30/5 were higher in the PCR group.

Study Limitations

K1 and Ki values could be calculated by evaluating the kinetic analysis of dynamic studies through a special program. However, the program was not available on our workstation. A separate statistical evaluation according to receptor subgroups could not be made due to the small number of patients.

Conclusion

In conclusion, dynamic imaging is a component that can be used in specific patient groups and can be easily added to standard imaging. Semiquantitative parameters for dynamic ^{18}F-FDG can predict the response to NAC. Percentage changes in 2 minVol can identify non-responding patients.

Ethics

Ethics Committee Approval: Ethics Committee approval was obtained from Hacettepe University Faculty of Medicine (approval no: GO 13/45-29).

Informed Consent: Written informed consent forms were obtained from the patients who agreed to participate in the study.

Peer-review: Externally and internally peer-reviewed.

Authorship Contributions

Concept: O.K., M.T., P.Ö.K., M.G.A., K.A., F.B.D., B.E., Design: O.K., M.T., M.G.A., K.A., F.B.D., B.E., Data Collection or Processing: O.K., M.T., P.Ö.K., M.G.A., K.A., F.B.D., B.E., Analysis or Interpretation: O.K., B.E., Literature Search: O.K., B.E., Writing: O.K., B.E.

Conflict of Interest: No conflict of interest was declared by the authors.

Financial Disclosure: The authors declared that this study has received no financial support.

References

1. Wolff AC, Davidson NE. Primary systemic therapy in operable breast cancer. J Clin Oncol 2000;18:1558-1569.
2. Rastogi P, Anderson SJ, Bear HD, Geyer CE, Kahlenberg MS, Robidoux A, Margolese RG, Hoehn JL, Vogel VG, Dakhil SR, Tamkus D, King KM, Pajon ER, Wright MJ, Robert J, Paik S, Mamounas EP, Wolmark N. Preoperative

chemotherapy: updates of National Surgical Adjuvant Breast and Bowel Project Protocols B-18 and B-27. J Clin Oncol 2008;26:778-785.

3. Kuerer HM, Newman LA, Smith TL, Ames FC, Hunt KK, Dhingra K, Theriault RL, Singh G, Binkley SM, Sneige N, Buchholz TA, Ross MI, McNeese MD, Buzdar AU, Hortobagyi GN, Singletary SE. Clinical course of breast cancer patients with complete pathologic primary tumor and axillary lymph node response to doxorubicin-based neoadjuvant chemotherapy. J Clin Oncol 1999;17:460-469.
4. Buzdar AU, Ibrahim NK, Francis D, Booser DJ, Thomas ES, Theriault RL, Pusztai L, Green MC, Arun BK, Giordano SH, Cristofanilli M, Frye DK, Smith TL, Hunt KK, Singletary SE, Sahin AA, Ewer MS, Buchholz TA, Berry D, Hortobagyi GN. Significantly higher pathologic complete remission rate after neoadjuvant therapy with trastuzumab, paclitaxel, and epirubicin chemotherapy: results of a randomized trial in human epidermal growth factor receptor 2-positive operable breast cancer. J Clin Oncol 2005;23:3676-3685.
5. Tian F, Shen G, Deng Y, Diao W, Jia Z. The accuracy of 18F-FDG PET/CT in predicting the pathological response to neoadjuvant chemotherapy in patients with breast cancer: a meta-analysis and systematic review. Eur Radiol 2017;27:4786-4796.
6. Dimitrakopoulou-Strauss A, Strauss LG, Egerer G, Vasamiliette J, Mechtersheimer G, Schmitt T, Lehner B, Haberkorn U, Stroebel P, Kasper B. Impact of dynamic 18F-FDG PET on the early prediction of therapy outcome in patients with high-risk soft-tissue sarcomas after neoadjuvant chemotherapy: a feasibility study. J Nucl Med 2010;51:551-558.
7. Strauss LG, Pan L, Cheng C, Haberkorn U, Dimitrakopoulou-Strauss A. Shortened acquisition protocols for the quantitative assessment of the 2-tissue-compartment model using dynamic PET/CT 18F-FDG studies. J Nucl Med 2011;52:379-385.
8. unnwald LK, Doot RK, Specht JM, Gralow JR, Ellis GK, Livingston RB, Linden HM, Gadi VK, Kurland BF, Schubert EK, Muzi M, Mankoff DA. PET tumor metabolism in locally advanced breast cancer patients undergoing neoadjuvant chemotherapy: value of static versus kinetic measures of fluorodeoxyglucose uptake. Clin Cancer Res 2011;17:2400-2409.
9. Payan N, Presles B, Brunotte F, Coutant C, Desmoulins I, Vrigneaud JM, Cochet A. Biological correlates of tumor perfusion and its heterogeneity in newly diagnosed breast cancer using dynamic first-pass 18F-FDG PET/CT. Eur J Nucl Med Mol Imaging 2020;47:1103-1115.
10. Kajáry K, Lengyel Z, Tőkés AM, Kulka J, Dank M, Tőkés T. Dynamic FDG-PET/CT in the initial staging of primary breast cancer: clinicopathological correlations. Pathol Oncol Res 2020;26:997-1006.
11. Edge SB, Compton CC. The American Joint Committee on Cancer: the 7th edition of the AJCC cancer staging manual and the future of TNM. Ann Surg Oncol 2010;17:1471-1474.
12. Strauss LG, Koczan D, Klippel S, Pan L, Willis S, Sachpekidis C, Dimitrakopoulou-Strauss A. Dynamic PET with (18)F-Deoxyglucose (FDG) and quantitative assessment with a two-tissue compartment model reflect the activity of glucose transporters and hexokinases in patients with colorectal tumors. Am J Nucl Med Mol Imaging 2013;3:417-424.
13. Specht JM, Kurland BF, Montgomery SK, Dunnwald LK, Doot RK, Gralow JR, Ellis GK, Linden HM, Livingston RB, Allison KH, Schubert EK, Mankoff DA. Tumor metabolism and blood flow as assessed by positron emission tomography varies by tumor subtype in locally advanced breast cancer. Clin Cancer Res 2010;16:2803-2810.
14. Dunnwald LK, Gralow JR, Ellis GK, Livingston RB, Linden HM, Specht JM, Doot RK, Lawton TJ, Barlow WE, Kurland BF, Schubert EK, Mankoff DA. Tumor metabolism and blood flow changes by positron emission tomography: relation to survival in patients treated with neoadjuvant chemotherapy for locally advanced breast cancer. J Clin Oncol 2008;26:4449-4457.
15. Partridge SC, Vanantwerp RK, Doot RK, Chai X, Kurland BF, Eby PR, Specht JM, Dunnwald LK, Schubert EK, Lehman CD, Mankoff DA. Association between serial dynamic contrast-enhanced MRI and dynamic 18F-FDG PET measures in patients undergoing neoadjuvant chemotherapy for locally advanced breast cancer. J Magn Reson Imaging 2010;32:1124-1131.
16. Rusten E, Rødal J, Revheim ME, Skretting A, Bruland OS, Malinen E. Quantitative dynamic ^{18}FDG-PET and tracer kinetic analysis of soft tissue sarcomas. Acta Oncol 2013;52:1160-1167.
17. Tuncel M, Kupik O, Kiratli P, Erbas B. Practical measures of dynamic 18 FDG time-activiy curves. Eur J Nucl Med Mol Imaging. 2015(Suppl 1):375.
18. Dimitrakopoulou-Strauss A, Pan L, Strauss LG. Quantitative approaches of dynamic FDG-PET and PET/CT studies (dPET/CT) for the evaluation of oncological patients. Cancer Imaging 2012;12:283-289.

Original Article
Mol Imaging Radionucl Ther 2023;32:103-111 DOI:10.4274/mirt.galenos.2022.36097

The Evaluation of Sentinel Lymph Node Biopsy Using Radiocolloid in First Stage Endometrial Cancer

Birinci Evre Endometrial Kanserde Radyokolloid Kullanılarak Yapılan Sentinel Lenf Nodu Biyopsisinin Değerlendirilmesi

Anamarija Jankulovska[1], Sinisha Stojanoski[1], Sasho Stojcevski[2], Igor Aluloski[2], Rubens Jovanovic[3], Slavica Kostadinova Kunovska[3], Mile Tanturovski[2], Nevena Manevska[1], Gordana Petrusevska[3], Daniela Miladinova[1]

[1]University of "Ss. Cyril and Methodius" Faculty of Medicine, Institute of Pathophysiology and Nuclear Medicine, Skopje, Republic of North Macedonia
[2]University Clinic for Obstetrics and Gynecology, Skopje, Republic of North Macedonia
[3]University of "Ss. Cyril and Methodius" Faculty of Medicine, Department of Pathology, Skopje, Republic of North Macedonia

Abstract

Objectives: Detection of a sentinel lymph node (SLN) in patients with endometrial cancer (EC) reduces the rate of unnecessary systemic lymph dissection. The aim of this study was to assess the SLN detection rate, accuracy of the method using Tc-99m-SENTI-SCINT and the rate of metastatic nodal involvement in patients with preoperative first stage EC.

Methods: A prospective study of SLN biopsy of 41 patients with stage I EC was conducted after cervical application of 4mCi Tc-99m-SENTI-SCINT. Planar lymphoscintigraphy and single-photon emission computed tomography/computed tomography (SPECT/CT) of the pelvis were performed, followed by site-specific lymphadenectomy in intermediate-risk patients if no SLN was detected per hemipelvis and pelvic lymphadenectomy in all high-risk patients.

Results: Pre-operative detection rate of planar lymphoscintigraphy was 80.49 [95% confidence interval (CI): 68.36-92.62] and of SPECT/CT 95.12 (95% CI: 88.52-101.7). The total intraoperative SLN detection rate was 95.12 (95% CI: 88.52-101.7) per patient and 26.83 (95% CI: 19.91-33.75) bilaterally. The average number of SLNs removed was 1.6±0.8. The most common anatomical location of SLN was the right external iliac region. The SLN metastatic rate was 17%. Both sensitivity and negative predictive value regarding metastatic involvement were 100%.

Conclusion: The SLN detection rate, sensitivity and negative predictive value using Tc-99m-SENTI-SCINT in patients with EC in our study were high. The application of ultra-staging in the histopathological analysis of SLN increases the detection of nodal metastases and improves the staging in these patients.

Keywords: Endometrial carcinoma, sentinel lymph node, ultra-staging, SPECT/CT

Öz

Amaç: Endometriyal kanserli (EK) hastalarda sentinel lenf nodu (SLN) saptanması gereksiz sistemik lenf diseksiyonu oranını azaltır. Bu çalışmanın amacı, preoperatif birinci evre EK'li hastalarda SLN saptama oranını, Tc-99m-SENTI-SCINT kullanılan yöntemin doğruluğunu ve metastatik nodal tutulum oranını değerlendirmekti.

Yöntem: 4mCi Tc-99m-SENTI-SCINT'nin servikal uygulamasından sonra evre I EK'li 41 hastanın SLN biyopsisini içeren prospektif bir çalışma yapıldı. Pelvisin planar lenfosintigrafisi ve tek foton emisyonlu bilgisayarlı tomografisi/bilgisayarlı tomografisi (SPECT/BT) çekildi, ardından hemipelvis başına SLN saptanmadıysa orta riskli hastalarda bölgeye özgü lenfadenektomi ve tüm yüksek riskli hastalarda pelvik lenfadenektomi uygulandı.

Address for Correspondence: Anamarija Jankulovska MD, University of "Ss. Cyril and Methodius" Faculty of Medicine, Institute of Pathophysiology and Nuclear Medicine, Skopje, Republic of North Macedonia
Phone: +023112831 **E-mail:** anamarija.jovanovska90@gmail.com ORCID ID: orcid.org/0000-0002-7261-5915
Received: 25.05.2022 **Accepted:** 25.08.2022

Bulgular: Planar lenfosintigrafinin ameliyat öncesi saptama oranı 80,49 iken [%95 güven aralığı (GA): 68,36-92,62] SPECT/BT'nin saptama oranı 95,12 (%95 GA: 88,52-101,7) idi. Toplam intraoperatif SLN saptama oranı hasta başına 95,12 (%95 GA: 88,52-101,7) ve bilateral olarak 26,83 (%95 GA: 19,91-33,75) idi. Çıkarılan ortalama SLN sayısı 1,6±0,8 idi. SLN'nin en yaygın anatomik yerleşim yeri sağ eksternal iliak bölge idi. SLN metastatik oranı %17 idi. Metastatik tutulumla ilgili hem duyarlılık hem de negatif öngörü değeri %100 idi.

Sonuç: Çalışmamızda EK'li hastalarda Tc-99m-SENTI-SCINT kullanılarak SLN saptama oranının ve Tc-99m-SENTI-SCINT'nin duyarlılığının ve negatif prediktif değerinin yüksek olduğu gösterildi. Ultra evrelemenin SLN'nin histopatolojik analizinde uygulanması nodal metastazların saptanmasını arttırır ve bu hastalarda evrelemeyi geliştirir.

Anahtar kelimeler: Endometriyal karsinom, sentinel lenf nodu, ultra evreleme, SPECT/BT

Introduction

Endometrial carcinoma (EC) is the sixth most common cancer among women worldwide, with 417,367 new cases registered in 2020 (1). The surgical treatment includes hysterectomy with adnexectomy for histopathological analysis of the tumor, further with pelvic lymphadenectomy, with or without para-aortic lymphadenectomy, for nodal staging (2). Radical lymphadenectomy in EC is a current topic of a debate and is very controversial, on one hand due to lack of impact on the overall survival and recurrence of the disease, while on the other could lead to frequent complications such as lymphedema/lymphocyst, pelvic infections, nerve injury, and/or deep vein thrombosis (3,4).

To improve the quality of EC treatment in 2020, the existing guidelines have been updated and new recommendations have been established in terms of patient management. Sentinel lymph node (SLN) biopsy has been proposed as a viable alternative to conventional lymphadenectomy to evaluate the nodal status in tumor stage I/II (5). The SLN, as first described by Gould et al. (6), is the first drainage lymph node of the tumor area and thus has the highest probability to be the carrier of metastatic cells. Therefore, if the SLN is negative for metastatic disease, it is assumed that all lymph nodes in the same lymph pathway are also free of metastasis. This concept of SLN removal in EC patients would provide an adequate approach between sub-treatment (no lymphadenectomy) and over-treatment (radical lymphadenectomy) with a significant risk of complications.

The cervical application of Tc-99m labeled colloid particles 2-24 hours before the operation allows the tracer to be trapped by phagocytosis by the SLNs so they can be detected preoperatively either on planar lymphoscintigraphy and/or single-photon emission computed tomography/computed tomography (SPECT/CT), which is not the case when other tracers/techniques are being used. Planar images show two-dimensional mapping of the lymphatic drainage and the SLN, while SPECT/CT provides important information about its anatomical location, facilitating surgical detection (7). SLNs are detected intraoperatively with a hand-held gamma detector probe, following its acoustic signal and determining the counts per second (8). In this way, lymph nodes at atypical locations are detected, especially locations where lymphadenectomy would not commonly be performed, in the immediate vicinity of blood vessels. An important advantage of the SLN concept is the possibility of detecting small-volume metastases by detailed histopathological analysis that otherwise would have been missed by routine procedures (9).

SLN mapping with radiocolloid has already been established at our Institution and incorporated as a part of the surgical staging of patients with breast cancer, melanoma, and colorectal cancer. Using this knowledge, we established a nuclear medicine method for SLN biopsy in EC patients with presumed first stage of the disease. Furthermore, purpose of our study was to evaluate the detection rate of SLN in preoperative imaging and intraoperative during SLN biopsy using the Tc-99m-SENTI-SCINT as a tracer, the diagnostic accuracy of SLN biopsy procedure for detecting nodal metastases (sensitivity and negative predictive value), lymphatic drainage, and the rate of metastatic lymph nodes in these patients.

Materials and Methods

Study Design

This is a prospective interventional study that included 41 patients with preoperative (presumed) International Federation of Gynecology and Obstetrics first stage EC who met the inclusion criteria (histopathologically verified EC, T1; N0; M0; patients over 18 years of age, signed informed consent for the procedures and participation in this study) for the SLN biopsy. Patients with EC who had any of the following exclusion criteria were not included in the study: presumed disease stage II-IV (confirmed by ultrasound, computed tomography or magnetic resonance imaging); patients who refused to sign the informed consent for the procedure and participation in this study; a documented contraindication for application of radioactive tracer; existence of contraindications for surgical treatment; and patients who have received neoadjuvant therapy).

The study was approved by the Ethics Committee of the Medical Faculty in Skopje (approval number: 03-366/8).

Procedures

In the morning on the day of the surgical intervention, 37MBq Tc-99m-SENTI-SCINT (Tc-99m marked human serum albumin millimicroaggregate-colloidal particles with a diameter of 100-600 nm) was applied in four cervical quadrants (3, 6, 9 and 12 o'clock positions) by a specialist in gynecology and obstetrics. Planar lymphoscintigraphy and SPECT/CT for SLN detection were than performed to the following acquisition protocol as recommended by the EANM guidelines (8):

- Static images (600 seconds) at 30, 60 and 120 min after application (anteroposterior) position, and if necessary in left lateral and/or right lateral position (gamma camera Mediso DHV Nucline Spirit).

- SPECT/CT at 120-180 minutes (SPECT/CT camera OPTIMA NM/CT 640 GE Healthcare dual detector/4 slice CT).

Intraoperative detection of SLN was performed with a hand-held gamma detector probe (EUROPROBE SYSTEM III), taking into account the results of lymphoscintigraphy and SPECT/CT. In patients with more than one hot node per hemipelvis, we followed the 10% rule. In this regard, all lymph nodes that had 10% higher counts per second than those of the hottest node were also treated as SLNs and were removed (8).

In intermediate-risk patients (endometrioid histology with histological grade 1-2 and more than 50% myometrial invasion or histological grade 3 and less than 50% myometrial invasion) where no SLN was detected in either half of the pelvis, site-specific lymphatic dissection was performed. Pelvic lymphadenectomy was performed in all high-risk patients (non-endometrioid histology; grade 3 endometrioid adenocarcinoma with more than 50% myometrial invasion). The surgical method was laparotomy. After SLN biopsy, all patients underwent abdominal hysterectomy with bilateral salpingo-oophorectomy.

Histopathological Evaluation

The operative material was analyzed at the Institute of Pathology, where a macroscopic evaluation was performed with isolation of SLNs. After fixation in 10% neutral formalin, tissue specimens were paraffin embedded, serially cut, and stained with standard hematoxylin and eosin (H&E) staining for microscopic analysis.

In SLNs where no metastatic deposits were found on the initial sections, two additional sections were done, every 20 microns deep, one of which was stained with standard H&E staining, and the second immunohistochemically for cytokeratin AE1/AE3, in order to detect the presence of low-volume metastasis. Briefly, the paraffin tissue sections were cut (3-5 μm) and mounted on silanized glass slides, followed by deparaffinization in the thermostat at 58-60 °C. PT Link pretreatment was performed in Autostainer Link instrument with diluted EnVision Flex Target Retrieval solution in deionized water for 30 minutes at 97 °C. After cooling the slides to 65 °C, the sections were rinsed in diluted EnVision Flex Wash Buffer for 5 min. DAKO FLEX Ready to Use primary antibody-cytokeratin AE1/AE3 by using Dako EnVision FLEX+ detection system was applied by pre-programmed Autostainer Link Software on Autostainer PT LINK platform. We used Flex + Mouse and Flex+ Mouse 2x5 DAB (Linker) protocol. When the staining procedure was completed, the specimens were mounted with Neo-clear (xylene substitute) after the procedure of dehydrating and clearing the sections. Positive and negative tissue controls were used at the same time.

Detection of malignant cells in the lymph nodes was defined according to the recommendations of the American Joint Committee on Cancer:

- The presence of macrometastasis (MM): focus on metastatic tumor cells larger than 2 mm in diameter,

- The presence of micrometastasis (Mm): focus on metastatic tumor cells 0.2-2 mm in diameter,

- The presence of isolated tumor cells (ITCs): microscopic clusters and single cells less than 0.2 mm in diameter.

Statistical Analysis

Statistical analysis was performed using SPSS 23.0. Categorical (attributive) variables were represented by absolute and relative numbers. Numerical (quantitative) variables were represented by average, standard deviation, minimum, and maximum values. The detection rate of SLN on planar lymphoscintigraphy, SPECT/CT, and intraoperatively was defined as the ratio between the number of patients with at least 1 detected SLN on planar lymphoscintigraphy, SPECT/CT, and intraoperatively with the total number of subjects in the study. Bilateral detection rate was defined as the ratio between the number of patients with at least 1 intraoperatively removed SLN in each hemipelvis and the total number of subjects in the study. The status of the SLN after histopathological examination was defined as true positive-if SLN contained malignant cells regardless of the pathological status of the subsequent non-SLNs in the pelvis (the other lymph nodes in the pelvis); true negative-if SLN did not contain malignant cells and the subsequent non-SLNs in the pelvis were also negative for metastasis or false negative- if SLN did not contain malignant cells but at least one subsequent removed non-SLN in the pelvis was

positive for metastasis. No false positive SLN status was evaluated because positivity of the SLN guaranties nodal metastatic disease. The sensitivity and negative predictive value of SLN biopsy for detecting nodal metastasis were analyzed on a per-patient basis. We used and compared the pathological status of SLNs and non-SLNs to determine if radionuclide mapping and SLN biopsy accurately detected SLN (through finding if the pathological status of the SLN reflects the same pathological status of the non-SLNs). Considering this, the estimated sensitivity and negative predictive value were referred to the SLN biopsy procedure and consequentially (secondarly) to the imaging modality (planar lymphoscintigraphy and SPECT/CT). The sensitivity of SLN biopsy was calculated as the ratio between patients with true positive SLN and patients with true positive SLN and false negative SLN. Negative predictive value of SLN biopsy was calculated as the ratio between patients with true negative SLN and all patients with negative SLN (true negative and false negative).

Results

Demographics

The mean age of the patients was 60.2±7.9 years. The body mass index (BMI) had a mean value of 32.3±5.9 kg/m^2, while the average age of menarche was 12.9±1.3 years. Thirty nine patients were in menopause at the time of EC diagnosis with an average age at menopause occurring at 50.1±4.0 years. Only four patients had a family history of malignancy (9.8%).

Endometrial Carcinoma Characteristics

The characteristics of EC are shown in Table 1. The results of fractional curettage of the endometrium presented endometrioid adenocarcinoma as the most common histopathological type (78.05%). Preoperatively, most carcinomas were intermediate differentiated (46.34%) and in stage IA (82.92%). Endometrioid adenocarcinoma was also the dominant postoperative histological type, proven in 82.9% patients, followed by serous type in 9.75% patients. Postoperative histopathological analysis presented the largest number of carcinomas in stage IA (70.7%) and grade 2 (68.3%) with a size of 2 cm and larger (63.4%). Lymphovascular space invasion and invasion of the myometrium greater than 50% were in 11 (26%) carcinomas. The mean duration of surgery with SLN biopsy was 2.26±0.5 hours, ranging from 1.15 to 3.35 h.

Sentinel Lymph Node Detection

The detection rate of the SLN (hot spots referred as SLNs) on planar lymphoscintigraphy was 33/41=80.49% [95% confidence interval (CI): 68.36-92.62]; while on SPECT/CT 39/41=95.12% (95% CI: 88.52-101.7); the total intraoperative detection rate of SLN was 39/41=95.12% (95% CI 88.52-101.7); the bilateral intraoperative detection rate of SLN was 11/41=26.83% (95% CI: 19.91-33.75). The SLN presentation on planar lymphoscintigraphy and on SPECT/CT is shown in Figures 1 and 2. Table 2 presents the distribution of SLNs detected on planar lymphoscintigraphy and SPECT/CT. Comparing the pre-operative SPECT/CT and intraoperative findings, total concordance was obtained in 35 patients (85.4%), while partial concordance was noticed in 6 patients (14.6%). In these 6 patients, we removed the "hottest" SLN detected by both preoperative imaging and gamma probe (fist echelon). The additional hot spots (n=10), detected on SPECT/CT were not registered by the gamma probe or had activity below 10% counts from the "hottest" SLN and thus were not removed. These nodes were characterized as second echelon nodes and were located in the common iliac region (9) and internal iliac region (1) on SPECT/CT. In two patients, no SLN was detected by both preoperative imaging and gamma probe (4.8%).

Table 1. Characteristics of EC (n=41). Results are present as number and percent

	Preoperative characteristics	Postoperative characteristics
Histological type n (%)		
Endometrioid adenocarcinoma	32 (78.05)	34 (82.93)
Serous	4 (9.75)	4 (9.75)
Mixed form	1 (2.44)	1 (2.44)
Undifferentiated	1 (2.44)	1 (2.44)
Mucinous	3 (7.32)	1 (2.44)
Grade n (%)		
1	13 (31.70)	5 (12.19)
2	19 (46.34)	28 (68.29)
3	9 (21.95)	8 (19.51)
Stage n (%)		
IA		29 (70.73)
IB	34 (82.92)	7 (17.07)
II	7 (17.07)	1 (2.44)
IIIC		4 (9.76)
Size of the carcinoma (cm)		
<2		15 (36.58)
≥2		26 (63.41)
Lymphovascular space invasion		
Present		11 (26.83)
Absent		30 (73.17)
Myometrial invasion		
None		2 (4.88)
<50%	30 (73.17)	28 (68.29)
>50%	11 (26.83)	11 (26.83)

EC: Endometrial cancer

In half of the patients, more than one SLN was removed. The total number of SLNs removed was 66, and the average number was 1.6±0.8. Metastatic deposits in the SLN were detected in 8 SLNs in 7 (17.1%) patients, of which 3 were MM, 1 Mm, and 4 were ITCs. Micrometastatic deposit in a SLN is shown in Figure 3. The total number of non-SLNs removed during site-specific lymphadenectomy (in 4 patients) and pelvic lymphadenectomy (in 8 patients) was 154. In 2 patients, metastatic deposits were in both SLNs and non-SLNs. The sensitivity of the SLN biopsy regarding nodal metastasis was 100%. The true negative rate was 100%. No false negative SLN was found, and the negative predictive value was 100%. The data for intraoperative SLN detection are presented in Table 3. There were no adverse events during cervical application of the tracer, SLN mapping on nuclear medicine imaging, and during surgery regarding radiocolloid and SLN biopsy.

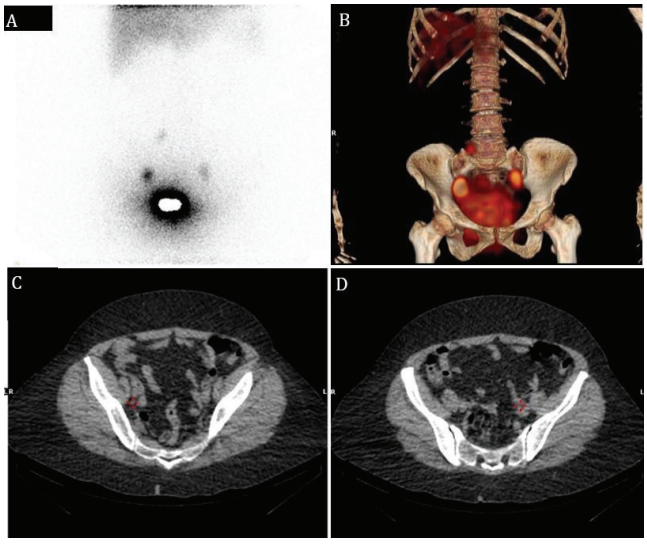

Figure 1. Planar lymphoscintigraphy and SPECT/CT in a 51-year-old patient with grade 3 mixed form of endometrial adenocarcinoma. Planar lymphoscintigraphy (A) and SPECT/CT (B) showed drainage to the bilateral pelvic regions. The hot spots refereed as SLNs were further localized on the axial CT image in the right external iliac region (C) and in the left external iliac region (D). The second hot spot in the right hemipelvis was characterized as second echelon node and was located in the right common iliac region

SPECT/CT: Single-photon emission computed tomography/computed tomography, SLN: Sentinel lymph node

The most common anatomical location of the SLN was the right external iliac region, followed by the left external iliac region and the right obturator regions. SLNs with metastatic deposits were most often located in the right external iliac region. Only in the left obturator region was no SLN with metastatic deposits found. Data for the anatomical localization of the SLN and the distribution of the SLN with metastatic deposits are presented in Table 4.

Discussion

The concept of SLN detection in the EC has been controversial for a long time due to the central position of the uterus and thus the complex lymphatic drainage as well as the heterogeneity of the used techniques. Although it was first applied in 1996 by Burke et al. (10), this procedure was not accepted as a possible alternative to complete lymphadenectomy until 2014 (11). Two uterine lymphatic drainage pathways are identified in the pelvis: the upper paracervical pathway with drainage to the external iliac and/or obturator lymph nodes and the lower paracervical pathway with drainage to the internal iliac and/or presacral lymph nodes (12). Mainly the upper lymph nodes and only part of the lower paracervical pathway are removed by conventional lymphadenectomy, which leaves the possibility of some nodal metastases to be missed. During SLN biopsy, a specific lymph node is removed regardless of the location, including those detected in less typical places such as parametrium, interiliac region, presacral region etc. (13,14). At the same time, the detection

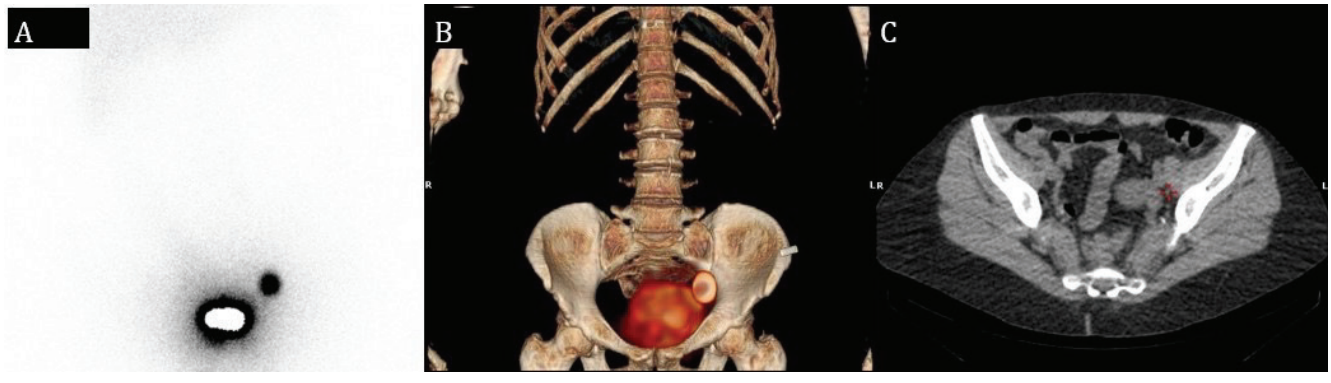

Figure 2. Planar lymphoscintigraphy and SPECT/CT in a 54-years old patient with grade 2 endometrioid adenocarcinoma. Planar lymphoscintigraphy (A) and SPECT/CT (B) showed intensive focal accumulation in the left hemipelvis, corresponding to a left obturator node on the axial CT image (C)

SPECT/CT: Single-photon emission computed tomography/computed tomography, SLN: Sentinel lymph node

Table 2. Patients (n=41) distribution according to the number of SLNs detected on planar lymphoscintigraphy and SPECT/CT. Results are presented as number and percent

Visualization of hot spots referred as SLNs on gamma camera	Number of hot spots referred as SLNs	
	Planar lymphoscintigraphy n (%)	SPECT/CT n (%)
0	8 (19.51)	2 (4.88)
1	17 (41.46)	18 (43.90)
2	12 (29.27)	13 (31.71)
3	3 (7.32)	5 (12.19)
4	1 (2.44)	3 (7.32)
Total number of hot spots referred as SLNs	62	72
Mean ± SD	1.3±0.9	1.7±0.9

SLN: Sentinel lymph node, SPECT/CT: Single-photon emission computed tomography/computed tomography, SD: Standard deviation

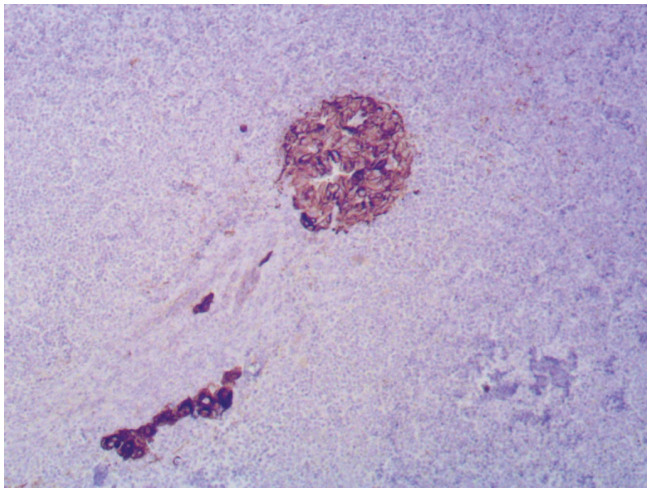

Figure 3. A positive sentinel lymph node for micrometastasis (immunohistochemistry with cytokeratin 7; magnification, x40)

rate of nodal metastases was increased compared with lymphadenectomy (14.7% vs. 9.9%; p=0.002) (15).

Several tracers for identification of the SLN and techniques for their application have been reported (16,17,18,19,20). The total detection rate varies and it is lowest for blue dye as a single tracer 71-76% (14,16), while the best results are obtained using the double-tracer (dual detection) method, which combines radiocolloid and indocyanine green, with a detection rate of 91-100% and a bilateral detection rate of 69-87.3% (17,18,19). Furthermore, future studies concerning SLN biopsy in EC with hybrid tracer (fluorescent and radioactive tracer) would be beneficial as this tracer contains advantages of both compounds.

Table 3. Data for intraoperative SLN detection. Results are presented as number and percent

Variable	Statistical parameter
SLN detection n (%) Unilateral pelvic Bilateral pelvic Unsuccessful detection	 28 (68.29) 11 (26.83) 2 (4.88)
Number of removed SLNs Total number Mean ± SD	 66 1.6±0.8
Lymphatic metastases in SLN n (%) Yes No	 7 (17.07) 34 (82.93)
Macrometastasis Micrometastasis Isolated tumor cells	3 (7.32) 1 (2.44) 3 (7.32)

SLN: Sentinel lymph node

Table 4. Distribution of the SLNs in the pelvis by anatomical regions and localization of SLNs with metastatic deposits

Anatomical location of the SLN in the pelvis	Total number of SLN	Positive for metastatic deposits
Right hemipelvis n (%)	37	5/37 (13.51%)
Right common iliac region	8/37 (21.62%)	1/5 (20%)
Right external iliac region	15/37 (40.54%)	2/5 (40%)
Right internal iliac region	4/37 (10.87%)	1/5 (20%)
Right obturator region	10/37 (27.03%)	1/5 (20%)
Left hemipelvis n (%)	29	3/29 (10.34%)
Left common iliac region	7/29 (24.14%)	1/3 (33.33%)
Left external iliac region	11/29 (37.93%)	1/3 (33.33%)
Left internal iliac region	3/29 (10.34%)	1/3 (33.33%)
Left obturator region	8/29 (27.59%)	0/3 (0%)

SLN: Sentinel lymph node

Several places of tracer application are being proposed: cervical, hysteroscopic-endometrial, and subserosal/myometrial. Cervical injection is most commonly used because of its easy access to the cervix and the highest pelvic detection rate (20). However, the para-aortic SLN count is significantly lower compared with endometrial injection (21). Another concern is that the cervical injection site of Tc-99m-colloid can stimulate gamma detectors, making it difficult to distinguish it from parametrial SLNs (22).

In our study, we used Tc-99m-SENTI-SCINT applied cervically at the 3, 6, 9 and 12 o'clock positions of the uterine cervix, and the total intraoperative detection rate was high, 95.12%. A lower detection rate of 80% was published when only two cervical injections of Tc-99m-labeled tracer were used at the 3 and 9 o'clock positions (21).

Various factors affecting the SLN detection rate have been published. In their study, Restaino et al. (23) pointed out that older patients with higher BMI and non-endometrioid histology were more likely to have no SLN mapping. The SLN in our study was not detected by both SPECT/CT and handheld gamma probes in two patients. Both patients had low grade endometrioid type adenocarcinoma on final histopathology, but were obese as the possible reason for mapping failure.

For a hot spot to be considered as SLN on preoperative imaging, some criteria should be fulfilled, such as lymphatic duct visualization, first appearing node in the lymphatic basin, and high intensity of lymph node uptake. These factors further determine the probability of SLN identification (24). Total concordance between preoperative imaging and intraoperative SLN detection was achieved in 85.4% and partial concordance in the rest of the cases in our study. Elisei et al. (25) published a moderate concordance (73% of the cases) between SPECT/CT and intraoperative findings with a gamma probe, with SPECT/CT having the highest detection rate. Furthermore, Sawicki et al. (26) found 35 false-positive hot spots detected on SPECT/CT that were not found by gamma probe intraoperatively. This could be due to misinterpreting a lymphatic duct or a lymphatic lake for an SLN or a higher echelon lymph node with mild activity below 10% of the counts of the hottest node.

The diagnostic accuracy of SLN biopsy in EC was evaluated by a meta-analysis (34 studies) of How et al. (27), with a pooled sensitivity of 94% (95% CI: 91-96%) and negative predictive value of 100% (95% CI: 99-100%). To calculate the above mentioned parameters, a complete pelvic lymphadenectomy is required. However, lymph node dissection does not provide any therapeutic benefit except adding prognostic information in low-risk ECs. Considering this, we decided not to perform lymphadenectomy besides SLN biopsy in these patients. Complete pelvic lymphadenectomy and site-specific lymphadenectomy were performed in 12 patients. These non-SLNs were further analyzed for sensitivity and negative predictive value of the procedure. Specificity and positive predictive values were not analyzed because false-positive results for SLN can not occur. If a SLN is found positive for metastasis, it would remain unchanged by histopathological analysis of the additional non-SLNs removed at systematic lymphadenectomy. The sensitivity and negative predictive value was 100% in our study, which indicates the high accuracy of the technique although the sample of patients was small.

The most common anatomical localization of SLN in the pelvis regardless of the tracer used is the external iliac region, followed by the obturator region (17,20). These results were also confirmed .

The second advantage of SLN detection is the extensive histopathological analysis with the possibility of detecting low volume deposits of tumor cells (Mm and ITCs). Ultra-staging is expensive and prolongs the processing time, making it impossible to apply to several lymph nodes. In contrast to radical lymphadenectomy, SLN biopsy removes a few lymph nodes, which can be histopathologically analyzed in more detail. Thus, the SLN concept offers an increase in the sensitivity of detecting nodal metastases, especially since Mm is also considered N1 and such patients are classified into stage III of the disease (5,28).

In our study, 57% of the patients positive for nodal metastases had low-volume metastases, of which Mm was found in one patient, with the final stage being IIIC. This patient would have been missed and misclassified as stage I by conventional histopathology. Patients with Mm/ITCs have a higher relative risk of recurrence compared with patients without nodal metastases. However, the importance of the ITCs is still not clear enough, so it does not affect the staging for the time being. In addition, it is recommended that ITCs be noted in the surgical pathology report but designated as pNo(i+) (29). Large, randomized studies are needed to assess their impact on recurrence and overall survival (30).

Study Limitations

Limitations of the study include the small sample size and not performance of para-aortic lymph node dissection as there was no case of first echelon para-aortic lymph node visualization on planar lymphoscintigraphy/SPECT/CT. Additionally, pelvic lymphadenectomy was not performed in patients with low-risk EC. Therefore, we could not analyze the sensitivity and negative predictive value of the method in low-risk EC.

Conclusion

Our study indicates that SLN biopsy is a safe, non-invasive, and effective alternative for lymph node assessment in EC patients. The present results point out the high detection rate and diagnostic accuracy of the lymphoscintigraphy method for detecting SLN with cervical application of Tc-99m-SENTI-SCINT in patients with apparently uterine-confined EC. Furthermore, the application of immunohistochemical analysis of the SLN increases the detection of low-volume metastases in the lymph nodes, contributing to more

accurate staging and thus appropriate adjuvant treatment in these patients. Additionally, since the lymphatic drainage of the uterus is complex and there could be more than one drainage region and therefore more than one SLN, we recommend following the 10% rule and removal of all lymph nodes with counts per second higher than 10% of the counts of the hottest SLN.

Ethics

Ethics Committee Approval: The study was approved by the Ethics Committee of the Medical Faculty in Skopje (approval number: 03-366/8).

Informed Consent: Consent has been taken.

Peer-review: Externally and internally peer-reviewed.

Authorship Contributions

Surgical and Medical Practices: A.J., S.S., Sa.S., I.A., R.J., M.T., S.K.K., N.M., G.P., D.M., Concept: A.J., D.M., Design: A.J., S.S., Sa.S., I.A., G.P., D.M., Data Collection or Processing: A.J., D.M., Analysis or Interpretation: S.S., G.P., D.M., Literature Search: A.J., D.M., Writing: J.A., N.M., S.S., G.P., D.M.

Conflict of Interest: No conflict of interest was declared by the authors.

Financial Disclosure: The authors declared that this study has received no financial support.

References

1. Sung H, Ferlay J, Siegel RL, Laversanne M, Soerjomataram I, Jemal A, Bray F. Global Cancer Statistics 2020: GLOBOCAN Estimates of Incidence and Mortality Worldwide for 36 Cancers in 185 Countries. CA Cancer J Clin 2021;71:209-249.
2. Brooks RA, Fleming GF, Lastra RR, Lee NK, Moroney JW, Son CH, Tatebe K, Veneris JL. Current recommendations and recent progress in endometrial cancer. CA Cancer J Clin CA Cancer J Clin 2019;69:258-279.
3. Frost JA, Webster KE, Bryant A, Morrison J. Lymphadenectomy for the management of endometrial cancer. Cochrane Database Syst Rev 2017;10:CD007585.
4. Ignatov A, Ivros S, Bozukova M, Papathemelis T, Ortmann O, Eggemann H. Systematic lymphadenectomy in early stage endometrial cancer. Arch Gynecol Obstet 2020;302:231-239.
5. Concin N, Matias-Guiu X, Vergote I, Cibula D, Mirza MR, Marnitz S, Ledermann J, Bosse T, Chargari C, Fagotti A, Fotopoulou C, Gonzalez Martin A, Lax S, Lorusso D, Marth C, Morice P, Nout RA, O'Donnell D, Querleu D, Raspollini MR, Sehouli J, Sturdza A, Taylor A, Westermann A, Wimberger P, Colombo N, Planchamp F, Creutzberg CL. ESGO/ESTRO/ESP guidelines for the management of patients with endometrial carcinoma. Int J Gynecol Cancer 2021;31:12-39.
6. Gould EA, Winship T, Philbin PH, Kerr HH. Observations on a 'sentinel node' in cancer of the parotid. Cancer 1960;13:77-78
7. Rychlik A, Zalewski K. Tracers and corresponding detection devices: technetium colloids, blue dyes & NIR fluorescence. Chin Clin Oncol 2021;10:16.
8. Giammarile F, Bozkurt MF, Cibula D, Pahisa J, Oyen WJ, Paredes P, Olmos RV, Sicart SV. The EANM clinical and technical guidelines for lymphoscintigraphy and sentinel node localization in gynaecological cancers. Eur J Nucl Med Mol Imaging 2014;41:1463-1477.
9. Ballester M, Dubernard G, Lécuru F, Heitz D, Mathevet P, Marret H, Querleu D, Golfier F, Leblanc E, Rouzier R, Daraï E. Detection rate and diagnostic accuracy of sentinel-node biopsy in early stage endometrial cancer: a prospective multicentre study (SENTI-ENDO). Lancet Oncol 2011;12:469-476.
10. Burke TW, Levenback C, Tornos C, Morris M, Wharton JT, Gershenson DM. Intraabdominal lymphatic mapping to direct selective pelvic and paraaortic lymphadenectomy in women with high-risk endometrial cancer: results of a pilot study. Gynecol Oncol 1996;62:169-173.
11. olombo N, Creutzberg C, Amant F, Bosse T, González-Martín A, Ledermann J, Marth C, Nout R, Querleu D, Mirza MR, Sessa C; ESMO-ESGO-ESTRO Endometrial Consensus Conference Working Group. ESMO-ESGO-ESTRO Consensus Conference on Endometrial Cancer: diagnosis, treatment and follow-up. Ann Oncol 2016;27:16-41.
12. Geppert B, Lönnerfors C, Bollino M, Arechvo A, Persson J. A study on uterine lymphatic anatomy for standardization of pelvic sentinel lymph node detection in endometrial cancer. Gynecol Oncol 2017;145:256-261.
13. How J, Boldeanu I, Lau S, Salvador S, How E, Gotlieb R, Abitbol J, Halder A, Amajoud Z, Probst S, Brin S, Gotlieb W. Unexpected locations of sentinel lymph nodes in endometrial cancer. Gynecol Oncol 2017;147:18-23.
14. How J, Gotlieb WH, Press JZ, Abitbol J, Pelmus M, Ferenczy A, Probst S, Gotlieb R, Brin S, Lau S. Comparing indocyanine green, technetium, and blue dye for sentinel lymph node mapping in endometrial cancer. Gynecol Oncol 2015;137:436-442.
15. Bogani G, Murgia F, Ditto A, Raspagliesi F. Sentinel node mapping vs. lymphadenectomy in endometrial cancer: A systematic review and meta-analysis. Gynecol Oncol 2019;153:676-683.
16. Frumovitz M, Plante M, Lee PS, Sandadi S, Lilja JF, Escobar PF, Gien LT, Urbauer DL, Abu-Rustum NR. Near-infrared fluorescence for detection of sentinel lymph nodes in women with cervical and uterine cancers (FILM): a randomised, phase 3, multicentre, non-inferiority trial. Lancet Oncol 2018;19:1394-1403.
17. Cabrera S, Bebia V, Franco-Camps S, Forcada C, Villasboas-Rosciolesi D, Navales I, Pérez-Benavente A, Gil-Moreno A. Technetium-99m-indocyanine green versus technetium-99m-methylene blue for sentinel lymph node biopsy in early-stage endometrial cancer. Int J Gynecol Cancer 2020;30:311-317.
18. Tal O, Grinstein E, Goshen E, Oksman Y, Lorberboym M, Elyashiv O, Ben Shem E, Peled O, Levy T. Anatomic Asymmetry in Sentinel Lymph Node Detection in Endometrial Cancer. J Minim Invasive Gynecol 2021;28:1531-1535.
19. Kataoka F, Susumu N, Yamagami W, Kuwahata M, Takigawa A, Nomura H, Takeuchi H, Nakahara T, Kameyama K, Aoki D. The importance of para-aortic lymph nodes in sentinel lymph node mapping for endometrial cancer by using hysteroscopic radio-isotope tracer injection combined with subserosal dye injection: Prospective study. Gynecol Oncol 2016;140:400-404.
20. Eriksson AGZ, Davidson B, Bjerre Trent P, Eyjólfsdóttir B, Dahl GF, Wang Y, Staff AC. Update on Sentinel Lymph Node Biopsy in Surgical Staging of Endometrial Carcinoma. J Clin Med 2021;10:3094.
21. Gezer Ş, Duman Öztürk S, Hekimsoy T, Vural Ç, İşgören S, Yücesoy İ, Çorakçı A. Cervical versus endometrial injection for sentinel lymph node detection in endometrial cancer: a randomized clinical trial. Int J Gynecol Cancer 2020;30:325-331.
22. Zhai L, Zhang X, Cui M, Wang J. Sentinel Lymph Node Mapping in Endometrial Cancer: A Comprehensive Review. Front Oncol 2021;11:701758.

23. Restaino S, Buda A, Puppo A, Capozzi VA, Sozzi G, Casarin J, Gallitelli V, Murgia F, Vizzielli G, Baroni A, Corrado G, Pasciuto T, Ferrari D, Novelli A, Berretta R, Legge F, Vizza E, Chiantera V, Ghezzi F, Landoni F, Scambia G, Fanfani F. Anatomical distribution of sentinel lymph nodes in patients with endometrial cancer: a multicenter study. Int J Gynecol Cancer 2022;32:517-524.
24. Valdés Olmos RA, Rietbergen DDD, Vidal-Sicart S. SPECT/CT and sentinel node lymphoscintigraphy. Clin Transl Imaging 2014;2:491-504.
25. Elisei F, Crivellaro C, Giuliani D, Dolci C, De Ponti E, Montanelli L, La Manna M, Guerra L, Arosio M, Landoni C, Buda A. Sentinel-node mapping in endometrial cancer patients: comparing SPECT/CT, gamma-probe and dye. Ann Nucl Med 2017;31:93-99.
26. Sawicki S, Kobierski J, Łapińska-Szumczyk S, Lass P, Cytawa W, Bianek-Bodzak A, Wydra D. Comparison of SPECT-CT results and intraoperative detection of sentinel lymph nodes in endometrial cancer. Nucl Med Commun 2013;34:590-596.
27. How JA, O'Farrell P, Amajoud Z, Lau S, Salvador S, How E, Gotlieb WH. Sentinel lymph node mapping in endometrial cancer: a systematic review and meta-analysis. Minerva Ginecol Minerva Ginecol 2018;70:194-214.
28. Burg LC, Hengeveld EM, In 't Hout J, Bulten J, Bult P, Zusterzeel PLM. Ultrastaging methods of sentinel lymph nodes in endometrial cancer - a systematic review. Int J Gynecol Cancer 2021;31:744-753.
29. Singh N, Hirschowitz L, Zaino R, Alvarado-Cabrero I, Duggan MA, Ali-Fehmi R, Euscher E, Hecht JL, Horn LC, Ioffe O, Matias-Guiu X, McCluggage WG, Mikami Y, Ordi J, Parkash V, Quddus MR, Quick CM, Staebler A, Zaloudek C, Nucci M, Malpica A, Oliva E. Pathologic Prognostic Factors in Endometrial Carcinoma (Other Than Tumor Type and Grade). Int J Gynecol Pathol 2019;38(Suppl 1):93-113.
30. Gómez-Hidalgo NR, Ramirez PT, Ngo B, Pérez-Hoyos S, Coreas N, Sanchez-Iglesias JL, Cabrera S, Franco S, Benavente AP, Gil-Moreno A. Oncologic impact of micrometastases or isolated tumor cells in sentinel lymph nodes of patients with endometrial cancer: a meta-analysis. Clin Transl Oncol 2020;22:1272-1279.

Original Article
Mol Imaging Radionucl Ther 2023;32:112-116 DOI:10.4274/mirt.galenos.2022.05826

Comparison of Radioactive Iodine Activities in Terms of Short- and Long-term Results in Ablation Therapy in Patients with Low-risk Differentiated Thyroid Cancer

Düşük Risk Grubundaki Diferansiye Tiroid Kanseri Hastalarında Ablasyon Tedavisinde Radyoaktif İyot Aktivitelerinin Kısa ve Uzun Dönem Sonuçları Açısından Karşılaştırılması

Seray Saraçoğlu[1], Osman Güven[1], Gündüzalp Buğrahan Babacan[1], Savaş Karyağar[1], Tamer Özülker[1], Sadık Ergür[2], Sevda Sağlampınar Karyağar[1]

[1]*University of Health Sciences Turkey, Prof. Dr. Cemil Taşcıoğlu City Hospital, Clinic of Nuclear Medicine, İstanbul, Turkey*
[2]*Bursa City Hospital, Clinic of Nuclear Medicine, Bursa, Turkey*

Abstract

Objectives: The aim of this study was to compare the treatment responses after ablation with 30-50 mCi radioactive iodine (RAI) and 100 mCi RAI in patients with differentiated thyroid cancer (DTC) who were in the low-risk group according to 2015 American Thyroid Associations Classification (ATA 2015) criteria.

Methods: Between February 2016 and August 2018, 100 patients who received RAI treatment in our clinic after total thyroidectomy and who were in the low-risk group DTC were included in this retrospective study. These patients were divided into 2 groups: low-activity (30-50 mCi) (group 1) and high-activity (100 mCi) (group 2). While 54 patients were treated with low activity, 46 patients received high activity RAI. The 2 groups were compared according to the 1st- and 3rd-year treatment response status.

Results: According to the first-year follow-up, 15 patients were accepted as indeterminate response and 85 patients as excellent response. Three (5.5%) of the patients who were accepted as indeterminate response were in group 1 and 12 (26%) were in group 2. According to the third year follow-up, 1 patient in group 1 and 3 patients in group 2 were accepted as indeterminate response. No biochemical incomplete response or recurrent disease was detected. In the chi-square analysis performed to investigate the relationship between the first-year treatment response and RAI activities, a significant relationship was found (p=0.004). In the Mann-Whitney U test performed to investigate the parameters that may be effective in the treatment response, only the preablative serum thyroglobulin value was shown to have a significant difference between the two groups (p=0.01). In the long-term follow-up of the patients, based on the third year treatment response data, chi-square analysis was performed to evaluate the two groups in terms of treatment responses, and no statistically significant relationship was found (p=0.73).

Conclusion: Ablation with 30-50 mCi can be safely applied in DTC patients who are in the ATA 2015 low-risk group and are planned for RAI ablation treatment.

Keywords: Differentiated thyroid carcinoma, low-risk, radioiodine, remnant ablation

Öz

Amaç: Bu çalışmanın amacı, 2015 Amerikan Tiroid Dernekleri Sınıflandırması (ATA 2015) kriterlerine göre düşük risk grubunda olup radyoaktif iyot ile ablasyon (RAİ) tedavisi almış olan diferansiye tiroid kanseri (DTK) hastalarında, 30 veya 50 mCi RAİ ile 100 mCi RAİ ile ablasyon sonrası tedavi yanıtlarının karşılaştırılmasıdır.

Address for Correspondence: Seray Saraçoğlu MD, University of Health Sciences Turkey, Prof. Dr. Cemil Taşcıoğlu City Hospital, Clinic of Nuclear Medicine, İstanbul, Turkey
Phone: +90 554 619 13 94 **E-mail:** seraysaracoglu@gmail.com ORCID ID: orcid.org/0000-0002-8815-0729
Received: 14.05.2022 **Accepted:** 25.08.2022

Yöntem: Şubat 2016-Ağustos 2018 tarihleri arasında kliniğimizde total tiroidektomi sonrası RAİ tedavisi alan ve düşük risk grubu DTK olan 100 hasta bu retrospektif çalışmaya dahil edildi. Bu hastalar düşük doz (30-50 mCi) (grup 1) ve yüksek doz (100 mCi) (grup 2) olarak 2 gruba ayrıldı. Elli dört hasta düşük doz ile tedavi edilirken, 46 hasta yüksek doz RAİ aldı. İki grup 1. ve 3. yıl tedavi yanıt durumuna göre karşılaştırıldı.

Bulgular: Birinci yıl takibine göre 15 hasta belirsiz yanıt, 85 hasta mükemmel yanıt olarak kabul edildi. İndetermine yanıt olarak kabul edilen hastaların 3'ü (%5,5) grup 1'de, 12'si (%26) grup 2'deydi. Üçüncü yıl takibine göre grup 1'de 1, grup 3'te 2 hasta indetermine yanıt olarak kabul edildi. Hiçbir hastada biyokimyasal yetersiz yanıt veya nüks hastalık saptanmadı. Birinci yıl tedavi yanıtı ile RAİ dozları arasındaki ilişkiyi araştırmak için yapılan ki-kare analizinde anlamlı ilişki bulundu (p=0,004). Tedavi yanıtında etkili olabilecek parametreleri araştırmak için yapılan Mann-Whitney U testinde sadece preablatif serum tiroglobulin değerinin mükemmel yanıt ve indetermine yanıt gösteren hasta grupları arasında anlamlı fark gösterdiği tespit edildi (p=0,01). Hastaların uzun dönem takiplerinde üçüncü yıl tedavi yanıt verilerine göre iki grubu tedavi yanıtları açısından değerlendirmek için ki-kare analizi yapıldı ve istatistiksel olarak anlamlı bir ilişki bulunamadı (p=0,73).

Sonuç: ATA 2015 düşük risk grubunda yer alan ve RAİ ablasyon tedavisi planlanan DTK hastalarında 30-50 mCi ile ablasyon güvenle uygulanabilir.

Anahtar kelimeler: Diferansiye tiroid kanseri, düşük risk, radyoaktif iyot, remnant ablasyonu

Introduction

Differentiated thyroid carcinomas (DTC) usually show a slow course of progression and patients diagnosed with DTC have a long life expectancy. A significant increase has been observed in the incidence of DTC with the widespread use of imaging modalities recently (1,2). An important reason for this is thought to be the incidental detection of small-sized nodules, which would not normally cause any symptoms in the patient, in imaging studies such as computed tomography (CT), magnetic resonance imaging (MRI), ultrasonography (USG), and positron emission tomography (PET)/CT applied to the patient for other reasons. This has led to a significant increase in the incidence of especially low-risk thyroid cancer through the early diagnosis of slow-progressing malignant thyroid nodules.

According to the 2015 American Thyroid Associations Classification (ATA 2015), patients without risk factors such as extrathyroidal extension, distant metastasis, or aggressive histological subtype are defined as low-risk (3). In these patients, the recurrence of the disease or disease-related mortality after treatment is extremely rare. It has been reported that when patients with DTC undergo successful radioactive iodine (RAI) remnant ablation after total thyroidectomy, less than 1-4% of patients have disease recurrence (4,5,6,7). The very slow course of the disease and the very low rate of recurrence have led to the emergence of very different clinical approaches, and there is no consensus among physicians yet on the necessity of RAI in these patients and the activity to be administered if necessary. This situation often leads to overtreatment of these patients, resulting in undesirable results such as unnecessary radiation exposure, an increase in the frequency of side effects and secondary malignancies, and cost increase (8,9). The aim of this study was to compare the treatment responses after ablation with low-activity (30-50 mCi) RAI and high-activity (100 mCi) RAI in patients with DTC who were in the low-risk group according to ATA 2015 criteria.

Materials and Methods

Patients

Between February 2016 and August 2018, 100 patients (97 patients with papillary, and 3 patients with follicular carcinoma) who received RAI treatment in our clinic after total thyroidectomy and who were in the low-risk group DTC were included in this retrospective study.

The inclusion criteria were as follows: age at diagnosis ≥18 years; patients undergoing total or near-total thyroidectomy; low-risk DTC; and primary RAI therapy after surgery. The exclusion criteria were the presence of aggressive histologic subtypes, high preablative serum anti-thyroglobulin (anti-Tg) levels, vascular invasion, microscopic or gross extrathyroidal extension, metastatic lymph nodes of any size, any RAI-avid metastatic foci outside the thyroid bed on the first posttreatment whole-body RAI scan indicating distant metastasis, and secondary malignancy. These patients were divided into two groups: low-activities (30-50 mCi) (group 1) and high-activity (100 mCi) (group 2). While 54 patients were treated with low activity (6 patients with 30 mCi and 48 with 50 mCi), 46 patients received high activity RAI. The 2 groups were compared according to the 1st- and 3rd-year treatment response status.

Radioactive Iodine Administration

Patients admitted to our clinic in the 1-6 months postoperative period were prepared with thyroid hormone withdrawal for 4 weeks and a low-iodine diet for 2 weeks. Patients with thyroid-stimulating hormone (TSH) level ≥30 mU/L were evaluated for RAI activity determination by serum Tg and anti-Tg levels, neck USG, and technetium-99m pertechnetate thyroid scintigraphy. Four to 7 days after RAI treatment, a post-therapy I-131 whole-body scan (WBS) was performed using a Mediso Anyscan SC-SN-

3s-60R high energy parallel hole collimator. Scan images were reviewed by 2 consultant nuclear physicians before reporting.

Response to Therapy

The ATA 2015 guideline has a dynamic risk assessment system that classifies the patient based on the response to therapy (excellent, indeterminate, biochemical incomplete, and structural incomplete response) using serum Tg level, anti-Tg antibodies, USG, diagnostic wholebody scan, CT, PET/CT, and MRI (3). In this study, response to therapy assessment was performed twelve months and three years after RAI treatment based on the ATA 2015 risk assessment system.

Thus, an excellent response was defined as negative imaging with TSH-stimulated Tg <1 ng/mL or suppressed Tg <0.2 ng/mL.

Meanwhile, an incomplete response was defined as one of the following:

1. Biochemical incomplete response was defined as negative imaging with abnormal suppressed Tg (≥1 ng/mL) and/or stimulated Tg values (≥10 ng/mL) or rising anti-Tg.

2. Structural incomplete response was defined as locoregional or distant metastases on USG and/or WBS (independent of Tg and anti-Tg).

Lastly, indeterminate response was defined as non-specific findings on imaging studies, non-stimulated Tg between 0.2 and 1 ng/mL, stimulated Tg between 1 and 10 ng/mL, or anti-Tg stable or declining in the absence of structural or functional disease.

University of Health Sciences Turkey, Prof. Dr. Cemil Taşcıoğlu City Hospital Ethics Committee approval was obtained on 09.05.2022 with decision number 147 for this clinical study, which was designed retrospectively.

Statistical Analysis

Data were analyzed using IBM SPSS Statistics 26.0 for Windows. Results were expressed as mean ± standard deviation. Comparisons of the data were performed by Mann-Whitney U and chi-square tests. Results were considered statistically significant when the two-tailed p value was less than 0.05.

Results

Of the 100 patients included in the study, 79 were female and 21 were male. The mean age of the patients was 47±13 (range 19-75 years), while the mean tumor diameter was 19.40±10.68 millimeters. The mean preablative Tg value was calculated as 2.92 (0.04-82.55) in all patients in the study group. While there were 7 T1a, 38 T1b, 8 T2, 1 T3 stage patients in group 1, which consisted of patients who received low-activity (30-50 mCi) RAI treatment, there were 3 T1a, 21 T1b, 19 T2, 3 T3 stage patients in group 2, which consisted of patients who received high-activity (100 mCi) RAI treatment. In group 1, 25 patients had unifocal and 29 patients had multifocal disease, while in group 2, 23 patients had unifocal and 23 patients had multifocal disease. While the mean primary tumor diameter was 21.62±7.39 (4-45) mm in group 1, it was 23.11±12.69 (3-65) mm in group 2. Preablative serum Tg value was 1.81 (0.04-34) ng/mL in group 1 and 4.25 (0.05-82.55) ng/mL in group 2. The demographic and clinical features of the patients in this study are summarized in Table 1.

According to the first-year follow-up, 15 patients were accepted as indeterminate response and 85 patients as an excellent response. Three (5.5%) of the patients who were accepted as indeterminate response were in group 1 and 12 (26%) were in group 2. According to the 3rd year follow-up, 1 patient in group 1 and 3 patients in group 2 were accepted as indeterminate response. No biochemical incomplete response or recurrent disease was detected in any patient in either patient group. The treatment responses of the patients at the end of the 1st and 3rd years according to the administered RAI activities are summarized in Table 2.

In the chi-square analysis performed to investigate the relationship between the first-year treatment response and RAI activities, a significant relationship was found (p=0.004). Accordingly, group 2 had significantly more patients who were accepted as indeterminate response than group 1 at the end of the first year. It was investigated which parameters had a statistically significant difference between patients with excellent response and patients

Table 1. Patient characteristics

Parameters	n	
Gender	Female	79
	Male	21
Age	47±13 years	
Mean tumor diameter	19.9±10.68 milimeters	
Mean preablative Tg	2.92 ng/mL	
T stage	T1a	10
	T1b	59
	T2	27
	T3	4
Tumor multifocality	Unifocal	48
	Multifocal	52

Tg: Thyroglobulin

Table 2. The treatment responses of the two patient groups at the end of the 1st and 3rd years, according to the administered RAI activities

	1st year treatment response		3rd year treatment response	
	Excellent	Indeterminate	Excellent	Indeterminate
Group 1 (30-50 mCi)	51	3	53	1
Group 2 (100 mCi)	34	12	40	6

RAI: Radioactive iodine

with indeterminate response. In the Mann-Whitney U test performed for this purpose, only the preablative serum Tg value was shown to have a significant difference between patients with excellent and indeterminate response (p=0.010), and tumor size, patient age, and preablative anti-Tg levels were found to be not statistically significant factors (p=0.083; 0.38; 0.80; respectively).

The mean preablative serum Tg value was 2.14 (0.04-85.55) ng/mL in patients with excellent response at 1st year after treatment and 6.21 (0.83-41) ng/mL in patients with indeterminate response. In the long-term follow-up of the patients, based on the third year treatment response data, chi-square analysis was performed to evaluate the two groups in terms of treatment responses, and no statistically significant relationship was found (p=0.73).

Discussion

The ATA 2015 guideline does not recommend routine RAI ablation in low-risk thyroid cancer patients but recommends the application of low-activity RAI if ablation is required. Similarly, there are multiple studies that have shown that a low activity of RAI is as effective as a high activity for thyroid remnant ablation in low- and intermediate-risk patients. However, due to changes in definitions of response to treatment and patient selection criteria, the rate of ablation success may differ between these studies.

In this study, we found that 85 out of 100 patients with low-risk DTC showed excellent response to treatment 1 year after RAI treatment. Similarly, in a single-center randomized study by Dong et al. (10), it was found that RAI ablation was successful at 6 months after RAI in 412 of the 474 (87.5%) low-intermediate risk patients. In the same study, it was reported that the successful ablation rates between the patients who received high- and low-activity RAI were similar (87.5% vs. 86.5%; respectively). Comparably, in another study that included 34 patients by Yasmin et al. (11), it was reported that no statistically significant difference concerning the treatment response was found between high- and low-activity RAI receiving patients at 1 year after RAI treatment [82% vs. 76%, respectively (p=0.671)]. As opposed to these studies, in the present study, there was a statistically significant difference between the two groups 1 year after RAI treatment. In this study, the successful ablation rates 1 year after treatment were 94.5% at low- and 74% at high-activity RAI receive patients (p=0.004). This variability among these past studies and this study could be due to different study populations and different definitions of treatment response. In the Mann-Whitney U test performed to investigate the parameters that may be effective in the significant difference in treatment responses in the current study, only the preablative serum Tg value was shown to have a significant difference between the two groups (p=0.01); and tumor size, patient age, preablative anti-Tg levels were found to be not statistically significant factors (p=0.083; 0.38; 0.80; respectively).

In the present study, the mean preablative serum Tg value was 2.14 (0.04-85.55) ng/mL in patients with excellent response at 1st year after treatment and 6.21 (0.83-41) ng/mL in patients with indeterminate response. In a different study by Ha et al. (12), it was reported that 121 of 176 (68.8%) patients with low-risk DTC had successful ablation after receiving low-activity RAI. Although the successful ablation rate was lower in the study by Ha et al. (12), it was also discovered similarly to our study that the pre-ablative serum Tg levels were the only independent factor related to the treatment response (1.2±2.3 ng/mL in successful, vs. 6.2±15.2 ng/mL in unsuccessful ablation, p=0.027).

In two major open-label, randomized, controlled trials, there was no statistically significant correlation found between high- and low-activity RAI receiving low-intermediate risk patients, considering the treatment response in long-term follow-up. In the HiLo study including 434 patients by Dehbi et al. (13), the successful ablation rates were similar between the high- and low-activity RAI groups at 3-5 years after treatment (98.5% vs. 97.9% at 3 years and 97.9% vs. 97.3% at 5 years after RAI, respectively). Likewise, in the ESTIMABL1 study including 752 patients by Schlumberger et al. (14), 98% of the low-risk DTC patients had excellent response to treatment at 5 years after RAI. Of the 11 patients who showed evidence of disease 5 years after RAI, 5 had previously received high-activity and 6 had received low-activity RAI treatment. Similar to these studies, in this study, no statistically significant difference was found

between the high- and low-activity RAI groups at 3 years after treatment (98% vs. 87%, respectively, p=0.73).

Study Limitations

The limitations of this study were the retrospective design, limited number of patients, and relatively short follow-up time of 3 years. As previously stated, DTC is a disease that can progress over a long period of time. Thus, extending this period may have some positive impacts on patient outcome.

Conclusion

In conclusion, although the data obtained in our study revealed that there was a statistically significant difference between the high- and low-activity RAI groups at the end of the first year, there was no statistically significant difference in long-term follow-up. Therefore, considering the unwanted effects of high-activity RAI treatment such as side effects, cost increase, and secondary malignancy, ablation with 30-50 mCi can be safely applied in DTC patients who are in the ATA 2015 low-risk group and are planned for RAI ablation treatment.

Ethics

Ethics Committee Approval: University of Health Sciences Turkey, Prof. Dr. Cemil Taşcıoğlu City Hospital Ethics Committee approval was obtained on 09.05.2022 with decision number 147 for this clinical study, which was designed retrospectively.

Informed Consent: All patients signed written informed consent.

Peer-review: Externally peer-reviewed.

Authorship Contributions

Surgical and Medical Practices: S.K., S.S.K., Concept: S.K., Design: T.Ö., Data Collection or Processing: S.S., G.B.B., Analysis or Interpretation: O.G., Literature Search: S.E., Writing: S.S.

Conflict of Interest: No conflict of interest was declared by the authors.

Financial Disclosure: The authors declared that this study has received no financial support.

References

1. Stewart B, Wild CP: World cancer report 2014. World: 2015. http://publications.iarc.fr/Non-Series-Publications/World-Cancer-Reports/World-Cancer- Report-2014
2. Dal Maso L, Tavilla A, Pacini F, Serraino D, van Dijk BAC, Chirlaque MD, Capocaccia R, Larrañaga N, Colonna M, Agius D, Ardanaz E, Rubió-Casadevall J, Kowalska A, Virdone S, Mallone S, Amash H, De Angelis R; EUROCARE-5 Working Group. Survival of 86,690 patients with thyroid cancer: a population-based study in 29 European countries from EUROCARE-5. Eur J Cancer 2017;77:140-152.
3. Haugen BR, Alexander EK, Bible KC, Doherty GM, Mandel SJ, Nikiforov YE, Pacini F, Randolph GW, Sawka AM, Schlumberger M, Schuff KG, Sherman SI, Sosa JA, Steward DL, Tuttle RM, Wartofsky L. 2015 American Thyroid Association Management Guidelines for Adult Patients with Thyroid Nodules and Differentiated Thyroid Cancer: The American Thyroid Association Guidelines Task Force on Thyroid Nodules and Differentiated Thyroid Cancer. Thyroid 2016;26:1-133.
4. Rosario PW, Mineiro Filho AF, Prates BS, Silva LC, Calsolari MR. Postoperative stimulated thyroglobulin of less than 1 ng/ml as a criterion to spare low-risk patients with papillary thyroid cancer from radioactive iodine ablation. Thyroid 2012;22:1140-1143.
5. Soyluk O, Boztepe H, Aral F, Alagol F, Özbey NC. Papillary thyroid carcinoma patients assessed to be at low or intermediary risk after primary treatment are at greater risk of long term recurrence if they are thyroglobulin antibody positive or do not have distinctly low thyroglobulin at initial assessment. Thyroid 2011;21:1301-1308.
6. Tuttle RM, Tala H, Shah J, Leboeuf R, Ghossein R, Gonen M, Brokhin M, Omry G, Fagin JA, Shaha A. Estimating risk of recurrence in differentiated thyroid cancer after total thyroidectomy and radioactive iodine remnant ablation: using response to therapy variables to modify the initial risk estimates predicted by the new American Thyroid Association staging system. Thyroid 2010;20:1341-1349.
7. Pelttari H, Välimäki MJ, Löyttyniemi E, Schalin-Jäntti C. Post-ablative serum thyroglobulin is an independent predictor of recurrence in low-risk differentiated thyroid carcinoma: a 16-year follow-up study. Eur J Endocrinol 2010;163:757-763.
8. Iyer NG, Morris LG, Tuttle RM, Shaha AR, Ganly I. Rising incidence of second cancers in patients with low-risk (T1N0) thyroid cancer who receive radioactive iodine therapy. Cancer 2011;117:4439-4446.
9. Haymart MR, Banerjee M, Stewart AK, Koenig RJ, Birkmeyer JD, Griggs JJ. Use of radioactive iodine for thyroid cancer. JAMA 2011;306:721-728.
10. Dong P, Wang L, Qu Y, Huang R, Li L. Low - and high-dose radioiodine ablation for low-/intermediate-risk differentiated thyroid cancer in China: large randomized clinical trial. Head Neck 2021;43:1311-1320.
11. Yasmin T, Adnan S, Younis MN, Fatima A, Shahid A. Comparing high and low-dose radio-iodine therapy in thyroid remnant ablation among intermediate and low-risk papillary thyroid carcinoma patients-single centre experience. Dose Response 2021;19:15593258211062775.
12. Ha S, Oh SW, Kim YK, Koo do H, Jung YH, Yi KH, Chung JK. Clinical Outcome of remnant thyroid ablation with low dose radioiodine in korean patients with low to intermediate-risk thyroid cancer. J Korean Med Sci 2015;30:876-881.
13. Dehbi HM, Mallick U, Wadsley J, Newbold K, Harmer C, Hackshaw A. Recurrence after low-dose radioiodine ablation and recombinant human thyroid-stimulating hormone for differentiated thyroid cancer (HiLo): long-term results of an open-label, non-inferiority randomised controlled trial. Lancet Diabetes Endocrinol 2019;7:44-51.
14. Schlumberger M, Leboulleux S, Catargi B, Deandreis D, Zerdoud S, Bardet S, Rusu D, Godbert Y, Buffet C, Schvartz C, Vera P, Morel O, Benisvy D, Bournaud C, Toubert ME, Kelly A, Benhamou E, Borget I. Outcome after ablation in patients with low-risk thyroid cancer (ESTIMABL1): 5-year follow-up results of a randomised, phase 3, equivalence trial. Lancet Diabetes Endocrinol 2018;6:618-626.

Original Article
Mol Imaging Radionucl Ther 2023;32:117-122 DOI:10.4274/mirt.galenos.2021.65902

Gastric Emptying Scintigraphy: Diagnostic Value of Delayed Imaging and the Impact on Reclassification of Diagnosis

Mide Boşalma Sintigrafisi: Gecikmiş Görüntülemenin Tanısal Değeri ve Tanının Yeniden Sınıflandırılmasına Etkisi

Mohsen Qutbi[1], Reyhane Ahmadi[2], Elinaz Hosseinzadeh[1], Ali Asadi[1]

[1]Department of Nuclear Medicine, Taleghani Hospital Clinical Research Development Unit, School of Medicine, Shahid Beheshti University of Medical Sciences, Tehran, Iran
[2]Department of Nuclear Medicine and Molecular Imaging, Farshchian Heart Center, School of Medicine, Hamadan University of Medical Sciences, Hamadan, Iran

Abstract

Objectives: To investigate the added diagnostic value of delayed imaging at 3 and 4 h compared to 2 h imaging as well as scanning up to 4 h compared to 3, and by this means, diagnosis reclassification or changes in diagnosis across various time points.

Methods: Seventeen patients clinically suspected of gastroparesis, 8 (47.1%) men and 9 (52.9%) women, according to the standard procedural guidelines, underwent gastric emptying scintigraphy after ingesting a standard meal. One-minute static images in anterior and posterior projections were acquired immediately after ingestion and then at 1-, 2-, 3- , and 4 h time points. For image analysis, a manual region-of-interest was drawn, and then, count of stomach in each projection was used to calculate geometric mean for each time point. Decay correction was applied. At 2-, 3- and 4 h time points, percentage of retained activity was compared to standard values; therefore, each patient was labeled as normal or delayed.

Results: Pairwise correlation between time points was statistically significant. Value of hour 3 shows an extremely strong correlation with the value of hour 4 ($r=0.951$, $p<0.001$). In hour 2, of 17 participants, 11 (64.7%) were diagnosed as normal and 6 (35.3%) as delayed. In hour 3, the diagnosis made as delayed rose to 9 (52.9%), whereas normal was 8 (47.1%). Finally, in hour 4, results were 10 (58.8%) as delayed and 7 (41.2%) as normal. All subjects who were labeled as delayed in hour 3 remained with the same diagnosis and 1 out of 8 subjects categorized as normal in hour 3 changed to delayed. For testing agreement, coefficient of kappa was computed between each pair. Agreement between diagnosis in hour 2 with hours 3 or 4 was not strong (kappa <0.6 for both pairs). However, a strong agreement was found between diagnosis in hours 3 and 4 (kappa: 0.881).

Conclusion: Because of excellent correlation between values of hours 3 and 4 and strong agreement between the diagnosis in those time points, extending acquisition from 3 to 4 h adds little to the final diagnosis and may not be noticeably meaningful, especially in the clinical setting.

Keywords: Gastric emptying scintigraphy, delayed imaging, diagnostic value, reclassification of diagnosis

Öz

Amaç: İkinci saatteki görüntülemeye kıyasla üçüncü ve dördüncü saatteki gecikmeli görüntülemenin ve üçüncü saatteki görüntülemeye kıyasla dördüncü saatteki görüntülemenin tanıya katkısını araştırarak bu sayede tanının yeniden sınıflandırılmasını veya çeşitli zaman noktalarında tanıdaki değişikliklerin tespit edilmesi.

Address for Correspondence: Asst. Prof. Mohsen Qutbi, Department of Nuclear Medicine, Taleghani Hospital Clinical Research Development Unit, School of Medicine, Shahid Beheshti University of Medical Sciences, Tehran, Iran
Phone: +0982123031250 **E-mail:** mohsen.qutbi@gmail.com ORCID ID: orcid.org/0000-0002-8347-605X
Received: 15.06.2021 **Accepted:** 15.10.2021

Yöntem: Standart prosedür kılavuzlarına göre klinik olarak gastroparezi şüphesi olan 8'i (%47,1) erkek ve 9'u (%52,9) kadın 17 hastaya, standart bir yemek yedikten sonra mide boşalma sintigrafisi uygulandı. Anterior ve posterior projeksiyonlardaki bir dakikalık statik görüntüler, yemek yedikten hemen sonra ve ardından 1-, 2-, 3- ve 4 saatlik zaman noktalarında elde edildi. Görüntü analizi için, manuel bir ilgi bölgesi çizildi ve ardından, her bir zaman noktası için geometrik ortalamayı hesaplamak için her projeksiyondaki mide sayısı kullanıldı. Parçalanma düzeltilmesi uygulandı. 2-, 3- ve 4 saatlik zaman noktalarında tutulan aktivite yüzdesi standart değerlerle karşılaştırıldı; bunun için, her hasta normal veya gecikmiş olarak etiketlendi.

Bulgular: Zaman noktaları arasındaki ikili korelasyon istatistiksel olarak anlamlıydı. Üçüncü saat değeri 4. saat değeri ile son derece güçlü bir korelasyon göstermekteydi (r=0,951, p<0,001). İkinci saatte 17 katılımcının 11'i (%64,7) normal, 6'sı (%35,3) gecikmiş olarak teşhis edildi. Üçüncü saatte gecikmiş tanı 9'a (%52,9), normal tanı ise 8'e (%47,1) çıktı. Son olarak, 4. saatte katılımcıların 10'u (%58,8) gecikmiş ve 7'si (%41,2) normal olarak teşhis edildi. Üçüncü saatte gecikmiş olarak etiketlenen tüm denekler aynı teşhiste kaldı ve 3. saatte normal olarak sınıflandırılan 8 kişiden 1'i teşhisi gecikmiş olarak değişti. Uyumu test etmek için, her çift arasında kappa kat sayısı hesaplandı. İkinci saatteki tanı ile 3. veya 4. saatteki tanı arasındaki uyum güçlü değildi (her iki çift için kappa <0,6). Ancak 3. ve 4. saatlerdeki tanı arasında güçlü bir uyum bulundu (kappa: 0,881).

Sonuç: Üçüncü ve dördüncü saat değerleri arasındaki mükemmel korelasyon ve bu zaman noktalarındaki tanılar arasındaki güçlü uyum nedeniyle, görüntülemeyi 3. saatten 4. saate uzatmak nihai tanıya çok az katkıda bulunur ve özellikle klinik uygulamada anlamlı bir etkisi olmayabilir.

Anahtar kelimeler: Mide boşalma sintigrafisi, gecikmiş görüntüleme, tanı değeri, tanının yeniden sınıflandırılması

Introduction

Gastric emptying scintigraphy (GES) is currently the standard and validated method to non-invasively evaluate patients suspected of gastroparesis. This method enables us to quantitatively measure the speed and timing of the emptying function of the stomach (1). Because of the high reliability and reproducibility of GES (1), it helps monitor patients on serial imaging in addition to its role in making the initial diagnosis. The American Neurogastroenterology and Motility Society and the Society of Nuclear Medicine have published consensus recommendations to help health professionals apply standardized protocols of performance and interpretation of GES across the world. Accordingly, imaging at several time points, including 0, 1, 2, 3, and 4 h after ingestion of a low-fat eggwhite meal is recommended as a solution to maximize the sensitivity of the test (2,3). However, there is some uncertainty about the compliance and adherence of nuclear medicine laboratories to follow these guidelines (4). One such issue is the time points at which the images should be acquired. Some centers only perform imaging up to hour 2 post-ingestion, but others extend the duration of imaging to 4 h. There are a number of investigations that have found the superiority of delayed imaging (5,6,7,8). The extent to which delayed imaging, i.e., in 3 and 4 h, improves the diagnostic power of GES is yet to be elucidated. Additionally, the percentage of patients in whom the diagnosis is changed between consecutive time points and the added value of extending the scanning time is almost unknown. In this study, it is intended to investigate the added diagnostic value of delayed imaging at 3 and 4 h and thereby the changes in diagnosis from one time point to another.

Materials and Methods

Study Subjects

Seventeen patients clinically suspected of gastroparesis were referred by a referral gastroenterology center to our laboratory for GES for further evaluation of gastrointestinal symptoms, of whom 8 (47.1%) were male and 9 (52.9%) were female with a mean age of 49.3±21.1, from 15 to 77. All patients were initially examined clinically for their complaints and a thorough pertinent history was taken including prior esophageal and gastric surgeries, current prokinetic medications (metoclopramide, domperidone, etc.) and history of reflux or other esophageal problems. Patients who underwent recent upper endoscopic procedures were excluded from the study. Informed consent was obtained from all participants and the study has been approved by the Affairs-Shahid Beheshti University of Medical Sciences Ethics Committee (approval no: IR.SBMU.RETECH.REC.1402.058, date: 16.04.2023).

Patient Preparation and Study Procedure

According to the standard procedural guidelines and consensus recommendations for performing and interpreting GES, all patients were advised to keep a 4 h period of fasting before imaging and to discontinue taking any prokinetic or anti-motility medications for at least 2 days. Also, blood testing was performed for all participants to measure serum glucose using a glucometer shortly before initiation of the procedure. Those with serum glucose higher than 200-250 mg/dL were excluded. Patients were also asked to abstain from smoking from a few hours before until the end of study. Each patient was provided a standard meal containing the white of 4 eggs, two slices of toasted bread and 30 g or a spoonful of jam and then mixed with 18-20 MBq of Tc-99m-sulfur colloid

cooked in an oven until being firm and patients were instructed to eat the meal, prepared as a small sandwich, within 10 min. Each patient was also given a glass of water (about 200 mL) to help them swallow their meal. Immediately after ingestion of meal, for each patient, 1 min static images (matrix size of 128x128) in anterior and posterior projections of the trunk were acquired (as time 0) using a single-headed gamma camera in an upright position, in a way that their body touched the detector surface. Acquisition was repeated at 1-, 2-, 3- and 4-hour time points post-ingestion for all participants with the same protocol (1,3,4). Patients who were experiencing episodes of vomiting during the procedure were excluded from the study as well. Besides, the process of meal ingestion by patients was monitored uninterruptedly to ensure that the meal was ingested sufficiently. Participants were requested to avoid intense physical activity for usual daily movement.

Image Analysis and Gastric Emptying Calculation

Before analyzing images, all were inspected for quality to ensure that no esophageal reflux or overlapping of the intestinal loop containing radioactivity in the stomach existed. Then, in each projection, a region-of-interest is manually drawn around the stomach (Figure 1). Care was taken not to include interfering intestinal activity. The count of the stomach in each projection was determined. For each time point, the geometric mean was calculated by the following formula: squared root of the product of counts of anterior and posterior projections. For 1-, 2-, 3- and 4 h time points, decay correction was employed using coefficients from the physical decay table of Tc-99m (fraction remaining after 1, 2, 3 and 4 h are 0.891, 0.794, 0.708 and 0.631 respectively) (9). Decay-corrected geometric mean of each time point was divided by that of time 0 so that the percentage of the activity retained in the stomach was computed. At 2-, 3- and 4-hour time points, the percentage of retained activity was compared to standard or reference values (values higher than 90%, 60%, 30% and 10% at 1-, 2-, 3- and 4-hours post-ingestion respectively are considered abnormal) and therefore were labeled dichotomously as normal or abnormal (delayed). The images and the pattern of emptying or approximate curve was observed to ensure proper labeling.

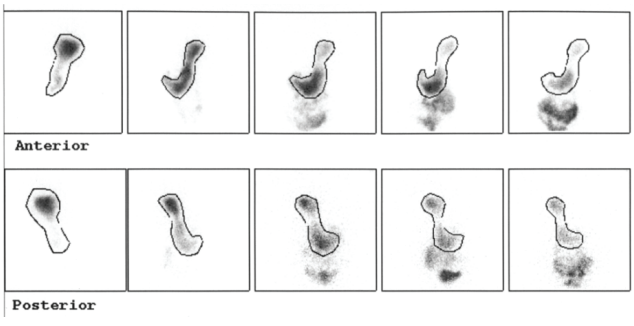

Figure 1. Planar images in anterior and posterior projections at five time points: 0 (immediately after ingestion), 1, 2, 3 h. Regions of interest of the stomach are manually drawn in a way that no other interfering activity gets included in it. Upper and lower rows demonstrate anterior and posterior projections, respectively, from left (hour 0) to right (hour 4)

Statistical Analysis

Mean and standard deviation, median, and quartiles of the percentages retained in the stomach at five time points (0, 1, 2, 3, and 4) were calculated. Error bar plot and box plot were used to display the results. Pairwise correlation testing was conducted between various time points, and Pearson's correlation coefficient was computed and graphed in matrix scatterplot. To compare diagnosis (labeled as normal or delayed) at 2-, 3-, and 4 h time points, an agreement test was employed between pairs and the kappa coefficient was computed. All statistical analyses were conducted and graphs were plotted in the SPSS software package (version 24), and a significance level of 0.05 was considered.

Results

Mean and standard deviation, median, and quartiles of the percentages retained in the stomach at each time point are summarized in Table 1. These values are graphically displayed in the error bar plot and box plot in Figure 2. Pairwise correlations between time points were statistically significant and are presented in Table 2. The value at hour 1 is strongly correlated with that at hour 2 but weak to moderate to those at hours 3 and 4. The value of hour 3 shows an extremely strong correlation with the value of hour 4 ($r=0.951$, $p<0.001$). The correlation coefficients of hour 2 are also moderate to strong with hours 3 and 4. Figure 3 presents the matrix scatterplot. Figure 4 depicts a stacked bar chart for diagnosis at different time points. Diagnosis was determined based on comparison with reference values recommended by standard guidelines. In hour 2 of 17 participants, 11 (64.7%) were diagnosed as normal and 6 (35.3%) as delayed. In hour 3, the diagnosis

Table 1. Values of mean, median, and quantiles of the percentage retained in the stomach at 4 time points

Time point	Mean (SD)	Median	Quartiles		
			25	50	75
Hour 1	75.36 (11.84)	78.00	64.50	78.00	85.00
Hour 2	50.05 (18.42)	56.00	33.00	56.00	67.00
Hour 3	31.28 (20.98)	34.00	8.25	34.00	48.50
Hour 4	21.62 (19.33)	17.00	3.35	17.00	38.75

SD: Standard deviation

Table 2. Results of correlation testing between pairs of time points			
Pairwise correlation between variables		**Correlation coefficient**	**p value**
Hour 1	Hour 2	0.797	0.000
	Hour 3	0.569	0.017
	Hour 4	0.569	0.017
Hour 2	Hour 3	0.756	0.000
	Hour 4	0.727	0.001
Hour 3	Hour 4	0.951	0.000

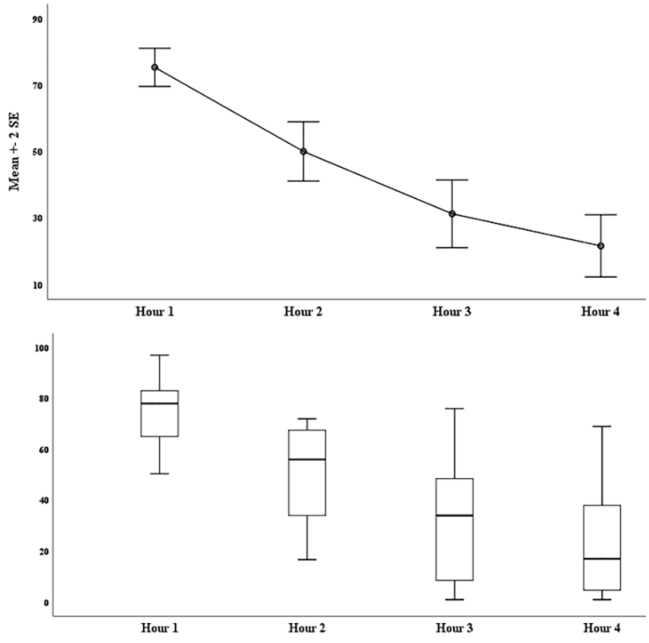

Figure 2. Error bar plot and box plot of the amount of retained activity in the stomach at various time points. The line connecting the means or medians seems to be fitted to an exponential curve

made as delayed rose to 9 (52.9%), whereas the normal was 8 (47.1%). Finally, at hour 4, the results were 10 (58.8%) as delayed and 7 (41.2%) as normal. As can be seen in Table 3, from the 2 h to 3 h time point, 4 subjects who were normal were rediagnosed as delayed and vice versa, and one subject who was delayed in hour 2 was reclassified as normal. All subjects who were labeled as delayed in hour 3 remained with the same diagnosis and 1 out of 8 subjects categorized as normal in hour 3 changed to delayed. For testing agreement, the coefficient of kappa was computed between each pair. The agreement between diagnosis in hour 2 and hours 3 or 4 was not strong (kappa <0.6 for both pairs). However, a strong agreement was found between diagnosis in hours 3 and 4 (kappa: 0.881) (Table 4).

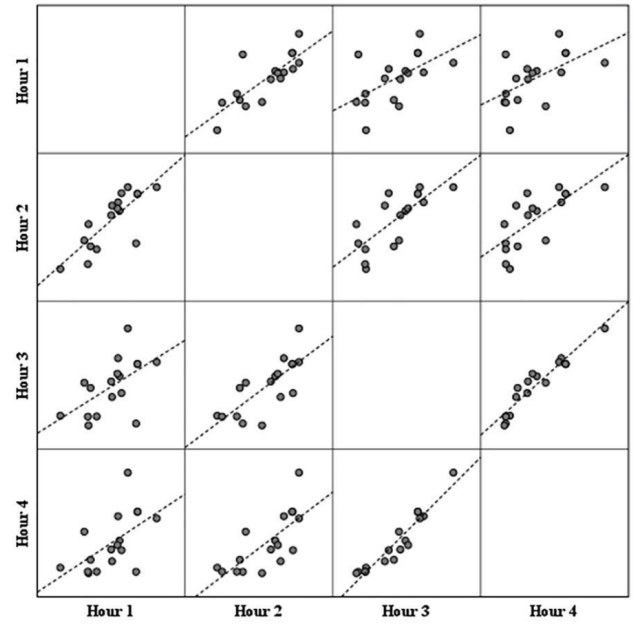

Figure 3. Matrix scatterplot of pairs at various time points. Pairs of hours 3 and 4 show the strongest correlation.

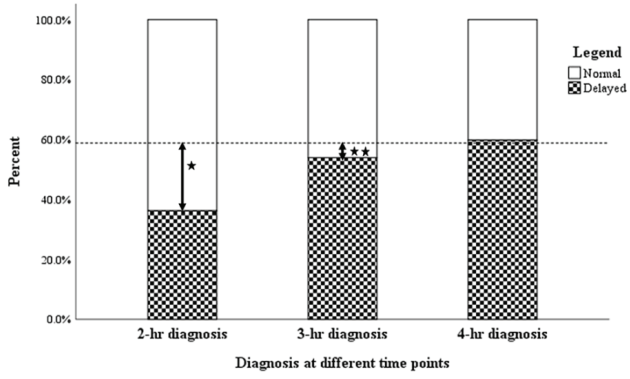

Figure 4. Stacked bar chart for diagnosis at time points of 2, 3 and 4 h. The dotted horizontal line represents the percentage of patients diagnosed as delayed (patterned part of the bar). As can be seen, the difference between hours 2 and 4 (shown by asterisk) is noticeable compared to that between hours 3 and 4 (shown by double asterisk), in which the difference is negligible

Discussion

GES as a useful tool for non-invasive evaluation of the physiology of the stomach still need to be standardized in performance of the procedure and interpretation. Several mathematical methods for measuring the emptying rate of the stomach have been proposed. Some methods derive parameters from a dynamic image continuously acquired from ingestion up to a desired time, for example, 1 or 2 h. Other methods employ static images obtained at various

Table 3. Reclassification of the diagnosis of subjects from hour 2 to hours 3 and 4 and from hour 3 to hour 4

Initial diagnosis at each time point			Reclassification of diagnosis the following time extension			
			To 3 h		To 4 h	
Time point	Diagnosis	Number (%)	Diagnosis	Number (%)	Diagnosis	Number (%)
Diagnosis at hour 2	Normal	11 (64.7%)	Normal	7 (63.6%)	Normal	7 (63.6%)
			Delayed	4 (36.4%)	Delayed	4 (36.4%)
	Delayed	6 (35.3%)	Normal	1 (16.7%)	Normal	0 (0.0%)
			Delayed	5 (83.3%)	Delayed	6 (100%)
Diagnosis at hour 3	Normal	8 (47.1%)	N/A	N/A	Normal	7 (87.5%)
			N/A	N/A	Delayed	1 (12.5%)
	Delayed	9 (52.9%)	N/A	N/A	Normal	0 (0.0%)
			N/A	N/A	Delayed	9 (100%)

N/A: Not applicable

Table 4. Results of the agreement test between diagnosis at different pairs of time points

The test of agreement between variables pairwise		Kappa coefficient	p value
2 hr diagnosis	3 hr diagnosis	0.422	0.064
	4 hr diagnosis	0.553	0.011
3 hr diagnosis	4 hr diagnosis	0.881	0.000

time points and provide parameters different from the former. Each has its own advantages and disadvantages (2,3,10,11). The method that is used more commonly in clinical settings and is recommended by consensus guidelines is imaging at 1 h intervals up to 4 h to maximize the sensitivity. Although the lag phase and emptying half-time cannon be computed, this method is sufficiently reliable and easy to perform in imaging centers. It has been shown that delayed imaging improves the diagnostic accuracy of GES and finds patients with delayed emptying whose scan up to 2 h is indicated as a normal result. However, to what extent the imaging in 4 h compared to 3 h scanning improves the diagnostic accuracy and what percentage of patients would benefit from is still under debate. In other words, it is less known how much extending the scanning up to 4 h outweighs and prevails over the one up to 3 h. In our study, correlation testing showed that consecutive time points were well correlated. Particularly, pairs of 3 and 4 h depicted an excellent correlation (r=0.951). Additionally, based on dichotomous diagnosis (normal versus delayed), a strong agreement was found between the diagnosis in hour 3 compared to hour 4. According to the results presented in Table 3, in patients whose diagnosis was normal in hour 3, 12.5% changed to delayed and likewise, in those with diagnosis labeled as delay in hour 3, none reclassified in terms of diagnosis. We think that the difference between scanning up to 3 h in comparison to 4 h adds little to the final diagnosis and may not be noticeably meaningful, especially in clinical practice. Our study results agreed with previous investigations (5,6,7,8). However, we emphasized and focused our attention on the respective difference between numerical results and diagnosis in hours 3 and 4, contrary to previous research that investigated the difference between hours 2 and 4 (5,6,7,8). Another point worth noting is that making a diagnosis based on numbers or numerical values may lead to false-positive and false-negative results. Visual interpretation to recognize the pattern ought to be used as an adjunct to quantitative analysis to maximize the accuracy of GES (12). We are aware that the number of participants in our study was, to some degree, low and this may affect the conclusion, particularly in calculating the percentages of patients with reclassification of diagnosis. An innate shortcoming of such quantitative methods and comparing the results of each time point with constant reference values may lead to discordant results with the physician's clinical suspicion and impression.

Study Limitations

One of the limitations of our study is that the clinical data of the participants were excluded from the analysis and the interpretation was only the results of scans, although the patients who were clinically suspected of gastroparesis were included. Another issue is the number of subjects enrolled in the study, which might affect the results.

Conclusion

Because of excellent correlation between values of hours 3 and 4 and strong agreement between the diagnosis in those time points, extending acquisition from 3 to 4 h

adds little to final diagnosis and may not be noticeably meaningful, especially in the clinical setting with high throughput.

Ethics

Ethics Committee Approval: Affairs-Shahid Beheshti University of Medical Sciences Ethics Committee (approval no: IR.SBMU.RETECH.REC.1402.058, date: 16.04.2023).

Informed Consent: Informed consent was obtained from all participants.

Peer-review: Externally and internally peer-reviewed.

Authorship Contributions

Concept: M.Q., A.A., Design: M.Q., E.H., R.A., Data Collection or Processing: M.Q., R.A., Analysis or Interpretation: M.Q., E.H., R.A. A.A., Literature Search: E.H., R.A., Writing: M.Q., E.H., R.A. A.A.

Conflict of Interest: No conflict of interest was declared by the authors.

Financial Disclosure: Mohsen Qutbi receives a grant with partial financial support from Taleghani Educational Hospital, School of Medicine, Shahid Beheshti University of Medical Sciences. Reyhane Ahmadi, Elinaz Hosseinzadeh, and Ali Asadi have nothing to disclose regarding funding.

References

1. Donohoe KJ, Maurer AH, Ziessman HA, Urbain JL, Royal HD, Martin-Comin J; Society for Nuclear Medicine; American Neurogastroenterology and Motility Society. Procedure guideline for adult solid-meal gastric-emptying study 3.0. J Nucl Med Technol 2009;37:196-200.
2. Abell TL, Camilleri M, Donohoe K, Hasler WL, Lin HC, Maurer AH, McCallum RW, Nowak T, Nusynowitz ML, Parkman HP, Shreve P, Szarka LA, Snape WJ Jr, Ziessman HA; American Neurogastroenterology and Motility Society and the Society of Nuclear Medicine. Consensus recommendations for gastric emptying scintigraphy: a joint report of the American Neurogastroenterology and Motility Society and the Society of Nuclear Medicine. J Nucl Med Technol 2008;36:44-54.
3. Abell TL, Camilleri M, Donohoe K, Hasler WL, Lin HC, Maurer AH, McCallum RW, Nowak T, Nusynowitz ML, Parkman HP, Shreve P, Szarka LA, Snape WJ Jr, Ziessman HA; American Neurogastroenterology and Motility Society and the Society of Nuclear Medicine. Consensus recommendations for gastric emptying scintigraphy: a joint report of the American Neurogastroenterology and Motility Society and the Society of Nuclear Medicine. Am J Gastroenterol 2008;103:753-763.
4. Farrell MB, Costello M, McKee JD, Gordon LL, Fig LM. Compliance with gastric-emptying scintigraphy guidelines: an analysis of the intersocietal accreditation commission database. J Nucl Med Technol 2017;45:6-13.
5. Guo JP, Maurer AH, Fisher RS, Parkman HP. Extending gastric emptying scintigraphy from two to four hours detects more patients with gastroparesis. Dig Dis Sci 2001;46:24-29.
6. Pathikonda M, Sachdeva P, Malhotra N, Fisher RS, Maurer AH, Parkman HP. Gastric emptying scintigraphy: is four hours necessary? J Clin Gastroenterol 2012;46:209-215.
7. Chogle A, Saps M. Gastroparesis in children: the benefit of conducting 4-hour scintigraphic gastric-emptying studies. J Pediatr Gastroenterol Nutr 2013;56:439-442.
8. Alipour Z, Khatib F, Tabib SM, Javadi H, Jafari E, Aghaghazvini L, Mahmoud-Pashazadeh A, Nabipour I, Assadi M. Assessment of the prevalence of diabetic gastroparesis and validation of gastric emptying scintigraphy for diagnosis. Mol Imaging Radionucl Ther 2017;26:17-23.
9. Ziessman HA, O'Malley JP, Thrall JH. Radiopharmaceuticals. Nuclear Medicine, The Requisites. Philadelphia, PA, Elsevier Saunders, 2014;1-15.
10. Podczeck F, Course NJ, Newton JM. Determination of the gastric emptying of solid dosage forms using gamma-scintigraphy: a problem of image timing and mathematical analysis. Eur J Nucl Med 1999;26:373-378.
11. Camilleri M, Shin A. Novel and validated approaches for gastric emptying scintigraphy in patients with suspected gastroparesis. Dig Dis Sci 2013;58:1813-1815.
12. Ora M, Nazar AH, Parashar A, Kheruka S, Gambhir S. Gastric emptying scintigraphy: beyond numbers - an observational study to differentiate between various etiologies and a step toward personalized management. Indian J Nucl Med 2019;34:194-200.

Original Article
Mol Imaging Radionucl Ther 2023;32:123-130 DOI:10.4274/mirt.galenos.2022.08860

Potential Role of Somatostatin Receptor Scintigraphy for *In Vivo* Imaging of Vulnerable Atherosclerotic Plaques and Its Association with Myocardial Perfusion Imaging Finding: A Preliminary Study

Hassas Aterosklerotik Plakların İn Vivo Görüntülenmesinde Somatostatin Reseptör Sintigrafisinin Potansiyel Rolü ve Bunun Miyokardiyal Perfüzyon Görüntüleme Bulgusu ile İlişkisi: Bir Ön Çalışma

Abdullatif Amini[1], Esmail Jafari[2], Mohammad Reza Pourbehi[1], Dariush Iranpour[1], Reza Nemati[3], Hojjat Ahmadzadehfar[4], Majid Assadi[2]

[1]Bushehr University of Medical Sciences Faculty of Medicine, Bushehr Medical Heart Center, Bushehr, Iran
[2]The Persian Gulf Nuclear Medicine Research Center, Bushehr Medical University Hospital, School of Medicine, Bushehr University of Medical Sciences, Department of Molecular Imaging and Theranostics, Bushehr, Iran
[3]Bushehr University of Medical Sciences, Bushehr Medical University Hospital, Department of Neurology, Bushehr, Iran
[4]Klinikum Westfalen, Department of Nuclear Medicine, Dortmund, Germany

Abstract

Objectives: This study was conducted to detect atherosclerotic plaques with somatostatin receptor scintigraphy (SRS) using Tc-99m-octreotide that binds to somatostatin receptor-2.

Methods: Of the 783 patients referred for myocardial perfusion imaging (MPI), 52 underwent additional chest single-photon emission computed tomography (SPECT) with Tc-99m-octreotide and participated in this study. In addition, 43 patients who underwent Tc-99m-octreotide scan for neuroendocrine tumor (NET) also received cardiac SPECT. Angiography was performed within 1 month after SRS for 19 patients who showed intensive uptake in SRS and had cardiac risk factors.

Results: Of 52 patients who underwent MPI and SRS, 15 showed intensive cardiac uptake in SRS. Moreover, of 43 patients who were referred for NET, 4 patients had marked cardiac uptake in SRS in the heart. Nineteen patients including 12 women and 7 men aged 28 to 84 (58±8.04) years underwent coronary angiography. SRS and angiography in the left anterior descending territory were concordant in 15/19 (79%) patients, whereas only 7/15 (46%) cases had concordant MPI and angiography results. In the right coronary artery territory, SRS and angiography were concordant in 16/19 (84%) cases, while MPI and angiography were concordant in 11/15 (73%) cases. In the left circumflex artery territory, SRS and angiography were concordant in 15/19 (79%) cases, whereas MPI and angiography were concordant in 6/15 (40%) cases. In the remaining 76 patients who did not undergo coronary angiography based on cardiovascular profile and SRS, no cardiac events occurred in a follow-up of 2-11 months (7.52±2.71).

Conclusion: Tc-99m-octreotide uptake was more concordant with coronary plaques relative to MPI findings, suggesting a potential role for Tc-99m-octreotide in the evaluation of atherosclerosis.

Keywords: Tc-99m-octreotide, somatostatin receptor-2 (SSTR-2), myocardial perfusion scintigraphy, coronary angiography

Address for Correspondence: Prof. Majid Assadi, MD, FASNC, The Persian Gulf Nuclear Medicine Research Center, Bushehr Medical University Hospital, School of Medicine, Bushehr University of Medical Sciences, Department of Molecular Imaging and Theranostics, Bushehr, Iran
Phone: +0098-771-2580169 **E-mail:** asadi@bpums.ac.ir, assadipoya@yahoo.com ORCID ID: orcid.org/0000-0002-2166-3765
Received: 02.05.2022 **Accepted:** 15.08.2022

Öz

Amaç: Bu çalışma, somatostatin reseptör-2'ye bağlanan Tc-99m-oktreotid kullanılarak somatostatin reseptör sintigrafisi (SRS) ile aterosklerotik plakların saptanması amacıyla yapılmıştır.

Yöntem: Miyokardiyal perfüzyon görüntülemesi (MPI) için sevk edilen 783 hastadan 52'sine ek olarak Tc-99m-oktreotid ile göğüs tek foton emisyonlu bilgisayarlı tomografisi (SPECT) uygulandı ve bu hastalar çalışmaya katıldı. Ayrıca, nöroendokrin tümör (NET) için Tc-99m-oktreotid taraması yapılan 43 hastaya da kardiyak SPECT uygulandı. SRS'de yoğun tutulum gösteren ve kardiyak risk faktörü taşıyan 19 hastaya SRS'den sonraki 1 ay içinde anjiyografi yapıldı.

Bulgular: MPI ve SRS uygulanan 52 hastanın 15'inde SRS'de yoğun kardiyak tutulum görüldü. Ayrıca NET için yönlendirilen 43 hastanın 4'ünde kalpte SRS'de belirgin kardiyak tutulum saptandı. Yaşları 28 ile 84 (58±8,04) arasında değişen 12'si kadın, 7'si erkek olmak üzere 19 hastaya koroner anjiyografi yapıldı. SRS ve sol ön inen arter bölgesinde anjiyografi 15/19 (%79) hastada uyumlu iken, sadece 7/15 (%46) hastada uyumlu MPI ve anjiyografi sonuçları vardı. Sağ koroner arter bölgesinde 16/19 (%84) hastada SRS ve anjiyografi, 11/15 (%73) hastada MPI ve anjiyografi uyumluydu. Sol sirkumfleks arter bölgesinde 15/19 (%79) hastada SRS ve anjiyografi, 6/15 (%40) hastada MPI ve anjiyografi uyumluydu. Kardiyovasküler profil ve SRS'ye göre koroner anjiyografi yapılmayan geri kalan 76 hastada 2-11 aylık takipte (7,52±2,71) kardiyak olay gelişmedi.

Sonuç: Miyokardiyal perfüzyon görüntülemesi bulgularına göre Tc-99m-oktreotid alımının koroner plaklarla daha uyumlu olması, aterosklerozun değerlendirilmesinde Tc-99m-oktreotidin potansiyel bir rolü olduğunu düşündürmektedir.

Anahtar kelimeler: Tc-99m-oktreotid, somatostatin reseptör-2 (SSTR-2), miyokardiyal perfüzyon sintigrafisi, koroner anjiyografi

Introduction

Cardiovascular diseases are the main cause of about one-third of deaths in men and women across the world. It is estimated that more than 19 million patients worldwide suffer from cardiovascular disease annually. One common cause of cardiac events is the buildup of fats, cholesterol, and any other compounds in the arterial wall leading to the formation of plaques, known as vulnerable atherosclerotic plaques (VAPs) (1,2).

VAP formation in coronary arteries is one of the common causes of cardiac disease, which can lead to cardiac events and death. These plaques develop gradually and mild plaques usually have no complications. The complications of atherosclerosis start when the artery becomes occluded due to plaque formation, leading to inadequate blood supply to the tissues. A VAP may restrict coronary blood flow leading, leading myocardial infarction and death. A VAP consists of a fine fibrous cap and a vast lipid core, resulting in the accumulation of activated macrophages. The activated macrophages may rupture the VAP, resulting in sudden cardiac events and death. Given the importance of this issue, the detection of early changes in the coronary walls is of enormous importance (3,4). VAP, which is prone to rupture, usually does not cause marked stenosis; therefore, it is not diagnosed by myocardial perfusion imaging (MPI), the procedure commonly used for ischemia evaluation. Many preclinical and clinical studies have been conducted to understand VAP recently (5).

The standard methods for diagnosis of VAP include physical examination, laboratory tests, ankle/brachial index, electrocardiogram, and ultrasound examination, as well as invasive methods including intravascular coronary ultrasound, angiography, and angioscopy (6,7). All these procedures have differences in terms of sensitivity, specificity, availability, and reproducibility. Nowadays, molecular and cellular imaging has made it possible to evaluate early changes in the arterial walls toward VAP formation, opening new windows in detecting VAP in subclinical and clinical stages.

As mentioned earlier, VAPs result in the accumulation of activated macrophages, therefore imaging macrophages can be used as a potential target for the characterization and diagnosis of VAP. It has been indicated that somatostatin receptor-2 (SSTR-2) is overexpressed by activated macrophages (8). Several radiotracers have an affinity for somatostatin receptors, including SSTR-2, and are used for imaging and management of patients with neuroendocrine tumors (NETs) in multiple centers around the world, such as ^{68}Ga-DOTATATE positron emission tomography (PET) and Tc-99m-octreotide single-photon emission computed tomography (SPECT) (9,10,11,12).

The potential role of several radiotracers such as ^{68}Ga-DOTATATE and ^{18}F sodium florine PET in the evaluation of inflammatory processes and detection of VAP has been investigated in several studies (4,13,14,15,16). Therefore, this study was conducted to detect atherosclerotic plaques by somatostatin receptor scintigraphy (SRS) using Tc-99m-octreotide SPECT and to compare SRS with coronary angiography for detection of atherosclerotic plaques and its association with MPI using Tc-99m-MIBI SPECT finding.

Materials and Methods

Study Population

In this study, VAP was evaluated using Tc-99m-octreotide SPECT in the following patients at Bushehr Nuclear Medicine Department:

1. Patients who were referred for MPI were asked to perform an additional Tc-99m-octreotide SPECT for evaluation of VAP within 3 to 7 days following MPI.

2. Patients who were referred for evaluation of NETs by Tc-99m-octreotide and had cardiac risk factors underwent cardiac Tc-99m-octreotide SPECT in addition to the whole-body scan for evaluation of VAP (Figure 1).

A detailed history including age, hypertension, angina, diabetes, hyperlipidemia, smoking, family history of cardiac diseases, obesity and history of cardiac attack was taken from all patients for evaluation of cardiac risk factors. The inclusion criteria were age >18 and the presence of cardiac risk factors. In addition, because of the possibility of false-positive results, patients with a history of interventional coronary therapy such as CABG or stent were excluded from the study. The images were evaluated by nuclear medicine physicians. Patients who showed significant uptake of Tc-99m-octreotide in the heart and had cardiac risk factors were asked to undergo angiography for the evaluation of VAP in coronary arteries. This study was approved by a local ethics committee, and written consent was obtained from all patients before each stage of the study. The Ethical Committee of Bushehr University of Medical Sciences approved this study (IR.BPUMS.REC.1401.175).

Image Acquisition

SPECT Images

Patients fasted overnight and all cardiovascular medications were discontinued at least 2 days before the study. An intravenous line of normal saline solution was connected to the antecubital vein using a 20-gauge cannula. Dipyridamole (0.56 mg/kg) was infused above 4 min. Patients' symptoms and three-lead electrocardiography were monitored continuously. A dose of 740 MBq of Tc-99m-sestamibi as a compact bolus was injected 4 min after the initiation of the infusion. Sixty minutes later, the patients were asked to eat a fatty meal to accelerate hepatobiliary clearance of Tc-99m sestamibi, and imaging was performed 90 min after the initial infusion of dipyridamole. The rest phase was performed next day.

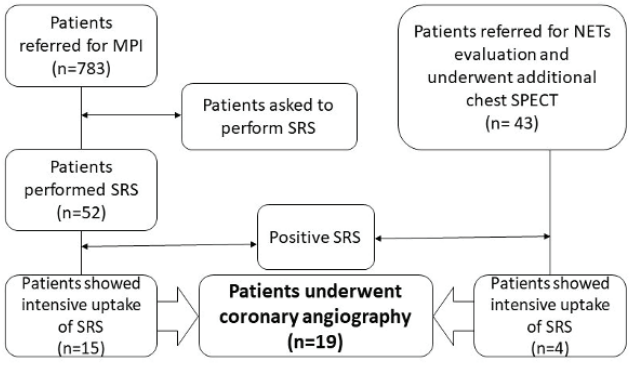

Figure 1. Study design
MPI: Myocardial perfusion imaging, SRS: Somatostatin receptor scintigraphy, NETs: Neuroendocrine tumors, SPECT: Single-photon emission computed tomography

The one-day stress-rest protocol was used for MPI. Patients fasted overnight and all cardiovascular drugs were stopped at least 2 days before the examination. In the stress phase, the patients underwent treadmill testing or pharmacologic stress with the infusion of 0.56 mg/kg dipyridamole over 5 min. Then 370-555 MBq (10-15 mCi) Tc-99m-sestamibi (ParsIsotope Co., Iran) was administered at the peak of stress. SPECT images were acquired 30-45 minutes after stress. Four hours after the stress phase, the rest phase was performed with an injection of 740-925 MBq (20-25 mCi) Tc-99m-sestamibi. SPECT images were acquired 60-90 minutes after the radiotracer injection.

For SRS, 60 to 90 min following injection of 740-925 MBq (20-25 mCi) Tc-99m-octreotide, SPECT imaging of the heart was performed in addition to a whole-body scan.

The scans were acquired using a dual-head gamma camera (ADAC-Pegasys) equipped with a low-energy high-resolution collimator, a 140 keV photopeak with a 20% energy window, and a matrix size of 64x64. The SPECT images were acquired with 32 projections (20 seconds/projection) 180° rotations from RAO to LPO for MPI and with 64 projections (20 seconds/projection) and 360° rotations for SRS. Image reconstruction was performed using the filtered back projection method (Wiener filter; cut-off: 0.66, order: 5). The images were evaluated by a nuclear medicine specialist.

Coronary Angiography

Angiography was performed using the standard Judkins method. A cardiologist who was not aware of the scintigraphic results analyzed the angiograms.

Image Analysis

In this study, a blinded cardiologist evaluated the angiographic data and a blinded nuclear medicine specialist evaluated the scintigraphic data. The coronary arteries are divided into three main arteries, including the left anterior descending (LAD), right coronary artery (RCA), and left circumflex artery (LCx), according to angiographic standards. In scintigraphic images, the left ventricular wall was mapped to the standard 17-segment model.

For MPI, a 17-segment model was used for interpretation. According to this model, the left ventricle was divided into three main coronary arteries. For the evaluation of each segment, changes in radiotracer uptake in stress and rest phases were evaluated. A decreased radiotracer uptake

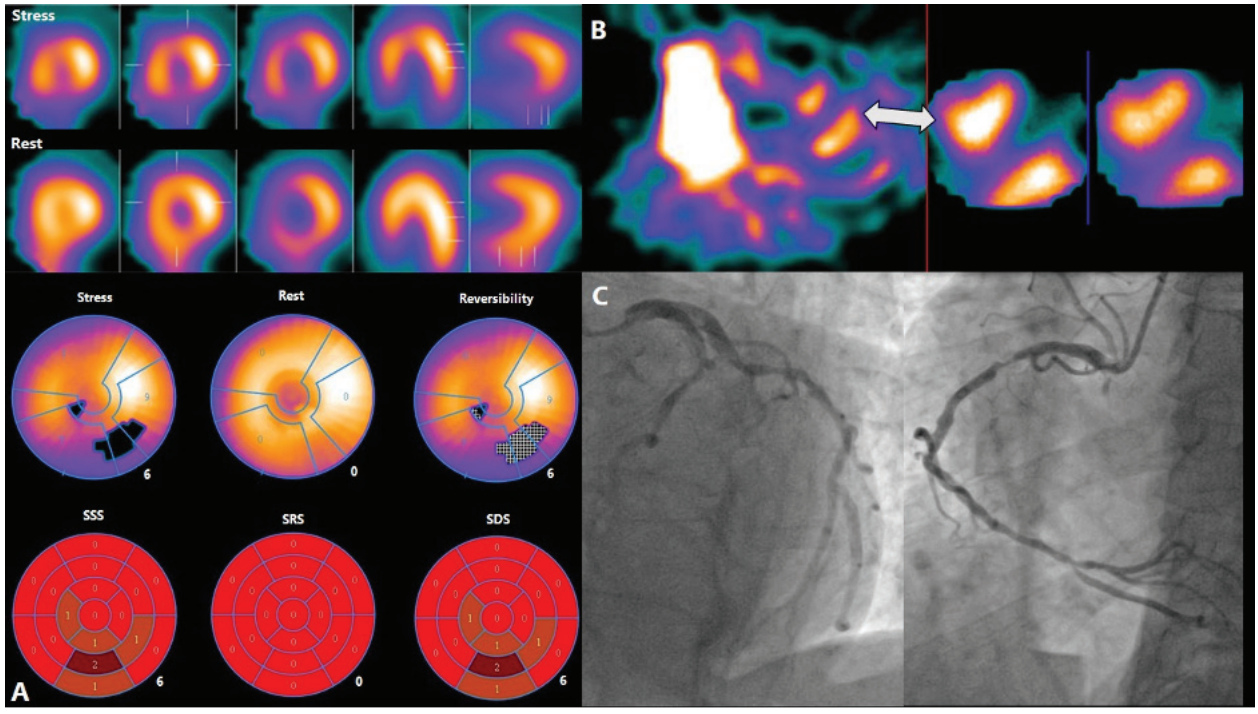

Figure 2. Myocardial perfusion imaging (MPI) single-photon emission computed tomography (SPECT) of a 64-year-old woman with non-specific chest symptoms who was referred from the department of cardiology for assessment of the perioperative risk of ischemic cardiac events. MPI SPECT showed only mild ischemia in the inferoseptal wall (A). Somatostatin receptor scintigraphy using Tc-99m-octreotide SPECT in the same patient showed intense uptake areas in the inferior and anterior regions (B). Coronary angiography showed a severe left anterior descending lesion just after the diagonal branch, cut-off diagonal branch, multiple non-significant plaques in the left circumflex, severe proximal right coronary artery lesion, and a severe lesion of the PDA origin (C)

(defect) observed in the stress phase that improved on rest was considered an ischemic defect, and a stress defect that did not improve was considered a fixed defect. In this study, any myocardial defect observed in the region of interest was considered abnormal.

For SRS, similar to MPI, the left ventricle was mapped into 17 segments and then divided into three main coronary arteries. For interpretation, any marked radiotracer uptake in these 17 regions as compared to background tissue was considered VAP in that region.

Statistical Analysis

Statistical analysis was performed using SPSS software version 21 for Windows. The continuous variables are expressed as median ± standard error of mean.

Results

Of 783 patients with suspected coronary artery disease who presented to Bushehr Nuclear Medicine Department for MPI, 52 consented to perform additional SRS and were included in the final study cohort. In addition, 43 patients who underwent Tc-99m-octreotide scan for NET also underwent cardiac SPECT. In total, 95 cases had cardiac Tc-99m-octreotide SPECT for evaluation of VAP. Of these 95 patients, 19 patients, including 12 women and 7 men aged 28 to 84 (58±8.04) years) who showed marked radiotracer uptake in SRS, underwent coronary angiography. An example of such a case is presented in Figure 2. Four out of 19 patients were NET patients who did not undergo MPI. Angiography was abnormal in all 19 patients, while MPI was normal in one of them. The baseline characteristics of the patients are shown in Table 1.

As for concordance between scintigraphic data and angiography in three main arteries, the results of SRS and angiography were concordant in the LAD territory in 15/19 (79%) patients, while only 7/15 (46%) cases had concordant MPI and angiography results. In the RCA territory, the results of SRS and angiography were concordant in 16/19 (84%) cases, while MPI and angiography results were concordant in 11/15 (73%) cases. In the LCx territory, the results of SRS and angiography were concordant in 15/19 (79%) cases, while MPI and angiography were concordant in 6/15 (40%) cases. Table 2 shows the results in detail. A false positive and false negative case is presented in Figure 3.

Table 1. Baseline characteristics of patients	
	Patients (n=19)
Age (mean ± SD)	58±8.04
Sex (female)	12 (63.2)
Chest pain	8 (42.1%)
Cardiac risk factor	
Hypertension	11 (57.9%)
Diabetes	9 (47.4)
Smoking	7 (36.8%)
Hyperlipidemia	8 (42.1%)
Family history	3 (15.8%)
Obesity	3 (15.8%)
Cardiac attack	3 (15.8%)
SD: Standard deviation	

As for the scintigraphic data, the results of SRS and MPI were concordant in 11/15 (73%), 10/15 (66%), and 10/15 (66%) patients in the LAD, RCA, and LCx territories, respectively (Table 3).

Cardiac events were not observed in a follow-up period of 2-11 months (7.52±2.71) in any of the remaining 76 patients who did not undergo coronary angiography based on the cardiovascular profile. Interestingly, they did not show a remarkable uptake on SRS.

Discussion

This study was conducted to evaluate coronary VAP using SRS and compare it with MPS and angiography for the first time. Several studies have evaluated PET radiotracers

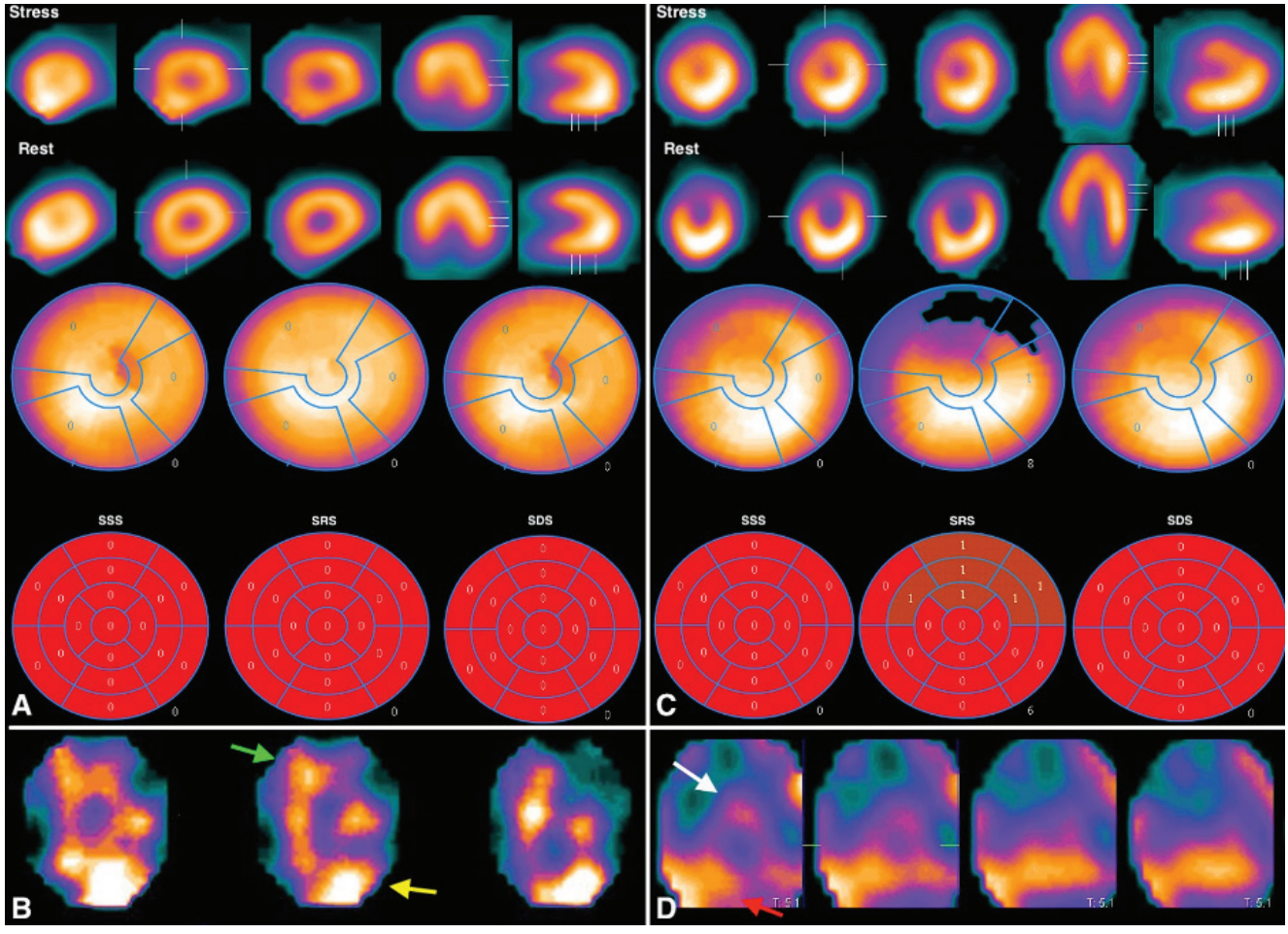

Figure 3. The cardiac examination of a 58-year-old woman presented with normal myocardial perfusion imaging (MPI) (A). Somatostatin receptor scintigraphy (SRS) single-photon emission computed tomography indicated uptake in anteroseptal [left anterior descending (LAD)] (green arrow) and inferior wall [right coronary artery (RCA)] (yellow arrow) (B) but angiography showed LAD lesion and normal RCA resulted in false positive in SRS, which may be due to liver uptake. In another case, cardiac examination of a 64-year-old woman presented with a defect in the anteroseptal wall according to MPI (C). In SRS, only uptake in the anterolateral wall (LAD) (white arrow) was reported and uptakes in the inferior and inferoseptal (RCA) (red arrow) were considered as liver uptake (D), but lesions were observed in both LAD and RCA in coronary angiography, which resulted in false negatives, which may be due to liver uptake

Table 2. Concordance between coronary angiography and SRS and MPI

		Angiography								
		LAD			RCA			LCx		
		Negative	Positive	Concordance	Negative	Positive	Concordance	Negative	Positive	Concordance
SRS	Negative	4	3	15/19 (79%)	5	2	16/19 (84%)	7	0	15/19 (79%)
	Positive	1	11		1	11		4	8	
MPI	Negative	3	7	7/15 (46%)	4	4	11/15 (73%)	4	4	6/15 (40%)
	Positive	1	4		0	7		5	2	

SRS: Somatostatin receptor scintigraphy, MPI: Myocardial perfusion imaging, LAD: Left anterior descending, RCA: Right coronary artery, LCx: Left circumflex artery

Table 3. Concordance between SRS and MPI

		SRS								
		LAD			RCA			LCx		
		Negative	Positive	Concordance	Negative	Positive	Concordance	Negative	Positive	Concordance
MPI	Negative	6	0	11/15 (73%)	4	4	10/15 (66%)	4	4	10/15 (66%)
	Positive	4	5		1	6		1	6	

MPI: Myocardial perfusion imaging, SRS: Somatostatin receptor scintigraphy, LAD: Left anterior descending, RCA: Right coronary artery, LCx: Left circumflex artery

such as ^{68}Ga-DOTATATE, ^{18}F-fluorodeoxyglucos (FDG), and ^{18}F sodium florine for VAP (4,7,15,16,17); however, no study has investigated SPECT radiotracers. We previously reported the role of SRS in a case of myocarditis (18).

It has been shown that about 50% of cardiovascular-related mortality is due to acute myocardial infarction. About 75% of myocardial infarctions are due to an acute thrombotic event because of the rupture of a VAP, and plaque erosion is responsible for the remaining 25% (19). Because of the importance of this subject, early detection of VAP is of great significance.

Clinically, according to the guidelines (20,21), invasive coronary angiography is considered the gold standard investigation in patients presenting with symptoms of CAD and angina. MPI is performed when the diagnosis is equivocal or to evaluate the functional significance of a familiar coronary lesion. CT coronary angiography (CTa) is another modality that may help to avoid invasive methods. Except for CTa, other above-mentioned modalities are only used for detection of obstructive intraluminal stenosis and therefore provide little information on the nature of plaques and cannon determine the vulnerability of plaques (22). It has been shown that multicontrast magnetic resonance imaging (MRI) has the highest potential for evaluation of carotid plaque and interrogation of the fibrous cap, but its high cost and lengthy procedure are its major limitations (23,24).

Molecular imaging procedures have attracted attention for the evaluation of VAP, which provide additional information about the process of VAP formation such as calcification, apoptosis, hypoxia, and neovascularization as a non-invasive method. Moreover, these procedures can lead to early diagnosis of high-risk patients with prospective culprit lesions and help to prevent subsequent cardiovascular events with proper management (22). Clinically, many studies have investigated two molecular imaging protocols including ultrasmall superparamagnetic iron oxide-contrast-enhanced MRI and ^{18}F-FDG-PET (25). Although ^{18}F-FDG-PET is the most common radiotracer for nuclear plaque imaging, some other PET radiotracers, including 11C and ^{18}F-choline, 11C-PK11195, 11C-acetate, ^{18}F-sodium fluoride, and ^{68}Ga-DOTATATE, have also been studied for plaque imaging (4,13,14).

Biologically, VAP formation occurs following endothelial injury and accumulation of low-density lipoprotein cholesterol in the intimal layer of the coronary wall. Monocytes are recruited into the damaged wall in response to damage and transform into macrophages (26). This inflammatory process following the accumulation of activated macrophages on the coronary wall can lead to destabilization, progression, initiation, and finally rupture of the VAP, which causes the cardiac event. Therefore, this inflammatory process can be used for imaging and diagnosis of VAP (17).

Because of the overexpression of SSTR-2 on activated macrophages, ^{68}Ga-DOTATATE PET and Tc-99m-octreotide, which have a high affinity for SSTR-2 and an unremarkable uptake in the normal myocardium, can be used for the evaluation of VAP. The role of ^{68}Ga-DOTATATE in the evaluation of VAP has been demonstrated in several

studies. Rominger et al. (13) studied the uptake of ^{68}Ga-DOTATATE in the LAD and showed a significantly increased ^{68}Ga-DOTATATE uptake in the LAD, suggesting the potential role of this tracer for plaque imaging in the coronary arteries. Mojtahedi et al. (4) evaluated the uptake of ^{68}Ga-DOTATATE in the coronary arteries for the detection of VAP. They reported a significantly increased uptake in fibrotic and VAPs compared with normal coronary arteries (4). In addition, previous studies have shown the superiority of ^{68}Ga-DOTATATE for detecting VAP compared to ^{18}F-FDG (14,17).

In this study, all patients with significant uptake of the radiotracer in SRS had abnormal coronary angiography. The results showed a high concordance between SRS and coronary angiography in three main coronary arteries; therefore, SRS can be used as a non-invasive and widely available modality for the assessment of VAP. The higher concordance of SRS with coronary angiography compared to MPI may be due to the inability of MPI to detect plaques without remarkable coronary stenosis, which can be detected by SRS. Therefore, early VAPs can be detected using SRS, which prevents future cardiac events. In conclusion, SRS and MPI complete each other in the assessment of coronary artery diseases.

Finally, it should be mentioned that PET radiotracers, including ^{68}Ga-DOTATATE and ^{18}F-FDG, are the best radiotracers for nuclear plaque imaging because in comparison between PET and SPECT, PET has a higher spatial resolution and sensitivity. Moreover, absolute quantification of radionuclide uptake can be performed by PET. However, SPECT has advantages that cannot be ignored including lower costs, wider availability, and better physical properties of its radionuclides such as longer half-life. Therefore, the SPECT protocol is more applicable than PET for evaluating VAP, especially in regions where PET is less available.

Study Limitations

The limitations of this study include its small sample size and lack of PET/CT and SPECT/CT for anatomical assessment. Therefore, studies with larger populations are warranted for the validation of the clinical use of SPECT with somatostatin receptor imaging for evaluating VAP. In addition, due to ethical considerations, coronary angiography was only performed for patients according to cardiovascular guidelines, which may limit the accuracy of the findings due to the lack of angiography results in all SRS participants. It is necessary to perform accurate diagnostic tests, e.g. IVUS, accompanied by histological examinations for all patients undergoing SRS to improve the results. Another limitation of the study is that not all ischemic lesions diagnosed on MPI are due to plaque formation in the coronary arteries; therefore, plaque detection is not a good measure for comparing these two tests. Further well-designed studies are required to verify these preliminary findings.

Conclusion

The results of Tc-99m-octreotide uptake were more concordant with coronary plaques than Tc-99m-MIBI SPECT, suggesting a potential role for Tc-99m-octreotide in the evaluation of atherosclerosis. In addition, coronary uptake may provide a molecular guide for coronary atherosclerotic lesions. Specific regional uptake should be ascertained by histology.

Ethics

Ethics Committee Approval: The Ethical Committee of Bushehr University of Medical Sciences approved this study (IR.BPUMS.REC.1401.175).

Informed Consent: All participants provided written informed consent before participation

Peer-review: Externally and internally peer-reviewed.

Authorship Contributions

Surgical and Medical Practices: A.A., M.R.P., D.I., H.A., M.A., Concept: A.A., M.R.P., R.N., H.A., M.A., Design: E.J., D.I., R.N., H.A., M.A., Data Collection or Processing: A.A., E.J., M.R.P., D.I., H.A., M.A., Analysis or Interpretation: E.J., R.N., H.A., M.A., Literature Search: E.J., Writing: E.J., H.A., M.A.

Conflict of Interest: No conflict of interest was declared by the authors.

Financial Disclosure: The authors declared that this study has received no financial support.

References

1. Lambert MA, Weir-McCall JR, Salsano M, Gandy SJ, Levin D, Cavin I, Littleford R, MacFarlane JA, Matthew SZ, Nicholas RS, Struthers AD, Sullivan F, Henderson SA, White RD, Belch JJF, Houston JG. Prevalence and distribution of atherosclerosis in a low- to intermediate-risk population: assessment with whole-body MR angiography. Radiology 2018;287:795-804.
2. Ghanem AM, Hamimi AH, Matta JR, Carass A, Elgarf RM, Gharib AM, Abd-Elmoniem KZ. Automatic coronary wall and atherosclerotic plaque segmentation from 3D coronary CT angiography. Sci Rep 2019;9:47.
3. Bentzon JF, Otsuka F, Virmani R, Falk E. Mechanisms of plaque formation and rupture. Circ Res 2014;114:1852-1866.
4. Mojtahedi A, Alavi A, Thamake S, Amerinia R, Ranganathan D, Tworowska I, Delpassand ES. Assessment of vulnerable atherosclerotic and fibrotic plaques in coronary arteries using (68)Ga-DOTATATE PET/CT. Am J Nucl Med Mol Imaging 2015;5:65-71.
5. Dickson BC, Gotlieb AI. Towards understanding acute destabilization of vulnerable atherosclerotic plaques. Cardiovasc Pathol 2003;12:237-248.

6. Gallino A, Stuber M, Crea F, Falk E, Corti R, Lekakis J, Schwitter J, Camici P, Gaemperli O, Di Valentino M, Prior J, Garcia-Garcia HM, Vlachopoulos C, Cosentino F, Windecker S, Pedrazzini G, Conti R, Mach F, De Caterina R, Libby P. "In vivo" imaging of atherosclerosis. Atherosclerosis 2012;224:25-36.
7. Malmberg C, Ripa RS, Johnbeck CB, Knigge U, Langer SW, Mortensen J, Oturai P, Loft A, Hag AM, Kjær A. 64Cu-DOTATATE for noninvasive assessment of atherosclerosis in large arteries and its correlation with risk factors: head-to-head comparison with 68Ga-DOTATOC in 60 patients. J Nucl Med 2015;56:1895-1900.
8. Armani C, Catalani E, Balbarini A, Bagnoli P, Cervia D. Expression, pharmacology, and functional role of somatostatin receptor subtypes 1 and 2 in human macrophages. J Leukoc Biol 2007;81:845-855.
9. Al Bulushi N, Al Suqri B, Al Aamri M, Al Hadidi A, Al Jahdami H, Al Zadjali M, Al Risi M. Diagnostic accuracy of technetium-99m-octreotide in imaging neuroendocrine tumors, Oman hospital experience with literature review. World J Nucl Med 2019;18:137-142.
10. Pirayesh E, Amoui M, Assadi M. Uptake difference by somatostatin receptors in a patient with neuroendocrine tumor: 99mTc-octreotide uptake in the lung without uptake in liver lesions. Mol Imaging Radionucl Ther 2015;24:128-131.
11. H Haug AR, Cindea-Drimus R, Auernhammer CJ, Reincke M, Wängler B, Uebleis C, Schmidt GP, Göke B, Bartenstein P, Hacker M. The role of 68Ga-DOTATATE PET/CT in suspected neuroendocrine tumors. J Nucl Med 2012;53:1686-1692.
12. Haug AR, Cindea-Drimus R, Auernhammer CJ, Reincke M, Beuschlein F, Wängler B, Uebleis C, Schmidt GP, Spitzweg C, Bartenstein P, Hacker M. Neuroendocrine tumor recurrence: diagnosis with 68Ga-DOTATATE PET/CT. Radiology 2014;270:517-525.
13. Rominger A, Saam T, Vogl E, Ubleis C, la Fougère C, Förster S, Haug A, Cumming P, Reiser MF, Nikolaou K, Bartenstein P, Hacker M. In vivo imaging of macrophage activity in the coronary arteries using 68Ga-DOTATATE PET/CT: correlation with coronary calcium burden and risk factors. J Nucl Med 2010;51:193-197.
14. Tarkin JM, Joshi FR, Evans NR, Chowdhury MM, Figg NL, Shah AV, Starks LT, Martin-Garrido A, Manavaki R, Yu E, Kuc RE, Grassi L, Kreuzhuber R, Kostadima MA, Frontini M, Kirkpatrick PJ, Coughlin PA, Gopalan D, Fryer TD, Buscombe JR, Groves AM, Ouwehand WH, Bennett MR, Warburton EA, Davenport AP, Rudd JH. Detection of atherosclerotic inflammation by ^{68}Ga-DOTATATE PET compared to [^{18}F]FDG PET imaging. J Am Coll Cardiol 2017;69:1774-1791.
15. Høilund-Carlsen PF, Piri R, Constantinescu C, Iversen KK, Werner TJ, Sturek M, Alavi A, Gerke O. Atherosclerosis imaging with ^{18}F-sodium fluoride PET. Diagnostics (Basel) 2020;10:852.
16. Lee R, Seok JW. An Update on [18F] fluoride PET imaging for atherosclerotic disease. J Lipid Atheroscler 2020;9:349-361.
17. Li X, Samnick S, Lapa C, Israel I, Buck AK, Kreissl MC, Bauer W. 68Ga-DOTATATE PET/CT for the detection of inflammation of large arteries: correlation with18F-FDG, calcium burden and risk factors. EJNMMI Res 2012;2:52.
18. Amini A, Dehdar F, Jafari E, Gholamrezanezhad A, Assadi M. Somatostatin receptor scintigraphy in a patient with myocarditis. Mol Imaging Radionucl Ther 2021;30:50-53.
19. Leccisotti L, Nicoletti P, Cappiello C, Indovina L, Giordano A. PET imaging of vulnerable coronary artery plaques. Clin Transl Imaging 2019;7:267-284.
20. Fox K, Garcia MA, Ardissino D, Buszman P, Camici PG, Crea F, Daly C, De Backer G, Hjemdahl P, Lopez-Sendon J, Marco J, Morais J, Pepper J, Sechtem U, Simoons M, Thygesen K, Priori SG, Blanc JJ, Budaj A, Camm J, Dean V, Deckers J, Dickstein K, Lekakis J, McGregor K, Metra M, Morais J, Osterspey A, Tamargo J, Zamorano JL; Task Force on the Management of Stable Angina Pectoris of the European Society of Cardiology; ESC Committee for Practice Guidelines (CPG). Guidelines on the management of stable angina pectoris: executive summary: The Task Force on the Management of Stable Angina Pectoris of the European Society of Cardiology. Eur Heart J 2006;27:1341-1381.
21. Fihn SD, Gardin JM, Abrams J, Berra K, Blankenship JC, Dallas AP, Douglas PS, Foody JM, Gerber TC, Hinderliter AL, King SB 3rd, Kligfield PD, Krumholz HM, Kwong RY, Lim MJ, Linderbaum JA, Mack MJ, Munger MA, Prager RL, Sabik JF, Shaw LJ, Sikkema JD, Smith CR Jr, Smith SC Jr, Spertus JA, Williams SV; American College of Cardiology Foundation; American Heart Association Task Force on Practice Guidelines; American College of Physicians; American Association for Thoracic Surgery; Preventive Cardiovascular Nurses Association; Society for Cardiovascular Angiography and Interventions; Society of Thoracic Surgeons. 2012 ACCF/AHA/ACP/AATS/PCNA/SCAI/STS Guideline for the diagnosis and management of patients with stable ischemic heart disease: a report of the American College of Cardiology Foundation/American Heart Association Task Force on Practice Guidelines, and the American College of Physicians, American Association for Thoracic Surgery, Preventive Cardiovascular Nurses Association, Society for Cardiovascular Angiography and Interventions, and Society of Thoracic Surgeons. J Am Coll Cardiol 2012;60:44-164.
22. Tarkin JM, Joshi FR, Rudd JH. Advances in molecular imaging: plaque imaging. Current Cardiovascular Imaging Reports 2013;6:358-368.
23. Owen DR, Lindsay AC, Choudhury RP, Fayad ZA. Imaging of atherosclerosis. Annu Rev Med 2011;62:25-40.
24. Vancraeynest D, Pasquet A, Roelants V, Gerber BL, Vanoverschelde JL. Imaging the vulnerable plaque. J Am Coll Cardiol 2011;57:1961-1979.
25. Osborn EA, Jaffer FA. The year in molecular imaging. JACC Cardiovasc Imaging 2009;2:97-113.
26. Krishnan S, Otaki Y, Doris M, Slipczuk L, Arnson Y, Rubeaux M, Dey D, Slomka P, Berman DS, Tamarappoo B. Molecular imaging of vulnerable coronary plaque: a pathophysiologic perspective. J Nucl Med 2017;58:359-364.

Original Article
Mol Imaging Radionucl Ther 2023;32:131-137 DOI:10.4274/mirt.galenos.2022.72593

Comparison of Regadenoson and Dipyridamole Safety Profiles During Stress Myocardial Perfusion Imaging

Stres Miyokardiyal Perfüzyon Görüntüleme Esnasında Regadenozon ve Dipiridamol Güvenlik Profillerinin Karşılaştırılması

Jan Roczniak[1], Justyna Bączalska[1], Gabriela Kanclerz[1], Weronika Zielińska[1], Joanna Ożga[1], Błażej Cymerman[1], Agnieszka Stępień[2], Magdalena Kostkiewicz[2,3], Katarzyna Holcman[2,3]

[1]*Jagiellonian University Medical College, Students' Scientific Group Medical Imaging in Cardiology, Kraków, Poland*
[2]*John Paul II Hospital, Jagiellonian University Medical College, Department of Cardiac and Vascular Diseases, Kraków, Poland*
[3]*John Paul II Hospital, Department of Nuclear Medicine, Kraków, Poland*

Abstract

Objectives: The pharmacological stress test with vasodilator agents is an alternative cardiological diagnostic tool for patients with contraindications to the classical stress test provided by physical activity during single-photon emission computed tomography (SPECT) myocardial perfusion imaging (MPI). The study compared the frequency of the side effects of regadenoson and dipyridamole during a SPECT MPI.

Methods: This retrospective study included data of 283 consecutive patients who underwent pharmacological stress tests in years 2015-2020. The study group consisted of 240 patients who had received dipyridamole and 43 patients who had received regadenoson. The collected data included the patients' characteristics, the occurrence of side effects (divided into mild: headache, vertigo, nausea, vomiting, dyspnea, chest discomfort, hot flushes, general weakness and severe: bradycardia, hypotension, loss of consciousness), and blood pressure values/measurements.

Results: Overall, complications occurred relatively often (regadenoson: 23.2%, dipirydamol: 26.7%, p=0.639). Procedure discontinuation was necessary in 0.7% of examinations, whereas pharmacological support was necessary in 4.7%. There was no difference in the prevalence of mild (regadenoson: 16.2%, dipirydamol: 18.3%, p=0.747) and severe complications (regadenoson: 11.6%, dipyridamole: 15.0%, p=0.563). However, regadenoson has been found to cause a significantly smaller mean decrease of systolic blood pressure (SBP) (regadenoson: -2.6±10.0 mmHg, dipyridamole: -8.7±9.6 mmHg, p=0.002), diastolic blood pressure (DBP) (regadenoson: -0.9±5.4 mmHg, dipyridamole: -3.6±6.2 mmHg, p=0.032), as well as mean arterial pressure (MAP) (regadenoson: -1.5±5.6 mmHg, dipyridamole: -5.4±6.5 mmHg, p=0.001).

Conclusion: Regadenoson and dipyridamole presented a similar safety profile during SPECT MPI. However, regadenoson has been found to cause significantly smaller decreases in SBP, DBP, and MAP.

Keywords: Regadenoson, dipyridamole, myocardial perfusion imaging, vasodilators, stress test, single photon emission computed tomography

Öz

Amaç: Vazodilatör ajanlarla yapılan farmakolojik stres testi, tek foton emisyonlu bilgisayarlı tomografi (SPECT) miyokardiyal perfüzyon görüntülemesi (MPI) sırasında fiziksel aktivite ile sağlanan klasik stres testinin uygulanmasının kontrendike olduğu hastalar için alternatif bir kardiyolojik tanı aracıdır. Bu çalışmada, SPECT MPI sırasında regadenozon ve dipiridamolün yan etkilerinin sıklığı karşılaştırıldı.

Yöntem: Bu retrospektif çalışma, 2015-2020 yıllarında farmakolojik stres testi uygulanan ardışık 283 hastanın verilerini içermektedir. Dipiridamol alan 240 hasta ve regadenozon alan 43 hasta çalışma grubunu oluşturdu. Toplanan veriler içinde hastaların özellikleri, ortaya çıkan yan etkiler (baş

Address for Correspondence: Jan Roczniak MD, Jagiellonian University Medical College, Students' Scientific Group Medical Imaging in Cardiology, Krakow, Poland
Phone: +12 614 22 87 **E-mail:** roczniakjan@gmail.com ORCID ID: orcid.org/0000-0003-2536-2633
Received: 22.05.2022 **Accepted:** 15.08.2022

ağrısı, vertigo, mide bulantısı, kusma, nefes darlığı, göğüs rahatsızlığı, sıcak basması ve genel halsizlik hafif yan etkiler; bradikardi, hipotansiyon ve bilinç kaybı şiddetli yan etkiler olarak sınıflandırıldı) ve kan basıncı değerleri/ölçümleri bulunmaktaydı.

Bulgular: Genel olarak, komplikasyonlar nispeten sık meydana geldi (regadenozon: %23,2, dipiridamol: %26,7, p=0,639). Muayenelerin %0,7'sinde işlem sona erdirilirken, %4,7'sinde farmakolojik destek gerekliydi. Hafif (regadenozon: %16,2, dipiridamol: %18,3, p=0,747) ve ağır komplikasyonların (regadenozon: %11,6, dipiridamol: %15,0, p=0,563) prevalansları açısından fark yoktu. Bununla birlikte, regadenozonun sistolik kan basıncında (SBP) (regadenozon: -2,6±10,0 mmHg, dipiridamol: -8,7±9,6 mmHg, p=0,002), diyastolik kan basıncında (DBP) (regadenozon: -0,9±5,4 mmHg, dipiridamol: -3,6±6,2 mmHg, p=0,032) ve ortalama arter basıncında (MAP) (regadenozon: -1,5±5,6 mmHg, dipiridamol: -5,4±6,5 mmHg, p=0,001) anlamlı olarak daha az düşüş ile ilişkili bulunmuştur.

Sonuç: Regadenozon ve dipiridamol, SPECT miyokard perfüzyon görüntülemesi sırasında benzer bir güvenlik profili sergilemiştir. Bununla birlikte, regadenozonun SBP'de, DBP'de ve MAP'de anlamlı olarak daha az düşüşe neden olduğu bulunmuştur.

Anahtar kelimeler: Regadenozon, dipiridamol, miyokardiyal perfüzyon görüntüleme, vazodilatörler, stres testi, tek foton emisyonlu bilgisayarlı tomografi

Introduction

Coronary artery disease (CAD) is a cardiovascular condition that involves atherosclerotic plaque formation in the vessel lumen. Due to impairment in the blood flow, oxygen delivery to the myocardium is disturbed (1). For this reason, CAD is proved to be one of the main causes of death in developed and developing countries and should be properly diagnosed and treated (2). The single-photon emission computed tomography (SPECT) myocardial perfusion imaging (MPI) is a non-invasive diagnostic tool that is performed in patients with suspected CAD. This method is a superior alternative to the treadmill electrocardiography test, especially in patients with single-vessel CAD, with superior safety profile compared to the invasive diagnostic procedure, namely coronary arteriography (3,4). This imaging technique shows myocardial perfusion and the effects of stress on the heart muscle. SPECT MPI is a nuclear medicine imaging technique using gamma rays and radiopharmaceuticals such as Technetium-99m; it may be performed in a one- or two-day protocol (5). In the one-day protocol, the patient undergoes a rest SPECT scan in the morning and then a SPECT stress scan after 4 h. In the 2-day protocol, only one SPECT scan is taken daily. There are two strategies for stress testing. The most common is exercise on a treadmill with constant heart rate, blood pressure, and electrocardiographic monitoring. The second technique is pharmacological and is used if the exercise test is contraindicated (6). During this method, the patient receives one of the coronary vasodilators adenosine agonists: adenosine, regadenosine, or dipyridamole. Dipyridamole is an indirect adenosine agonist, and regadenosine and adenosine are direct agonists. Regadenoson is a selective α(2A) receptor agonist, whereas dipyridamole and adenosine can activate adenosine α(1), α(2A), α(2B) and α(3) receptors. These substances mimic physical exercise on the heart muscle (5). Each of the drugs applied to simulate cardiovascular stress causes various adverse effects due to stimulation of adenosine receptors, most commonly: headache, chest pain, decrease in blood pressure, nausea (5). Therefore, it is important to compare the most commonly used vasodilators in terms of their safety profiles. The study compared regadenoson and dipyridamole in terms of complications and impact on blood pressure during SPECT examination.

Materials and Methods

The study included 283 consecutive patients who underwent pharmacological stress SPECT in years 2015-2020 in the John Paul II Hospital in Kraków, Poland. The study population consisted of two groups: 240 patients who had received dipyridamole (Persantin, Boehringer Ingelheim Pharmaceuticals Inc, Germany) and 43 patients who had received regadenoson (Rapiscan, GE Healthcare AS, Norway). The inclusion criteria were having undergone a pharmacological stress SPECT with the administration of dipyridamole or regadenoson and age above 18 years. Each patient included in the study gave informed consent to perform pharmacological stress SPECT. The exclusion criteria were the contraindications to the pharmacological stress with vasodilators (a history of severe bronchospasm, asthma during physical activity, severe aortic stenosis, severe obstructive hypertrophic cardiomyopathy, pregnancy or lactation, 2° or 3° degree, atrioventricular block and atrial node disease, arterial hypotension (SP <90 mmHg), or history of allergic reaction to the previously mentioned drugs) (7). The collected data included the characteristics of the patients such as sex, age, body mass index (BMI), medical information regarding chronic diseases like diabetes, hypertension, atherosclerosis, hyperlipidemia as well as past myocardial infarction (MI) or heart failure and the history of medical procedures [percutaneous coronary interventions (PCI), and coronary artery bypass graft surgery (CABG)] as well as information regarding to the stress MPI procedure: side effects (divided into mild: headache,

vertigo, nausea, vomiting, dyspnea, chest discomfort, hot flushes, overall weakness, and severe: bradycardia (defined as heart rate below 60), hypotension [defined as systolic blood pressure (SBP), <90 or mean blood pressure (MBP) <70 and loss of consciousness] and blood pressure measurements: before the procedure, 5 times during the procedure (every minute) and 4 times after the procedure (every minute). Standard descriptive statistics were used to describe the data. Categorical variables were presented as percentages. Quantitative data were presented as mean value ± 1 standard deviation for data with normal distribution or median with interquartile range quartile 1 and 3, respectively for data with distribution other than normal.

Statistical Analysis

The normality of the data was assessed using the Shapiro-Wilk test for samples smaller than 50 or Kolmogorov-Smirnov test for samples greater than 50. Quantitative variables with a normal distributions were compared using the Student's t-test. Non-normally distributed quantitative variables were compared using Mann-Whitney Wilcoxon U test. Categorical variables were compared using Pearson's chi-square test. The statistical significance was set at $p \leq 0.05$. All analyses were carried out with the software TIBCO Software Inc. (2017). Statistical (data analysis software system) version 13. http://statistica.io.

The study was provided with the ethical principles for clinical research based on the Declaration of Helsinki. Every patient included in the study gave informed consent for the SPECT examination. The Bioethics Committee of Jagiellonian University approved this study (approval no: 1072.6120.155.2021). It gave consent to the use of patient health data related directly to the perfusion SPECT (the course of the procedure, complications, the measure given) as well as general information containing demographic data and information on general health for conducting the study. The bioethics committee waived the obligation to obtain informed consent from enrolled patients due to the retrospective nature of the study.

Results

The study group consisted of 283 patients who underwent pharmacological stress tests, 240 of whom had been administered dipyridamole and 43 regadenoson. The most common chronic condition was hypertension, followed by hyperlipidemia, atherosclerosis, and obesity. Both groups were comparable in terms of chronic diseases, BMI, past cardiovascular history MI, PCI, and CABG. The full characteristics of patients are presented in the table below (Table 1).

Overall, complications occurred relatively often (regadenoson: in 10 of 43;23.2%, dipyridamole: in 64 of 240; 26.7%, p=0.639). The majority was mild complications (regadenoson: in 7 of 43; 16.2%, dipyridamole: in 44 of 240; 18.3%, p=0.747); however, therewas also a high occurrence of severe complications (regadenoson: in 5 of 43; 11.6%, dipyridamole: in 36 of 240; 15.0%, p=0.563). The difference between the two vasodilator drugs in terms of specific and pooled complications was not significant. A detailed comparison has been presented in Table 2.

The differences in MBP values SBP, diastolic blood pressure (DBP), and mean arterial pressure (MAP) during and

Table 1. Characteristics of the study group

	Total	Regadenoson (n=43)	Dipirydamol (n=240)	p value
Age (years)	70.4±9.2	71.0±7.4	70.3±9.5	0.638
Male sex	158 (55.8%)	24 (55.8%)	134 (55.8%)	0.993
BMI (kg/m^2)	29.7±5.15	30.3±6.9	29.8±4.6	0.892
Obesity (BMI >30)	123 (43.5%)	17 (39.5%)	106 (44.2%)	0.639
Diabetes mellitus type 2	87 (30.9%)	10 (23.3%)	77 (32.2%)	0.241
Hypertension	227 (80.5%)	30 (69.8%)	197 (82.4%)	0.054
Atherosclerosis	139 (49.3%)	20 (46.5%)	119 (49.8%)	0.692
Hyperlipidemia	197 (69.5%)	31 (72.1%)	166 (69.5%)	0.729
Past MI	86 (30.5%)	11 (25.6%)	75 (31.4%)	0.447
Past PCI	89 (31.6%)	12 (27.9%)	77 (32.2%)	0.576
Past CABG	28 (9.93%)	4 (9.3%)	24 (10.0%)	0.881
Heart failure	118 (41.8%)	15 (34.9%)	103 (43.1%)	0.315

Quantitative data with normal distribution has been presented as mean ± standard deviation. Categorical variables have been presented as counts with percentages in brackets. BMI: Body mass index, MI: Myocardial infarction, PCI: Percutaneous coronary intervention, CABG: Coronary artery bypass grafting

Table 2. Detailed comparison of complications				
	Total	**Regadenoson (n=43)**	**Dipyridamole (n=240)**	**p value**
Complications	74 (26.1%)	10 (23.2%)	64 (26.7%)	0.639
Mild complications	51 (18.0%)	7 (16.2%)	44 (18.3%)	0.747
-Headache	15 (5.3%)	0	15 (6.25%)	0.092
-Vertigo	4 (1.4%)	1 (2.3%)	3 (1.3%)	0.582
-Nausea	1 (0.4%)	0	1 (0.4%)	0.672
-Vomiting	0	0	0	1.0
-Dyspnea	14 (4.9%)	3 (7.0%)	11 (4.6%)	0.505
-Chest discomfort	8 (2.8%)	0	8 (3.3%)	0.224
-Hot flushes	5 (1.8%)	0	5 (2.1%)	0.340
-Overall weakness	9 (3.1%)	2 (4.6%)	7 (2.9%)	0.551
Severe complications	41 (14.4%)	5 (11.6%)	36 (15.0%)	0.563
-Bradycardia	6 (2.1%)	2 (4.7%)	4 (1.7%)	0.211
-Hypotension	38 (13.4%)	5 (11.6%)	33 (13.75%)	0.707
-Loss of consciousness	0	0	0	1
Procedure discontinuation	2 (0.7%)	0	2 (0.8%)	0.548
Aminophylline administration	14 (4.9%)	2 (4.7%)	12 (5.0%)	0.922
Oxygen administration	5 (1.8%)	2 (4.7%)	3 (1.3%)	0.119
Categorical variables have been presented as counts with percentages in brackets				

before the procedure are presented in Table 3. Changes in SBP, DBP and MAP values in time compared between dipyridamole and regadenoson have been presented in Figure 1. Regadenoson has been found to cause a significantly smaller mean decrease of SBP (regadenoson: -2.6±10.0 mmHg, dipyridamole: -8.7±9.6 mmHg, p=0.002) and DBP (regadenoson: -0.9±5.4 mmHg, dipyridamole: -3.6±6.2 mmHg, p=0.032), as well as MAP (regadenoson: -1.5±5.6 mmHg, dipyridamole: -5.4±6.5 mmHg, p=0.001) compared with the value before the procedure (Table 3) (Figure 2A, B, C).

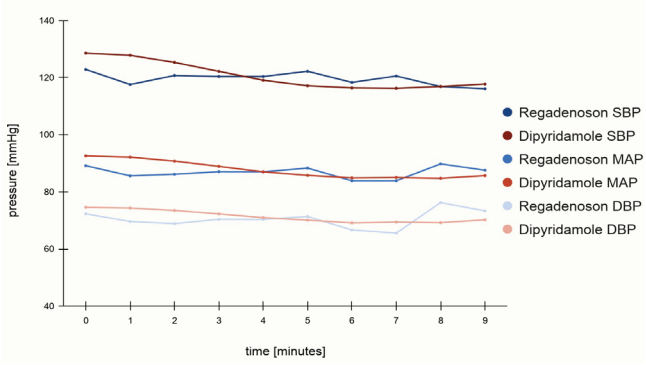

Figure 1. Change of blood pressure values in time (mmHg)
SBP: Systolic blood pressure, DBP: Diastolic blood pressure, MAP: Mean arterial pressure

Discussion

In this study of the vasodilators' safety profile during MPI, the administration of dipyridamole was associated with a significant decrease in systolic (8.7±9.6 mmHg versus 2.6±10 mmHg, p=0.002), diastolic (3.6±6.2 mmHg versus 0.9±5.4 mmHg, p=0.032) and MAP (5.4±6.5 mmHg versus 1.5±5.6 mmHg, p=0.001), in comparison to regadenoson. No such differences between the vasodilators were observed in terms of the symptoms reported by patients undergoing the procedure and the need for oxygen or aminophylline administration. The occurrence of any side effects was observed in 10 of 43 patients (23.2%) in regadenoson and 64 of 240 patients (26.7%) in the dipyridamole group (p=0.639). The main adverse effects of vasodilator administration were: hypotension (reported by 38 of 283 patients, 13.4%, p=0.707), headache (15 of 283, 5.3%, p=0.092), and dyspnea (14 of 283, 4.9%, p=0.505). Presented data may suggest that regadenoson is safer than dipyridamole.

In the study conducted by Amer et al. (8), regadenoson was associated with more frequent adverse effects (241 of 284, 84.9%) than dipyridamole (161 of 284, 56.7%) in patients undergoing MPI, with a p value <0.0001. There were particular types of complaints, which were statistically rarely observed in the dipyridamole group compared to regadenoson, which were: dyspnea (2.1% vs. 52.5%,

Table 3. Average change of blood pressure values during the procedure				
	Total	**Regadenoson (n=27)**	**Dipyridamole (n=240)**	**p value**
SBP change (mmHg)	**-8.1±9.8**	**-2.6±10.0**	**-8.7±9.6**	**0.002**
SBP change (% of initial value)	**-5.6 (-9.5)-(-1.0)**	**0 (-7.6)-(6.0)**	**-6.0 (-9.7)-(-1.7)**	**0.002**
DBP change (mmHg)	**-1.1 (-6.6)-(0.0)**	**0 (-4.0)-(0.0)**	**-1.1 (-7.8)-(0.0)**	**0.032**
DBP change (% of initial value)	-1.4 (-9.3)-(0.0)	0 (-5.0)-(0.0)	-1.6 (-9.7)-(0.0)	0.051
MAP change (mmHg)	**-4.0 (-8.1)-(-0.6)**	**-1.0 (-4.0)-(2.0)**	**-4.1 (-8.6)-(-1.2)**	**0.001**
MAP change (% of initial value)	**-4.1 (-8.73)-(-0.6)**	**-1.0 (-5.0)-(2.8)**	**-4.3 (-8.8)-(-1.2)**	**0.002**

Quantitative variables which followed normal distribution have been presented as mean ± standard deviation. Results with significant p values have been presented in **bold**.
Positive value = increase, negative value = decrease
SBP: Systolic blood pressure, DBP: Diastolic blood pressure, MAP: Mean arterial pressure

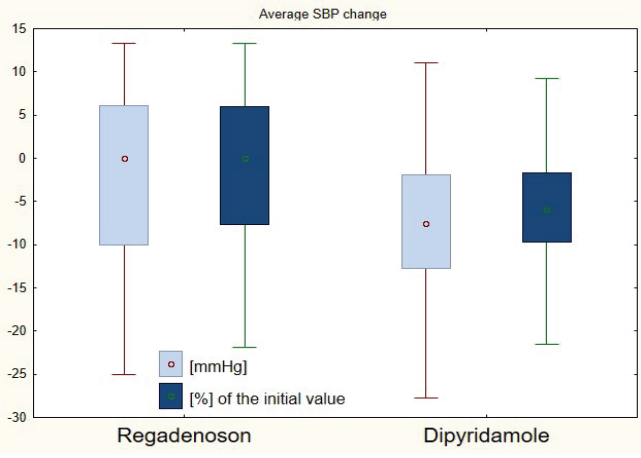

Figure 2A. Average SBP change during and after the procedure. Data has been presented as median, quartiles and non-outlier range
SBP: Systolic blood pressure

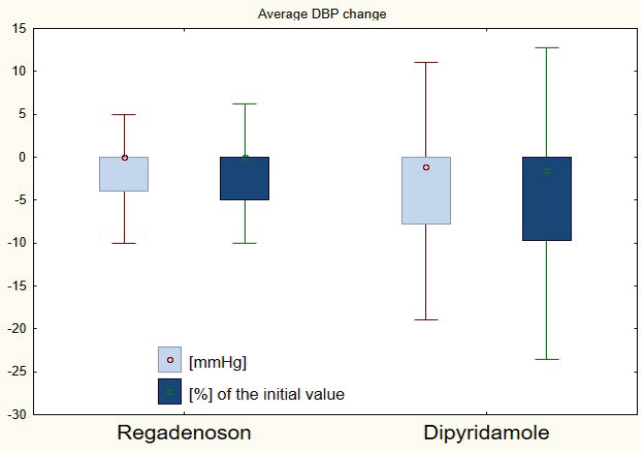

Figure 2B. Average DBP change during and after the procedure. Data has been presented as median, quartiles and non-outlier range
DBP: Diastolic blood pressure

p<0.0001), gastrointestinal discomfort (8.1% vs. 27.8%, p<0.0001) and chest pain (3.9 vs. 15.8%, p<0.0001). Hypotension was very rare: 1.1% in the regadenoson group

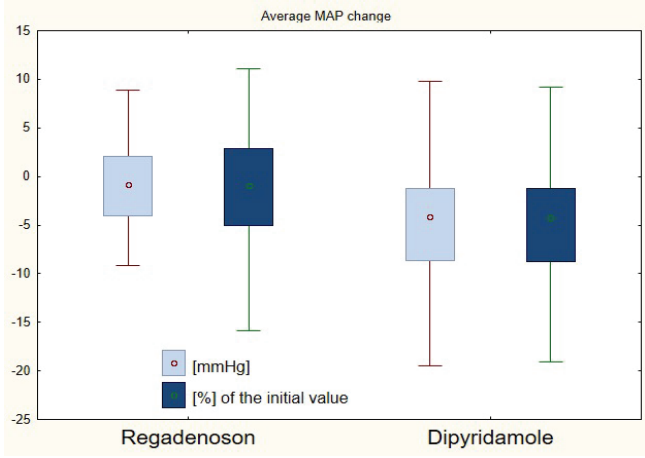

Figure 2C. Average MAP change during and after the procedure. Data has been presented as median, quartiles and non-outlier range
MAP: Mean arterial pressure

and 0% in the dipyridamole group (8). In our study, there was no statistically significant difference in dyspnea in the dipyridamole group compared with regadenoson (4.6% vs. 7%, p=0.505). Hypotension was the most common complication in both the dipyridamole and regadenoson groups. Overall, complications were rarely observed in our study than in the study by Amer et al. (8).

Goudarzi et al. (9) investigated the hemodynamic responses to regadenoson and dipyridamole. The increase in the heart rate was significantly higher in the regadenoson group than in patients who received dipyridamole (34±14 vs. 23±10 beats per minute increase from baseline; p<0.01). Stress myocardial body flow and myocardial flow reserve were not different between the groups (2.2±0.6 vs. 2.1±0.6 mL/min/g, p=0.39, and 2.9±0.8 vs. 2.8±0.7, p=0.31, respectively). If we consider the most common side effects of regadenoson, in a study conducted by Katsikis et al. (10), in the group of patients who underwent the MPI stress test, 197 of 279 women (71%) and 162 of 279 men (58%) experienced side effects of regadenoson. The following side effects occurred more frequently in women: chest

pain (65 of 279, 23% versus 33 of 279, 12%, p=<0.001), gastrointestinal discomfort (55 of 279, 20% versus 33 of 279, 12%, p=0.01) dizziness (35 of 279, 12% versus 14 of 279, 5%, p=0.002) and headache (56 of 279, 20% versus 37 of 279, 13%, p=0.03) respectively in women and men. Other adverse effects appear to be unrelated to gender (10) In another study, the most common side effects of regadenoson were: dyspnea (149 of 232 patients, 64%), headache (45 of 232, 19%), and chest pain (39 of 232, 17%). Three patients (1.3%) required administration of pharmaceuticals or hemodynamic support to relieve their symptoms. If hemodynamic responses are considered, a significant (p<0.0001) drop in SBP and DBP was observed as well as an increase in the heart rate (11). Complications of regadenoson in our study were observed more rarely compared to those studies; dyspnea was present in 7% of patients, followed by overall weakness (4.6%), and no cases of headache and chest discomfort were reported. Hypotension occurred in 11.6% and bradycardia in 4.7% of patients administered regadenoson. On the other hand, additional support was more often necessary; 4.7% of participants required administration of aminophylline and 4.7%-oxygen.

Considering the relative potency of vasodilators, regadenoson produces higher stress myocardial blood flow (95±11 vs. 86±12 beats/minute) and myocardial perfusion reserve (3.11±0.63 vs. 2.61±0.57) than dipyridamole and, if adjusted to the heart rate, has a much higher heart rate response. This means that regadenoson has superior vasodilator efficacy to dipyridamole; therefore, it could be a better agent to perform the stress MPI test (12). In a survey-based study by Friedman et al. (13), regadenoson and dipyridamole were compared in terms of duration of MPI test (156 vs. 191 min, respectively) and time from the administration to the start of the imaging procedure, including the dose calculation and infusion time, which were also shorter for regadenoson (mean difference: 12 min). Also, the time to manage the occurring adverse events was shorter in regadenoson (13).

It is worth adding that in the literature there is a certain trend in the popularity of using various vasodilators. In a survey study from 2013, the responders group consisted of the employees of healthcare facilities that perform MPI stress studies on the territory of the United States of America. In 93 of 141 (69%) imaging laboratories that took part in the survey, only one agent had been used: 38 (28%) adenosine, 27 (20%) dipyridamole, and 28 (21%) regadenoson. From 141 labs, 36 (27%) used two agents: 21 (16%) adenosine and regadenoson, 8 (6%) adenosine and dipyridamole, and 7 (5%) dipyridamole and regadenoson. Only 6 (4%) labs used all three agents (13). In a similar study from 2020, 35 of 50 (70%) participating labs were using only regadenoson, and dipyridamole or adenosine were both used in only 3 (6%) of responders' places of work. There were 10 labs (20%) using two agents, one of which was regadenoson. In 7 (14%), the other one was dipyridamole and in 3 (6%), it was adenosine. Only 2 (4%) centers used all three agents (14).

Study Limitations

This is a retrospective observational study with all its inherent biases. There was a difference in the size of the groups in this study, which could have impacted the results of statistical analysis. The duration of the symptoms was not taken into consideration because it was not available in the documentation.

Conclusion

Overall, based on our findings, regadenoson, and dipyridamole presented a similar safety profile during a SPECT MPI. There was no significant difference in the assessed complications. The occurrence of complications was high overall: 26.1%, mild: 18.0%, severe: 14.4%. Procedure discontinuation was necessary in 0.7% of examinations, whereas pharmacological support was necessary in 4.7%. However, regadenoson has been found to cause a significantly smaller decrease in SBP, DBP, and MAP, so it might be preferred for patients with lower blood pressure or a known tendency for hypotony.

Ethics

Ethics Committee Approval: The study was provided with the ethical principles for clinical research based on the Declaration of Helsinki. Every patient included in the study gave informed consent for the SPECT examination. The Bioethics Committee of Jagiellonian University approved this study (approval no: 1072.6120.155.2021).

Informed Consent: Each patient included in the study gave informed consent to perform pharmacological stress SPECT.

Peer-review: Externally and internally peer-reviewed.

Authorship Contributions

Surgical and Medical Practices: A.S., M.K., K.H., Concept: J.R., J.B., G.K., W.Z., J.O., B.C., A.S., M.K., K.H., Design: J.R., J.B., G.K., W.Z., J.O., B.C., A.S., M.K., K.H., Data Collection or Processing: J.R., J.B., G.K., W.Z., J.O., B.C., Analysis or

Interpretation: J.R., J.B., G.K., W.Z., J.O., B.C., A.S., M.K., Literature Search: J.R., J.B., G.K., W.Z., J.O., B.C., Writing: J.R., J.B., G.K., W.Z., J.O., B.C., A.S., M.K., K.H.

Conflict of Interest: No conflict of interest was declared by the authors.

Financial Disclosure: The authors declared that this study has received no financial support.

References

1. Shahjehan RD, Bhutta BS. Coronary Artery Disease. [Updated 2021 Aug 7]. In: StatPearls [Internet]. Treasure Island (FL): StatPearls Publishing; 2021. Available from: https://www.ncbi.nlm.nih.gov/books/NBK564304/
2. Malakar AK, Choudhury D, Halder B, Paul P, Uddin A, Chakraborty S. A review on coronary artery disease, its risk factors, and therapeutics. J Cell Physiol 2019;234:16812-16823.
3. Bokhari S, Shahzad A, Bergmann SR. Superiority of exercise myocardial perfusion imaging compared with the exercise ECG in the diagnosis of coronary artery disease. Coron Artery Dis 2008;19:399-404.
4. Knuuti J, Wijns W, Saraste A, Capodanno D, Barbato E, Funck-Brentano C, Prescott E, Storey RF, Deaton C, Cuisset T, Agewall S, Dickstein K, Edvardsen T, Escaned J, Gersh BJ, Svitil P, Gilard M, Hasdai D, Hatala R, Mahfoud F, Masip J, Muneretto C, Valgimigli M, Achenbach S, Bax JJ; ESC Scientific Document Group. 2019 ESC Guidelines for the diagnosis and management of chronic coronary syndromes. Eur Heart J 2020;41:407-477. Erratum in: Eur Heart J 2020;41:4242.
5. Henzlova MJ, Duvall WL, Einstein AJ, Travin MI, Verberne HJ. ASNC imaging guidelines for SPECT nuclear cardiology procedures: stress, protocols, and tracers. J Nucl Cardiol 2016;23:606-639. Erratum in: J Nucl Cardiol 2016;23:640-642.
6. Lak HM, Ranka S, Goyal A. Pharmacologic Stress Testing. 2021 Aug 2. In: StatPearls [Internet]. Treasure Island (FL): StatPearls Publishing; 2021. PMID: 32310423.
7. Rodrigues CVB, Oliveira A, Wiefels CC, Leão MS, Mesquita CT. Current practices in myocardial perfusion scintigraphy in Brazil and Adherence to the IAEA Recommendations: results of a cross-sectional study. Arq Bras Cardiol 2018;110:175-180.
8. Amer KA, Hurren JR, Edwin SB, Cohen G. Regadenoson versus dipyridamole: a comparison of the frequency of adverse events in patients undergoing myocardial perfusion imaging. Pharmacotherapy 2017;37:657-661.
9. Goudarzi B, Fukushima K, Bravo P, Merrill J, Bengel FM. Comparison of the myocardial blood flow response to regadenoson and dipyridamole: a quantitative analysis in patients referred for clinical 82Rb myocardial perfusion PET. Eur J Nucl Med Mol Imaging 2011;38:1908-1916.
10. Katsikis A, Kyrozi E, Manira V, Theodorakos A, Malamitsi J, Tsapaki V, Iakovou I, Voudris V, Kolovou G, Koutelou M. Gender-related differences in side-effects and hemodynamic response to regadenoson in patients undergoing SPECT myocardial perfusion imaging. Eur J Nucl Med Mol Imaging 2019;46:2590-2600.
11. Pape M, Zacho HD, Aarøe J, Eggert Jensen S, Petersen LJ. Safety and tolerability of regadenoson for myocardial perfusion imaging - first Danish experience. Scand Cardiovasc J 2016;50:180-186.
12. Vasu S, Bandettini WP, Hsu LY, Kellman P, Leung S, Mancini C, Shanbhag SM, Wilson J, Booker OJ, Arai AE. Regadenoson and adenosine are equivalent vasodilators and are superior than dipyridamole- a study of first pass quantitative perfusion cardiovascular magnetic resonance. J Cardiovasc Magn Reson 2013;15:85.
13. Friedman M, Spalding J, Kothari S, Wu Y, Gatt E, Boulanger L. Myocardial perfusion imaging laboratory efficiency with the use of regadenoson compared to adenosine and dipyridamole. J Med Econ 2013;16:449-460.
14. Yang H, Faust E, Gao E, Sethi S, Kitt TM, Kristy RM, Spalding JR, Xu Y. Evaluating the use of pharmacological stress agents during single-photon emission computed tomography myocardial perfusion imaging tests after inadequate exercise stress test. J Nucl Cardiol 2022;29:1788-1795.

Original Article
Mol Imaging Radionucl Ther 2023;32:138-145 DOI:10.4274/mirt.galenos.2022.68094

Clinical Utility of CT-based Attenuation-correction in Myocardial Perfusion SPECT Imaging

Miyokard Perfüzyon SPECT Görüntülemede, BT Bazlı Atenüasyon Düzeltmenin Klinik Yararı

Filiz Hatipoğlu[1], Neslihan Çetin[2]

[1]*İzmir Atatürk Training and Research Hospital, Clinic of Nuclear Medicine, İzmir, Turkey*
[2]*Ümraniye Training and Research Hospital, Clinic of Nuclear Medicine, İstanbul, Turkey*

Abstract

Objectives: We aimed to investigate and compare the role of computed tomography (CT)-based attenuation-corrected images (AC) with non-attenuation-corrected images (NAC) obtained by single-photon emission computed tomography/computed tomography (SPECT/CT) myocardial perfusion imaging (MPI).

Methods: The data of 124 patients who were applied one-day stress-rest Tc-99m sestamibi SPECT/CT MPI and who had coronary angiography (CAG) results within ±3 months were retrospectively reviewed. AC and NAC images were visually evaluated by two nuclear medicine specialists in a consensus. CAG results were used as the reference standard.

Results: Specificity, sensitivity, and accuracy were calculated as 66%, 61%, 71%, 79% and 69%, 70% for AC and NAC imaging in the whole group, respectively. There was no statistically significant difference between AC and NAC images for specificity, sensitivity, and accuracy in the male and female subgroups. In the diagnosis of right coronary artery (RCA) disease, CT AC significantly increased the specificity from 87% to 96%. However, in the left anterior descending artery (LAD) region, the specificity was significantly reduced from 95% to 77%.

Conclusion: CT-based AC did not significantly contribute to diagnostic performance for increased specificity for the RCA and reduced specificity in the LAD region. Therefore, AC images should always be evaluated side by side with NAC images to benefit from the different advantages of both techniques.

Keywords: Myocardial perfusion, scintigraphy, attenuation correction

Öz

Amaç: Miyokard perfüzyon görüntülemede, atenüasyon artefaktları tetkik spesifitesini etkilemektedir. Çalışmamızda tek foton emisyonlu bilgisayarlı tomografi/bilgisayarlı tomografi (SPECT/BT) sistemi ile elde edilen atenüasyon düzeltmesi yapılmış görüntüler, düzeltme yapılmamış görüntüler ile karşılaştırıldı. Bilgisayarlı tomografi (BT) bazlı atenüasyon düzeltmenin klinik pratiğe katkısı araştırıldı.

Yöntem: Tek gün protokolü ile strest-rest Tc-99m sestamıbı SPECT/BT yapılan ve ±3 ay içinde koroner anjiyografi (CAG) sonuçları mevcut olan 53 kadın, 71 erkek 124 hastanın datası retrospektif olarak incelendi. Atenüasyon düzeltmesi yapılmış ve yapılmamış görüntüler iki nükleer tıp uzmanı tarafından vizüel olarak değerlendirildi. Bulgular referans standart kabul edilen CAG sonuçları ile karşılaştırıldı.

Bulgular: Atenüasyon düzeltmesi yapılmış ve yapılmamış görüntüleme için sırasıyla tüm grupta, spesifite %66, %60; sensitivite %71, %79 ve doğruluk %69, %70 olarak hesaplandı (p>0,05). Kadın ve erkek subgruplarında da atenüasyon düzeltmesi yapılmış ve yapılmamış görüntüler arasında, spesifite, sensitivite ve doğruluk için istatistiksel olarak anlamlı fark saptanmadı. Sağ koroner arter (RCA) hastalığının dedekte edilmesinde

Address for Correspondence: Filiz Hatipoğlu MD, İzmir Atatürk Training and Research Hospital, Clinic of Nuclear Medicine, İzmir, Turkey
Phone: +90 232 244 44 44 **E-mail:** karagozfiliz@yahoo.com ORCID ID: orcid.org/0000-0002-6893-434X
Received: 16.05.2022 **Accepted:** 07.08.2022

BT ile atenüasyon düzeltmesi, spesifiteyi %87'den %96'ya yükseltti. Ancak sol ön inen arter (LAD) alanında BT bazlı atenüasyon düzeltme ile spesifitenin %95'ten %77 ye gerilediği görüldü (p=<0,0001).

Sonuç: BT bazlı atenüasyon düzeltmesi, RCA alanı için artan spesifite dışında tüm hasta grubunda tanısal performansa anlamlı bir katkı sağlamamış, LAD alanında da spesifiteyi azaltmıştır. Bu nedenle atenüasyon düzeltmesi yapılmış görüntüler, düzeltme yapılmamış görüntüler ile yan yana, klinik veriler eşliğinde değerlendirilmelidir.

Anahtar kelimeler: Miyokard perfüzyon, sintigrafi, atenüasyon düzeltme

Introduction

Myocardial perfusion imaging (MPI) is a non-invasive diagnostic test applied in the evaluation of functional severity of known or suspected coronary artery disease (CAD) (1,2). Although the diagnostic currency of MPI is accepted, attenuation developing secondary to the photon absorption caused by soft tissues such as the breast, diaphragm, thoracic wall, and prominent subdiaphragmatic gastrointestinal activity can cause the artifacts. These artifacts can ultimately affect the diagnostic performance of the test (3). Many methods such as electrocardiogram (ECG) gated imaging, prone imaging, and transmission mapping with external radioactive sources have been developed to overcome attenuation artifacts (4,5). Attenuation artifacts are partially eliminated by ECG-gated single-photon emission computed tomography (SPECT) imaging, which is frequently used in clinical practice to assess regional myocardial contractility (6). However, in inhomogeneous attenuation regions, such as thorax, attenuation maps obtained by transmission imaging are thought to be more effective than ECG-gated SPECT in attenuation correction (7). Transmission imaging conducted with external radioactive sources brings several disadvantages, such as cross-talk between emission and transmission energies and suboptimal image quality (8,9). Recently developed combined SPECT and low dose computed tomography (CT) devices can generate the transmission maps with high count and resolution in a short time, and enhance the image quality (10). Many previous studies have shown that SPECT/CT MPI has high diagnostic accuracy in the evaluation of CAD (11). Nevertheless, it increases radiation exposure, can mask some perfusion defects, and reveal false-positive defects with new unexpected artifacts (10,12). Therefore, the discussions continue on the routine usage of SPECT/CT MPI in clinical practice.

Materials and Methods

Patients

A total of 124 patients in the age group of 35-82 (median age 61.8±11.4 years), including 71 males (57.3%) and 53 females (42.7%), who were referred to our clinic for evaluation of myocardial perfusion in 2012 and 2014 with the diagnosis of known or suspected CAD, were enrolled in our retrospective study. One-day stress-rest Tc-99m sestamibi (MIBI) ECG gated SPECT/CT imaging was applied to all subjects. All patients had available CAG data within three months before or after MPI.

Patients who were not able to perform treadmill exercise test due to their clinical condition, who had undergone pharmacological stress, and patients with left bundle branch block or arrhythmia causing insufficient counting statistics/quality in ECG-gated imaging were excluded from the study. The cases were divided into subgroups of females and males. Patients were instructed to read the detailed information form before the procedure and signed the consent form. The study protocol was approved by the Ethics Committee of Clinical Investigations of our hospital with decision number 372/2-97 dated 06.06.2016. The study was performed in accordance with the ethical standards laid down by the Declaration of Helsinki in 1964 and all its subsequent revisions. The medical history and symptoms of the patients are given in Table 1.

Patient Preparation and SPECT/CT Myocardial Perfusion Imaging Protocol

After at least 4 h of fasting, an exercise stress test was performed in patients according to modified Bruce protocol. Calcium channel blockers or beta-blockers were stopped 48 hours before imaging and long-acting nitrates

Table 1. Symptoms and medical history of the patients

Variables	n	Percentile (%)
Hypertension	81	65.3
Hyperlipidemia	62	50
Diabetes	34	27.4
Smoking	60	48.4
Typical angina pectoris	34	27.4
Atypical chest pain	30	24.2
Asymptomatic	60	48.4
Myocardial infarction	12	9.7
Coronary artery bypass grafting	16	12.9
Percutaneous coronary intervention	36	29

were discontinued the day before the study if there was no medical contraindication. 8-10 millicuries (mCi) [296-370 megabecquerels (MBq)] Tc-99m MIBI was injected to each patient during exercise when target heart rate was reached or an indication for the exercise termination (physical fatigue, progressive angina, systolic blood pressure lower than 20 mmHg, systolic blood pressure higher than 250 mmHg, ST depression more than 3 mm, etc.) was observed. After the injection, patients were fed with greasy foods that accelerated the hepatobiliary clearance of the radiopharmaceutical. ECG stress images were recorded after about 45 minutes. At least 2 h after the stress test, 24-30 mCi (888-1110 MBq) of Tc-99 m MIBI injected intravenously and resting ECG-gated images were obtained after approximately 45 min following injection. Studies were conducted using a Siemens Symbia T6 (Healthcare, Erlangen, Germany) dual-head SPECT/CT hybrid camera equipped with high-resolution low energy parallel hole collimators. When the patients were in the supine position and the angle between the collimators was 90°, in a 64×64 matrix, a total of 60 projections were acquired using a step & shot technique over a 180° rotation from the 45° right anterior oblique to the 45° left posterior oblique, in 20% energy window centered on the 140 keV energy peak of Tc-99m MIBI and with a zoom factor of 1.33.

For ECG-gated SPECT imaging, all patients were monitored with a 3-lead ECG. Images were gated at 8 frames per cardiac cycle. A low-dose CT study (140 kV, 2.5 mA) of the chest was performed for attenuation mapping during both stress and rest imaging following the emission study. Obtained SPECT and AC images were automatically reconstructed using standard filtered back-projection technique and FLASH 3D iterative reconstruction algorithm, respectively. Emission and transmission data were visually inspected on axial, sagittal, and coronal fusion plans, and misalignments were manually corrected in 50 patients (40.3%).

Evaluation

Analysis of AC and NAC images was performed visually by two nuclear medicine specialists in consensus. Sections on the short, vertical, and horizontal axes obtained by the Cedars Sinai Quantitative Perfusion Gated SPECT (QPS-QGS) software packages (Cedars Sinai Medical Center, Los Angeles, CA) were evaluated.

The left ventricle was evaluated in association with the presence or absence of perfusion defects based on a 17-segment model of three main coronary arterial territories left anterior descending (LAD), left circumflex (LCx), and right coronary arteries (RCA) recommended by the American Heart Association (13).

MPI results were reported as normal in the absence of perfusion defects in both stress and rest images. If the perfusion was normal in resting images in areas where a perfusion defect was detected in stress images, ischemia (reversible defect) was reported. MPI result was reported as infarct (fixed defect) in the presence of a matched perfusion defect in both stress and rest images. However, when NAC images were reported, ECG-gated images were taken into account and areas with a fixed perfusion defect without any wall motion abnormality was interpreted as artifacts.

Coronary Angiography

CAG results of 124 patients obtained within ±3 months were analyzed. CAG findings served as the reference standard for the diagnostic performance of MPI. A reduction in the luminal diameter of ≥50% in at least one of the three coronary arteries was defined as a significant stenosis.

Statistical Analysis

All statistical analysis were performed using the IBM SPSS version 21.0 for Windows program (SPSS, Chicago, Ill.). The mean, standard deviation, minimum, and maximum values of all numerical variables were calculated. NAC and AC images were compared in terms of sensitivity, specificity, and accuracy. The McNemar test was used for statistical difference analysis in assessing the diagnostic accuracy (sensitivity, specificity, accuracy) obtained by NAC and AC imaging. Results with a p value of less than 0.05 were regarded as statistically significant.

Results

Myocardial Perfusion Imaging

In NAC images, perfusion defects were compatible with ischemia and infarction in 48 (38.7%) and 17 (%13.7) cases, respectively. Both ischemia and infarction were detected in 10 cases (8.1%). In 8 cases (6.5%) with a fixed perfusion defect in the inferior myocardial wall, MPI results were evaluated favorably for diaphragmatic attenuation because wall motion was normal in these cases. In 41 patients (33%), MPI findings were reported as normal. When the AC images of all patients were assessed, 39 cases (31.4%) were diagnosed with ischemia, 19 cases (15.3) were diagnosed with infarction, 9 cases (7.3%) were found to have both ischemia and infarction. MPI findings were reported as normal according to AC images in 57 (46%) patients.

Coronary Angiography

There was significant stenosis in 66 cases according to CAG results. Of the cases, 9 had three vessels, 17 had two

vessels, 40 had single-vessel stenosis. 58 (46.8%) patients had no critical stenosis. Table 2 summarizes the MPI results of NAC and AC images according to CAG findings.

In the entire study group, CT increased specificity (60% and 66% for NAC and AC imagings, respectively) and decreased sensitivity and accuracy (79%, 71%, and 70% and 69% for NAC and AC imagings, respectively) (Table 3). However, the results were not statistically significant. Moreover no significant effect of AC imaging was found in the male and female subgroups (Table 3).

Table 2. Compliance with CAG findings of AC and NAC MPI results

			CAG (-)		CAG (+)		Total
			Male	Female	Male	Female	
	NAC	-	20	15	9	5	124
		+	6	17	36	16	
	AC	-	20	18	14	5	124
		+	6	14	31	16	
LCx	NAC	-	46	40	10	3	124
		+	2	6	13	4	
	AC	-	54	36	8	7	124
		+	3	1	6	9	
RCA	NAC	-	38	43	9	6	124
		+	11	1	13	3	
	AC	-	45	44	11	6	124
		+	4	0	11	3	
LAD	NAC	-	45	30	9	8	124
		+	0	4	17	11	
	AC	-	39	25	10	5	124
		+	6	13	16	10	

CAG: Coronary angiography, AC: CT-based attenuation corrected images, NAC: Non-attenuation corrected images, LAD: Left anterior descending artery, RCA: Right coronary artery, LCx: Left circumflex artery, MPI: Myocardial perfusion imaging

In the diagnosis of RCA disease, the sensitivity decreased slightly according to AC imaging. Furthermore, for the RCA region, CT-AC increased specificity and accuracy both in the entire study population and subgroups (there was statistical significance in the study group and the male subgroup regarding specificity). In the LCx territory with AC imaging, sensitivity decreased mildly, while a slight increase was observed in terms of specificity and accuracy. However, CT had no statistically significant effect on the diagnostic performance in the entire group and subgroups of patients in the LCxterritory. In the detection of LAD artery stenosis, with the effect of CT-AC, the sensitivity and accuracy did not significantly change, while specificity significantly decreased. This reduction of specificity, which was determined by attenuation correction in the LAD region, was observed similarly in subgroups as well (Table 4).

Discussion

When evaluating CAD, in addition to morphological information about the location and grade of coronary artery stenosis, functional severity should be determined for the selection of the patient group that will benefit from revascularization (1,14). There are several studies showing the prognostic value of SPECT MPI used for this purpose in evaluating known or suspected CAD (15). However, the diagnostic performance of SPECT MPI is limited by low spatial resolution. The artifacts caused by soft tissue attenuation and subdiaphragmatic activity affect the diagnostic accuracy of SPECT MPI, especially by reducing specificity. Therefore,artifacts reduce the cost-effectiveness of this technique (16). Methods such as ECG-gated imaging, prone imaging, and transmission mapping have been developed for the elimination of attenuation artifacts, but all methods have some limitations. For instance, ECG-gated SPECT, which is very practical for clinical routine use, is problematic in distinguishing artifacts from ischemic tissue.

Table 3. Diagnostic value of NAC versus AC images

	Sensitivity %	p value	Specificity %	p value	Accuracy %	p value
Total (n=124)						
NAC	79 (0.67-0.88)	0.146	60 (0.47-0.73)	0.328	70 (0.61-0.78)	0.864
AC	71 (0.59-0.82)		66 (0.52-0.78)		69 (0.60-0.77)	
Males (n=71)						
NAC	80 (0.65-0.90)	0.134	77 (0.56-0.91)	1.000	79 (0.68-0.88)	0.333
AC	69 (0.53-0.82)		77 (0.56-0.91)		72 (0.60-0.82)	
Females (n=53)						
NAC	76 (0.53-0.92)	1.000	47 (0.29-0.65)	0.356	58 (0.44-0.72)	0.528
AC	76 (0.53-0.92)		56 (0.38-0.74)		64 (0.50-0.77)	

AC: CT-based attenuation corrected images, NAC: Non-attenuation corrected images

While prone imaging, which is used to solve inferior wall artifacts, occasionally causes new artifacts in the anterior wall and prolongs the imaging time. Moreover, transmission maps generated by external radioactive sources, which seem to be more effective in inhomogeneous attenuation regions, also have disadvantages such as suboptimal quality transmission images and additional imaging time (8,9). In the transmission study conducted with the combined SPECT/CT system, the imaging time is not prolonged and the image quality increases due to high counting and resolution. However, new artifacts may arise and additional radiation exposure occurs (9,10).

Some studies evaluating the diagnostic efficiency of AC MPI reported that CT-AC increased specificity and accuracy significantly, while others reported that it decreased sensitivity in CAD detection with the improvement of specificity (17,18,19). In a study conducted with 120 patients, when AC images were compared with NAC imagings, the overall sensitivity decreased significantly from 87% to 70%. Overall specificity increased from 54% to 62%, although it was not statistically significant. In addition, the accuracy did not show any significant difference (12). In our study, there was no statistically significant difference between AC and NAC imaging regarding sensitivity specificity and accuracy. In the entire study group, CT-AC increased specificity from 60% to 66% and decreased sensitivity and accuracy from 79% to 71% and from 70% to 69%, respectively. However, their

Table 4. Diagnostic value of NAC vs AC images according to coronary arterial territories

	Sensitivity (%)	p value	Specificity (%)	p value	Accuracy	p value
RCA						
NAC	52 (0.34-0.69)	NS	87 (0.80-0.94)	0.011	78 (0.70-0.85)	NS
AC	45 (0.28-0.63)		96 (0.92-1.00)		83 (0.75-0.89)	
LCx						
NAC	57 (0.37-0.74)	NS	91 (0.84-0.96)	NS	83 (0.75-0.89)	NS
AC	50 (0.31-0.69)		96 (0.89-0.99)		85 (0.77-0.91)	
LAD						
NAC	62 (0.47-0.76)	NS	95 (0.88-0.99)	<0.0001	83 (0.75-0.89)	NS
AC	63 (0.47-0.78)		77 (0.67-0.86)		73 (0.64-0.80)	
RCA, males						
NAC	59 (0.39-0.80)	NS	78 (0.66-0.89)	0.019	72 (0.60-0.82)	NS
AC	50 (0.29-0.71)		92 (0.84-1.00)		79 (0.68-0.88)	
RCA, females						
NAC	33 (0.03-0.64)	NS	98 (0.93-1.00)	NS	87 (0.75-0.95)	NS
AC	33 (0.03-0.64)		100 (1.00-1.00)		89 (0.77-0.96)	
LCx, males						
NAC	57 (0.34-0.77)	NS	96 (0.86-0.99)	NS	83 (0.72-0.91)	NS
AC	43 (0.18-0.71)		95 (0.85-0.99)		85 (0.74-0.92)	
LCx, females						
NAC	57 (0.20-0.94)	NS	87 (0.77-0.97)	NS	83 (0.70-0.92)	NS
AC	56 (0.30-0.80)		97 (0.86-1.00)		85 (0.72-0.93)	
LAD, males						
NAC	65 (0.44-0.83)	NS	100 (0.92-1.00)	0.0017	87 (0.77-0.94)	NS
AC	62 (0.41-0.80)		87 (0.73-0.95)		77 (0.66-0.87)	
LAD, females						
NAC	58 (0.34-0.80)	NS	88 (0.73-0.97)	0.0074	77 (0.64-0.88)	NS
AC	67 (0.38-0.88)		66 (0.49-0.80)		66 (0.52-0.78)	

(Data in parentheses are 95% confidence intervals). AC: CT-based attenuation-corrected images, NAC: Non-attenuation corrected images, LAD: Left anterior descending artery, RCA: Right coronary artery, LCx: Left circumflex artery, NS: Not statistically significant

differences were both non-significant. In the literature, CT-AC improves the specificity in a general manner, while it results in different conclusions in terms of sensitivity and accuracy (20). This difference of outcomes may also be related to group characteristics, subjectivity affecting visual image analysis, and individual differences in interpreters, as well as technical reasons such as software used for reconstruction of the study, the use of scatter correction and resolution recovery (21,22,23). The pattern of the patients in the study group and the effect of the individual trends of the interpreters are also observed in the work of Sharma et al. (19) which used the same method and the same equipment to interpret the image.

Many factors affecting the outcome of clinical trials make it difficult to determine the diagnostic efficacy of CT-AC in CAD detection. However, as AC imaging provides high left ventricular count homogeneity, attenuation correction is thought to facilitate the separation of patients with positive and negative data according to coronary angiography. In a study conducted by Płachcińska et al. (6), specificity and accuracy in CAD detection increased statistically through AC imaging, and the increase in specificity was also observed in the male and female subgroups. According to Huang et al. (24), CT-AC reduced the defect size in the inferior wall in both male and female groups; however, AC imaging was found to be more beneficial in male than in female subgroups as diaphragmatic attenuation artifact in the inferior wall was seen more frequently in men than in women. Moreover, according to this study, attenuation correction increased the specificity for RCA disease from 77.9% to 98.7%; hence, the contribution of attenuation correction was most commonly seen in the RCA territory (24). As the current study demonstrated, the vascular area that most benefited from attenuation correction was RCA. Similar to the literature, attenuation correction yielded a decrease in the sensitivity in the whole group, while the specificity increased in the whole group and male subgroup (6).

In our study, there was no statistically significant difference in sensitivity, specificity, and accuracy between AC and NAC images in the LCx territory, as in the literature, for both whole group and subgroups. Conflicting results are reported for the LAD region (25). There are also papers that have reported that attenuation correction increases the capacitance of the detection of LAD disease (26). In contrast to Wolak et al. (27), AC imaging has also been reported to be useful in female patients (6). Additionally, some publications have argued that apical defects observed in AC images may be secondary to true apical thinning (28). It has been reported that artifacts observed in the anterior wall of NAC images were corrected in AC images (29). In the current study, however, there was no statistically significant change in sensitivity in the whole group between AC and NAC imaging in LAD region, whereas the specificity was observed to decrease in the whole group, besides the subgroups (Figure 1). In accordance with the current study, it has been reported in the literature that CT-AC reduced specificity in LAD territory and it is not sufficient for the elimination of breast artifacts, as well as it has been informed that new defects occasionally arise from the apical, anterior and septal wall with AC imaging (24,30). It is known that the attenuation map (small field of view), which does not contain the entire thoracic wall, can cause these defects in oversized patients. Besides, the underestimation of the attenuation effect on the anterior thoracic wall due tomis registration of the emission and transmission images (caused by patient movement or respiratory motion) can also create new defects (31). Although re-registration seems beneficial, manual correction is based on the visual evaluation, and the correction process can vary depending on the user's experience (32). Furthermore, regardless of misalignment, overestimation of the attenuation correction in the inferior wall, hence, a relative decrease in other segments and false perfusion defects may occur (31). All misalignments in our study were corrected manually. Nonetheless, lower specificity and accuracy values were obtained in AC images in the LAD territory, and there was no statistically significant improvement in the LCx field with attenuation correction. This is thought to be caused by the effect of user-dependent realignment or overcorrection of the inferior wall, as mentioned in the literature.

Study Limitations

Our study was planned retrospectively with a single centered, relatively small patient sample. Another limitation of our study is that a functional diagnostic test such as SPECT MPI for the diagnosis of CAD is compared with an anatomical method such as invasive angiography as a reference method. Moreover, we did not have a prognostic value of AC MPI in our study because there were no follow-up details of the patients. According to our own clinical experience, AC imaging contributes to the detection of perfusion defects in the inferior wall; however, it reduces specificity in the evaluation of the anterior wall. Therefore, it should be kept in mind that the inferior wall defects, which are only observed in NAC images, and anterior wall defects, which are detected only in AC images, may be artefacts. It is thought that NAC images should be evaluated primarily for the findings of anterior, anteroseptal, anterolateral walls and apex.

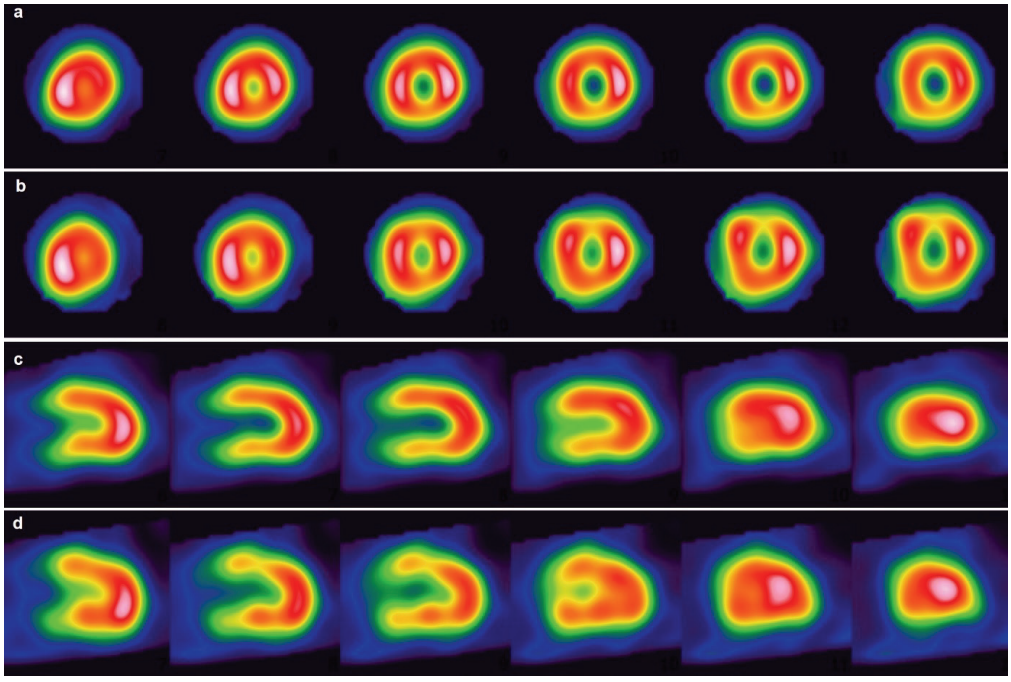

Figure 1. Non-attenuation corrected images (a, c) and CT-based attenuation corrected images (b, d) in short- and vertical long-axis planes. CT-based attenuation correction overcomes the perfusion defect related to diaphragmatic attenuation in the inferior myocardial wall. However, an anterior wall defect occurs as a new artifact
CT: Computed tomography

Conclusion

In conclusion, when using CT-based attenuation correction in MPI, a visual review of raw data along with the reconstructed images is required for the correct registration of the emission and transmission data. Additionally, AC images should always be evaluated side by side with NAC images to benefit from the different advantages of both techniques.

Ethics

Ethics Committee Approval: The study protocol was approved by the Ethics Committee of Clinical Investigations of our hospital with decision number 372/2-97 dated 06.06.2016. The study was performed in accordance with the ethical standards laid down by the Declaration of Helsinki in 1964 and all its subsequent revisions.

Informed Consent: Informed consent was obtained.

Peer-review: Externally and internally peer-reviewed.

Authorship Contributions

Surgical and Medical Practices: F.H., N.Ç., Concept: F.H., N.Ç., Design: F.H., N.Ç., Data Collection or Processing: F.H., N.Ç., Analysis or Interpretation: F.H., Literature Search: F.H., Writing: F.H.

Conflict of Interest: No conflict of interest was declared by the authors.

Financial Disclosure: The authors declared that this study has received no financial support.

References

1. Klocke FJ, Baird MG, Lorell BH, Bateman TM, Messer JV, Berman DS, O'Gara PT, Carabello BA, Russell RO Jr, Cerqueira MD, St John Sutton MG, DeMaria AN, Udelson JE, Kennedy JW, Verani MS, Williams KA, Antman EM, Smith SC Jr, Alpert JS, Gregoratos G, Anderson JL, Hiratzka LF, Faxon DP, Hunt SA, Fuster V, Jacobs AK, Gibbons RJ, Russell RO; American College of Cardiology; American Heart Association; American Society for Nuclear Cardiology. ACC/AHA/ASNC guidelines for the clinical use of cardiac radionuclide imaging–executive summary: a report of the American College of Cardiology/American Heart Association Task Force on Practice Guidelines (ACC/AHA/ASNC Committee to Revise the 1995 Guidelines for the Clinical Use of Cardiac Radionuclide Imaging). J Am Coll Cardiol 2003;42:1318-1333.
2. Nakajima K, Matsuo S, Okuyama C, Hatta T, Tsukamoto K, Nishimura S, Yamashina A, Kusuoka H, Nishimura T. Cardiac event risk in Japanese subjects estimated using gated myocardial perfusion imaging, in conjunction with diabetes mellitus and chronic kidney disease. Circ J 2012;76:168-175.
3. Corbett JR, Kritzman JN, Ficaro EP. Attenuation correction for single photon emission computed tomography myocardial perfusion imaging. Curr Cardiol Rep 2004;6:32-40.
4. 4 Okkalides D. Recent international regulations: low dose-low rate radiation protection and the demise of reason. Hell J Nucl Med 2008;11:86-90.

5. Kalantari F, Rajabi H, Saghar M. Quantification and reduction of attenuation related artifacts in SPET by applying attenuation model during iterative image reconstruction: a Monte Carlo study. Hell J Nucl Med 2011;14:278-283.
6. Płachcińska A, Włodarczyk M, Kovacevic-Kuśmierek K, Bieńkiewicz M, Drożdż J, Chiżyński K, Kasprzak JD, Peruga JZ, Kuśmierek J. Diagnostic performance of myocardial perfusion single-photon emission computed tomography with attenuation correction. Kardiol Pol 2016;74:32-39.
7. Zaidi H, Hasegawa B. Determination of the attenuation map in emission tomography. J Nucl Med 2003;44:291-315.
8. Garcia EV. SPECT attenuation correction: an essential tool to realize nuclear cardiology's manifest destiny. J Nucl Cardiol 2007;14:16-24.
9. Patton JA, Townsend DW, Hutton BF. Hybrid imaging technology: from dreams and vision to clinical devices. Semin Nucl Med 2009;39:247-263.
10. Dvorak RA, Brown RK, Corbett JR. Interpretation of SPECT/CT myocardial perfusion images: common artifacts and quality control techniques. Radiographics 2011;31:2041-2057.
11. Tonge CM, Manoharan M, Lawson RS, Shields RA, Prescott MC. Attenuation correction of myocardial SPECT studies using low resolution computed tomography images. Nucl Med Commun 2005;26:231-237.
12. Apostolopoulos DJ, Savvopoulos C. What is the benefit of CT-based attenuation correction in myocardial perfusion SPET? Hell J Nucl Med 2016;19:89-92.
13. Cerqueira MD, Weissman NJ, Dilsizian V, Jacobs AK, Kaul S, Laskey WK, Pennell DJ, Rumberger JA, Ryan T, Verani MS; American Heart Association Writing Group on Myocardial Segmentation and Registration for Cardiac Imaging. Standardized myocardial segmentation and nomenclature for tomographic imaging of the heart. A statement for healthcare professionals from the Cardiac Imaging Committee of the Council on Clinical Cardiology of the American Heart Association. Circulation 2002;105:539-542.
14. Silber S, Albertsson P, Avilés FF, Camici PG, Colombo A, Hamm C, Jørgensen E, Marco J, Nordrehaug JE, Ruzyllo W, Urban P, Stone GW, Wijns W; Task Force for Percutaneous Coronary Interventions of the European Society of Cardiology. Guidelines for percutaneous coronary interventions. The Task Force for Percutaneous Coronary Interventions of the European Society of Cardiology. Eur Heart J 2005;26:804-847.
15. Pazhenkottil AP, Ghadri JR, Nkoulou RN, Wolfrum M, Buechel RR, Küest SM, Husmann L, Herzog BA, Gaemperli O, Kaufmann PA. Improved outcome prediction by SPECT myocardial perfusion imaging after CT attenuation correction. J Nucl Med 2011;52:196-200.
16. Dvorak RA, Brown RK, Corbett JR. Interpretation of SPECT/CT myocardial perfusion images: common artifacts and quality control techniques. Radiographics 2011;31:2041-2057.
17. Ficaro EP, Fessler JA, Shreve PD, Kritzman JN, Rose PA, Corbett JR. Simultaneous transmission/emission myocardial perfusion tomography. Diagnostic accuracy of attenuation-corrected 99mTc-sestamibi single-photon emission computed tomography. Circulation 1996;93:463-473.
18. Genovesi D, Giorgetti A, Gimelli A, Kusch A, D'Aragona Tagliavia I, Casagranda M, Cannizzaro G, Giubbini R, Bertagna F, Fagioli G, Rossi M, Romeo A, Bertolaccini P, Bonini R, Marzullo P. Impact of attenuation correction and gated acquisition in SPECT myocardial perfusion imaging: results of the multicentre SPAG (SPECT Attenuation Correction vs Gated) study. Eur J Nucl Med Mol Imaging 2011;38:1890-1898.
19. Sharma P, Patel CD, Karunanithi S, Maharjan S, Malhotra A. Comparative accuracy of CT attenuation-corrected and non-attenuation-corrected SPECT myocardial perfusion imaging. Clin Nucl Med 2012;37:332-338.
20. Masood Y, Liu YH, Depuey G, Taillefer R, Araujo LI, Allen S, Delbeke D, Anstett F, Peretz A, Zito MJ, Tsatkin V, Wackers FJ. Clinical validation of SPECT attenuation correction using x-ray computed tomography-derived attenuation maps: multicenter clinical trial with angiographic correlation. J Nucl Cardiol 2005;12:676-686.
21. Links JM, Becker LC, Rigo P, Taillefer R, Hanelin L, Anstett F, Burckhardt D, Mixon L. Combined corrections for attenuation, depth-dependent blur, and motion in cardiac SPECT: a multicenter trial. J Nucl Cardiol 2000;7:414-425.
22. Hendel RC, Berman DS, Cullom SJ, Follansbee W, Heller GV, Kiat H, Groch MW, Mahmarian JJ. Multicenter clinical trial to evaluate the efficacy of correction for photon attenuation and scatter in SPECT myocardial perfusion imaging. Circulation 1999;99:2742-2749.
23. Johansen A, Grupe P, Veje A, Braad PE, Høilund-Carlsen PF. Scatter and attenuation correction changes interpretation of gated myocardial perfusion imaging. Eur J Nucl Med Mol Imaging. Eur J Nucl Med Mol Imag 2004;31:1152-1159.
24. Huang R, Li F, Zhao Z, Liu B, Ou X, Tian R, Li L. Hybrid SPECT/CT for attenuation correction of stress myocardial perfusion imaging. Clin Nucl Med 2011;36:344-349.
25. Ficaro EP. Should SPET attenuation correction be more widely employed in routine clinical practice? For. Eur J Nucl Med Mol Imaging 2002;29:409-412.
26. Shotwell M, Singh BM, Fortman C, Bauman BD, Lukes J, Gerson MC. Improved coronary disease detection with quantitative attenuation-corrected Tl-201 images. J Nucl Cardiol 2002;9:52-62.
27. Wolak A, Slomka PJ, Fish MB, Lorenzo S, Berman DS, Germano G. Quantitative diagnostic performance of myocardial perfusion SPECT with attenuation correction in women. J Nucl Med 2008;49:915-922.
28. Okuda K, Nakajima K, Matsuo S, Wakabayashi H, Taki J, Kinuya S. Cause of apical thinning on attenuation-corrected myocardial perfusion SPECT. Nucl Med Commun 2011;32:1033-1039.
29. Venero CV, Heller GV, Bateman TM, McGhie AI, Ahlberg AW, Katten D, Courter SA, Golub RJ, Case JA, Cullom SJ. A multicenter evaluation of a new post-processing method with depth-dependent collimator resolution applied to full-time and half-time acquisitions without and with simultaneously acquired attenuation correction. J Nucl Cardiol 2009;16:714-725.
30. Banzo I, Pena FJ, Allende RH, Quirce R, Carril JM. Prospective clinical comparison of non-corrected and attenuation- and scatter-corrected myocardial perfusion SPECT in patients with suspicion of coronary artery disease. Nucl Med Commun 2003;24:995-1002.
31. Fricke H, Fricke E, Weise R, Kammeier A, Lindner O, Burchert W. A method to remove artifacts in attenuation-corrected myocardial perfusion SPECT Introduced by misalignment between emission scan and CT-derived attenuation maps. J Nucl Med 2004;45:1619-1625.
32. Apostolopoulos DJ, Gąsowska M, Savvopoulos CA, Skouras T, Spyridonidis T, Andrejczuk A, Vassilakos PJ. The impact of transmission-emission misregistration on the interpretation of SPET/CT myocardial perfusion studies and the value of misregistration correction. Hell J Nucl Med 2015;18:114-121.

Interesting Image
Mol Imaging Radionucl Ther 2023;32:146-149 DOI:10.4274/mirt.galenos.2022.80774

^{68}Ga-FAPI-04 PET/CT Findings in Patients with Liver Cirrhosis

Karaciğer Sirozu Olan Hastalarda ^{68}Ga-FAPI-04 PET/BT Bulguları

Gamze Tatar[1], Ediz Beyhan[2], Özge Erol Fenercioğlu[2], İsa Sevindir[3], Nurhan Ergül[2], Tevfik Fikret Çermik[2]

[1]University of Health Sciences Turkey, İstanbul Bağcılar Training and Research Hospital, Clinic of Nuclear Medicine, İstanbul, Turkey
[2]University of Health Sciences Turkey, İstanbul Training and Research Hospital, Clinic of Nuclear Medicine, İstanbul, Turkey
[3]University of Health Sciences Turkey, İstanbul Training and Research Hospital, Clinic of Internal Medicine, Division of Gastroenterology, İstanbul, Turkey

Abstract

Fibroblast activation protein (FAP) is expressed as a pro-inflammatory agent from fibrous tissue in liver cirrhosis and in the tumor microenvironment. Cirrhosis is the last stage of any chronic liver disease, and the natural course of cirrhosis is the progression from the asymptomatic phase to the symptomatic decompensated phase with the development of ascites. Although various clinical features suggest cirrhosis in patients with chronic liver disease, non-invasive methods should follow the clinical approach before a definitive diagnosis. Herein, we present three cases of liver cirrhosis with fibroblast activation protein inhibitor (FAPI) uptake to demonstrate the usefulness of ^{68}Ga-FAPI-04 positron emission tomography/computed tomography (PET/CT) scan in cirrhosis.

Keywords: PET/CT, ^{68}Ga FAPI-04, cirrhosis, liver, molecular imaging

Öz

Fibroblast aktivasyon proteini (FAP), karaciğer sirozunda ve tümör mikroçevresinde fibröz dokudan proenflamatuvar bir ajan olarak eksprese edilir. Siroz, herhangi bir kronik karaciğer hastalığının son aşamasını gösterir ve sirozun doğal seyri, asit gelişimi ile asemptomatik fazdan semptomatik dekompanse faza ilerlemedir. Kronik karaciğer hastalığı olan hastalarda çeşitli klinik özellikler sirozu düşündürse de, kesin tanıdan önce invaziv olmayan yöntemler klinik yaklaşımı takip etmelidir. Burada, sirozda ^{68}Ga-fibroblast aktivasyon protein inhibitörü (FAPI)-04 pozitron emisyon tomografisi/bilgisayarlı tomografi taramasının yararlılığını göstermek için FAPI tutulumu olan üç karaciğer sirozu olgusunu sunuyoruz.

Anahtar kelimeler: PET/BT, ^{68}Ga FAPI-04, siroz, karaciğer, moleküler görüntüleme

Address for Correspondence: Gamze Tatar MD, University of Health Sciences Turkey, İstanbul Bağcılar Training and Research Hospital, Clinic of Nuclear Medicine, İstanbul, Turkey
Phone: +90 212 444 40 00 **E-mail:** gamze_tatar@hotmail.com ORCID ID: orcid.org/0000-0002-4187-755X
Received: 06.08.2022 **Accepted:** 12.12.2022

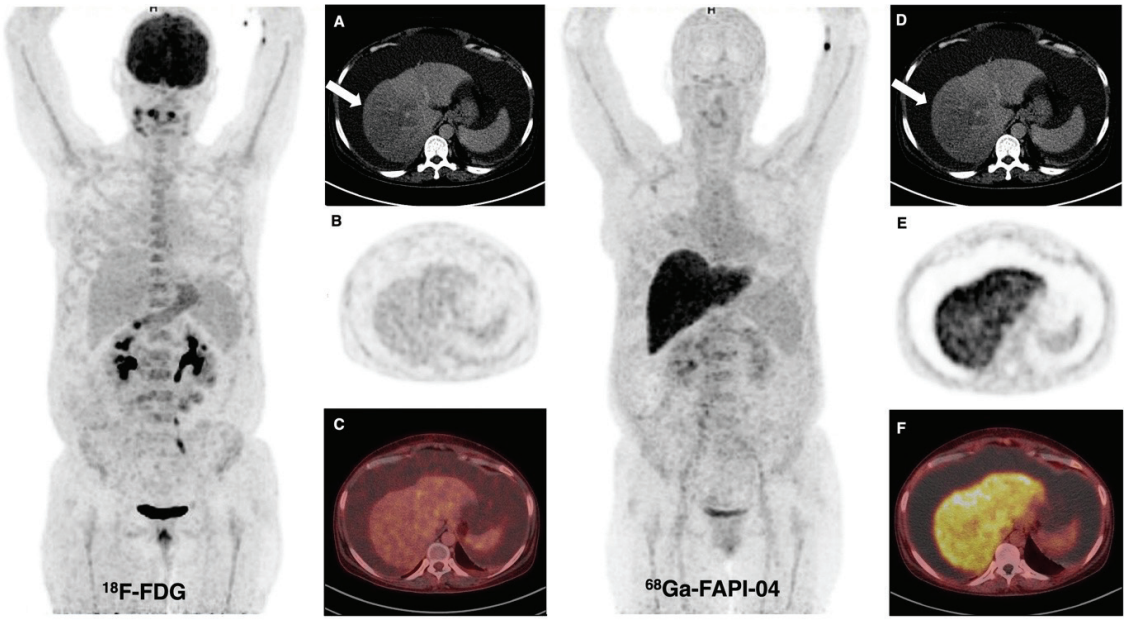

Figure 1. A 50-year-old woman patient presented with abdominal pain and was found to have massive ascites and had undergone ^{18}F-fluorodeoxyglucose (FDG) and ^{68}Ga-fibroblast activation protein inhibitor (FAPI)-04 positron emission tomography/computed tomography (PET/CT) imaging for a suspected gastric tumor. Abnormal liver activity was not observed on ^{18}F-FDG PET/CT, but diffuse intense FAPI uptake [maximum standardized uptake value (SUV_{max}): 11.2] was seen in the liver on ^{68}Ga-FAPI-04 PET/CT. The hypodense area detected in CT sections [(A, D) arrow] at the right lobe of the liver did not show prominent ^{18}F-FDG [(B) PET, (C) fusion images] or FAPI uptake [(E) PET, (F) fusion images] in the parenchyma. Also, no malignant cells were found in the peritoneal aspiration fluid. The patient is being followed up with the diagnosis of decompensated alcoholic cirrhosis.

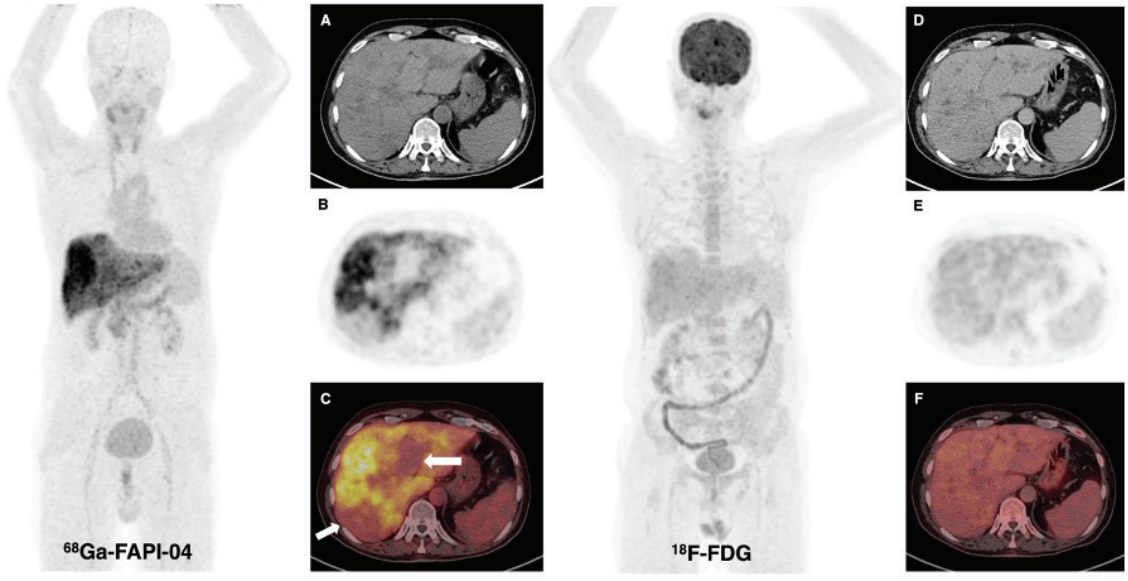

Figure 2. ^{18}F-FDG and ^{68}Ga-FAPI-04 PET/CT imaging were performed on a 55-year-old patient who was investigated for a liver malignancy that may occur on the basis of cirrhosis. Heterogeneous intense FAPI uptake was detected in the liver, especially in the right lobe, whereas there was no significant pathological uptake apart from parenchymal areas protected from cirrhosis [(C) arrows] [(A) CT, (B) PET, (C) fusion images] and no prominent liver activity on ^{18}F-FDG PET/CT [(D) CT, (E) PET, (F) fusion images]. In addition, mild to moderately increased thyroidal uptake suggestive of thyroiditis was revealed on the maximum intensity projection image of ^{68}Ga-FAPI-04 PET/CT.

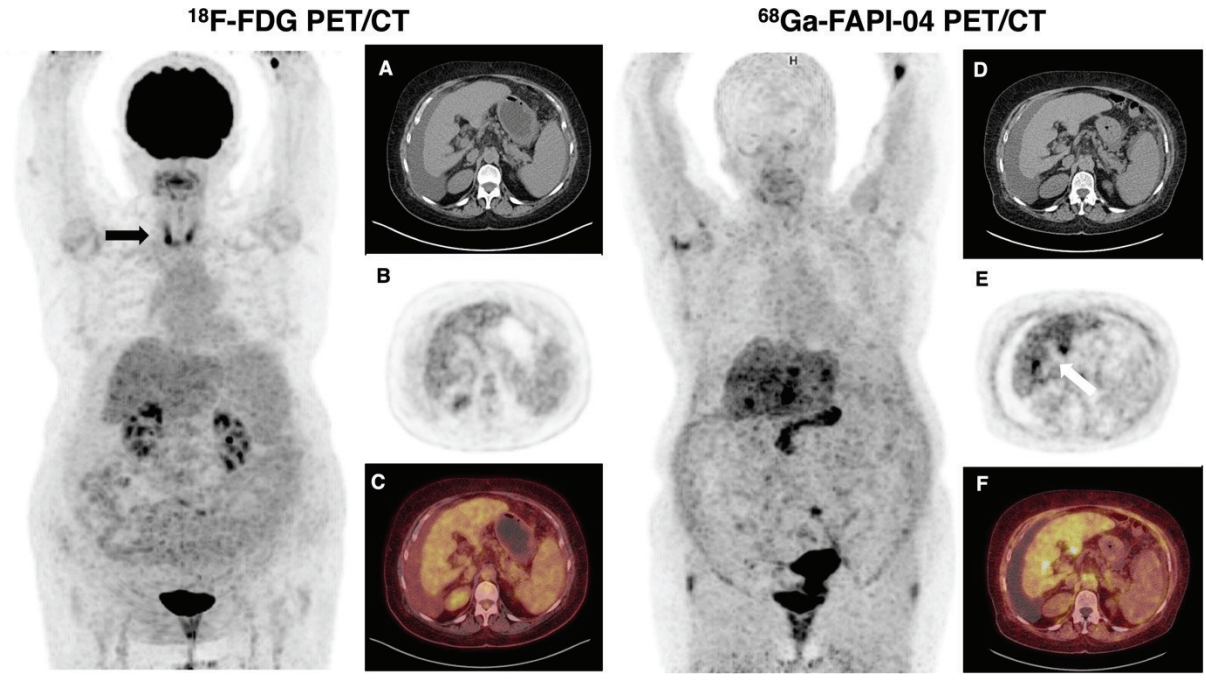

Figure 3. ^{18}F-FDG and ^{68}Ga-FAPI-04 PET/CT scans were obtained on a 70-year-old woman patient with free fluid in the peritoneum for the evaluation of liver cirrhosis [(A, D) CT)]. Slightly increased tracer activity in the liver [(B) PET, (C) fusion images] and diffusely increased thyroid uptake (arrow) indicated thyroiditis were seen on ^{18}F-FDG PET/CT. The axial view of PET (E) and fusion images (F) showed intense heterogeneous FAPI uptake (SUV_{max}: 9.7) in the liver, but no FAPI uptake in the thyroid gland on ^{68}Ga-FAPI-04 PET/CT.

The histological diagnosis of cirrhosis indicates the last stage of any chronic liver disease, and the natural course of cirrhosis is the progression from the asymptomatic phase to the symptomatic decompensated phase with the development of ascites (1,2). FAPI was superior to ^{18}F-FDG in detecting liver tumors and many types of cancer (3,4,5). In a few cases published in the literature, diffuse intense FAPI uptake in the liver has been defined in patients with cirrhosis and ^{68}Ga-FAPI-04 PET/CT has been shown to have a place in the differentiation of liver lesions due to its preferred image contrast (6). In a study evaluating liver lesions comparatively both with FAPI and ^{18}F-FDG PET/CT on twenty patients, ^{68}Ga-FAPI-04 PET/CT was found superior to ^{18}F-FDG in detecting liver lesions and Shi et al. (7) also detected significantly higher hepatic FAPI uptake in nine patients with cirrhosis than the non-cirrhotic study group. Low background activity is among the important advantages of imaging with FAPI, but high uptake on the liver in patients with cirrhosis may limit the evaluation of hepatic lesions in terms of malignant nature. Therefore, in patients without cirrhosis, some liver lesions may be better differentiated in the absence of intense FAPI uptake. However, Zhao et al. (8) reported a case of cirrhosis with multiple FAPI-negative benign hepatic nodules with increased liver FAPI uptake. According to this patient example, they stated that ^{68}Ga-FAPI-04 PET/CT might be an appropriate tool for differentiating benign nodular lesions from primary malignant tumors. Our results, together with the published cases, suggest that ^{68}Ga-FAPI-04 PET/CT may have a place in the treatment plan and management of liver cirrhosis in addition to tumor imaging in the future molecular era.

Ethics

Informed Consent: Informed consent was obtained from the patients included in the study.

Peer-review: Externally and internally peer-reviewed.

Authorship Contributions

Surgical and Medical Practices: G.T., E.B., Ö.E.F., İ.S., N.E., T.F.Ç., Concept: G.T., E.B., Ö.E.F., İ.S., N.E., T.F.Ç., Design: G.T., E.B., Ö.E.F., İ.S., N.E., T.F.Ç., Data Collection or Processing: G.T., E.B., Ö.E.F., İ.S., N.E., T.F.Ç., Analysis or Interpretation: G.T., E.B., Ö.E.F., İ.S., N.E., T.F.Ç., Literature Search: G.T., E.B., Ö.E.F., İ.S., Writing: G.T., T.F.Ç.

Conflict of Interest: No conflict of interest was declared by the authors.

Financial Disclosure: The authors declared that this study received no financial support.

References

1. Ginès P, Krag A, Abraldes JG, Solà E, Fabrellas N, Kamath PS. Liver cirrhosis. Lancet 2021;398:1359-1376.
2. Zhou WC, Zhang QB, Qiao L. Pathogenesis of liver cirrhosis. World J Gastroenterol 2014;20:7312-7324.
3. Çermik TF, Ergül N, Yılmaz B, Mercanoğlu G. Tumor imaging with 68Ga-DOTA-FAPI-04 PET/CT: comparison with 18F-FDG PET/CT in 22 different cancer types 2022;47:333-339.
4. Chen H, Zhao L, Ruan D, Pang Y, Hao B, Dai Y, Wu X, Guo W, Fan C, Wu J, Huang W, Lin Q, Sun L, Wu H. Usefulness of [^{68}Ga]Ga-DOTA-FAPI-04 PET/CT in patients presenting with inconclusive [^{18}F]FDG PET/CT findings. Eur J Nucl Med Mol Imaging 2021;48:73-86.
5. Ballal S, Yadav MP, Moon ES, Kramer VS, Roesch F, Kumari S, Tripathi M, ArunRaj ST, Sarswat S, Bal C. Biodistribution, pharmacokinetics, dosimetry of [^{68}Ga]Ga-DOTA.SA.FAPi, and the head-to-head comparison with [^{18}F]F-FDG PET/CT in patients with various cancers. Eur J Nucl Med Mol Imaging 2021;48:1915-1931.
6. Shi X, Xing H, Yang X, Li F, Yao S, Congwei J, Zhao H, Hacker M, Huo L, Li X. Comparison of PET imaging of activated fibroblasts and ^{18}F-FDG for diagnosis of primary hepatic tumours: a prospective pilot study. Eur J Nucl Med Mol Imaging 2021;48:1593-1603.
7. Shi X, Xing H, Yang X, Li F, Yao S, Zhang H, Zhao H, Hacker M, Huo L, Li X. Fibroblast imaging of hepatic carcinoma with ^{68}Ga-FAPI-04 PET/CT: a pilot study in patients with suspected hepatic nodules. Eur J Nucl Med Mol Imaging 2021;48:196-203.
8. Zhao L, Gu J, Fu K, Lin Q, Chen H. 68Ga-FAPI PET/CT in assessment of liver nodules in a cirrhotic patient. Clin Nucl Med 2020;45:430-432.

Interesting Image
Mol Imaging Radionucl Ther 2023;32:150-152 DOI:10.4274/mirt.galenos.2023.47550

Comparison of ^{68}Ga-PSMA PET/CT and ^{18}F-PSMA PET/CT of a Patient with Prostate Cancer Recurrence on Urinary Bladder Wall

Mesane Duvarında Prostat Kanseri Nüksü Tespit Edilen Hastanın ^{68}Ga-PSMA PET/BT ve ^{18}F-PSMA PET/BT Görüntülerinin Karşılaştırılması

Çiğdem Soydal, Burak Demir, Gizem Sütçü, Mine Araz, Nuriye Özlem Küçük

Ankara University Faculty of Medicine, Department of Nuclear Medicine, Ankara, Turkey

Abstract

Prostate cancer is one of the most prevalent cancers in the world. After radical prostatectomy, prostate-specific antigen (PSA) levels are usually used as a marker of recurrence for prostate cancer. In the case of increased PSA levels, ^{68}Ga-prostate-specific membrane antigen (PSMA) or ^{18}F-PSMA, a new alternative, can be performed for the detection of recurrent disease. We report a case of a 49-year-old male patient with increasing PSA levels who was previously operated 8 years ago. Although no obvious pathological uptake was detected in ^{68}Ga-PSMA positron emission tomography/computed tomography (PET/CT), ^{18}F-PSMA PET/CT revealed a lesion with pathological uptake on the urinary bladder wall.

Keywords: Cancer, prostate, positron emission tomography, ^{68}Ga-PSMA, ^{18}F-PSMA

Öz

Prostat kanseri dünyada en sık görülen kanserlerden biridir. Radikal prostatektomi operasyonu sonrasında prostat-spesifik antijen (PSA) düzeyleri genellikle prostat kanseri rekürrens için tümör belirteçi olarak kullanılmaktadır. Yüksek PSA düzeylerinde ise ^{68}Ga- prostat-spesifik membran antijeni (PSMA) pozitron emisyon tomografi/bilgisayarlı tomografi (PET/BT) veya daha yeni bir alternatifi olan ^{18}F-PSMA PET/BT rekürrensin tespitinde kullanılabilmektedir. Artan PSA düzeyleri tespit edilen ve 8 yıl önce opere edilmiş olan 49 yaşında prostat kanseri tanılı bir hastayı sunduk. Her ne kadar ^{68}Ga-PSMA PET/BT'de belirgin bir patolojik aktivite tutulumu izlenmese de, ^{18}F-PSMA PET/BT görüntülemesi sonucunda mesane duvarında patolojik tutulum gösteren lezyon tespit edildi.

Anahtar kelimeler: Kanser, prostat, pozitron emisyon tomografisi, ^{68}Ga-PSMA, ^{18}F-PSMA

Address for Correspondence: Burak Demir MD, Ankara University Faculty of Medicine, Department of Nuclear Medicine, Ankara, Turkey
Phone: +90 555 817 07 10 **E-mail:** 4burakfe@gmail.com ORCID ID: orcid.org/0000-0002-0966-9988
Received: 05.10.2022 **Accepted:** 15.01.2023

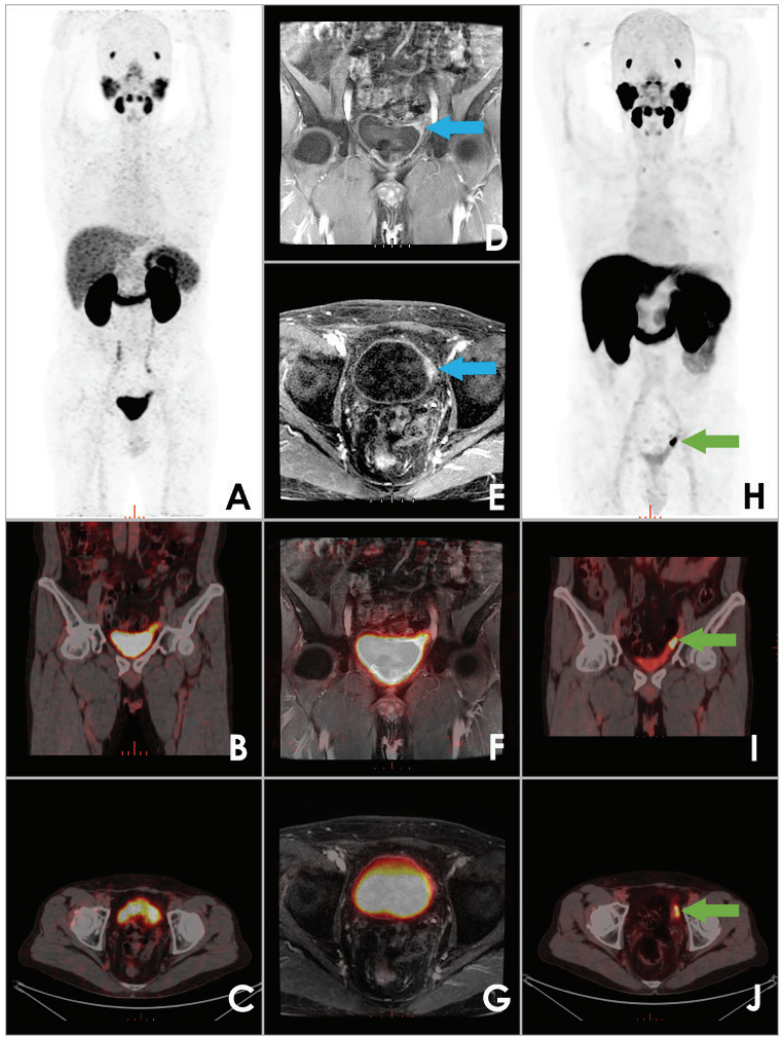

Figure 1. A 49-year-old man with a history of radical prostatectomy for prostate adenocarcinoma was referred for ^{68}Ga-prostate-specific membrane antigen (PSMA) positron emission tomography/computed tomography (PET/CT) because of increased levels of PSA as high as 0.52 ng/mL. There was no discernible pathological uptake on ^{68}Ga-PSMA PET/CT maximum intensity projection (MIP) (A), coronal (B), and axial (C) projections. After completing ^{68}Ga-PSMA whole-body PET/CT, pelvic PET/magnetic resonance imaging (MRI) with intravenous MRI contrast agent was performed to detect any local recurrence in the pelvis. In coronal (D) and axial (E) T1-weighted post-contrast MRI sequences, a lesion with contrast enhancement (blue arrows) was spotted on the left superior wall of the urinary bladder. However, in coronal (F) and axial (G) PET/MRI fusion images, no discernible uptake from radioactive urine could be detected. Three days later, the patient underwent a whole-body ^{18}F-PSMA PET/CT scan. Pathological uptake of ^{18}F-PSMA in the previously reported location in MRI scans has been observed (green arrows) in MIP (H), coronal (I), and axial (J) projections. In ^{18}F-PSMA PET/CT scans, there was a significant difference between activities detected in lesion and radioactive urine, unlike ^{68}Ga-PSMA PET scans. Prostate cancer is one of the most prevalent cancers in men worldwide (1). PSMA is a transmembrane protein that is highly expressed in prostate cancer cells (2). Its expression is increased in cases of more aggressive and dedifferentiated tumors (3). With the utilization of ^{68}Ga or ^{18}F labeled PSMA ligands, prostate cancer lesions can be imaged with positron emission tomography (4,5). Although ^{18}F-PSMA-1007 and ^{68}Ga-PSMA-11 are both PSMA ligands that can be used for imaging prostate cancer, there are some differences in their biodistribution and excretion mechanisms. Urinary extraction of ^{18}F-PSMA-1007 is minimal (5), unlike ^{68}Ga-PSMA-11, which can be an advantage in detecting local recurrences due to close proximity of the prostate gland and urinary bladder.

Ethics

Informed Consent: Written informed consent was obtained from the patient.

Peer-review: Externally peer-reviewed.

Authorship Contributions

Concept: N.Ö.K., G.S., M.A., Ç.S., Design: N.Ö.K., G.S., M.A., Ç.S., Analysis or Interpretation: B.D., Ç.S., Literature Search: B.D., G.S., Ç.S., Writing: B.D., Ç.S.

Conflict of Interest: No conflict of interest was declared by the authors.

Financial Disclosure: The authors declared that this study has received no financial support.

References

1. Rebbeck TR. Prostate cancer genetics: variation by race, ethnicity, and geography. Semin Radiat Oncol 2017;27:3-10.
2. Sweat SD, Pacelli A, Murphy GP, Bostwick DG. Prostate-specific membrane antigen expression is greatest in prostate adenocarcinoma and lymph node metastases. Urology 1998;52:637-640.
3. Ghosh A, Heston WDW. Tumor target prostate specific membrane antigen (PSMA) and its regulation in prostate cancer. J Cell Biochem 2004;91:528-539.
4. Fendler WP, Eiber M, Beheshti M, Bomanji J, Ceci F, Cho S, Giesel F, Haberkorn U, Hope TA, Kopka K, Krause BJ, Mottaghy FM, Schöder H, Sunderland J, Wan S, Wester HJ, Fanti S, Herrmann K. 68Ga-PSMA PET/CT: Joint EANM and SNMMI procedure guideline for prostate cancer imaging: version 1.0. Eur J Nucl Med Mol Imaging 2017;44:1014-1024.
5. Giesel FL, Hadaschik B, Cardinale J, Radtke J, Vinsensia M, Lehnert W, Kesch C, Tolstov Y, Singer S, Grabe N, Duensing S, Schäfer M, Neels OC, Mier W, Haberkorn U, Kopka K, Kratochwil C. F-18 labelled PSMA-1007: biodistribution, radiation dosimetry and histopathological validation of tumor lesions in prostate cancer patients. Eur J Nucl Med 2017;44:678-688.

Interesting Image
Mol Imaging Radionucl Ther 2023;32:153-155 DOI:10.4274/mirt.galenos.2022.99266

Cutaneous Metastase of Rectal Neuroendocrine Carcinoma Revealed on ^{18}F-FDG PET/CT

Rektal Nöroendokrin Karsinomun ^{18}F-FDG PET/BT'de Kutanöz Metastazı

Ömer Faruk Şahin, Rahime Şahin, Mehmet Can Baloğlu, Tevfik Fikret Çermik, Nurhan Ergül

University of Health Sciences Turkey, İstanbul Training and Research Hospital, Clinic of Nuclear Medicine, İstanbul, Turkey

Abstract

Rectal neuroendocrine carcinomas constitute <1% of all neuroendocrine carcinomas and <1% of all gastrointestinal tract malignancies. Cutaneous metastases of rectal neuroendocrine carcinoma are rarer than visceral metastases. We represent a 71-year-old man who was diagnosed with neuroendocrine tumor grade 3 originating from the rectum 1 year ago. He was referred for ^{18}F-fluorodeoxyglucose (FDG) positron emission tomography/computed tomography for restaging after 6 cycles of chemotherapy and radiotherapy. Intensely increased ^{18}F-FDG uptake in the right cutaneous inguinal region was consistent with neuroendocrine carcinoma metastasis with biopsy from the same region.

Keywords: ^{18}F-FDG-PET, rectal neuroendocrine carcinoma, cutaneous metastasis

Öz

Rektal nöroendokrin karsinomlar, tüm nöroendokrin karsinomların <%1'ini ve tüm gastrointestinal sistem malignitelerinin <%1'ini oluşturur. Rektal nöroendokrin karsinomun deri metastazı, viseral metastazlardan daha nadirdir. Bir yıl önce rektum kaynaklı nöroendokrin tümör grade 3 tanısı konan 71 yaşında bir erkek hastayı sunuyoruz. Hasta 6 kür kemoterapi ve radyoterapi sonrası yeniden evreleme için ^{18}F-florodeoksiglukoz (FDG) pozitron emisyon tomografisi/bilgisayarlı tomografiye yönlendirildi. Sağ kasık bölgesindeki deride yoğun artmış ^{18}F-FDG tutulumu aynı bölgeden alınan biyopsi sonucuyla birlikte nöroendokrin karsinom metastazı ile uyumluydu.

Anahtar kelimeler: ^{18}F-FDG-PET, rektal nöroendokrin karsinom, kutanöz metastaz

Address for Correspondence: Ömer Faruk Şahin MD, University of Health Sciences Turkey, İstanbul Training and Research Hospital, Clinic of Nuclear Medicine, İstanbul, Turkey
Phone: +90 212 45960 00 **E-mail:** dromersahin@yahoo.com ORCID ID: orcid.org/0000-0003-3931-4261
Received: 09.08.2022 **Accepted:** 04.10.2022

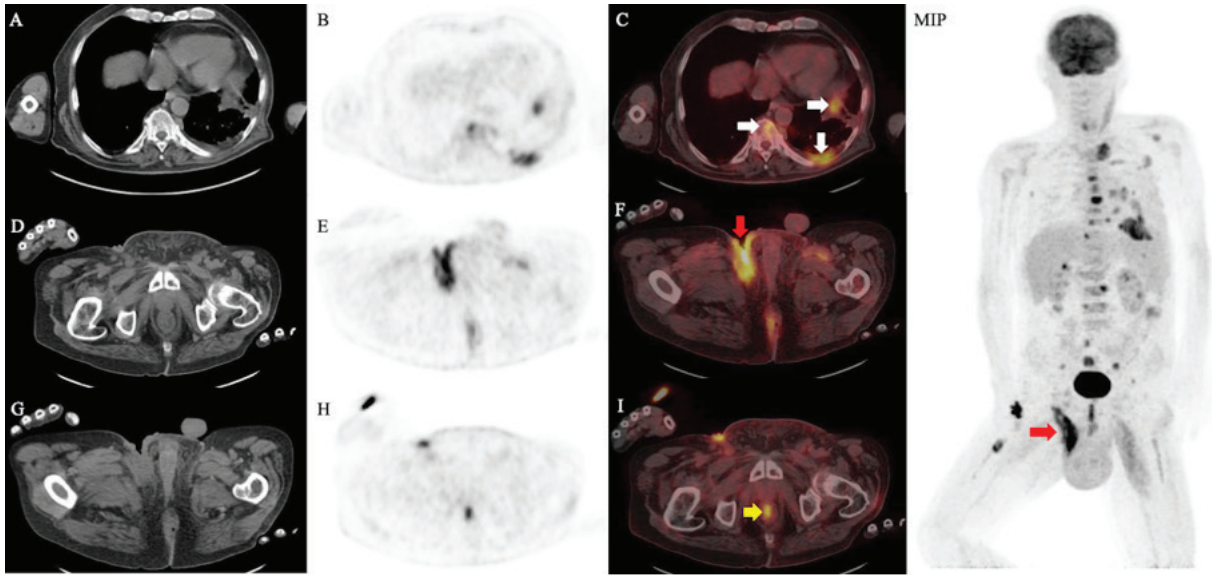

Figure 1. A 71-year-old man who was diagnosed with neuroendocrine tumor grade 3 originating from the rectum 1 year ago was referred to ^{18}F-fluorodeoxyglucose (FDG) positron emission tomography/computed tomography (PET/CT) for restaging after chemoradiotherapy. Axial CT, PET (A, B), and PET/CT fusion images (C) showed increased ^{18}F-FDG uptake related to metastatic lesions at vertebral regions and mass lesions at lingular segment of upper left lung and inferior anterobasal lobe of left lung [maximum standardized uptake value (SUV_{max}): 8.6] (white arrows). There was diffuse and intense ^{18}F-FDG uptake on skin at right inguinal region consistent with metastasis (SUV_{max}: 15.8) on axial CT, PET (D, E), and PET/CT fusion images (F) (red arrows). Also, a moderate uptake is seen at distal rectum and anal canal on axial CT, PET (G, H), and PET/CT fusion images (I) (SUV_{max}: 10.4) (yellow arrow). Rectal neuroendocrine carcinomas most commonly metastases to liver, followed by bone, lung, central nervous system, pleura, or mediastinum, while cutaneous metastases are considered rare (1). Primary cutaneous neuroendocrine carcinoma, also named Merkel cell carcinoma, is rare, accounting for less than 1% of all cutaneous malignancies and tends to spread quickly to the regional lymph nodes and then metastasizes to other organs, in particular the liver, bone, brain, and lungs (2). Secondary metastatic cutaneus neuroendocrine carcinoma is more commonly reported in the lung, less often in the larynx, gastrointestinal tract, pancreas, testicle, bladder, breast, uterus and rectum (3). Common regions for cutaneous metastasis of rectal neuroendocrine carcinomas include the scalp, abdomen, chest, back, and extremities. The appearance of cutaneous metastasis is a very poor prognostic sign (4). Up to now, 5 cases were reported that rectal neuroendocrine carcinoma metastases to skin. However, none of them include inguinal skin metastases and use ^{18}F-FDG PET/CT for imaging (5,6,7,8).

Ethics

Informed Consent: The patient consent was obtained.

Peer-review: Externally peer-reviewed.

Authorship Contributions

Surgical and Medical Practices: Ö.M.Ş., R.Ş., M.C.B., T.F.Ç., N.E., Concept: Ö.M.Ş., R.Ş., M.C.B., T.F.Ç., N.E., Design: Ö.M.Ş., R.Ş., M.C.B., T.F.Ç., N.E., Data Collection or Processing: Ö.M.Ş., R.Ş., M.C.B., T.F.Ç., N.E., Analysis or Interpretation: Ö.M.Ş., R.Ş., M.C.B., T.F.Ç., N.E., Literature Search: Ö.M.Ş., R.Ş., M.C.B., T.F.Ç., N.E., Writing: Ö.M.Ş., R.Ş., M.C.B., T.F.Ç., N.E.

Conflict of Interest: No conflict of interest was declare by the authors.

Financial Disclosure: The authors declared that this study received no financial support.

References

1. Voong KR, Rashid A, Crane CH, Minsky BD, Krishnan S, Yao JC, Wolff RA, Skibber JM, Feig BW, Chang GJ, Das P. Chemoradiation for high-grade neuroendocrine carcinoma of the rectum and anal canal. Am J Clin Oncol 2015;40:555-560.
2. Müller-Richter UDA, Gesierich A, Kübler AC, Hartmann S, Brands RC. Merkel cell carcinoma of the head and neck: recommendations for diagnostics and treatment. Ann Surg Oncol 2017;24:3430-3437.
3. Amorim GM, Quintella D, Cuzzi T, Rodrigues R, Ramos-E-Silva M. Cutaneous metastasis of neuroendocrine carcinoma with unknown primary site: case report and review of the literature. Case Rep Dermatol 2015;7:263-274.
4. Aldret S, Cotton L. Skin as a site of metastasis. Osteopathic Family Physician 2012;4:13-17.

5. Fluehler C, Quaranta L, di Meo N, Ulessi B, Trevisan G. Cutaneous metastasis of neuroendocrine carcinoma. Indian J Dermatol 2013;58:247.
6. 6.Lee WJ, Oh SH, Chang SE, Lee MW. Skin Metastasis of neuroendocrine carcinoma arising in the rectum. Ann Dermatol 2007;19:163-165.
7. Bell HK, Poston GJ, Vora J, Wilson NJ. Cutaneous manifestations of the malignant carcinoid syndrome. Br J Dermatol 2005;152:71-75.
8. Wang SM, Ye M, Ni SM. Multiple scalp metastases from colonic neuroendocrine carcinoma: case report and literature review. BMC Cancer 2014;14:305.

Interesting Image
Mol Imaging Radionucl Ther 2023;32:156-158 DOI:10.4274/mirt.galenos.2022.06926

Testicular Metastasis of Jejunal Neuroendocrine Tumor on ^{68}Ga-DOTATATE PET/CT

Jejunal Nöroendokrin Tümöre Sekonder Gelişen Bilateral Testiküler Metastazın ^{68}Ga-DOTATATE PET/BT Bulguları

Ömer Faruk Şahin, Özge Erol Fenercioğlu, Ediz Beyhan, Tevfik Fikret Çermik, Nurhan Ergül

University of Health Sciences Turkey, İstanbul Training and Research Hospital, Clinic of Nuclear Medicine, İstanbul, Turkey

Abstract

Neuroendocrine tumors are slow-growing tumors originating from neuroendocrine cells and capable of metastasis. Most of them are found in the gastrointestinal tract; however, they can also be rarely seen in other organs. Testicular neuroendocrine tumors account for less than 1% of all testicular neoplasms. They may present as primary testicular or secondary tumors from extratesticular sources. Jejunal neuroendocrine tumor metastasis to the testis is extremely rare. We present the case of a 61-year-old man with a jejunal neuroendocrine tumor and metastases to bilateral testicles revealed on Gallium-68-DOTATATE positron emission tomography/computed tomography.

Keywords: ^{68}Ga-DOTATATE, testicular metastasis, jejunal neuroendocrine tumor, PET/CT

Öz

İnce bağırsak nöroendokrin tümörleri; intestinal mukozadaki serotonin eksprese eden enterokromoffin hücrelerden köken alan, tüm gastrointestinal tümörlerin %1'inden daha azını oluşturan tümörlerdir. İnce bağırsak nöroendokrin tümörlerinin çoğu iyi diferansiye (G1-G2) tümörler olup en sık mezenterik lenf nodlarına, paraaortik lenf nodlarına ve karaciğere metastaz yaparlar. Jejunal nöroendokrin tümörlerin bilateral testise metastazı nadirdir. Testiküler nöroendokrin tümörler tüm testiküler neoplazmların %1'inden azını oluşturur. Nöroendokrin tümör tanılı 61 yaşında erkek hastaya ait testis metastazı görüntüleri sunulmuştur.

Anahtar kelimeler: ^{68}Ga-DOTATATE, testiküler metastaz, jejunal nöroendokrin tümör, PET/BT

Address for Correspondence: Ömer Faruk Şahin MD, University of Health Sciences Turkey, İstanbul Training and Research Hospital, Clinic of Nuclear Medicine, İstanbul, Turkey
Phone: +90 212 459 60 00 **E-mail:** dromersahin@yahoo.com ORCID ID: orcid.org/0000-0003-3931-4261
Received: 20.06.2022 **Accepted:** 09.10.2022

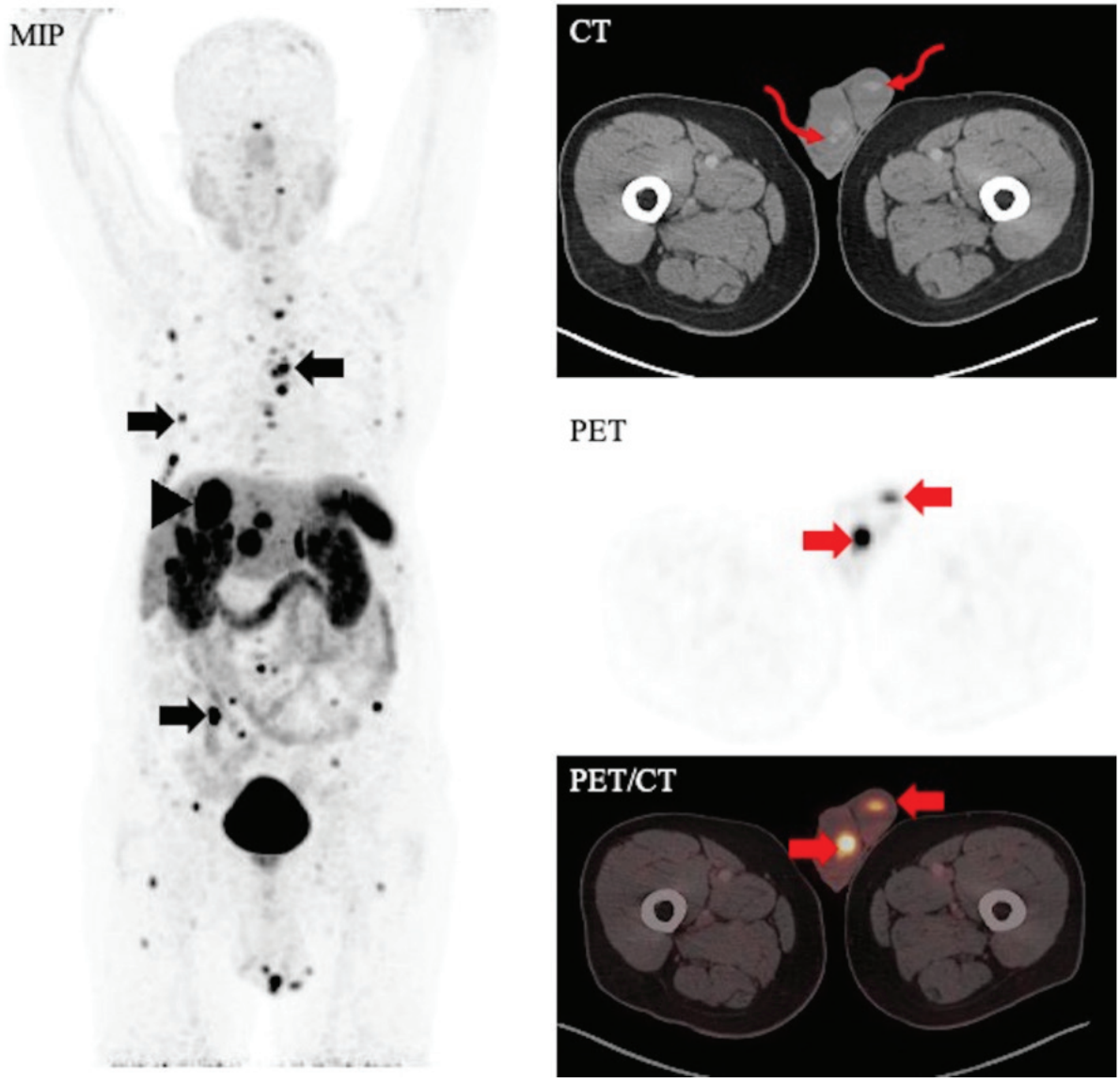

Figure 1. A 61-year-old man with metastatic jejunal neuroendocrine tumor was referred to Gallium-68 (^{68}Ga)-DOTATATE positron emission tomography/computed tomography (PET/CT) for restaging. He had a jejunal operation 18 years ago and was diagnosed with a jejunal neuroendocrine tumor. He had received 10 cycles of 177Lu-DOTATATE therapy and Y-90 microsphere therapy for metastatic lesions in his liver 5 years ago. He has been receiving IM Sandostatin LAR 30 mg monthly. A whole-body ^{68}Ga-DOTATATE PET/CT study maximum intensity projection image revealed multiple metastatic lesions in the whole body: a liver metastasis at segment 4A-8 [maximum standardized uptake value (SUV_{max}): 37.7] (black arrowhead), multiple metastatic foci at the vertebral colon, bilateral hemithorax ribs, and pelvic bones (black arrows). In addition, hyperintense lesions were observed in bilateral testicles on CT (red curved arrows), and these lesions showed intense ^{68}Ga-DOTATATE uptake (SUV_{max}: 28.28) in axial sections of PET and fusion images (red arrows). The testicular ultrasonography study was then applied and both testicular lesions were found to be compatible with metastasis. Approximately 70% of neuroendocrine tumors are located in the gastrointestinal tract, most commonly in the small bowel (45%). Hepatic metastases (45%) are the most common metastatic site of jejunal neuroendocrine tumors, while regional lymph nodes, peritoneum, lungs, bones, pancreas, testicles, ovaries, and myocardium are other rare documented sites of distant metastasis (1,2). ^{68}Ga-DOTATATE PET/CT is used to image primary tumors, metastasis, and recurrence of neuroendocrine tumors because of DOTATATE's high affinity for somatostatin receptors (3). Testicular neuroendocrine tumors account for less than 1% of all testicular neoplasms (4). Primary testicular neuroendocrine tumors usually metastasize to para-aortic lymph nodes, lungs, vertebrae, retroperitoneum, skin, and skeletal muscle (5). Metastatic testicular neuroendocrine tumors generally involve both testes and are associated with multifocality and vascular invasion (6). In the literature, it has been reported that gastrointestinal neuroendocrine tumors cause testicular metastasis in some cases, but none of them used ^{68}Ga-DOTATATE PET/CT for imaging (4,7,8,9,10,11,12,13).

Ethics

Informed Consent: The patient consent was obtained.

Peer-review: Externally and internally peer-reviewed.

Authorship Contributions

Surgical and Medical Practices: Ö.F.Ş., Ö.E.F., E.B., T.F.Ç., N.E., Concept: T.F.Ç., N.E., Design: Ö.F.Ş., Ö.E.F., E.B., N.E., Data Collection or Processing: Ö.F.Ş., Ö.E.F., E.B., Analysis or Interpretation: Ö.F.Ş., Ö.E.F., E.B., N.E., Literature Search: Ö.F.Ş., Writing: Ö.F.Ş.

Conflict of Interest: No conflict of interest was declared by the authors.

Financial Disclosure: The authors declared that this study has received no financial support.

References

1. Antoniadou F, Korkolis D, Koufopoulos N, Manatakis D, Sakellariou S. A well differentiated neuroendocrine tumor of the jejunum with peritoneal carcinomatosis: a case report. Mol Clin Oncol 2018;9:651-655.
2. Landerholm K, Falkmer S, Järhult J. Epidemiology of small bowel carcinoids in a defined population. World J Surg 2010;34:1500-1505.
3. Bodei L, Ambrosini V, Herrmann K, Modlin I. Current Concepts in ^{68}Ga-DOTATATE imaging of neuroendocrine neoplasms: interpretation, biodistribution, dosimetry, and molecular strategies. J Nucl Med 2017;58:1718-1726.
4. Amine MM, Mohamed B, Mourad H, Majed H, Slim C, Mehdi B, Hela M, Nouri R, Rim K, Tahya B, Nabil MM. Neuroendocrine testicular tumors: a systematic review and meta-analysis. Curr Urol 2017;10:15-25.
5. Wang WP, Guo C, Berney DM, Ulbright TM, Hansel DE, Shen R, Ali T, Epstein JI. Primary carcinoid tumors of the testis: a clinicopathologic study of 29 cases. Am J Surg Pathol 2010;34:519-524.
6. Manna S, Narayana SM, Premalata CS. Primary neuroendocrine tumor of the testis masquerading as germ cell tumor – a case report. Eur J Med Health Science 2020;2:518.
7. Fucs M, Romero FR, Germanos de Castro M, de Carvalho Fernandes R, Camara-Lopes LH, Cardenuto Perez MD. Testicular metastasis 10 years after resection of appendiceal carcinoid. Urology 2005;65:591.
8. Danikas D, Sachs R, Dressner RM, Arvanitis ML. Testicular metastasis from ileal carcinoid: report of a case. Dis Colon Rectum 2001;44:1365-1366.
9. Lau HY, Lai V. Metastatic testicular carcinoid tumour. Hong Kong J Radiol 2013;16:69-73.
10. Berdjis CC, Mostofi FK. Carcinoid tumors of the testis. J Urol 1977;118:777-782.
11. Stroosma OB, Delaere KP. Carcinoid tumours of the testis. BJU Int 2008;101:1101-1105.
12. Cope Z. Metastasis of an argentaffin carcinoma in the testicle. British Journal Urol 1930;2:268-272.
13. Blumberg JM, Sedberry S, Kazmi SO. Bilateral asynchronous metastatic carcinoid tumor of the testis. Urology 2005;65:174.

Interesting Image
Mol Imaging Radionucl Ther 2023;32:159-161 DOI:10.4274/mirt.galenos.2022.97268

^{18}F-FDG PET/MRI Image of Skin Metastasis of Ovarian Cancer

Over Kanserinde Deri Metastazının ^{18}F-FDG PET/MR Görüntüsü

Ali Kibar, Sertaç Asa, Rabia Lebriz Uslu Beşli, Muhammet Sait Sağer, Kerim Sönmezoğlu

İstanbul University-Cerrahpaşa, Cerrahpaşa Faculty of Medicine, Department of Nuclear Medicine, İstanbul, Turkey

Abstract

Ovarian cancer is one of the deadliest tumors among women. It mostly metastasizes to the liver, pleura, lungs, and bones. We present a sixty-six-year-old patient with skin lesions. The patient who underwent biopsy due to skin lesions was diagnosed with ovarian cancer. ^{18}F-fluorodeoxyglucose (FDG) positron emission tomography/magnetic resonance imaging (PET/MRI) performed for metastasis search shows widespread skin involvement, especially in the lower abdomen and legs. Skin involvement it ovarian cancer can be rarely seen, and in this article we would like to share ^{18}F-FDG PET/MRI of skin involvement in ovarian cancer.

Keywords: ^{18}F-FDG PET, PET/MRI, ovarian cancer, skin metastasis

Öz

Over kanseri, kadınlar arasında en ölümcül tümörlerden biridir. Çoğunlukla karaciğer, plevra, akciğer ve kemiklere metastaz yapar. Altmış altı yaşında kadın hasta deri lezyonlarıyla başvuruyor. Deri lezyonları sebebiyle biyopsi yapılan hasta over kanseri tanısı alıyor. Metastaz arama amacıyla yapılan ^{18}F-florodeoksiglukoz pozitron emisyon tomografi/manyetik rezonansta (PET/MR) özellikler alt batın ve bacaklarda yaygın deri tutulumları izleniyor. Over kanserinde deri tutulumları nadir olarak görülebilmektedir, bu yazıda over kanserinin deri tutulumunun ^{18}F-FDG PET/MR görüntülerini paylaşmak istiyoruz.

Anahtar kelimeler: ^{18}F-FDG PET, PET/MR, over kanseri, deri metastazı

Address for Correspondence: Ali Kibar MD, İstanbul University-Cerrahpaşa, Cerrahpaşa Faculty of Medicine, Department of Nuclear Medicine, İstanbul, Turkey
Phone: +90 212 414 34 34 **E-mail:** ali.kibar@iuc.edu.tr ORCID ID: orcid.org/0000-0003-0073-2343
Received: 24.05.2022 **Accepted:** 04.11.2022

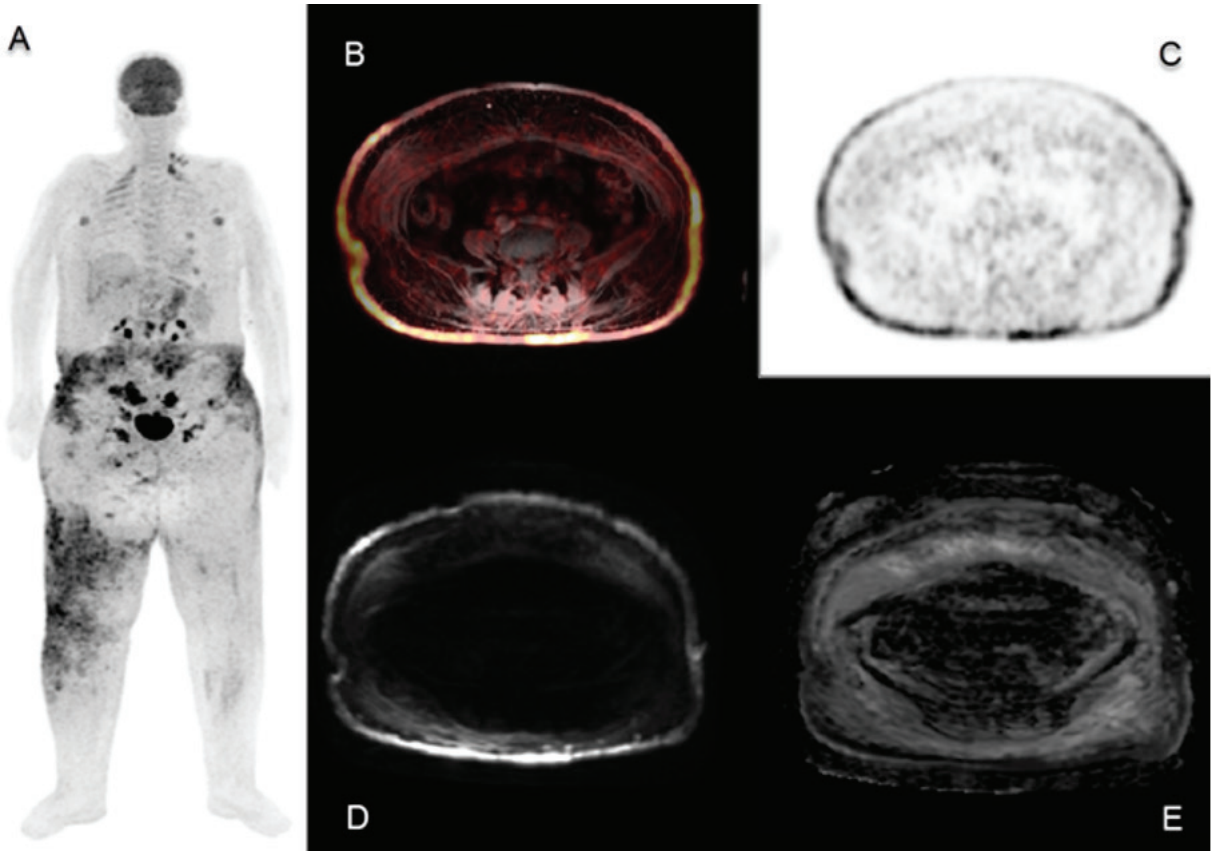

Figure 1. Ovarian cancer is responsible for most deaths among female reproductive system cancers and is also the fifth most common cause of death among all cancers in women according to the American Cancer Society. The most common distant metastatic sites are the liver, pleura, lung, bone, and brain. Skin metastasis is a rare feature of metastatic ovarian cancer. The prognosis of patients with skin metastasis varies greatly due to their heterogeneous sites and different times of appearance (1). Sixty six-year-old female developed skin lesions, mostly below abdominopelvic level. Biopsies of the lesions resulted in high-grade serous ovarian cancer. The patient underwent ^{18}F-fluorodeoxyglucose (FDG) positron emission tomography/magnetic resonance imaging (PET/MRI) for staging. Bilateral metabolically highly active adnexal lesions, primary tumor site, bilateral metabolically highly active inguinal and axillary lymphadenopathies, and pleural effusion are revealed. Skin lesions extending from the abdominopelvic level to lower extremities showed diffuse-increased ^{18}F-FDG uptake. All of these findings were consistent with the biopsy resulting in metastatic ovarian cancer. PET/MRI has a high soft-tissue resolution which makes it useful for tumors like ovarian cancer (2). ^{18}F-FDG PET/computed tomography (CT) has nearly 90% sensitivity and specificity for ovarian cancer (3). Maximum standardized uptake value has a positive correlation with Ki-67 index (4). ^{18}F-FDG PET/MRI combines both positive aspects of ^{18}F-FDG PET and MRI (5). PET differentiates metabolic characteristics of the lesions while MRI, using multiple sequences, provides high soft-tissue resolution and anatomical detail according to different signal intensities. MRI has been reported to have 95% sensitivity and 82% specificity (6), ^{18}F-FDG PET/MRI is more accurate than contrast-enhanced CT and pelvic dynamic MRI according to Tsuyoshi et al (7). PET/MRI has a lower radiation exposure level which adds another benefit to its use compared with PET/CT (8). As a result, PET/MRI can play an important role in soft tissue gynecological tumors such as ovarian cancer. Maximum intensity projection image (A) shows diffuse skin uptake of ^{18}F-FDG, particularly seen in lower abdomen and right leg; ovaries and multiple lymph nodes also show increased ^{18}F-FDG uptake. Selected axial fused T1 weighted water PET-MRI fusion slice (B) and selected axial PET-slice (C) show diffuse skin uptake due to tumor invasion; diffusion-weighted imaging b= 1000 MRI image (D) and apparent diffusion coefficient MRI image (E) show diffusion restriction, which is consistent with malignant invasion.

Ethics

Informed Consent: Obtained.

Peer-review: Externally peer-reviewed.

Authorship Contributions

Surgical and Medical Practices: A.K, S.A, R.L.U.B, M.S.S., K.S., Concept: A.K., S.A., Design: A.K., S.A., R.L.U.B., Data Collection or Processing: A.K., S.A., R.L.U.B., Analysis or Interpretation: A.K., S.A., Literature Search: A.K., Writing: A.K., S.A.

Conflict of Interest: No conflict of interest was declared by the authors.

Financial Disclosure: The authors declared that this study received no financial support.

References

1. Otsuka I. Cutaneous metastases in ovarian cancer. Cancers (Basel) 2019;11:1292.
2. Khiewvan B, Torigian DA, Emamzadehfard S, Paydary K, Salavati A, Houshmand S, Werner TJ, Alavi A. An update on the role of PET/CT and PET/MRI in ovarian cancer. Eur J Nucl Med Mol Imaging 2017;44:1079-1091.
3. Sun J, Cui XW, Li YS, Wang SY, Yin Q, Wang XN, Gu L. The value of 18F-FDG PET/CT imaging combined with detection of CA125 and HE4 in the diagnosis of recurrence and metastasis of ovarian cancer. Eur Rev Med Pharmacol Sci 2020;24:7276-7283.
4. Liu S, Feng Z, Wen H, Jiang Z, Pan H, Deng Y, Zhang L, Ju X, Chen X, Wu X. 18F-FDG PET/CT can predict chemosensitivity and proliferation of epithelial ovarian cancer via SUVmax value. Jpn J Radiol 2018;36:544-550.
5. Nie J, Zhang J, Gao J, Guo L, Zhou H, Hu Y, Zhu C, Li Q, Ma X. Diagnostic role of 18F-FDG PET/MRI in patients with gynecological malignancies of the pelvis: a systematic review and meta-analysis. PLoS One 2017;12:e0175401. Erratum in: PLoS One 2018;13:e0202314.
6. Tempany CM, Zou KH, Silverman SG, Brown DL, Kurtz AB, McNeil BJ. Staging of advanced ovarian cancer: comparison of imaging modalities--report from the Radiological Diagnostic Oncology Group. Radiology 2000;215:761-767.
7. Tsuyoshi H, Tsujikawa T, Yamada S, Okazawa H, Yoshida Y. Diagnostic value of [18F]FDG PET/MRI for staging in patients with ovarian cancer. EJNMMI Res 2020;10:117.
8. Nguyen NC, Beriwal S, Moon CH, D'Ardenne N, Mountz JM, Furlan A, Muthukrishnan A, Rangaswamy B. Diagnostic value of FDG PET/MRI in females with pelvic malignancy-a systematic review of the literature. Front Oncol 2020;10:519440.

Interesting Image
Mol Imaging Radionucl Ther 2023;32:162-164 DOI:10.4274/mirt.galenos.2022.90958

Brain Perfusion Changes in a Patient with Facial Trauma

Yüz Travmalı Bir Hastada Beyin Perfüzyon Değişiklikleri

Chrissa Sioka[1], Anastasia Zikou[2], Petros Petrikis[3], Asimakis Asimakopoulos[4], George Alexiou[5], Vasileios Ragos[6]

[1]*University of Ioannina Faculty of Medicine, Department of Nuclear Medicine, Ioannina, Greece*
[2]*University of Ioannina Faculty of Medicine, Department of Radiology, Ioannina, Greece*
[3]*University of Ioannina Faculty of Medicine, Department of Psychiatry, Ioannina, Greece*
[4]*University of Ioannina, Neurosurgical Institute, Ioannina, Greece*
[5]*University of Ioannina Faculty of Medicine, Department of Neurosurgery, Ioannina, Greece*
[6]*University of Ioannina Faculty of Medicine, Department of Maxillofacial Surgery, Ioannina, Greece*

Abstract

A 69-year-old male was admitted to our hospital because of left facial trauma with bone fractures, including the maxillary sinus, zygomatic arch, and ethmoid and sphenoid bones. Brain computed tomography was unremarkable but regional cerebral blood flow with hexamethyl-propylene-amine oxime single-photon emission computed tomography (SPECT) showed hypoperfusion of the left hemisphere, which was reversible since a repeat SPECT 4 months later was substantially improved. Brain perfusion SPECT may provide information on cerebrovascular status in some cases of facial injury.

Keywords: Brain perfusion imaging, cerebral blood flow, HMPAO, facial trauma, computed tomography, neuroimaging

Öz

Altmış dokuz yaşında erkek hasta, maksiller sinüs, zigomatik ark, etmoid ve sfenoid kemikleri içeren kemik kırıkları ile prezente sol yüz travması nedeniyle hastanemize başvurdu. Beyin bilgisayarlı tomografisinde özellik yoktu ancak hekzametil-propilen-amin oksim tek foton emisyonlu bilgisayarlı tomografi (SPECT) ile sol hemisferde bölgesel serebral kan akışında hipoperfüzyon görüldü. Bu hipoperfüzyon geçici olduğu ve 4 ay sonra tekrarlanan SPECT ile önemli ölçüde gerilediği gözlendi. Beyin perfüzyon SPECT, bazı yüz yaralanmalarında serebrovasküler durum hakkında bilgi sağlayabilir.

Anahtar kelimeler: Beyin perfüzyon görüntüleme, serebral kan akımı, HMPAO, yüz travması, bilgisayarlı tomografi, nörogörüntüleme

Address for Correspondence: Asst. Prof. Chrissa Sioka, University of Ioannina Faculty of Medicine, Department of Nuclear Medicine, Ioannina, Greece
Phone: +00302651099377 **E-mail:** csioka@yahoo.com ORCID ID: orcid.org/0000-0002-2184-4945
Received: 06.05.2022 **Accepted:** 15.11.2022

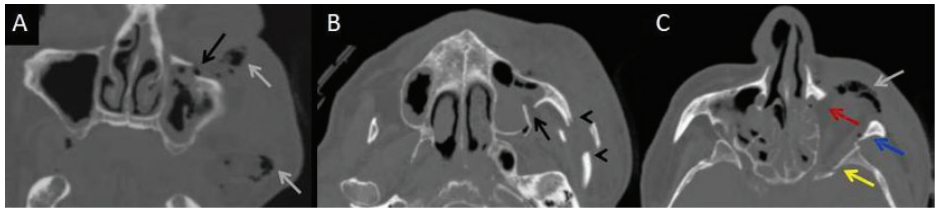

Figure 1. A 69-year-old male was admitted to our hospital because of left facial trauma with facial bone fractures (Figure 1). Axial computed tomography (CT) scan images showed several bone fractures and air bubbles (white arrows) in the left maxillary sinus (black arrows) (A, B) and the zygomatic arch (arrow head) (C), lamina papyracea of the ethmoid bone (red arrow) (C), greater wing of sphenoid (yellow arrow) (C), and zygomatic bone (blue arrow) (C). Brain CT was unremarkable (not shown).

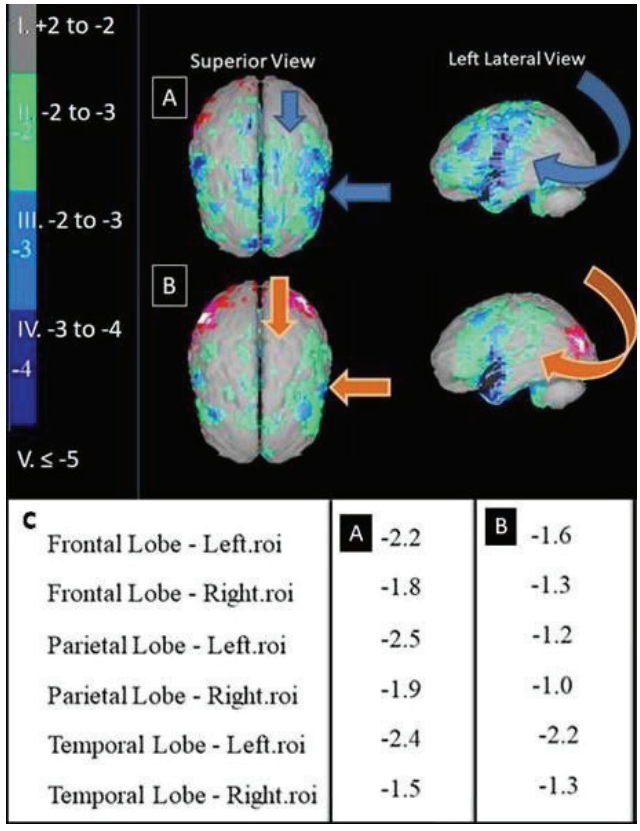

Figure 2. Further evaluation included regional cerebral blood flow (rCBF) distribution with Tc-99m hexamethyl-propylene-amine oxime (HMPAO) single-photon emission computed tomography (SPECT) using NeuroGam software for the semiquantitative evaluation of perfusion of left and right hemispheres. The standard deviation difference over 2-fold was considered an abnormal value. rCBF with HMPAO SPECT showed hypoperfusion of the left frontal and parietal lobes (Figure 2A), which was reversible since a repeat SPECT 4 months later was improved (Figure 2B). In the left temporal lobe, the second SPECT showed mild improvement in rCBF, which could have been related to the patient's psychological status after the accident, since this lobe has been linked to emotions such as depression (1).

SPECT cerebral perfusion imaging represents a sensitive method to assess brain perfusion changes even after minor traumatic brain injury (2). In addition, as in this case, it may show even subtle reversible changes in facial injury without brain damage. Figure 2 shows the reversibility of the perfusion deficit between the first (A) and the second examination (B). Blue arrows show the hypoperfused areas (A) and orange arrows show the reversibility (B). The colored scale in the image demonstrates the hypoperfused brain areas and their severity (≤-2) seen in the left frontal and parietal lobes.

This case demonstrated that during facial trauma without obvious cerebral abnormalities, brain perfusion was temporally reduced; however, this phenomenon was reversible. There is insufficient experience related to the impact of craniomaxillofacial injuries on the cerebrovascular bed. A recent retrospective study on 753 patients with such injuries demonstrated blunt cerebrovascular injuries in 3.1% of facial fracture patients (3). Similar results were reported in another study on 428 patients that showed that patients with craniofacial fractures exhibited a 3 to 4-fold increased risk for blunt cerebrovascular injuries (4). Thus, although brain imaging is not part of facial trauma evaluation, in some cases brain perfusion SPECT may provide further information on cerebrovascular status related to facial injury.

Ethics

Informed Consent: Written informed consent was obtained.

Peer-review: Externally peer-reviewed.

Authorship Contributions

Surgical and Medical Practices: C.S., A.Z., V.R., Concept: C.S., V.R., Design: A.Z., V.R., Data Collection or Processing: A.Z., P.P., A.A., Analysis or Interpretation: P.P., G.A., Literature Search: A.A., G.A., Writing: C.S., V.R.

Conflict of Interest: No conflict of interest was declared by the authors.

Financial Disclosure: The authors declared that this study received no financial support.

References

1. Ebmeier KP, Prentice N, Ryman A, Halloran E, Rimmington JE, Best JK, Goodwin GM. Temporal lobe abnormalities in dementia and depression: a study using high resolution single photon emission tomography and magnetic resonance imaging. J Neurol Neurosurg Psychiatry 1997;63:597-604.
2. Abu-Judeh HH, Parker R, Singh M, el-Zeftawy H, Atay S, Kumar M, Naddaf S, Aleksic S, Abdel-Dayem HM. SPET brain perfusion imaging in mild traumatic brain injury without loss of consciousness and normal computed tomography. Nucl Med Commun 1999;20:505-510.
3. Puolakkainen T, Vähäsilta L, Bensch F, Narjus-Sterba M, Wilson ML, Thorén H, Snäll J. Blunt cerebrovascular injuries in the craniofacial fracture population-are we screening the right patients? Int J Oral Maxillofac Surg 2021;50:463-470.
4. Varjonen EA, Bensch FV, Pyhältö TT, Koivikko MP, Snäll J. Remember the Vessels! Craniofacial Fracture Predicts Risk for Blunt Cerebrovascular Injury. J Oral Maxillofac Surg 2018;76:1509.

Interesting Image
Mol Imaging Radionucl Ther 2023;32:165-167 DOI:10.4274/mirt.galenos.2022.31032

Meningioma Mimicking Bone Metastasis in Breast Cancer

Meme Kanserinde Kemik Metastazını Taklit Eden Menenjiom

Oğuzhan Şahin, Gündüzalp Buğrahan Babacan, Tamer Özülker

University of Health Sciences Turkey, Prof. Dr. Cemil Taşcıoğlu City Hospital, Department of Nuclear Medicine, İstanbul, Turkey

Abstract

Meningiomas constitute 37% of primary central nervous system tumors and are more common in women. Also may occur with other primary malignancies, which can cause confusion with the metastasis in whole body bone scan (WBBS) imaging. A 58-year-old woman diagnosed with breast cancer was referred to the WBBS for the investigation of possible bone metastases. In the planar images, radiotracer uptake at multiple sites was detected on the anterior side of the skull base and the posterior side of the vertex of the cranium. Single photon emission computed tomography/computed tomography was performed for anatomical localization of possible metastatic lesions, and it revealed that detected accumulations of radiotracer did not belong to the bone metastases; uptakes were located at the cerebral parenchyma and the lesions in the falx cerebri. Patient history explained that she had been diagnosed with meningioma five years ago, which mimicked bone metastases in this study.

Keywords: Meningioma, bone scan, breast cancer

Öz

Menenjiomlar, primer santral sinir sistemi tümörlerinin %37'sini oluşturur ve kadınlarda daha sık görülür. Ayrıca, diğer primer malignitelere eşlik edebildiğinden tüm vücut kemik taraması (TVKT) görüntülerinde, metastaz ile karışıklığa neden olabilir. Elli sekiz yaşında meme kanseri tanısı konulan kadın hasta, olası kemik metastazlarının araştırılması amacıyla TVKT için nükleer tıp departmanına sevk edildi. Planar görüntülerde, kafa tabanının anteriorunda ve verteks bölgesinin posteriorunda multiple radyotraser akümülasyonları tespit edildi. Olası metastatik lezyonların anatomik lokalizasyonu için tek foton emisyon tomografisi/bilgisayarlı tomografi çalışması yapıldı ve saptanan radyotraser tutulumlarının kemik metastazlarına ait olmadığı, tutulumların serebral parankime ve lezyonların falks serebriye ait olduğu ortaya çıktı. Hastanın veri geçmişi, bu çalışmadaki kemik metastazlarını taklit eden bulguların, beş yıl önce konmuş olan menenjiom tanısı ile uyumlu olduğunu gösterdi.

Anahtar kelimeler: Menenjiom, kemik sintigrafisi, meme kanseri

Address for Correspondence: Oğuzhan Şahin MD, University of Health Sciences Turkey, Prof. Dr. Cemil Taşcıoğlu City Hospital, Clinic of Nuclear Medicine, İstanbul, Turkey
Phone: +90 212 314 55 55 **E-mail:** yunus.6489@gmail.com ORCID ID: orcid.org/0000-0001-5484-6798
Received: 25.08.2022 **Accepted:** 18.12.2022

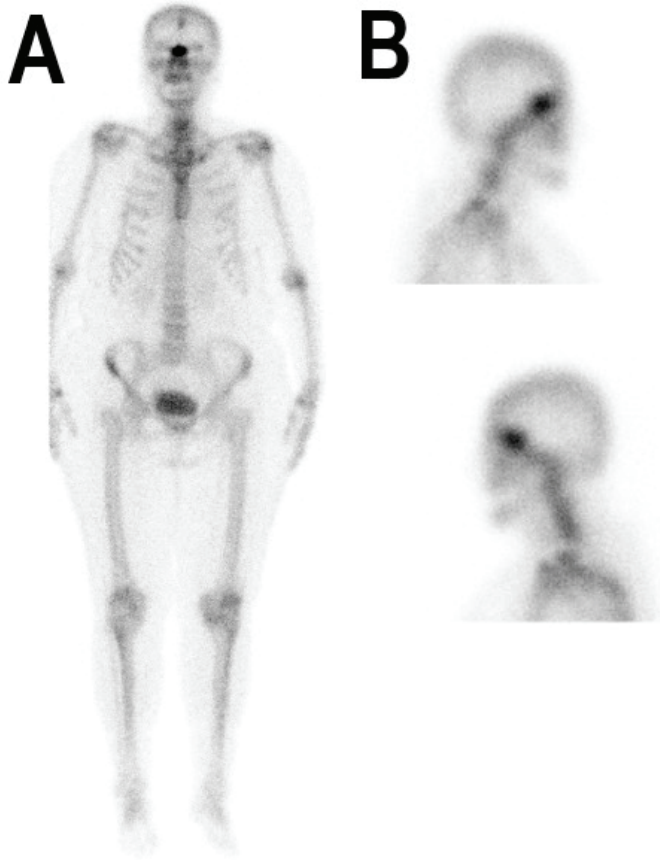

Figure 1. Anterior planar image (A) and lateral planar image (B) of a 58-year-old woman with a diagnosis of invasive ductal carcinoma presented with a complaint of shoulder pain during follow-up. Focal radiotracer uptake was observed anterior to the skull base and sagittal sinus areas.

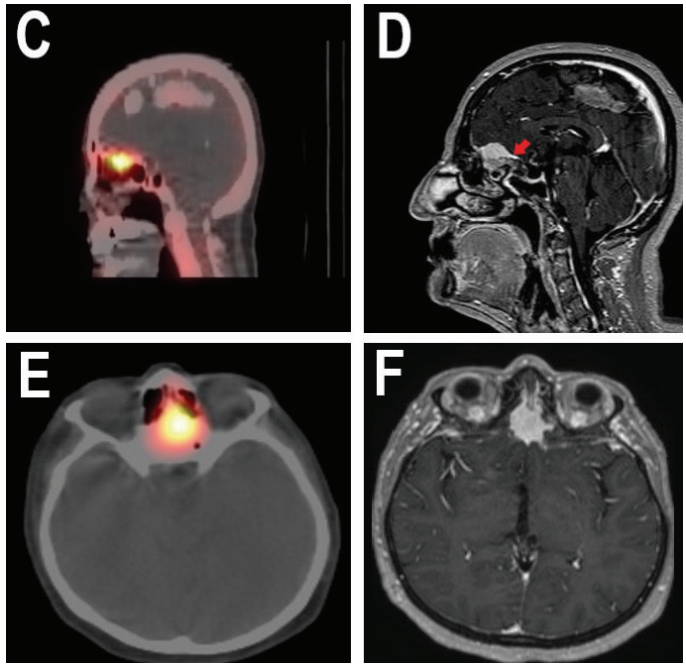

Figure 2. In the single photon emission computed tomography/computed tomography (SPECT/CT) images, increased radiotracer uptake was seen in the inferior frontal parenchymal tissue and the cerebral falx in the interhemispheric area in both sagittal and transaxial images (C, E).
In the T1-weighted sagittal and transaxial magnetic resonance imaging (D, F), a well-defined homogeneously avidly enhancing extraaxial mass at the planum sphenoidale with pathognomonic "dural tail sign" was demonstrated (red arrow).

Meningiomas are 37% of primary central nervous system tumors and are more common in women (1). Meningiomas can calcify in different ways (2). Meningiomas contains progesterone receptors similar to breast cancers (3). Clinicians can refer patients to whole-body bone scintigraphy in the follow-up of breast cancer, and it is recommended for high-risk patients (4). There are studies in the literature reported that patients with breast cancer have a higher risk of developing meningioma compared to the general population. Lopez-Rivera et al. (5) showed that the incidence of meningioma was 26% higher than the normal population in their cohort study of 5,000 breast cancer patients. In this case, we would like to present that bone metastasis can be interpreted with false positivity. Radiotracer can be obtained not only in meningioma but also in diseases such as cerebral infarction, brain abscess cerebritis, and chronic subdural hematoma in the cranial area (6,7). In WBBS studies, radiotracer uptake in unusual parts of the body history of disease other than metastasis should be questioned. Also, if available, SPECT/CT may be useful in confirming the findings.

Ethics

Informed Consent: Written informed consent was obtained.

Peer-review: Externally peer-reviewed.

Authorship Contributions

Surgical and Medical Practices: T.Ö., Concept: O.Ş., G.B.B., T.Ö., Design: O.Ş., G.B.B., T.Ö., Data Collection or Processing: O.Ş., T.Ö., Analysis or interpretation: G.B.B., T.Ö., Literature Search: O.Ş., T.Ö., Writing: O.Ş., G.B.B., T.Ö.

Conflict of Interest: No conflict of interest was declared by the authors.

Financial Disclosure: The authors declared that this study received no financial support.

References

1. Ogasawara C, Philbrick BD, Adamson DC. Meningioma: A review of epidemiology, pathology, diagnosis, treatment, and future directions. Biomedicines 2021;9:319.
2. Chotai SP, Mrak RE, Mutgi SA, Medhkour A. Ossification in an extra-intradural spinal meningioma-pathologic and surgical vistas. Spine J 2013;13:21-26.
3. Maiuri F, Mariniello G, de Divitiis O, Esposito F, Guadagno E, Teodonno G, Barbato M, Del Basso De Caro M. Progesterone receptor expression in meningiomas: pathological and prognostic implications. Front Oncol 2021;11:611218.
4. Costelloe CM, Rohren EM, Madewell JE, Hamaoka T, Theriault RL, Yu TK, Lewis VO, Ma J, Stafford RJ, Tari AM, Hortobagyi GN, Ueno NT. Imaging bone metastases in breast cancer: techniques and recommendations for diagnosis. Lancet Oncol 2009;10:606-614.
5. Lopez-Rivera V, Zhu P, Dono A, Lee S, Chen PR, Ballester LY, Sheth SA, Esquenazi Y. Increased risk of subsequent meningioma among women with malignant breast cancer. World Neurosurg 2020;139:271-285.
6. Wale DJ, Wong KK, Savas H, Kandathil A, Piert M, Brown RK. Extraosseous findings on bone scintigraphy using fusion SPECT/CT and correlative imaging. AJR Am J Roentgenol 2015;205:160-172.
7. Brill DR. Radionuclide imaging of nonneoplastic soft tissue disorders. Semin Nucl Med 1981;11:277-288.

Interesting Image
Mol Imaging Radionucl Ther 2023;32:168-170 DOI:10.4274/mirt.galenos.2022.59354

Unusual Case of Pseudomembranous Colitis Presenting as Fever of Unknown Origin Diagnosed by Tc-99m-HMPAO-labeled Leukocytes SPECT/CT

Nedeni Bilinmeyen Ateş ile Prezente olan ve Tc-99m-HMPAO İşaretli Lökosit SPECT/BT ile Teşhis Edilen Olağan Dışı Psödomembranöz Enterokolit Olgusu

Rosanna Del Carmen Zambrano-Infantino[1], Jean Félix Piñerúa-Gonsálvez[2], Noelia Alvarez-Mena[1], Sandra Izquierdo-Santervás[2], Noelia Alcaide[2], Maria Garcia-Aragon[1], Ricardo Ruano-Pérez[1]

[1]Hospital Clínico Universitario de Valladolid, Department of Nuclear Medicine, Valladolid, Spain
[2]Hospital Clínico Universitario de Valladolid, Department of Gastroenterology, Valladolid, Spain

Abstract

The fever of unknown origin (FUO) represents a complex diagnostic challenge due to the wide range of etiologies that could cause it, including neoplastic, infectious, rheumatic/inflammatory, and miscellaneous disorders. Several nuclear medicine techniques have proven to be valuable tools for guiding etiologic diagnosis in the setting of FUO. One of these is technetium-99m (Tc-99m)-hexamethylpropylene amine oxime (HMPAO)-labeled leukocyte scintigraphy, which is a diagnosis method that allows in most cases the localization and evaluation of the extension of an occult infection. This paper presents an uncommon case of pseudomembranous colitis without diarrhea as etiology of FUO diagnosed by Tc-99m-HMPAO-labeled leukocytes.

Keywords: Pseudomembranous colitis, fever of unknown origin, Tc-99m-HMPAO, single-photon emission computed tomography, radionuclide imaging

Öz

Nedeni bilinmeyen ateş (NBA), buna neden olabilecek neoplastik, enfeksiyöz, romatizmal/enflamatuvar ve çeşitli bozukluklar dahil olmak üzere çok çeşitli etiyolojiler nedeniyle tanısı zor bir durumdur. Birkaç nükleer tıp tekniğinin, NBA'da etiyolojik tanıya rehberlik etmek için değerli araçlar olduğu kanıtlanmıştır. Bunlardan biri, çoğu durumda gizli bir enfeksiyonun lokalizasyonuna ve yayılımının değerlendirilmesine olanak tanıyan bir tanı yöntemi olan teknesyum-99m (Tc-99m)-heksametilpropilen amin oksim (HMPAO) işaretli lökosit sintigrafisidir. Bu yazıda, Tc-99m-HMPAO işaretli lökositler ile teşhis edilen NBA etiyolojisi olarak diyarenin eşlik etmediği nadir bir psödomembranöz kolit olgusu sunulmaktadır.

Anahtar kelimeler: Psödomembranöz kolit, nedeni bilinmeyen ateş, Tc-99m-HMPAO, tek foton emisyonlu bilgisayarlı tomografi, radyonüklid görüntüleme

Address for Correspondence: Rosanna Del Carmen Zambrano-Infantino MD, Hospital Clínico Universitario de Valladolid, Department of Nuclear Medicine, Valladolid, Spain
Phone: +983420003 **E-mail:** rosannamedicina@hotmail.com ORCID ID: orcid.org/0000-0001-6876-5948
Received: 29.08.2022 **Accepted:** 25.12.2022

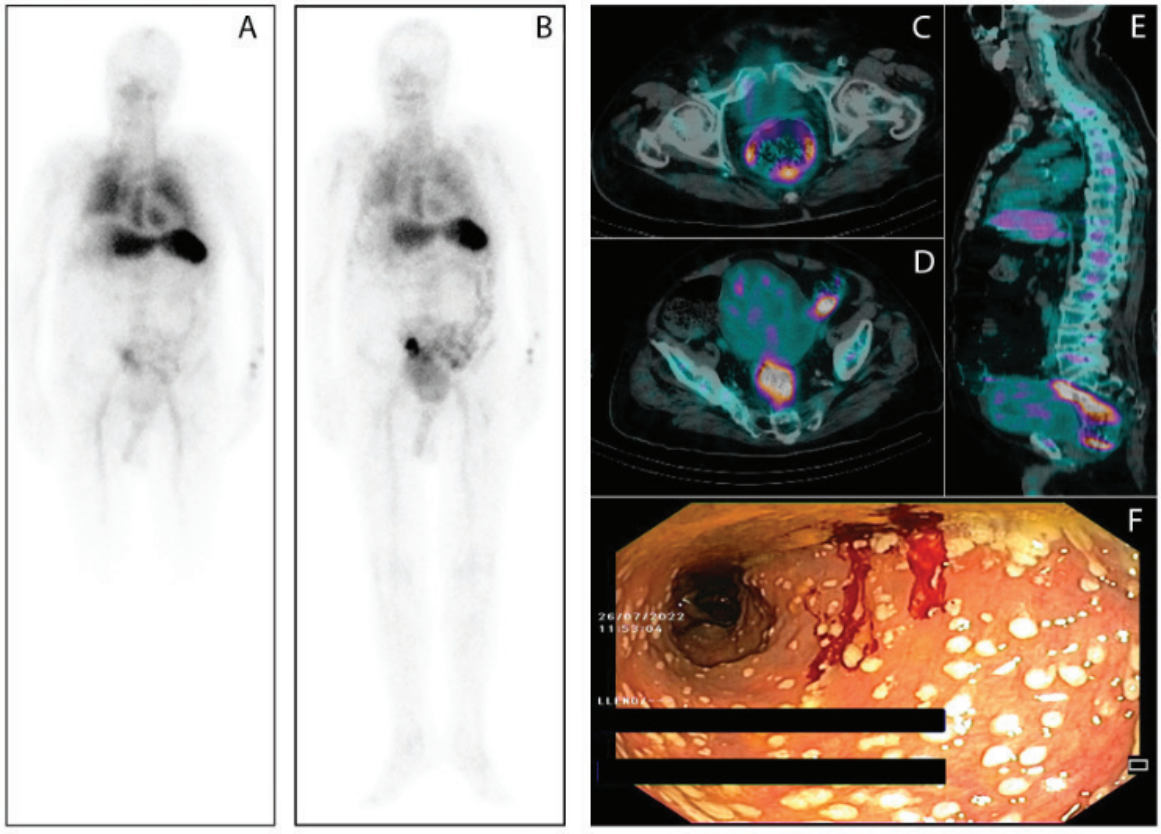

Figure 1. An 88-year-old man with a 1-month daily fever >38.5 °C and hyporexia. All other systems were reviewed and were negative. The patient had a past medical history of arterial hypertension and type 2 diabetes mellitus. There were no remarkable findings in the physical examination for a body temperature of 38.9 °C. At admission, the laboratory findings were as follows: hemoglobin, 9.8 gr/dL; white blood cell count, 18,840/mm^3; erythrocyte sedimentation rate, 10^3 mm/h; C-reactive protein, 215 mg/L; and procalcitonin, 1.38 ng/mL. Blood and urine cultures, viral serology, immunological profile, abdominal ultrasound, chest radiology, and echocardiogram were negative. Technetium-99m (Tc-99m)-hexamethylpropylene amine oxime (HMPAO)-labeled leukocytes single-photon emission computed tomography/computed tomography (SPECT/CT) was requested to identify the location of a probable occult infection. Planar images of the whole body were obtained after 30 min (A) and 3 h postinjection with thoraco abdomino pelvic SPECT/CT at 3 hours post injection. Planar images of the whole body at 3 h post-injection of Tc-99m-HMPAO-labeled leukocytes revealed increased uptake in the rectum and sigmoid colon (B). SPECT/CT fusion images showed pathological Tc-99m-HMPAO-labeled leukocytes uptake in the walls of the rectum, sigmoid, and descending colon (C, D, E). In view of the previous findings, colonoscopy was performed revealing multiple white-grey small plaques with mild erythema of the surrounding mucosa along the rectosigmoid and descending colon (F). These lesions were suggestive of pseudomembranous colitis, so rectal samples for microbiological studies and mucosal biopsies were taken. Polymerase chain reaction assays detected toxinogenic *Clostridium difficile* in the clinical isolates. Histological examination showed isolated focuses of ulceration and crypts with reactive changes and focal atrophy, neutrophil infiltration, and hyalinization of the lamina propriam. The patient was treated with oral vancomycin with subsequent cessation of fever and improvement of laboratory parameters. Fever of unknown origin (FUO) represents a complex diagnostic challenge due to the wide range of causes that could cause it including neoplastic, infectious, rheumatic/inflammatory, and miscellaneous disorders. This entity is defined by three criteria: 1) body temperature ≥38.3 °C, 2) minimum duration of 3 weeks, and 3) etiology unidentified despite an extended work-up (1). There are several nuclear medicine techniques that are valuable tools for guiding etiologic diagnosis in the setting of FUO (2). One of these is Tc-99m-HMPAO labeled leukocyte scintigraphy, which is a diagnosis method that allows in most cases the localization and evaluation of the extension of an occult infection (3,4). The usual clinical picture of pseudomembranous colitis includes diarrhea (the most common symptom), abdominal pain, fever, and elevated white blood cell counts. The absence of diarrhea is very infrequent in this setting, making its diagnosis difficult. Some unusual presentation forms include fulminant colitis, toxic megacolon, perforation, and intestinal pseudo-obstruction (5). This paper illustrated an uncommon case of pseudomembranous colitis presenting as FUO in which Tc-99m-HMPAO-labeled leukocytes were the key to achieving the diagnosis.

Ethics

Informed Consent: Informed consent was obtained by patient.

Peer-review: Externally peer-reviewed.

Authorship Contribution

Surgical and Medical Practices: S.I-S., N.A., Concept: R.D.C.Z-I., Design: R.D.C.Z-I., J.F.P-G., Data Collection or Processing: R.D.C.Z-I., J.F.P-G., Analysis or Interpretation: R.D.C.Z-I., J.F.P-G., N.A-M., M.G-A., R.R-P., Literature Search: R.D.C.Z-I., M.G-A., Writing: R.D.C.Z-I., J.F.P-G.

Conflict of Interest: No conflict of interest was declared by the authors.

Financial Disclosure: The authors declared that this study received no financial support.

References

1. Cunha BA, Lortholary O, Cunha CB. Fever of unknown origin: a clinical approach. Am J Med 2015;128:1138.
2. Cosma L, Frantellizzi V, Pontico M, De Vincentis G. Unexpected detection of abscessualized lung carcinoma on Tc-99m-HMPAO-labeled leukocytes scintigraphy misdiagnosed on chest computed tomography. Mol Imaging Radionucl Ther 2021;30:60-62.
3. de Vries EF, Roca M, Jamar F, Israel O, Signore A. Guidelines for the labelling of leucocytes with (99m)Tc-HMPAO. Inflammation/infection taskgroup of the European Association of Nuclear Medicine. Eur J Nucl Med Mol Imaging 2010;37:842-848.
4. Sc Schönau V, Vogel K, Englbrecht M, Wacker J, Schmidt D, Manger B, Kuwert T, Schett G. The value of 18F-FDG-PET/CT in identifying the cause of fever of unknown origin (FUO) and inflammation of unknown origin (IUO): data from a prospective study. Ann Rheum Dis 2018;77:70-77.
5. Sheikh RA, Yasmeen S, Pauly MP, Trudeau WL. Pseudomembranous colitis without diarrhea presenting clinically as acute intestinal pseudo-obstruction. J Gastroenterol 2001;36:629-632.

Interesting Image
Mol Imaging Radionucl Ther 2023;32:171-174 DOI:10.4274/mirt.galenos.2023.27037

Urinary Bladder Carcinoma Demonstrated on Bone Scintigraphy and SPECT/CT Images

Kemik Sintigrafisi ve SPECT/BT ile Gösterilen Üriner Mesane Karsinomu

Sotiria Alexiou[1], Xanthi Xourgia[1], Pavlos Raptis[2], Dimitrios Baltogiannis[3], Chrissa Sioka[1]

[1]*University of Ioannina Faculty of Medicine, Department of Nuclear Medicine, Ioannina, Greece*
[2]*General Hospital of Lefkada, Department of Urology, Lefkada, Greece*
[3]*University of Ioannina Faculty of Medicine, Department of Urology, Ioannina, Greece*

Abstract

Bone scintigraphy with Tc-99m-diphosphonate analogs are widely used in staging, restaging, and monitoring the therapy effectiveness of various cancer types. Bone-seeking agents are excreted through urination, resulting in the visualization of either anatomical abnormalities or pathological conditions of the kidneys and bladder. We present a case of a 63-year-old man with urinary bladder carcinoma depicted on whole body planar and single-photon emission computed tomography/computed tomography images.

Keywords: Bone scintigraphy, SPECT/CT, urinary bladder carcinoma, nuclear medicine

Öz

Tc-99m-difosfonat analogları ile kemik sintigrafisi, çeşitli kanser türlerinin evrelemesinde, yeniden evrelemesinde ve tedavi etkinliğinin izlenmesinde yaygın olarak kullanılmaktadır. Kemik arayan ajanlar idrar yoluyla atılır, bu da böbreklerin ve mesanenin anatomik anormalliklerin ya da patolojik durumlarının görselleştirilmesini sağlar. Bu yazıda, mesane karsinomu tüm vücut düzlemsel ve tek foton emisyonlu bilgisayarlı tomografi/bilgisayarlı tomografi ile gösterilen 63 yaşında bir erkek hastayı sunuyoruz.

Anahtar kelimeler: Kemik sintigrafisi, SPECT/BT, mesane karsinomu, nükleer tıp

Address for Correspondence: Asst. Prof. Chrissa Sioka, University of Ioannina Faculty of Medicine, Department of Nuclear Medicine, Ioannina, Greece
Phone: +00302651099375 **E-mail:** csioka@yahoo.com ORCID ID: orcid.org/0000-0002-2184-4945
Received: 20.09.2022 **Accepted:** 08.01.2023

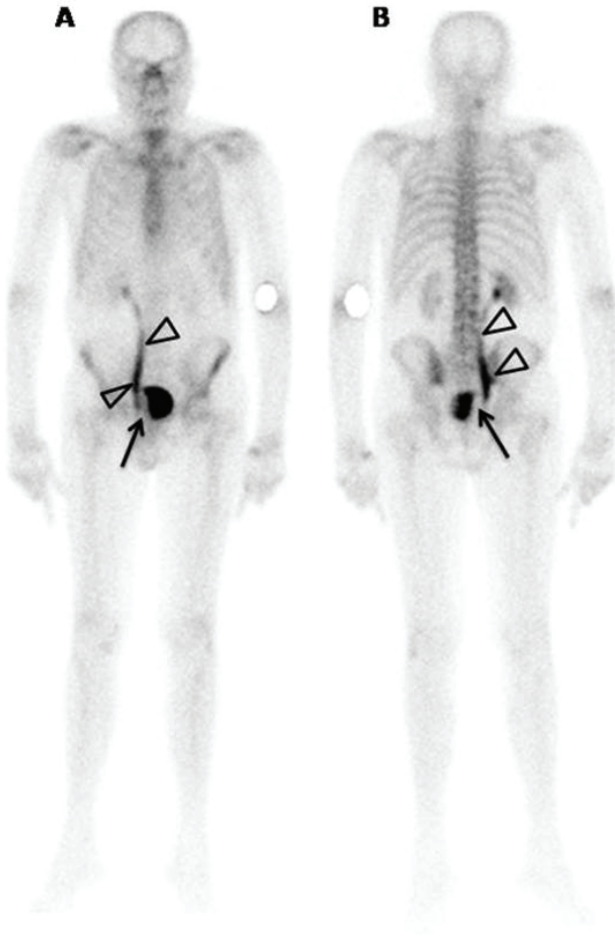

Figure 1. A 63-year-old man was admitted to the urology department of our hospital due to recent macroscopic hematuria and extremely low hematocrit levels. From his past medical history, he had been diagnosed with non-invasive urothelial carcinoma (high grade) seven years ago, for which he underwent transurethral resection with complementary Bacillus Calmette-Guerin intravesical therapy. Few weeks before his admission, he underwent routine cystoscopy in an outside facility, and he was informed that it showed urothelial papillomas, but he denied any therapeutic intervention at that time. Because of his prior history of urothelial carcinoma, an abdomen-pelvis computed tomography (CT) examination and bone scintigraphy was ordered. A whole-body scan was obtained 2 h after intravenous administration of 20 mCi (740 Mbq) Tc-99m methyl diphosphonate. Anterior (A) and posterior (B) images showed mild inhomogeneous radiopharmaceutical uptake in the lumbar spine, without having the typical appearance of osteoblastic metastatic osseous lesions. Moderately increased tracer accumulation was also observed in the cervical spine and joints of upper extremities, related to degenerative disorders. In the pelvic region, a cold photopenic area occupying the right portion of the urinary bladder was noticed (arrow). Additionally, dilatation and tracer retention was demonstrated in the right ureter, especially in the lower third (arrowheads).

Urinary tract abnormalities, such as filling defects of the urinary bladder, related to the presence of either intrinsic or extrinsic lesions have been previously reported on bone scintigrams. De Geeter and Goethals (1) in 2010 described three cases with similar appearance of the urinary bladder owing to carcinomas. Contrary to the above-mentioned reports, there are examples with intense tracer accumulation of urothelial carcinomas, pertained to tumor calcification (2,3). A case of complete absence of urinary bladder visualization caused by obstruction has also been mentioned (4). In male patients, regions with decreased tracer accumulation at the base of the urinary bladder, known as "inverted cups", have been attributed to prostate enlargement and surgical resection (5). Clots, hematomas, and ureterocele are some other possible explanations of cold lesions inside the bladder (6,7). Pelvic masses, such as colon tumors, can lead to the bladder defect formation by exerting external pressure (7,8). To ascertain the origin of our findings, a pelvic single-photon emission computed tomography (SPECT)/CT examination was performed.

Figure 2. On coronal SPECT images (A), a photopenic region, possessing part of the right side of the urinary bladder (orange arrows), with concomitant ureteral dilatation and tracer retention, especially in the lower third, was observed (black arrow). Additionally, a smaller cold region was depicted on the left part of the bladder (green arrow). The concurrent low-dose CT images (B) indicated an inhomogeneous appearance of the urinary bladder with the presence of large, hyperdense lesions on the left and right portion involving the right vesico-ureteral junction. Fused SPECT/CT images (C) revealed that our findings in the urinary tract system, as shown on bone scan, were caused by the existence of urinary bladder neoplasms (red arrows).

Figure 3. Furthermore, comparison with the enhanced coronal CT images confirmed the findings of fused SPECT/CT images (orange arrows). Conclusively, urinary tract abnormalities are an unexpected but possibly finding on bone scintigrams. Hybrid SPECT/CT technology providing additional anatomical information, represents a powerful tool in the correct and precise diagnostic interpretation of extraosseous findings on bone scintigraphy.

Ethics

Informed Consent: Written informed consent was obtained.

Peer-review: Externally peer-reviewed.

Authorship Contributions

Surgical and Medical Practices: S.A., X.X., P.R., D.B., Concept: S.A., C.S., Design: S.A., C.S., Data Collection or Processing: P.R., D.B., Analysis or Interpretation: X.X., C.S., Literature Search: S.A., C.S., Writing: S.A., C.S.

Conflict of Interest: No conflict of interest was declared by the authors.

Financial Disclosure: The authors declared that this study received no financial support.

References

1. De Geeter F, Goethals L. Utility of pelvic bone SPET in imaging urinary bladder filling defects in urinary bladder carcinoma. Hell J Nucl Med 2010;13:59-62.
2. Niederkohr RD, Chiu E, Katzel JA. 99mTc-oxidronate uptake within urothelial carcinoma confirmed with SPECT/CT imaging. Clin Nucl Med 2013;38:655-657.

3. Lin Y, Lu YY, Wang HY, Tsai SC, Lin WY. Accidental finding of bladder cancer in 99mTc methylene diphosphonate whole-body bone scan. Clin Nucl Med 2013;38:643-645.
4. Wright CL, Sharma A. Unusual appearance for urinary bladder obstruction detected with 99mTc-MDP bone scintigraphy. Clin Nucl Med 2015;40:967-968.
5. Bilchik TR, Spencer RP. Bladder variants on bone and renal imaging. Clin Nucl Med 1993;18:60-67.
6. Duong RB, Gelfand MJ, Volarich DT, Williams P. Urinary tract imaging – filling defect in the urinary bladder. Semin Nucl Med 1983;13:383-385.
7. Mandell GA, Harcke HT. Extrinsic causes of vesical filling defects on scintigraphy. Clin Nucl Med 1987;12:204-207.
8. Stewart CA, Siegel ME, NafisWA, Wood LA. Bone scan of recurrent colon carcinoma involving the sacrum and urinary bladder. Clin Nucl Med 1989;16:513-514.

Interesting Image
Mol Imaging Radionucl Ther 2023;32:175-177 DOI:10.4274/mirt.galenos.2023.24992

Incidental Spleen Cyst Mimicking Thyroid Carcinoma Metastasis: False-positive Uptake on Radioiodine Whole Body Scan

Tiroid Karsinom Metastazını Taklit Eden Rastlantısal Dalak Kisti: Radyoaktif İyot Tüm Vücut Taramada Yanlış Pozitif Tutulum

Mustafa Genç[1], Nazım Coşkun[2,3], Seyda Türkölmez[2,3]

[1]Sivas Numune Hospital, Clinic of Nuclear Medicine, Sivas, Turkey
[2]Ankara City Hospital, Clinic of Nuclear Medicine, Ankara, Turkey
[3]Ankara Yıldırım Beyazıt University Faculty of Medicine, Department of Nuclear Medicine, Ankara, Turkey

Abstract

In differentiated thyroid cancer, radioiodine therapy and whole body scans (WBS) are integral part of disease management. We present the case of a 33-year-old woman with multifocal thyroid carcinoma who was treated with radioiodine. Post-treatment WBS scintigraphy showed focal increased I-131 uptake in the spleen, although stimulated thyroglobulin level was not suggestive of distant metastasis. Dynamic magnetic resonance imaging performed later revealed that the finding was an incidental splenic cyst. Radioiodine uptake is not specific to the thyroid tissue. Benign pathologies showing increased radioiodine uptake should be considered in cases with splenic radioiodine accumulation in WBSs.

Keywords: Radioiodine therapy, thyroid cancer, spleen pathologies, whole body scan

Öz

Diferansiye tiroid kanserinde, radyoaktif iyot tedavisi ve tüm vücut tarama (TVT) sintigrafisi hastalık yönetiminin ayrılmaz bir parçasıdır. Radyoaktif iyot ile tedavi edilen multifokal tiroid karsinomlu 33 yaşında kadın hastayı sunuyoruz. Tedavi sonrası TVT sintigrafisinde, dalakta fokal artmış I-131 tutulumu saptandı. Ancak uyarılmış tiroglobulin düzeyi uzak metastaz ile uyumlu değildi. Daha sonra karaciğere yönelik yapılan dinamik manyetik rezonans görüntüleme bulgunun rastlantısal bir dalak kisti olduğunu ortaya çıkardı. Radyoaktif iyot tutulumu tiroid dokusuna özgü değildir. Radyoaktif iyot ile TVT'de dalakta aktivite tutulumu saptanan olgularda artmış radyoiyot tutulumu gösteren benign patolojiler de düşünülmelidir.

Anahtar kelimeler: Radyoaktif iyot tedavisi, tiroid kanseri, dalak patolojileri, tüm vücut tarama

Address for Correspondence: Mustafa Genç MD, Sivas Numune Hospital, Clinic of Nuclear Medicine, Sivas, Turkey
Phone: +90 346 215 08 44 **E-mail:** drmustafagenc@gmail.com ORCID ID: orcid.org/0000-0001-6580-311X
Received: 29.11.2022 **Accepted:** 08.01.2023

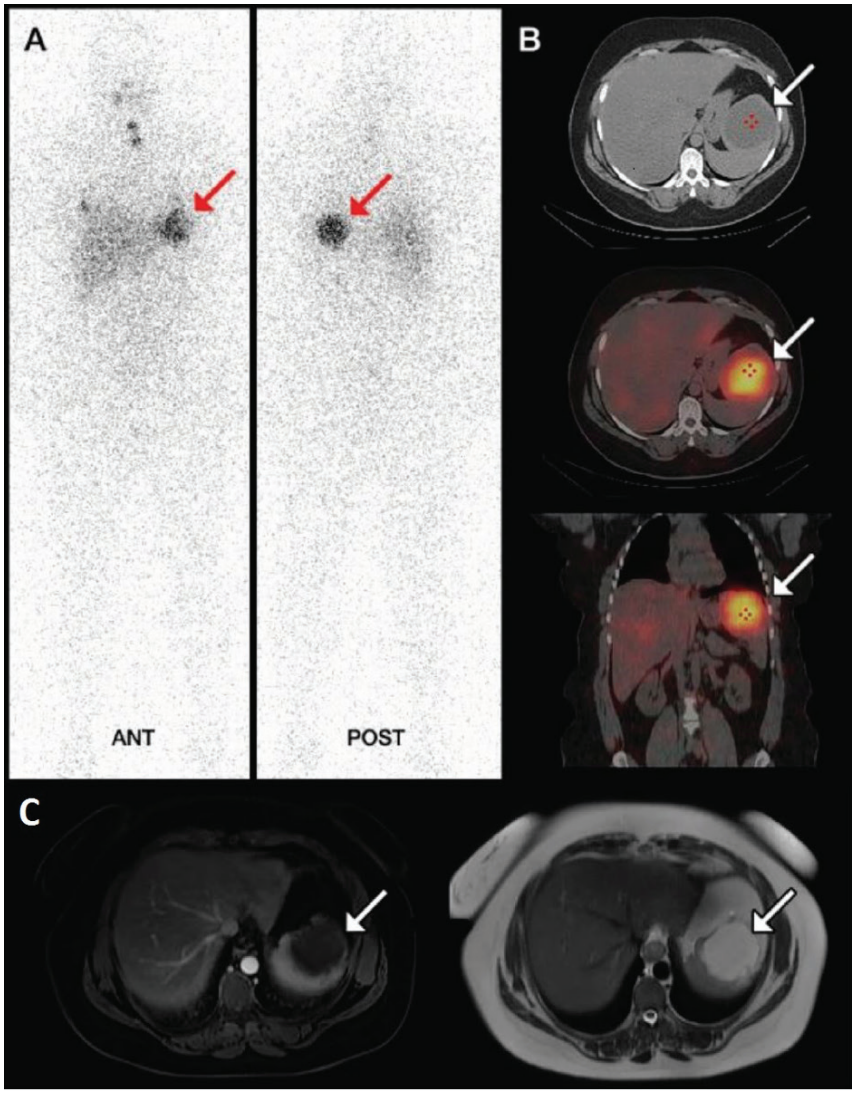

Figure 1. Total thyroidectomy was performed on a 33-year-old female patient with no known comorbidities. The pathology result was reported as diffuse sclerosing variant multifocal papillary thyroid carcinoma. Thereupon, 100 mCi radioactive iodine treatment was given to the patient in our clinic [thyroid stimulating hormone: 137.9, thyroglobulin (Tg): <0.20, anti-Tg: 92.2]. In the whole body scan (WBS) performed on the 7th day after the treatment, there were areas of activity uptake in the left thyroid lobe lodge and inferior proximity of the hyoid bone, possibly due to residual tissue and thyroglossal canal. In addition, focal activity uptake was observed in the left upper quadrant of the abdomen (Figure 1A). Radiopharmaceutical distribution in other areas was as expected. For anatomical correlation, single photon emission tomography/computed tomography imaging was performed by positioning the abdominal region in the field of view, which revealed a hypodense lesion measuring 83x71 mm in the superior anterior part of the spleen with a calcified appearance on the wall and increased I-131 uptake within the lesion (Figure 1B).
In the dynamic magnetic resonance imaging performed to clarify this finding, the lesion with a diameter of 8 cm in the upper pole of the spleen was evaluated as an unloculated cyst (Figure 1C).
Thyroid cancer accounts for 2.1% of all cancer cases worldwide. Approximately 90% of these cases are well-differentiated thyroid carcinoma (DTC) (1). Splenic metastasis is rare in DTC (2). Radioiodine has been used for more than fifty years in the diagnosis and treatment of patients with DTC (3). Radioiodine WBS is also an integral part of disease management (4). Radioiodine uptake is not specific to the thyroid tissue. There may be physiological uptake in the thymus, breast and gastrointestinal system. In addition, radioiodine uptake can be seen in benign conditions such as cysts and inflammation and in non-thyroid tumors (5). Radioiodine uptake in the spleen is very rare, with only 2 cases reported in the literature so far. In one of these cases, diffuse radioiodine uptake was detected in the spleen in post-treatment WBS, and thyroid cancer metastasis was proven by biopsy (2). On the other hand, radioiodine uptake was observed in the spleen in diagnostic WBS, and a littoral cell angioma was found in the biopsy result (6). In this study, we observed radioiodine uptake in benign spleen pathology. To our knowledge, radioiodine uptake of splenic cystic lesions has not been reported before. Splenic cystic lesions as a possible cause of false positive splenic radioiodine uptake mimicking metastasis should be kept in mind to avoid misdiagnosis in patients with DTC.

Ethics

Informed Consent: All appropriate patient consent forms were obtained. In this form, the patient gave consent for their pictures and other clinical information to be reported in the journal.

Peer-review: Externally peer-reviewed.

Authorship Contributions

Surgical and Medical Practices: M.G., N.C., S.T., Concept: M.G., N.C., S.T., Design: M.G., N.C., S.T., Data Collection or Processing: M.G., N.C., S.T., Analysis or interpretation: M.G., N.C., S.T., Literature Search: M.G., N.C., S.T., Writing: M.G., N.C., S.T.

Conflict of Interest: No conflict of interest was declared by the authors.

Financial Disclosure: The authors declared that this study received no financial support.

References

1. Kitahara CM, Sosa JA. The changing incidence of thyroid cancer. Nat Rev Endocrinol 2016;12:646-653.
2. Kand P, Asopa R. Metastatic involvement of the spleen in differentiated carcinoma of thyroid. Indian J Nucl Med 2010;25:171-172.
3. Wartofsky L, Van Nostrand D. Thyroid cancer: a comprehensive guide to clinical management. 2nd ed. Springer, 2006.
4. Haugen BR, Alexander EK, Bible KC, Doherty GM, Mandel SJ, Nikiforov YE, Pacini F, Randolph GW, Sawka AM, Schlumberger M, Schuff KG, Sherman SI, Sosa JA, Steward DL, Tuttle RM, Wartofsky L. 2015 American Thyroid Association Management Guidelines for Adult Patients with Thyroid Nodules and Differentiated Thyroid Cancer: The American Thyroid Association Guidelines Task Force on Thyroid Nodules and Differentiated Thyroid Cancer. Thyroid 2016;26:1-133.
5. Oh JR, Ahn BC. False-positive uptake on radioiodine whole-body scintigraphy: physiologic and pathologic variants unrelated to thyroid cancer. Am J Nucl Med Mol Imaging 2012;2:362-385.
6. Mohan V, Jones RC, Drake AJ 3rd, Daly PL, Shakir KM. Littoral cell angioma presenting as metastatic thyroid carcinoma to the spleen. Thyroid 2005;15:170-175.

Interesting Image
Mol Imaging Radionucl Ther 2023;32:178-180 DOI:10.4274/mirt.galenos.2023.81567

I-131 Avid Tumor Thrombus in a Case of Poorly Differentiated Thyroid Cancer

Kötü Diferansiye Tiroid Kanseri Olgusunda I-131 Tutan Tümör Trombüsü

Sana Munir Gill, Aamna Hassan, Humayun Bashir, Waqas Shafiq

Shaukat Khanum Memorial Cancer Hospital and Research Centre, Department of Nuclear Medicine, Lahore, Pakistan

Abstract

Intravenous tumor extension is a well-recognized phenomenon occurring in various malignancies but is a relatively rare entity in thyroid carcinoma. In patients with poorly differentiated thyroid cancer (pDTC), I-131 avid superior vena cava tumor (SVC) thrombus at initial presentation is infrequent and potential life threatening. Tumor thrombus can form either due to direct vascular extension of the primary mass or by hematogenous spread. Hybrid nuclear imaging can differentiate the two entities, which can impact the treatment plan of the patient. We present images of an interesting case of evolution of SVC thrombus in a 46-year-old woman with diagnosed pDTC over the span of two years.

Keywords: I-131 avid tumor thrombus, SPECT/CT, poorly differentiated thyroid cancer

Öz

İntravenöz tümör yayılımı, çeşitli malignitelerde ortaya çıkan iyi bilinen bir fenomendir, ancak tiroid karsinomunda nispeten nadir bir antitedir. Kötü diferansiye tiroid kanseri (pDTC) olan hastalarda, başlangıçta I-131 avid superior vena cava tümörü (SVC) trombüsü nadirdir ve potansiyel olarak yaşamı tehdit eder. Tümör trombüsü, primer kitlenin doğrudan vasküler yayılımı veya hematojen yayılım nedeniyle oluşabilir. Hibrit nükleer görüntüleme, hastanın tedavi planını etkileyebilecek bu iki antiteyi ayırt edebilir. Bu yazıda, pDTC tanısı konan 46 yaşındaki bir kadında ilginç bir SVC trombüs gelişiminin iki yıllık görüntülerini sunuyoruz.

Anahtar kelimeler: I-131 tutan tümör trombüsü, SPECT/BT, az diferansiye tiroid kanseri

Address for Correspondence: Aamna Hassan MD, Shaukat Khanum Memorial Cancer Hospital and Research Centre, Department of Nuclear Medicine, Lahore, Pakistan
Phone: +92 42 35905000 **E-mail:** aamnah@skm.org.pk ORCID ID: orcid.org/0000-0003-0026-0729
Received: 08.11.2022 **Accepted:** 22.01.2023

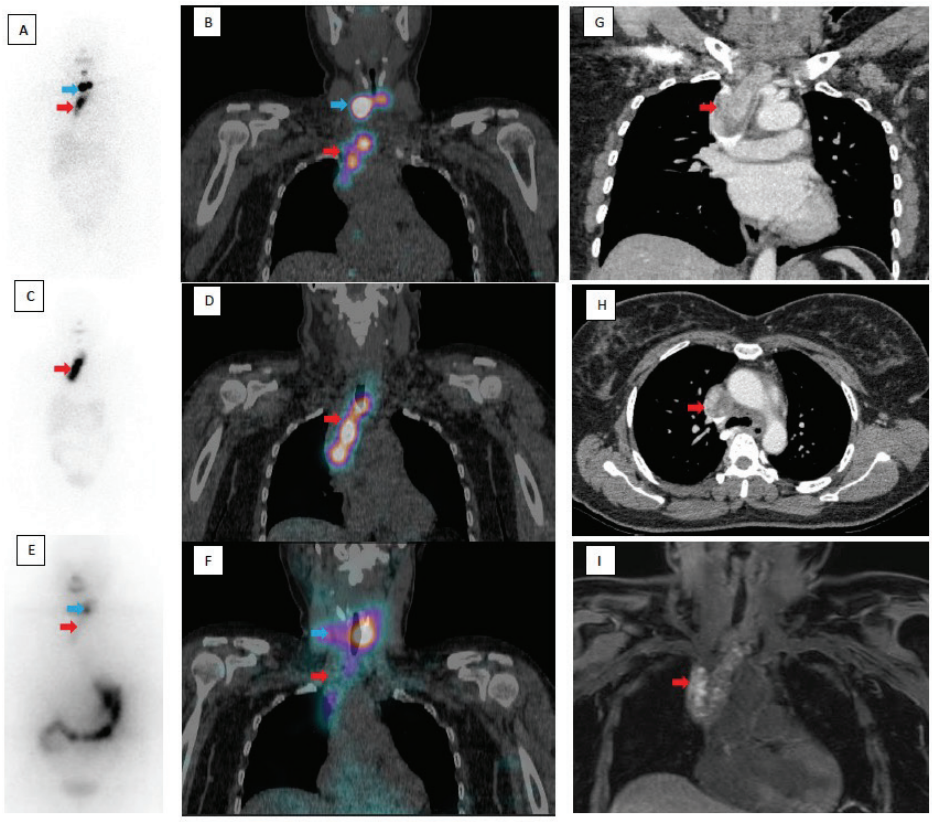

Figure 1. A 46-year-old female was referred for radioactive iodine (RAI) ablation therapy after total thyroidectomy. Histopathology revealed poorly differentiated thyroid carcinoma (pDTC). Per ATA guidelines, she was at highrisk for disease recurrence and was staged as T3aN1M0. A pre-therapy whole body scan (WBS) was performed 48 h after oral administration of 3.5 mCi of I131(A). It showed bifocal RAI (I-131) uptake in the thyroid bed (blue arrow) more prominent on the right side. Linear increased activity (red arrow) was confirmed to be a superior vena cava (SVC) tumor thrombus on a single-photon emission tomography/computed tomography (SPECT/CT) scan (fused coronal SPECT/CT, B). Stimulated thyroglobulin level was 11,135 ng/mL with normal anti-thyroglobulin antibody levels.

She received 100 mCi of RAI, which was well delivered to the thyroid remnant on post-therapy scan. The patient also had a CT thorax with contrast, which confirmed SVC thrombus extending into the left brachiocephalic vein with an enhancing component, consistent with tumor thrombus. Magnetic resonance imaging (MRI) thorax also showed a long segment thrombus of SVC with expansion (G, H, I). As iodinated contrast in CT scan can increase the total body iodine stores for up to 3 months, which can render subsequent RAI therapy ineffective, adequate interval was ensured between CT with contrast and RAI therapy. Subsequently, she developed facial swelling (SVC syndrome) and urgently received 800 cGy of palliative radiation to the mediastinum. SVC is rarely involved in thyroid carcinomas at initial presentation, and if present, it usually occurs with systemic disease (1). SVC tumor thrombus can result in severe symptoms due to vascular congestion.

Two months after radiotherapy, she received another 150 mCi of RAI. Post-therapy WBS and coronal SPECT/CT (C, D red arrow) showed a well-delivered dose to SVC tumor thrombus. No avidity was noted in the thyroid surgical bed. Stimulated thyroglobulin levels declined to 5788 ng/mL and anti-thyroglobulin levels remained normal.

pDTC has intermediate characteristics between well-differentiated thyroid carcinoma and anaplastic tumors (1). The incidence of pDTC has increased over the last few years with significant morbidity and mortality due to its aggressive behavior (2). Among thyroid cancers, it has an incidence of 0.23% to 2.6% (3). Thyroid carcinoma has a microscopic vascular invasion; however, gross venous thrombus is a rare occurrence (4). Conventional imaging such as MRI and CT is helpful in the diagnosis of venous thrombus (5). Doppler ultrasound has limited yield in this area as SVC is mostly obscured by adjacent structures (6). However, the differentiation of a tumor thrombus from other thrombi can be a challenge in conventional imaging. Thus, in iodine sensitive cases of thyroid carcinoma, hybrid nuclear scans such as I-131 planar images coupled with SPECT/CT are highly beneficial in identifying tumor thrombus versus benign thrombosis using the iodine avidity of the thrombus as in this case.

One year later, the patient had an evidence of recurrent disease on ultrasound in the left thyroid bed. pDTC is an aggressive tumor accounting for approximately 1-15% of thyroid carcinomas (7). More than 80% of patients with pDTC have good RAI uptake; however, 15% are non-avid iodine (8). As our patient had previously had iodine avid disease and had also shown response, she received a third dose of RAI, 200 mCi (cumulative dose 450 mCi). Post-therapy WBS and coronal SPECT/CT images (E,F, blue arrow) re-demonstrated ultrasound findings of soft tissue nodule in the left thyroid bed, which was iodine avid. Interval regression in the avidity of SVC tumor thrombus was also noted (E, F red arrow). She received 20 Gy radiation in 5 fractions to the thyroid. She is under regular follow-up and stable.

Ethics

Informed Consent: Written consent was taken from the patient.

Peer-review: Externally and internally peer-reviewed.

Authorship Contributions

Surgical and Medical Practices: A.H., H.B., W.S., Concept: A.H., H.B., Design: S.M.G., A.H., Data Collection or Processing: S.M.G., A.H., Analysis or Interpretation: A.H., H.B., Literature Search: S.M.G., Writing: A.H., H.B., W.S.

Conflict of Interest: No conflict of interest was declared by the authors.

Financial Disclosure: The authors declared that this study received no financial support.

References

1. Onoda N, Nakamura M, Hosono M, Sasaki Y, Kawajiri H, Takashima T, Ishikawa T, Hirakawa K. Successful surgical treatment of advanced follicular thyroid carcinoma with tumor thrombus infiltrating the superior vena cava: report of a case. Surg Today 2012;42:185-190.
2. Dettmer MS, Schmitt A, Komminoth P, Perren A. Poorly differentiated thyroid carcinoma: an underdiagnosed entity. Pathologe 2020;41(Suppl 1):1-8.
3. Yu MG, Rivera J, Jimeno C. Poorly differentiated thyroid carcinoma: 10-year experience in a Southeast Asian population. Endocrinol Metab (Seoul) 2017;32:288-295.
4. Kawano F, Tomita M, Tanaka H, Nagahama H, Tashiro K, Nakao H, Kataoka H, Nakamura K. Thyroid carcinoma with extensive tumor thrombus in the superior vena cava: a case report. Int J Surg Case Rep 2016;29:25-29.
5. Marcy PY, Thariat J, Bozec A, Poissonnet G, Benisvy D, Dassonville O. Venous obstruction of thyroid malignancy origin: the Antoine Lacassagne Institute experience. World J Surg Oncol 2009;7:40.
6. Hyer SL, Dandekar P, Newbold K, Haq M, Wechalakar K, Thway K, Harmer C. Thyroid cancer causing obstruction of the great veins in the neck. World J Surg Oncol 2008;6:36.
7. Ibrahimpasic T, Ghossein R, Carlson DL, Nixon I, Palmer FL, Shaha AR, Patel SG, Tuttle RM, Shah JP, Ganly I. Outcomes in patients with poorly differentiated thyroid carcinoma. J Clin Endocrinol Metab 2014;99:1245-1252.
8. Cherkaoui GS, Guensi A, Taleb S, Idir MA, Touil N, Benmoussa R, Baroudi Z, Chikhaoui N. Poorly differentiated thyroid carcinoma: a retrospective clinicopathological study. Pan Afr Med J 2015;21:137.

Interesting Image
Mol Imaging Radionucl Ther 2023;32:181-185 DOI:10.4274/mirt.galenos.2023.82712

Hypermetabolic Axillary Lymph Nodes Associated with COVID-19 Vaccination in Breast Cancer Management

Meme Kanseri Yönetiminde COVID-19 Aşısına Bağlı Hipermetabolik Aksiller Lenf Nodları

Cengiz Taşçı[1], Ahmet Dirican[2], Ethem Murat Sözbilen[3], Fatma Seher Pehlivan[4], Selim Serter[5]

[1]*İzmir University of Economics Faculty of Medicine, Medical Point Hospital, Department of Nuclear Medicine, İzmir, Turkey*
[2]*İzmir University of Economics Faculty of Medicine, Medical Point Hospital, Department of Medical Oncology, İzmir, Turkey*
[3]*İzmir University of Economics Faculty of Medicine, Medical Point Hospital, Department of General Surgery, İzmir, Turkey*
[4]*Private Mikro Pathology Lab, İzmir, Turkey*
[5]*İzmir University of Economics Faculty of Medicine, Medical Point Hospital, Department of Radiology, İzmir, Turkey*

Abstract

A 42-year-old female patient diagnosed with invasive ductal breast ca underwent ^{18}F-fluorodeoxyglucose (FDG) positron emission tomography/computed tomography (PET/CT) scan for staging, 1.5 cm diameter hypermetabolic lesion was observed in the lower inner quadrant of the right breast that was compatible with primary tumor [maximum standardized uptake value (SUV_{max}): 10.5]. No pathological ^{18}F-FDG uptake was observed in lymph nodes whose fatty hilum was seen in the right axilla. However, in the left axilla and left deep axilla, hypermetabolic lymph nodes with a maksimum diameter of 19 mm and fatty hilum were observed (SUV_{max}: 8.0). In a detailed CT evaluation, these lymph nodes have thicker walls than the ones in the right axilla. The patient was questioned again and coronavirus disease-2019 (COVID-19) vaccination history (with BNT162b2, COVID-19 mRNA vaccine) was determined that was administrated to the left arm 5 days ago. Tru-cut biopsy was performed from the left aksillary lymph nodes and proved to be reactive lymphoid tissue and there was no primary or metastatic tumor in these axillary lymph node tissues. The patient was given neoadjuvant chemotherapy 4.5 months after the first ^{18}F-FDG PET/CT, and the second was performed for the treatment response evaluation. Significant regression was determined from the findings. The patient underwent right total mastechtomy. She was being followed up with adjuvant chemotherapy and radiotherapy. In conclusion, hypermetabolic lymph nodes in the axillas should be interrogated for vaccination in patients with breast cancer. Hypermetabolic lymph nodes observed on the same side of the vaccinated arm in the ^{18}F-FDG PET/CT scan may be related to vaccine-induced reactive lymph node enlargement. Lymph node metastasis may be excluded, especially if there are hypermetabolic lymph nodes with preserved fatty hilum in the contralateral axilla on the same side as the vaccinated arm. Active lymph nodes reactive to the vaccine become inactive after a while.

Keywords: Axillary lymph nodes, COVID-19 vaccination, breast cancer, ^{18}F-FDG PET/CT

Öz

Kırk iki yaşında, invaziv duktal meme kanseri tanısı alan, evreleme için ^{18}F-florodeoksiglukoz (FDG) pozitron emisyon tomografi/bilgisayarlı tomografi (PET/BT) taraması yapılan kadın hastada, sağ meme alt iç kadranda primer tümörle uyumlu 1,5 cm çaplı hipermetabolik lezyon izlendi [maksimum standartlaştırılmış alım değeri (SUV_{maks}): 10,5]. Sağ aksillada yağlı hilusu görülen lenf nodlarında patolojik ^{18}F-FDG tutulumu izlenmedi. Ancak sol aksilla ve sol derin aksillada yağlı hilusu gözlenen 19 mm çaplı hipermetabolik lenf nodları mevcuttu (SUV_{maks}: 8,0). Ayrıntılı BT değerlendirmesinde, bu lenf bezlerinin duvarları sağ aksilladakilerden daha kalındı. Hasta tekrar sorgulandı ve 5 gün önce sol koluna uygulanan koronavirüs hastalığı-2019 (COVID-19) aşısı öyküsü (BNT162b2, COVID-19 mRNA aşısı ile) belirlendi. Sol aksiller lenf nodlarından yapılan tru-

Address for Correspondence: Asst. Prof. Cengiz Taşçı, İzmir University of Economics Faculty of Medicine, Medical Point Hospital, Department of Nuclear Medicine, İzmir, Turkey
Phone: +90 232 399 50 50 **E-mail:** cengiztasci68@hotmail.com ORCID ID: orcid.org/0000-0003-0962-7515
Received: 22.09.2022 **Accepted:** 22.01.2023

cut biyopsi sonucu reaktif lenfoid doku olarak geldi ve primer veya metastatik tümör izlenmediği rapor edildi. Hastaya neoadjuvan kemoterapi verildi. İlk ^{18}F-FDG PET/BT'den 4,5 ay sonra, tedaviye yanıt değerlendirmesi için ikincisi yapıldı. Bulgularda belirgin regresyon gözlendi. Hastaya sağ total mastektomi yapıldı. Hasta kemoterapi ve radyoterapi ile takip ediliyor. Sonuç olarak, pandemi günlerinde meme kanserli hastalarda aksiller hipermetabolik lenf nodları COVID-19 aşısı açısından sorgulanmalıdır. ^{18}F-FDG PET/BT taramasında aşılı kolun aynı tarafında gözlenen hipermetabolik lenf nodları, aşıya bağlı reaktif lenfadenomegali ile ilişkili olabilir. Özellikle memedeki kitleye göre kontralateral ancak aşı yapılan kol ile aynı taraftaki aksillada görülen yağlı hilusu korunmuş hipermetabolik lenf nodları, reaktif olarak değerlendirilerek lenf nodu metastazı dışlanabilir. Olguda aşıya bağlı reaktif (aktif) lenf nodlarının zamanla inaktif hale dönüşmesi gözlenmektedir.

Anahtar kelimeler: Aksiller lenf nodları, COVID-19 aşısı, meme kanseri, ^{18}F-FDG PET/BT

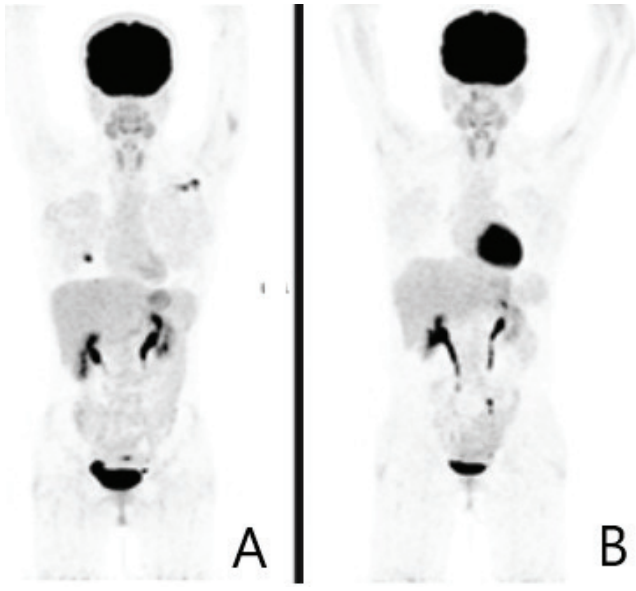

Figure 1. A) ^{18}F-fluorodeoxyglucose (FDG) positron emission tomography/computed tomography (PET/CT) scanning for staging purposes. A hypermetabolic lesion was observed in the lower inner quadrant of the right breast that was compatible with primary tumor [maximum standardized uptake value (SUV_{max}): 10.5]. No pathological ^{18}F-FDG uptake was observed in the right axilla. However, hypermetabolic lymph nodes were observed in the left axilla and left deep axilla (SUV_{max}: 8.0) which were confirmed to be related to the vaccination administrated to the left arm 5 days ago (1,2,3,4,5). No other pathological ^{18}F-FDG uptake was observed in all other body parts of the patient. B) The second ^{18}F-FDG PET/CT scan for neoadjuvant chemotherapy response evaluation, 4.5 months after the first scan. No ^{18}F-FDG avid malignancy finding was observed.

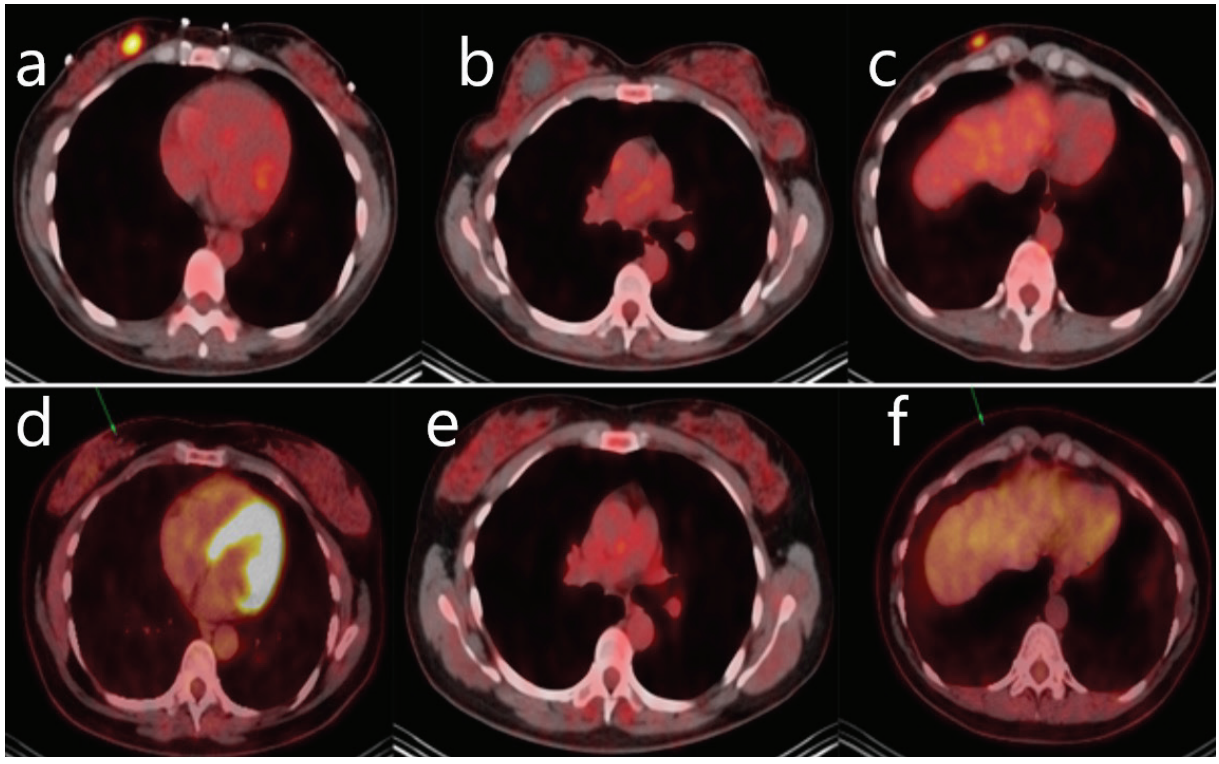

Figure 2. ^{18}F-FDG PET/CT scanning performed for staging at the beginning (a, b, c) and 4.5 months after the first one performed for neoadjuvant treatment response evaluation (d, e, f). A hypermetabolic lesion was observed in the lower inner quadrant of the right breast that was compatible with primary tumor (SUV_{max}: 10.5) (a). The primary tumor was reduced in size and its ^{18}F-FDG uptake was markedly decreased after neoadjuvant chemotherapy (d). Several hypometabolic cystic lesions were also observed in both breasts at the beginning. These lesions were interpreted as benign cystic lesions (fibrocystic changes?) (b). The hypometabolic cystic lesions were reduced in size at the second imaging (e) and confirmed by the postoperative pathology report. A 12 mm diameter hypermetabolic nodular lesion was observed in subcutaneous fatty tissue under the skin at the level of the 6th rib on the right anterior wall of the thorax at the initial imaging (SUV_{max}: 4.7) (c). This lesion was interpreted as an intramamarian lymph node metastasis (c). This nodular lesion disappeared on second imaging (f).

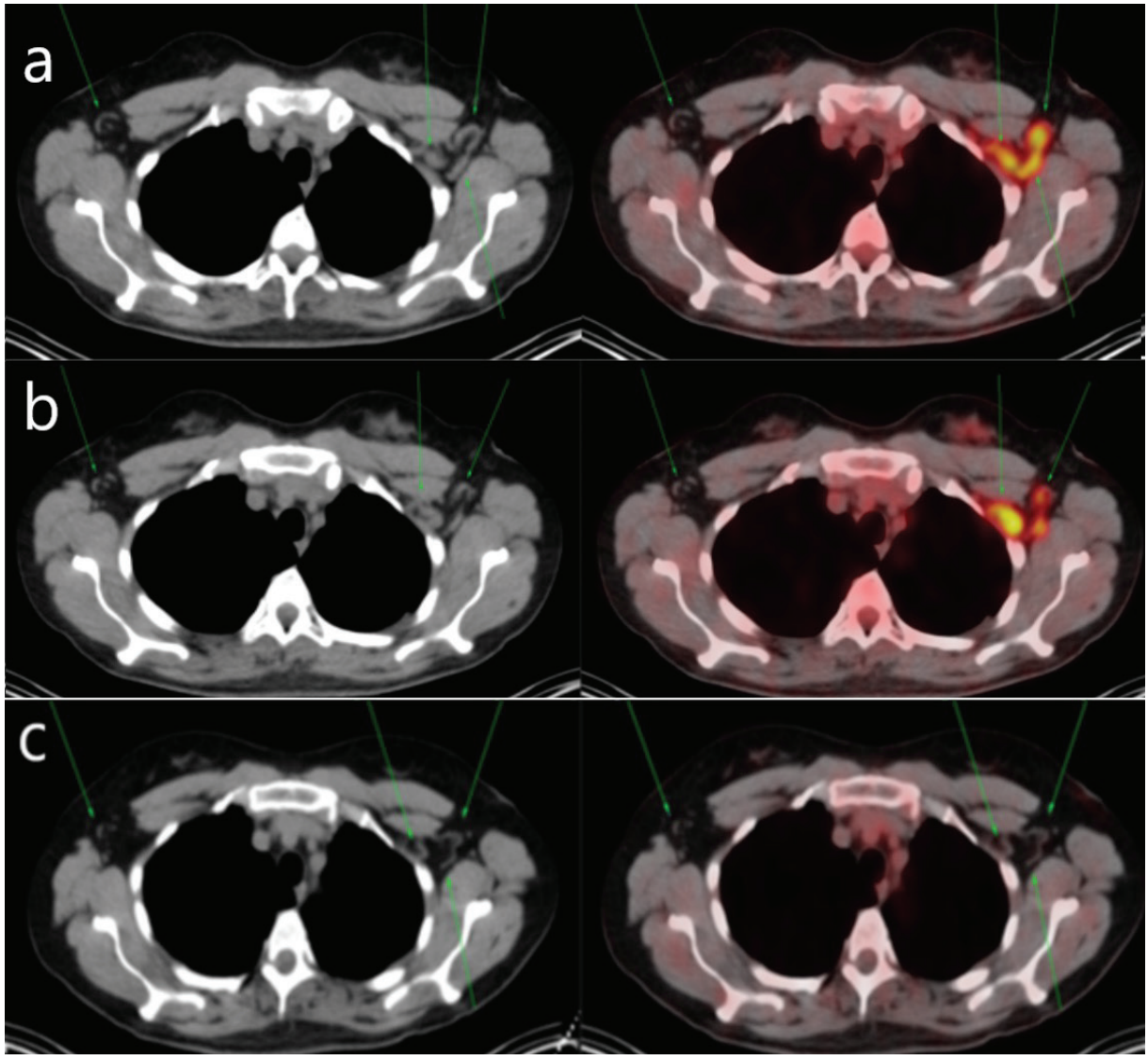

Figure 3. Hybrid images of ^{18}F-FDG PET/CT scanning performed for staging at the beginning (a, b). Initially, no pathological ^{18}F-FDG uptake was observed in lymph nodes that seemed inactive (non-metabolic) in the right axilla. However, there were hypermetabolic lymph nodes in the left axilla and left deep axilla (SUV_{max}: 8.0). On CT images of the same ^{18}F-FDG PET/CT scanning, the lymph nodes in the right axilla had fatty hiluses and thin walls, whereas the hypermetabolic lymph nodes in the left axilla and left deep axilla had fatty hiluses and thick walls (SUV_{max}: 8.0) (a, b). At the second ^{18}F-FDG PET/CT imaging after neoadjuvant chemotherapy, the lymph nodes in the left axilla were reduced in size and their ^{18}F-FDG uptake was markedly decreased. Yet, the ones in the right axilla stayed stable (c). At the initial imaging, active and inactive lymph nodes are seen together (a, b). The active to inactive transformation of the lymph nodes after vaccination has been visualized (a, b, c).

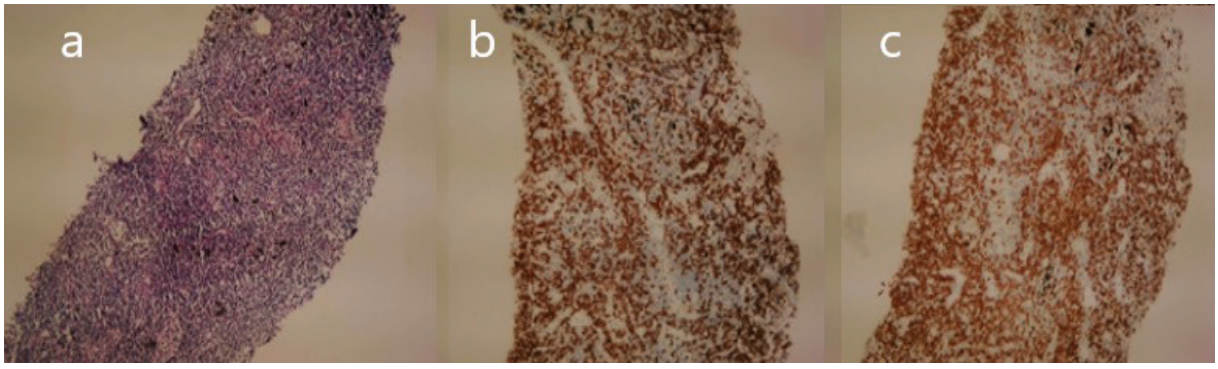

Figure 4. A mixed staining pattern was observed in staining with CD20 CD5 and pancytokeratin in immunochemical examination, (a) reactive lymph nodes including anthracnose pigment (x40; hematoxylin-eosin), (b) lymphoid cells stained positive with CD20 (x100; DAB), (c) lymphoid cells stained positive with CD3 (x100; DAB).

Hypermetabolic lymph nodes observed on the same side of the vaccinated arm in the ^{18}F-FDG PET/CT scan may be related to vaccine-induced reactive lymph node enlargement (1,2,3,4,5). Lymph node metastasis may be excluded, especially if there are hypermetabolic lymph nodes with preserved fatty hilum in the contralateral axilla on the same side as the vaccinated arm (2,3,4,5).

Ethics

Informed Consent: Written informed consent was obtained from the patient.

Peer-review: Externally peer-reviewed.

Authorship Contributions

Surgical and Medical Practices: C.T., E.M.S., Concept: C.T., A.D., E.M.S., F.S.P., S.S., Design: C.T., F.S.P., Data Collection or Processing: C.T., A.D., F.S.P., S.S., Analysis or Interpretation: C.T., A.D., E.M.S., F.S.P., S.S., Literature Search: C.T., Writing: C.T.

Conflict of Interest: No conflict of interest was declared by the authors.

Financial Disclosure: The authors declared that this study has received no financial support.

References

1. Özütemiz C, Krystosek LA, Church AL, Chauhan A, Ellermann JM, Domingo-Musibay E, Steinberger D. Lymphadenopathy in COVID-19 vaccine recipients: diagnostic dilemma in oncologic patients. Radiology 2021;300:296-300.
2. Otomi Y, Irahara S, Inoue H, Shinya T, Otsuka H, Harada M. Increased ^{18}F-FDG uptake in the axillary lymph nodes of the vaccinated side associated with COVID-19 vaccination. Mol Imaging Radionucl Ther 2023;32:169-171.
3. Nawwar AA, Searle J, Hopkins R, Lyburn ID. False-positive axillary lymph nodes on FDG PET/CT resulting from COVID-19 immunization. Clin Nucl Med 2021;46:1004-1005.
4. Eifer M, Eshet Y. Imaging of COVID-19 vaccination at FDG PET/CT. Radiology 2021;299:248.
5. Brown AH, Shah S, Groves AM, Wan S, Malhotra A. The Challenge of Staging Breast Cancer With PET/CT in the Era of COVID Vaccination. Clin Nucl Med 2021;46:1006-1010.

Interesting Image
Mol Imaging Radionucl Ther 2023;32:186-190 DOI:10.4274/mirt.galenos.2023.79095

Polyostotic Fibrous Dysplasia in a Six-year-Old Boy

Altı Yaşındaki Erkek Çocukta Poliostotik Fibröz Displazi

Nevena Manevska[1], Dushica Todorova-Stefanovski[2], Smiljana Bundovska Kocev[3], Sinisha Stojanoski[1], Tanja Makazlieva[1]

[1]*Ss. Cyril and Methodius University, Faculty of Medicine, Institute of Pathophisiology and Nuclear Medicine, Skopje, Macedonia*
[2]*University Institute for Positron Emission Tomography, Skopje, Macedonia*
[3]*Ss. Cyril and Methodius University, Faculty of Medicine, Institute of Radiology, Skopje, Macedonia*

Abstract

Fibrous dysplasia (FD) is a rare congenital benign bone disease that manifests as a defect in the bone remodeling process, affecting the function, differentiation, and maturation of osteoblasts. This process is located in the bone marrow, where the normal marrow tissue is replaced with immature bone islands and fibrous stroma. The etiology is unclear so far, but it is known to be connected with a point mutation of the gene that encodes Gs α protein at the time of embryogenesis, and because of that, all of the affected somatic cells become dysplastic. It is important to determine whether the mutation occurred earlier in the process of embryogenesis so that there will be more mutant cells and the disease will appear in a more severe form. The clinical presentation of FD is variable, so there are plenty of potential differential diagnoses. The most common include Paget disease, non-ossifying fibroma, osteofibrous dysplasia, aneurysmal bone cyst, adamantinoma, giant cell tumor, fracture callus, and low-grade central osteosarcoma.

Keywords: Fibrous dysplasia, bone scan, SPECT

Öz

Fibröz displazi (FD), osteoblastların işlevini, farklılaşmasını ve olgunlaşmasını etkileyen, kemiğin yeniden şekillenmesi sürecinde bir kusur olarak ortaya çıkan, nadir görülen, iyi huylu konjenital bir kemik hastalığıdır. Bu süreç, normal kemik iliği dokusunun olgunlaşmamış kemik adaları ve fibröz stroma ile yer değiştirdiği kemik iliğinde cereyan eder. Etiyoloji net değildir, ancak etiyolojinin embriyogenez sırasında Gs α proteinini kodlayan genin nokta mutasyonu ile bağlantılı olduğu bilinmektedir ve bu nedenle etkilenen tüm somatik hücreler displastik hale gelmektedir. Mutasyonun embriyogenez sürecinde daha erken meydana gelip gelmediğini belirlemek, daha fazla mutant hücre oluşması ve hastalığın daha şiddetli bir şekilde ortaya çıkması açısından önemlidir. FD'nin klinik prezentasyonu değişkendir, bu nedenle çok sayıda potansiyel ayırıcı tanı vardır. En yaygın olanları Paget hastalığı, ossifiye olmayan fibroma, osteofibröz displazi, anevrizmal kemik kisti, adamantinom, dev hücreli tümör, kırık kallus ve düşük dereceli santral osteosarkomdur.

Anahtar kelimeler: Fibröz displazi, kemik sintigrafisi, SPECT

Address for Correspondence: Asst. Prof. Nevena Manevska, Ss. Cyril and Methodius University, Faculty of Medicine, Institute of Pathophisiology and Nuclear Medicine, Skopje, Macedonia
Phone: +38970398042 **E-mail:** dr.nmanevska@gmail.com ORCID ID: orcid.org/0000-0001-7168-3775
Received: 08.09.2022 **Accepted:** 22.01.2023

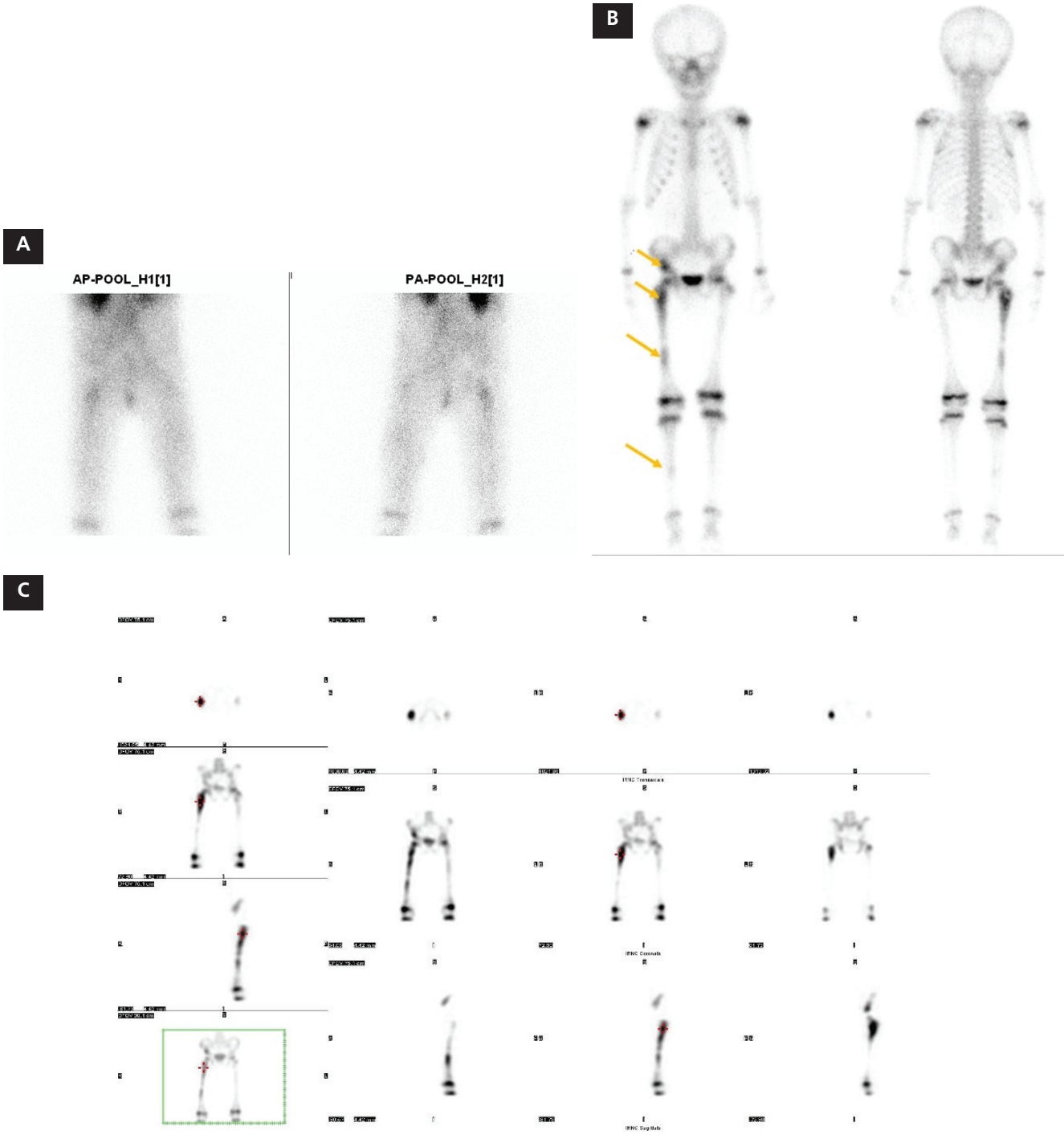

Figure 1. A We present a case of a 6-year-old boy complained of a right hip pain, especially at night and on exertion. He was diagnosed with a fracture of the subtrochanteric region of the right femur. The bone scan performed after an intravenous application of Tc-99m-methyl diphosphonate (MDP) revealed increased vascularization of the right hip in the early pool phase image (A). Whole-body images showed intensive uptake of Tc-99m-MDP in the right iliac bone and right femur (proximal diaphysis), with not very intense accumulation in the middle 1/3 of the right femur and right tibia (B). Single-photon emission computed tomography (SPECT) images confirmed the uptake in the iliac bone and the femur (C).
Fibrous dysplasia (FD) accounts for 7% of the benign bone tumors, primarily affecting young adolescents and young adults, with no gender predilection gender predilection. It may appear as monostotic (affecting one bone), polyostotic (multiple bones), or craniofacial FD (skull and facial bones alone).

Common sites of skeletal involvement are long bones, ribs, craniofacial bones, and the pelvis (2). The polyostotic form is found in 20-30% of cases. It presents earlier, typically in childhood (mean age of 8 years) with two/thirds being symptomatic by the age of 10. In early childhood, lesions are metabolically active and expand during linear growth. The lesions typically become static in size after puberty, and metabolic activity may decrease throughout adulthood (3). The polyostotic form of the disease is often accompanied by an endocrine disorder such as McCune-Albright syndrome. This kind of syndrome combines FD with other extraskeletal features, such as "café-au-lait" skin macules with characteristic distribution, gonadotropin-independent sex steroid production in girls and women or autonomous testosterone production in boys and men, thyroid lesions, growth hormone excess, neonatal hypercortisolism, and renal phosphate wasting (4). The bone scan shows increased uptake throughout life, but the uptake becomes less intense as the lesions mature. Some characteristic findings within lesions of FD are a bar-shaped pattern, whole bone involvement, and a close match between the size of the lesion on radiographs and the size of the area of uptake. The lesions show increased uptake of the tracer, but its intensity is variable, so sometimes false-negative results are detected. The mechanism of different degrees of Tc-99m-MDP metabolism of FD is unclear. As we know, FD is developmental failure in the remodeling of the primitive bone to a mature lamellar bone. Fibroblasts are the predominant proliferating cells in FD lesions, and the different degrees of 99mTc-MDP metabolism among them may be due to the difference in the vascular supply or the number of proliferating fibroblasts or their metabolic turnover (7).

Figure 2. Computed tomography image of the right femur. The coronal plane showed a changed skeletal structure of the diaphysis of the right femur with present multifocal ground-glass opacities and cystic components.

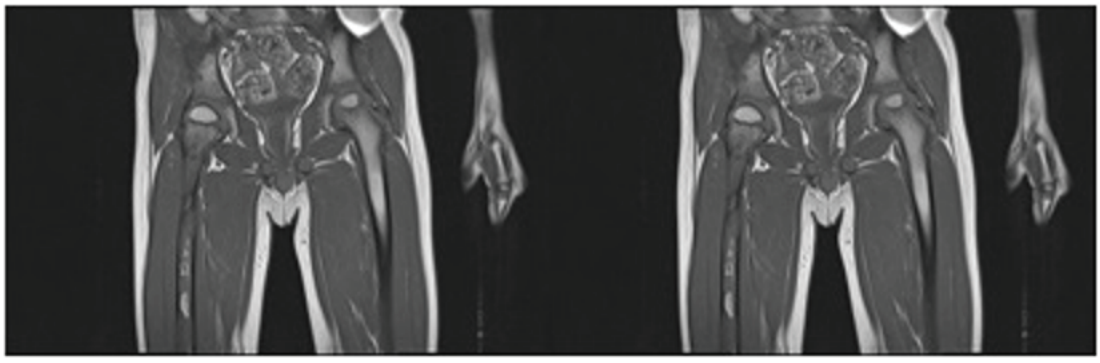

Figure 3. Magnetic resonance imaging (MRI) in 2019. There were multiple circumscribed lesions with ground-glass opacity in the right iliac bone, the superior ramus of the right ischiatic bone, and the right femur without involving the head. In the region of the right femoral neck and the intertrochanteric region, predominantly cystic and sclerotic components were delineated in the lesions. No cortical disruption or the cortical expansion was noted. There were signs of bone expansion in the inter- and subtrochanteric regions with cortical thinning but no disruption of the cortex.

Radiolucent ground glass matrix, which is smooth and homogeneous, is a typical FD lesion on radiography. Sometimes these lesions appear as completely radiolucent (cystic) lesions or sclerotic lesions, but mixed forms are also described. They have well-circumscribed thick sclerotic margins around the radiolucent lesion that can be interrupted, the so-called rind sign (5). MRI reports in patients with FD have been quite challenging, considering the high variability in the tumor signal on the MR examination..

Laboratory findings were as follows: C-reactive protein: 27.4 (<6 mg/L); white blood cells: 20.1 (4-9x109/L); alkaline phosphatase: 173 (36-126 U/L). These inflammatory markers are non-specific for FD, except for the alkaline phosphatase that can be high in patients with metabolic bone disease. Three months later, he underwent surgery with resection of the right fibula that was implanted on the site of the proximal diaphysis of the right femur.

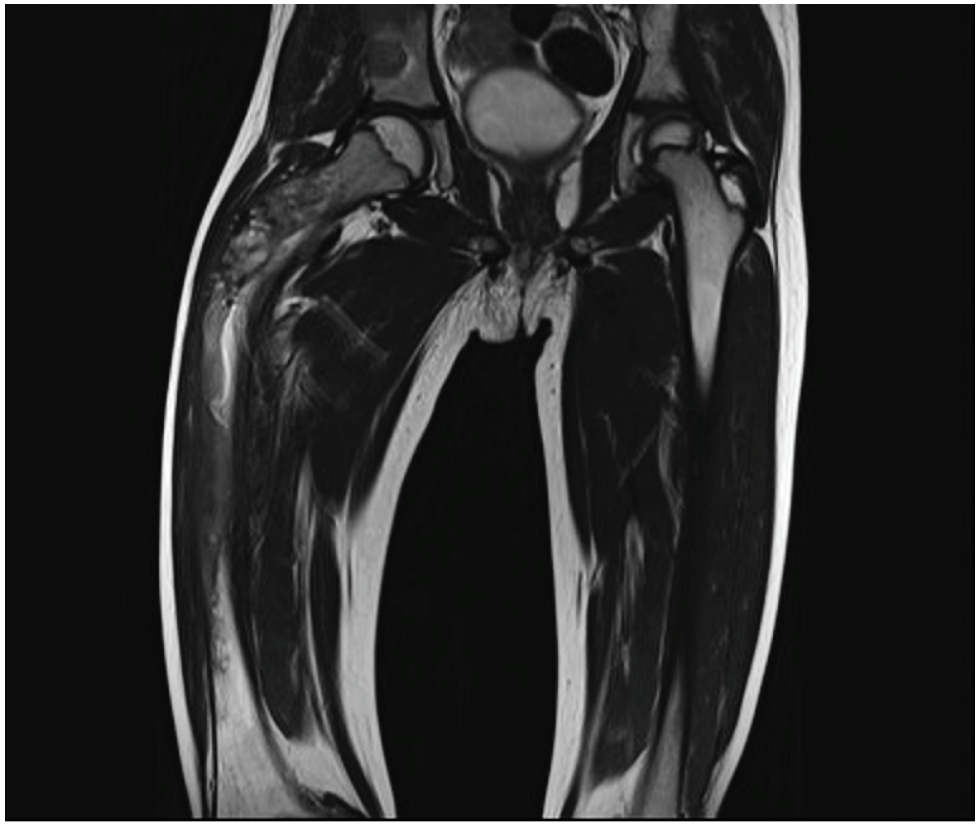

Figure 4. MRI images in 2021 there are predominantly fibrous and cystic lesions in the intertrochanteric region with mild bone expansion and endosteal scallopings. Changes in the skeletal structure in the basicervical, intertrochanteric, and proximal diaphyseal regions.
For confirming the diagnosis, biopsy is not always indicated. If there is a clear radiological finding for FD, only regular observation is needed. Follow-up radiographs should be made every six months to verify that there has been no progression. Bisphosphonates are the therapy of choice for pain relief and bone strengthening. Surgery is needed in rare cases only when complications such as fractures or deformities are present (8).

Ethics

Informed Consent: Written informed consent was obtained.

Peer-review: Externally peer-reviewed.

Authorship Contributions

Concept: N.M., Design: N.M., S.B.K., Data Collection or Processing: N.M., S.B.K., Analysis or interpretation:S.S., T.M., Literature Search: D.T-T., T.M., Writing: D.T-T., S.S., N.M.

Conflict of Interest: No conflict of interest was declared by the authors.

Financial Disclosure: The authors declared that this study received no financial support.

References

1. Jeyaraj P. Histological Diversity, Diagnostic Challenges, and Surgical Treatment Strategies of Fibrous Dysplasia of Upper and Mid-Thirds of the Craniomaxillofacial Complex. Ann Maxillofac Surg 2019;9:289-314.
2. DiCaprio MR, Enneking WF. Fibrous dysplasia. Pathophysiology, evaluation, and treatment. J Bone Joint Surg Am 2005;87:1848-1864.
3. https://radiopaedia.org/articles/fibrous-dysplasia
4. Javaid MK, Boyce A, Appelman-Dijkstra N, Ong J, Defabianis P, Offiah A, Arundel P, Shaw N, Pos VD, Underhil A, Portero D, Heral L, Heegaard AM, Masi L, Monsell F, Stanton R, Dijkstra PDS, Brandi ML, Chapurlat R, Hamdy NAT, Collins MT. Best practice management guidelines for fibrous dysplasia/McCune-Albright syndrome: a consensus statement from the FD/MAS international consortium. Orphanet J Rare Dis 2019;14:139.
5. Kushchayeva YS, Kushchayev SV, Glushko TY, Tella SH, Teytelboym OM, Collins MT, Boyce AM. Fibrous dysplasia for radiologists: beyond ground glass bone matrix. Insights imaging. Insights Imaging 2018;9:1035-1056.
6. Kinnunen AR, Sironen R, Sipola P. Magnetic resonance imaging characteristics in patients with histopathologically proven fibrous dysplasia-a systematic review. Skeletal Radiol 2020;49:837-845.
7. Zhang L, He Q, Li W, Zhang R. The value of 99mTc-methylene diphosphonate single photon emission computed tomography/computed tomography in diagnosis of fibrous dysplasia. BMC Med Imaging 2017;17:46.
8. Chapurlat RD. Medical therapy in adults with fibrous dysplasia of bone. J Bone Miner Res 2006;21(Suppl 2):114-119.